| AD NUMBER |
| --- |
| AD348620 |
| CLASSIFICATION CHANGES |
| TO: unclassified |
| FROM: confidential |
| LIMITATION CHANGES |
| TO:<br>Approved for public release, distribution unlimited |
| FROM:<br>Distribution authorized to U.S. Gov't. agencies and their contractors; Administrative/Operational Use; MAR 1964. Other requests shall be referred to Directorate of Armament Dev., Det 4, Research and Technology Div., AFSC, Eglin AFB, FL. |
| AUTHORITY |
| AFATL ltr, 28 Oct 1975; AFATL ltr, 28 Oct 1975 |

ATL-TDR-64-9 Copy of 184 Copies



(Unclassified Title)

# RADIALLY EXPANDING FRAGMENTATION WARHEAD STUDY

Summary Report for
16 November 1962 through 15 December 1963

ATL Technical Documentary Report No. 64-9
March 1964 Project No. 2855

Directorate of Armament Development
Det 4, Research and Technology Division
Air Force Systems Command
Eglin Air Force Base, Florida

(Prepared under Contract No. AF08(635)-5269 by the Armament Sciences Laboratory, Research Division, Martin Company, Orlando, Florida, W. R. Porter, Author).

Qualified requesters may obtain copies from DDC. Orders will be expedited if placed through the librarian or other person designated to request documents from DDC.

This document contains information affecting the national defense of the United States within the meaning of the Espionage Laws (Title 18, U.S.C., sections 793 and 794). Transmission or revelation in any manner to an unauthorized person is prohibited by law.

When US Government drawings, specifications, or other data are used for any purpose other than a definitely related government procurement operation, the government thereby incurs no responsibility nor any obligation whatsoever; and the fact that the government may have formulated, furnished, or in any way supplied the said drawings, specifications, or other data is not to be regarded by implication or otherwise, as in any manner licensing the holder or any other person or corporation, or conveying any rights or permission to manufacture, use, or sell any patented invention that may in any way be related thereto.

Do not return this copy. When not needed, destroy in accordance with pertinent security regulations.

KEYWORD LIST

Listed below are keywords which serve as an index to the contents of this report (AFR 80-29).

Fragmentation
Warheads
Expansion - radial

[redacted]

## FOREWORD

This report is a summary of investigations completed during the period from 16 November 1962 through 15 December 1963, under Contract AF 08(635)-3269. Further experimentation and analysis is in progress and is scheduled for completion in mid-April 1964. The contract is administered by the Weapons Division, Research and Technology Branch (ATWR), Detachment 4, RTD, Eglin Air Force Base, Florida. Project engineer for Detachment 4 is Mr. Edward C. Poston, Jr.

This research program is being accomplished by the Martin Company, Orlando Division, Orlando, Florida. Martin Company task leader for the overall effort is Mr. W. R. Porter. Other contributing Martin personnel include Mr. B. W. Gore, Jr., Mr. R. R. Boyce, Mr. D. R. Bragg, Mr. J. M. Allred, and Mr. T. D. Kitchin. This document was prepared by Mr. W. R. Porter under the direction of Mr. E. R. Caponi, Chief, Armament Sciences Laboratory, and Mr. C. A. Borcher, Manager, Structures and Mechanics Research Laboratories.

Acknowledgment is made to Mr. D. J. Dunn, Jr., and Mr. C. Graberick, Ballistic Research Laboratories, Aberdeen Proving Ground, Maryland, for review of design concepts and helpful suggestions. Detachment 4, RTD personnel Messrs. D. M. Davis, W. Dittrich, and E. C. Poston, Jr., have also contributed valuable design concepts and technical assistance.

[redacted]

[redacted]

## ABSTRACT

This report summarizes experimental and analytical accomplishments toward the objective of explosively projecting multilayers of preformed fragments into uniform radial disc patterns and at controlled velocities. The radial velocity of each fragment is to be proportional to its distance from the longitudinal axis of the warhead, and a predictable expansion pattern is to be between 500 feet per second and 2000 feet per second on the diameter.

The program approach emphasizes experimental investigations of various warhead design concepts that could possibly result in radial pattern distributions with controlled fragment velocities. Data are presented on four basic designs and variations thereof, which have been experimentally evaluated through warhead arena testing. Of the designs tested, an explosive layered concept provides the most promise for achieving program objectives. This design is comprised of a cylindrical package of alternating layers of preformed fragments and sheet explosive in either involute wrapping or concentric ring configurations.

Feasibility of the explosive layered concept is demonstrated with four-, six-, and eight-layered model test results. On the eight-layered design, fragment distributions over a 35-degree beam spray are uniform; and velocities of individual fragments range from less than 100 feet per second in the innermost layer to 2300 feet per second in the outermost layer. By varying the thickness of the explosive between fragment layers or the number of fragment layers between explosive layers, velocity gradients can be reduced or increased proportionately. An additional advantage to the explosive layered concept is that the above performance was achieved with a charge-to-metal ratio of only 0.082, excluding end-plate weight. With the energy coupling efficiencies achieved in this design, 1/4-inch diameter steel fragments, weighing 1 gram each, were dispensed in a controlled pattern for a total weight of approximately 35 pounds, including explosive, fragments, inert filler, and end plates.

The analytical portion of this study is oriented toward determining means of describing the physical behavior of multilayer fragments when subjected to an explosion in a radial direction. Classical hydrodynamic and spring mass theories are examined and found inadequate. A semi-empirical approach utilizing equations of the form $V = A \left(\frac{C}{M}\right)^b$ and experimental data are developed. Appropriate constants for both the spiral and

concentric ring configurations are derived, and detailed instructions for computing the $\frac{C}{M}$ values are given. It is shown that this approach provides a valid mathematical basis for predicting design parameters and for estimating fragment velocities.

Work items currently in progress include further experimentation toward devising practical means of initiating thin-gage sheet explosive and the development of minimum weight techniques for controlling beam spray angles. Current data indicate that thin-gaged sheet explosive can be initiated by a line wave generator and that hyperboloid models are feasible approaches to beam spray control.

Other topics presented in this document include discussions of test model fabrication techniques, test arrangements and instrumentation, data reduction procedures, and appendices of detailed design and test data.

**PUBLICATION REVIEW**

**This technical documentary report has been reviewed and is approved.**

Nicholas H. Cox, Col USAF
FOR BEN F. HARDAWAY
Colonel, USAF
Chief, Weapons Division

## LIST OF ILLUSTRATIONS

LIST OF TABLES

## SECTION 1 - INTRODUCTION

Preliminary experimentation and analysis of multilayer radial fragment projectors was initiated for the Air Force in November 1962 and supplemented for more detailed investigations in March 1963. Contract completion is scheduled for mid-April 1964. However, because of promising state-of-the-art advancements resulting from the current effort, this Summary Report is being published.

The objective of this program, as established by Reference 1, is to examine means of explosively projecting multilayers of fragments in a predictable uniform radial pattern, in such a way that the radial velocity of each fragment is proportional to its distance from the longitudinal axis of the pattern. Figure 1 illustrates the way in which such a warhead concept might be employed in a hypothetical space intercept situation.

Specific technical requirements of this program are:

1 By experimentation, devise and evaluate techniques or methods of explosively projecting multilayers of fragments in a radially expanding pattern.

2 Attempt to devise means of controlling radial velocity of each fragment so as to obtain a predictable uniform growth pattern between 500 feet per second and 2,000 feet per second on the diameter. The ratio of total fragment mass to explosive mass shall be the maximum commensurate with these growth rates.

3 Attempt to describe analytically the physical behavior of multilayer fragments when subjected to an explosive acceleration in a radial direction.

4 From conclusions drawn during this program make recommendations as to the need for future studies.

This report summarizes achievements in both the experimental and analytical phases of this program; describes detailed items such as experimental arrangements, fabrication techniques, and methods of reducing and presenting data; and gives complete data on the various design concepts tested for explosively projecting multilayers of fragments in a radially expanding pattern.

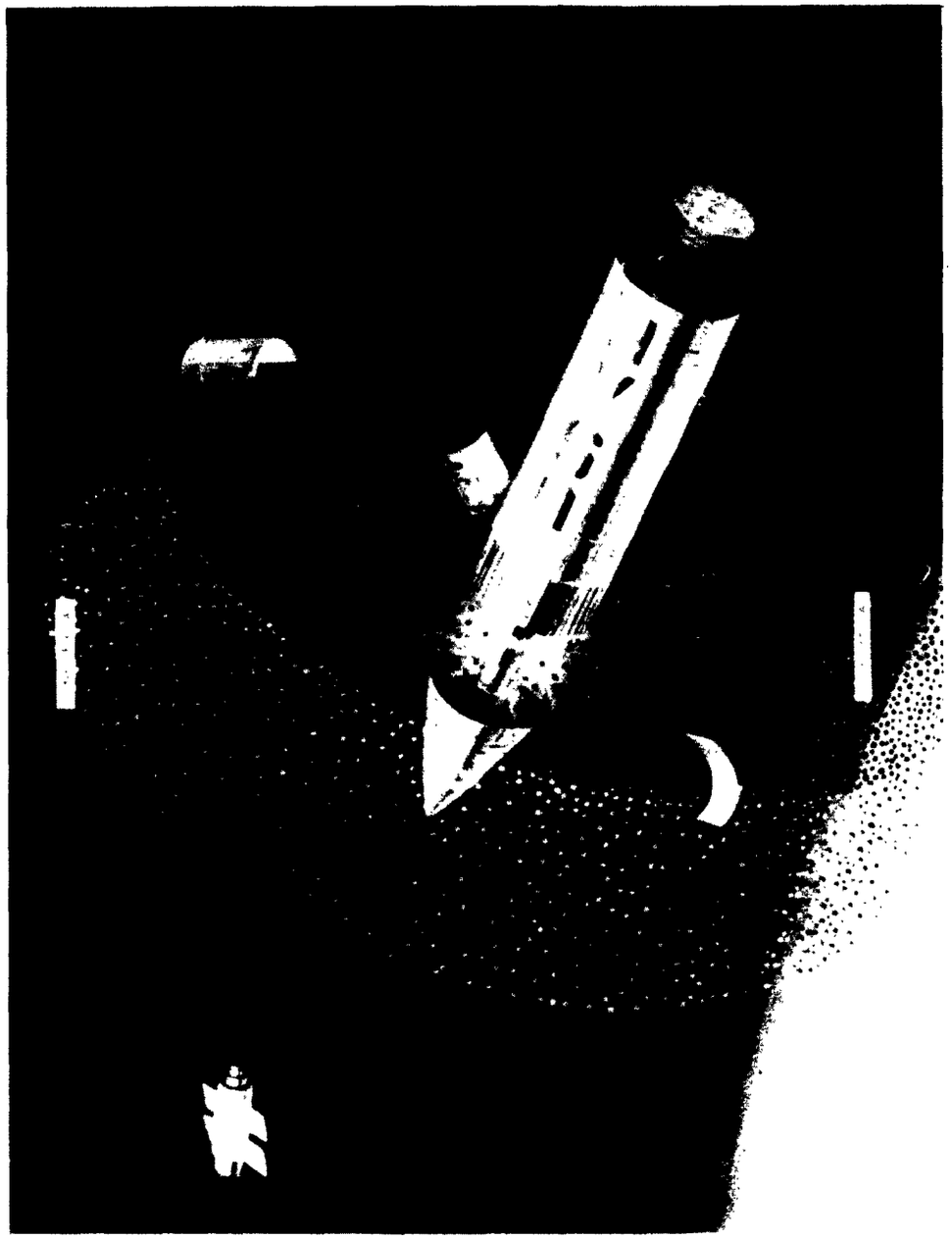

Figure 1. Artist's Concept of Hypotehtical Space Intercept

## SECTION 2 - EXPERIMENTAL PROGRAM

This section summarizes the experimental portion of the fragmentation warhead study. It discusses the approach followed, sets forth significant accomplishments, and describes techniques employed in the collection, reduction, and interpretation of experimental data. Detailed data pertinent to each test are included in the appendices of this report.

### A. APPROACH

The experimental approach consisted of testing four basic design concepts of explosive radial fragment projectors and variations thereof (Figure 2). The prime objective was to define those concepts that offered the most potential for achieving program requirements. After establishing this goal, more extensive testing of each model was conducted to determine more thoroughly the performance characteristics and effects of parameter variations.

The warhead models were tested in an arena, using an 8-foot by 8-foot by 12-inch celotex target to collect a 32-degree sector of the fragments. The fragments in this sector were marked so that their velocity and trajectory could be correlated with their location in the warhead. Initially, the beam spray was controlled by a massive fixture (Figure 3) so that parameters affecting velocity gradients could be isolated and controlled. When velocity gradients were successfully controlled, techniques for controlling beam spray were investigated.

### B. SIGNIFICANT RESULTS

Of the various design concepts initially investigated, experimental data show that the explosive-layered concept in either a spiral or concentric ring configuration (Figure 4) offers the most potential for achieving program objectives. Figure 5, a summary plot of fragment velocity gradients versus fragment row locations within the individual test models, illustrates this potential. In this presentation the various models tested are grouped under the headings of their basic design concept. The curves shown are fitted through the mean of each velocity interval determined for the fragments in that particular row location. The vertical extent of the heavy line on each fragment row indicates minimum and maximum velocities. Ideally, a straight-line slope with overlapping velocity intervals quite similar to those obtained for Round Nos. 30, 38, and 43 is sought.

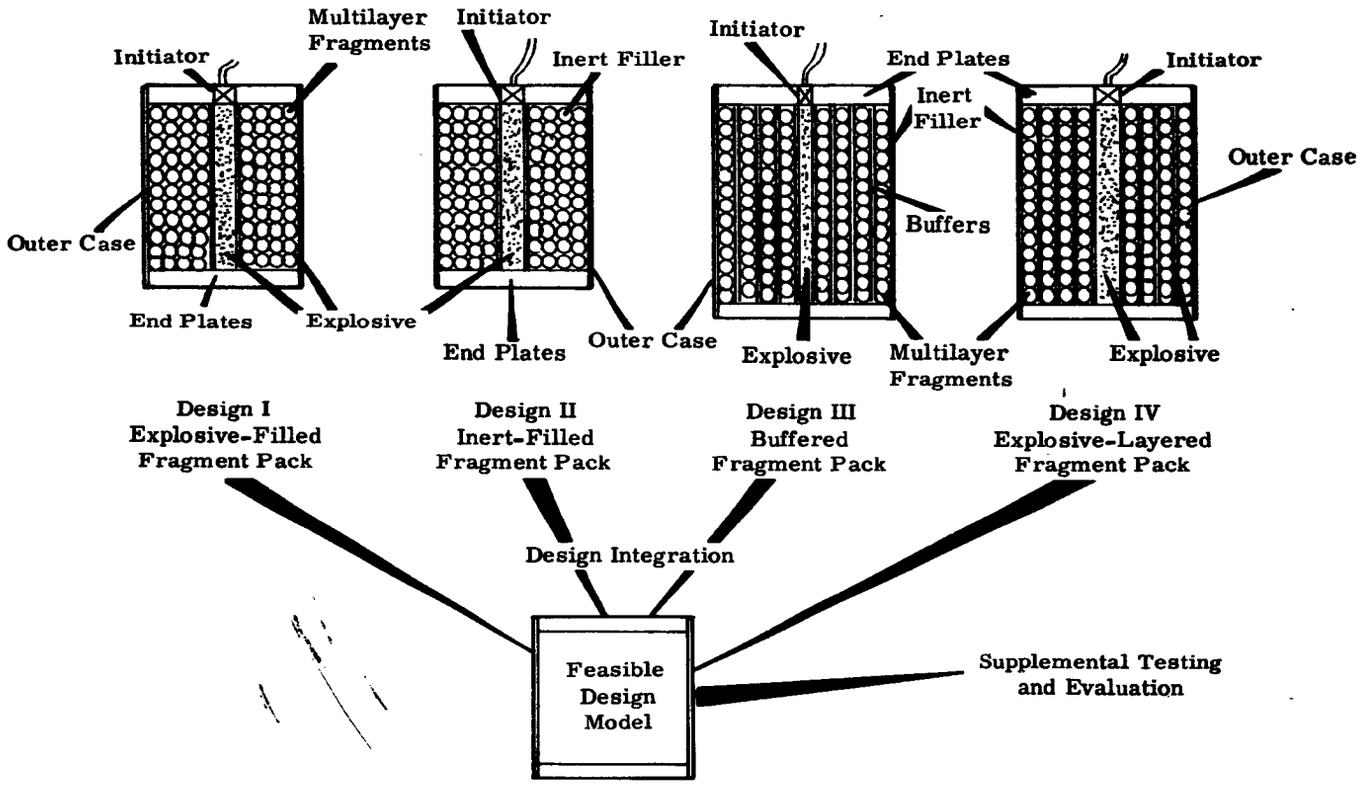


Figure 2. Basic Projector Designs

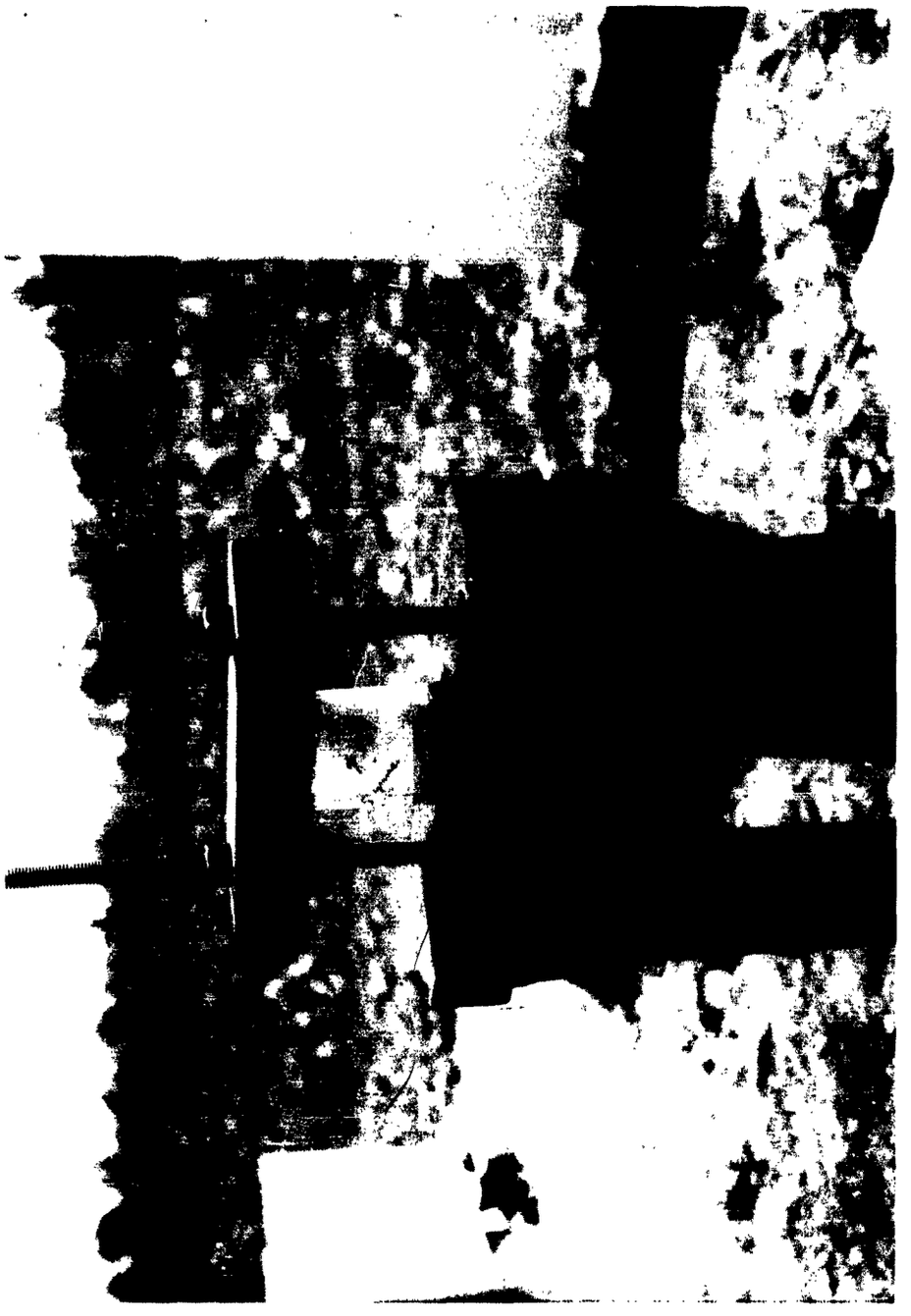

Figure 3. Firing Fixture

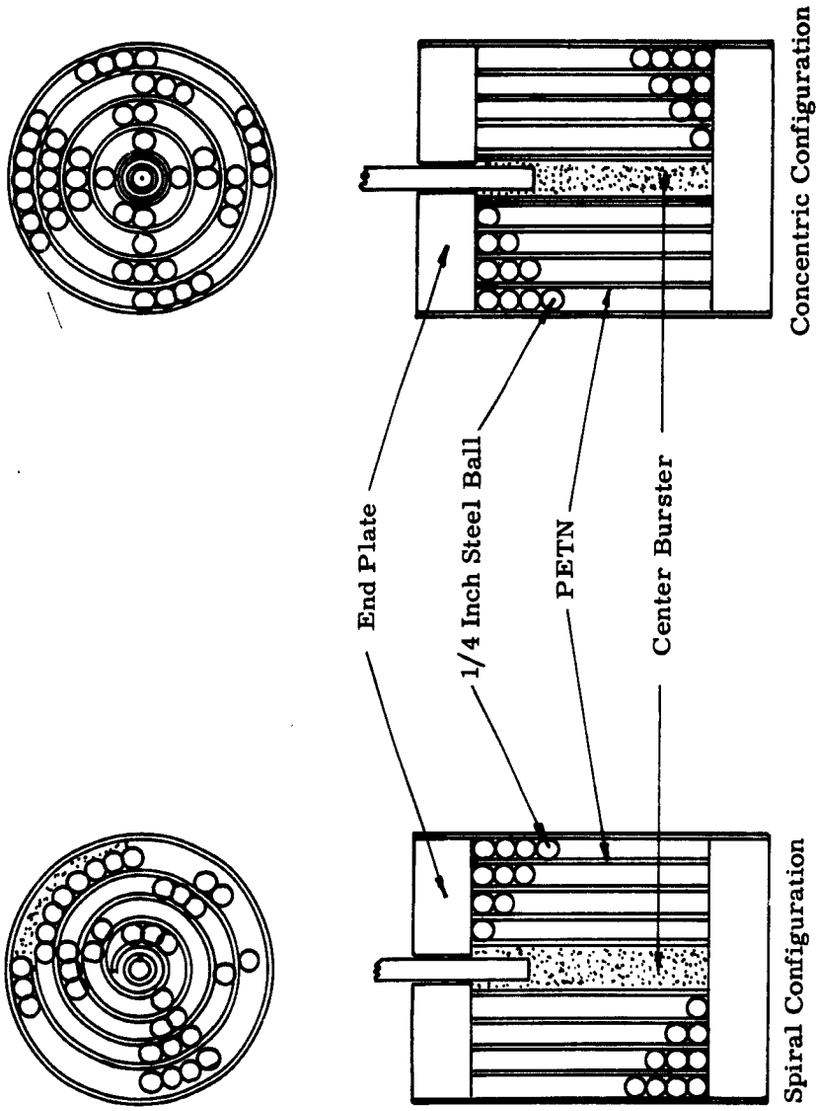


Figure 4. Explosive-Layered Design Models

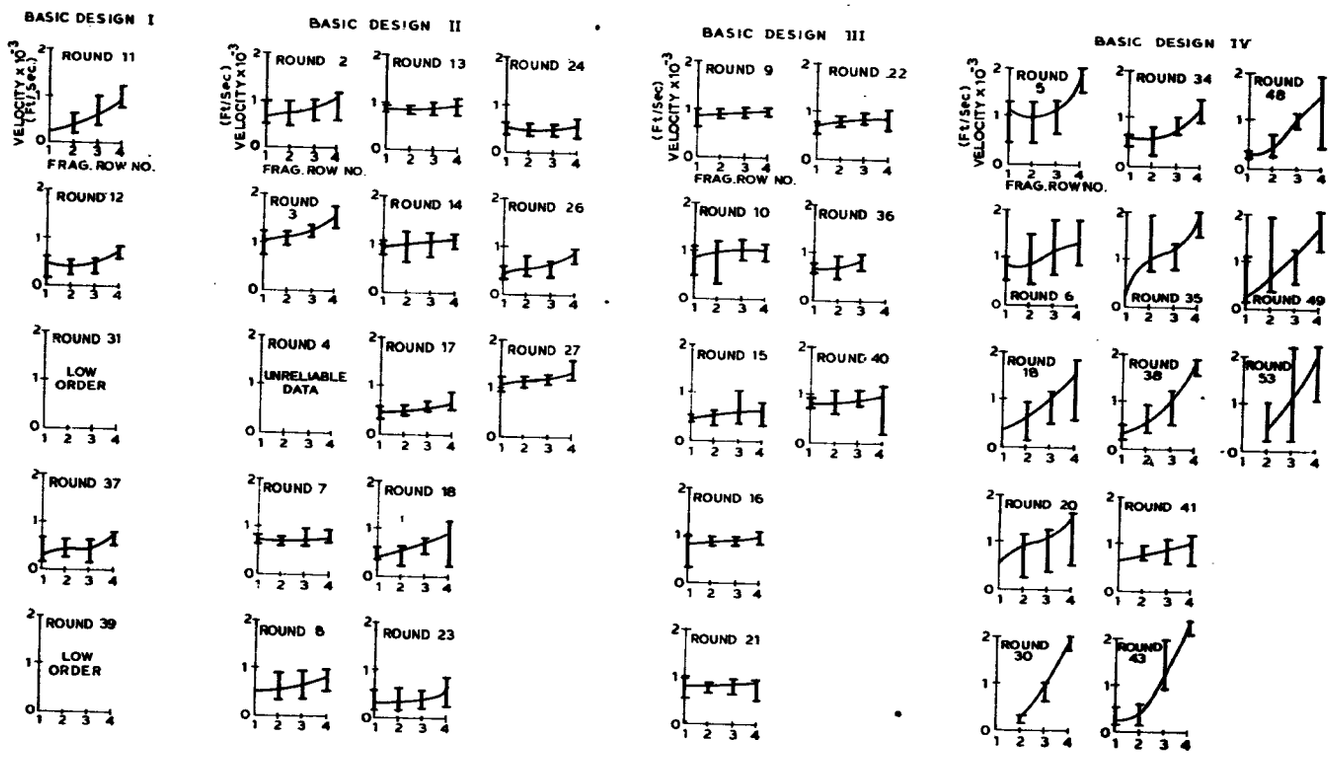


Figure 5. Preliminary Velocity Gradient Summary



CONFIDENTIAL

Further experimental evidence of the performance potential of the explosive-layered concept (Basic Design IV) is illustrated by the data presented in Figure 6. These are polar sectional plots* typical of the results obtained for each basic design. These presentations show how the fragments' velocity/space distributions would appear to an observer viewing the fragment pattern formation, at a given instant in time, down the warhaed model's longitudinal axis. By comparing these plots it is obvious that fragments from Basic Designs I, II, and III are projected as a solid group while those of Basic Design IV have the potential of moving in a graduated manner from some minimum velocity to a higher outer velocity. The angular banding or grouping effect evidenced on the Basic Design IV plot results from a fabrication characteristic that has subsequently been corrected.

The feasibility of the explosive-layered design concept to project multilayers of fragments radially into uniformly distributed patterns and at controlled velocity gradients has been confirmed through supplemental experimentation. Both six- and eight-layered models have been successfully tested without fragment break-up. Figure 7 is a polar sectional plot of average fragment velocity versus space distribution for an eight-layered test model, and Figure 8 is a similar presentation for a six-layered model.

The eight-layered test model contained 8000 fragments at a total weight of 19.4 pounds and only 2 pounds of explosive. The conventional charge-to-mass ratio is 0.082, exclusive of the weight for two half-inch-thick steel end plates. The six-layered model contained 4600 fragments for a total weight of 10.6 pounds and only 1 pound of explosive. The charge-to-metal ratio is 0.080, exclusive of two half-inch-thick steel end plates. In addition, results from several tests utilizing cubic and hexagonal shaped fragments instead of spherical fragments promise even further improvements in pattern distributions and average velocities as evidenced by deeper penetrations in the recovery target.

In the velocity distributions discussed above, the overall average fragment velocities are higher than believed necessary. The feasibility of reducing the average velocity for each layer by using thinner-gaged explosive between fragment layers has been demonstrated in subsequent experiments (Figure 9).

The results described were obtained in experiments wherein the warhead models were fired in a massive test fixture, thereby confining the ends of the model to retain the fragment-beam spray angle to the order of 35 de-

---

*For detailed explanations of these data presentations and the techniques employed in obtaining them, refer to paragraphs E and F of this chapter.

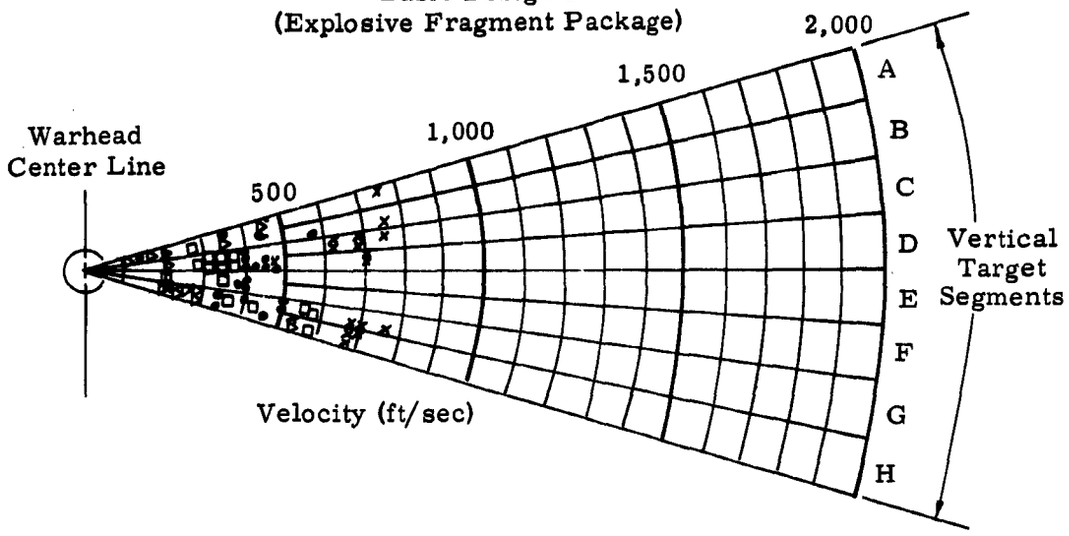
Basic Design I
(Explosive Fragment Package)
2,000
1,500
1,000
500
Warhead
Center Line
A
B
C
D
E
F
G
H
Vertical
Target
Segments
Velocity (ft/sec)

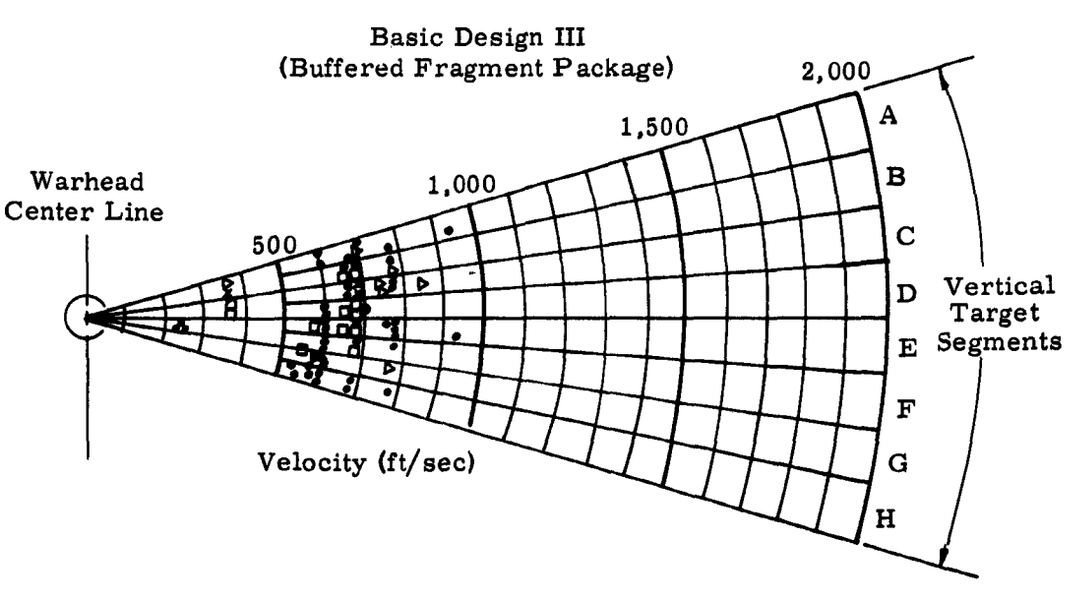
Basic Design III
(Buffered Fragment Package)
2,000
1,500
1,000
500
Warhead
Center Line
A
B
C
D
E
F
G
H
Vertical
Target
Segments
Velocity (ft/sec)

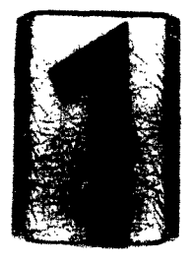

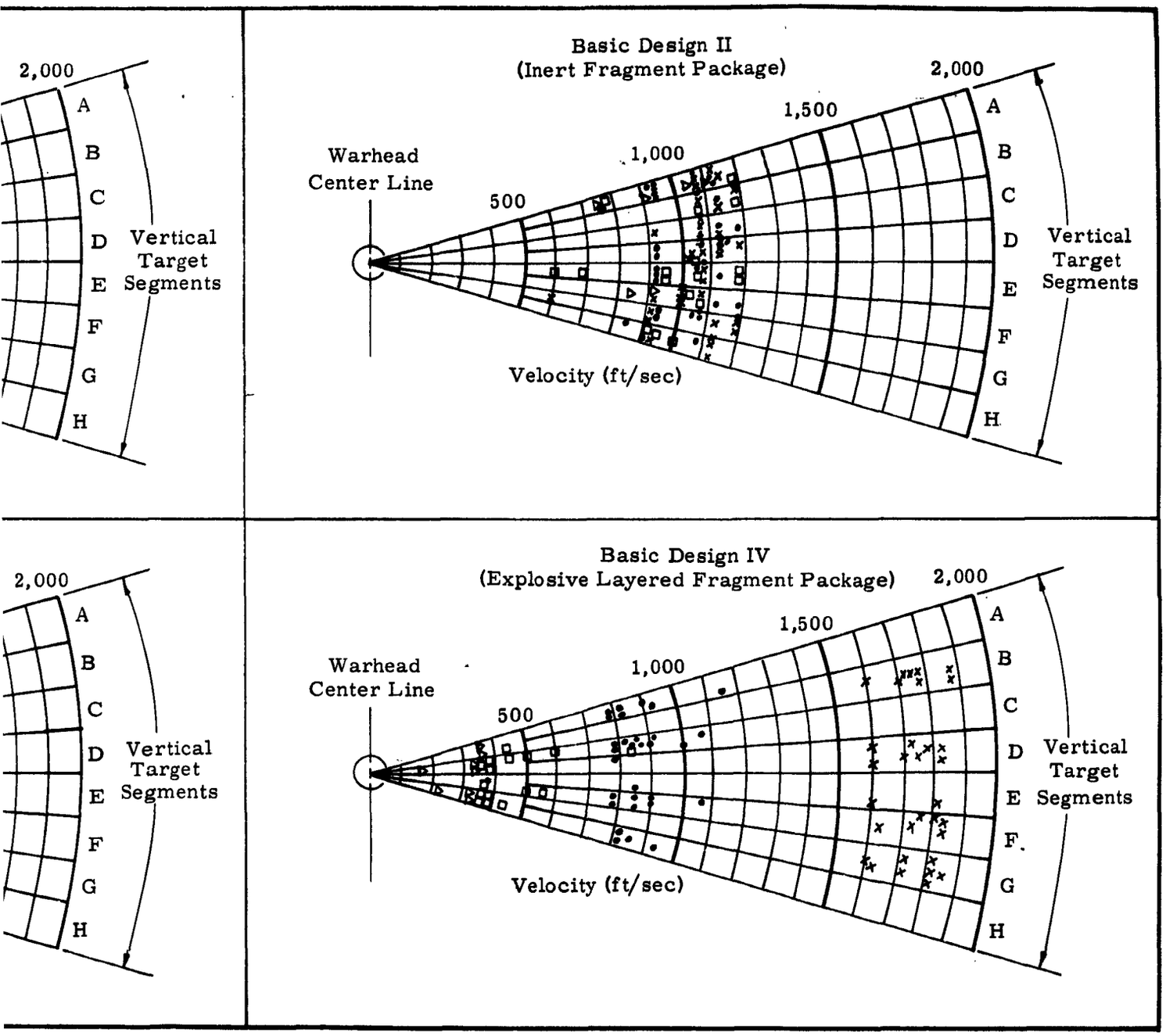


Figure 6. Basic Design Velocity-Space Distribution Comparison

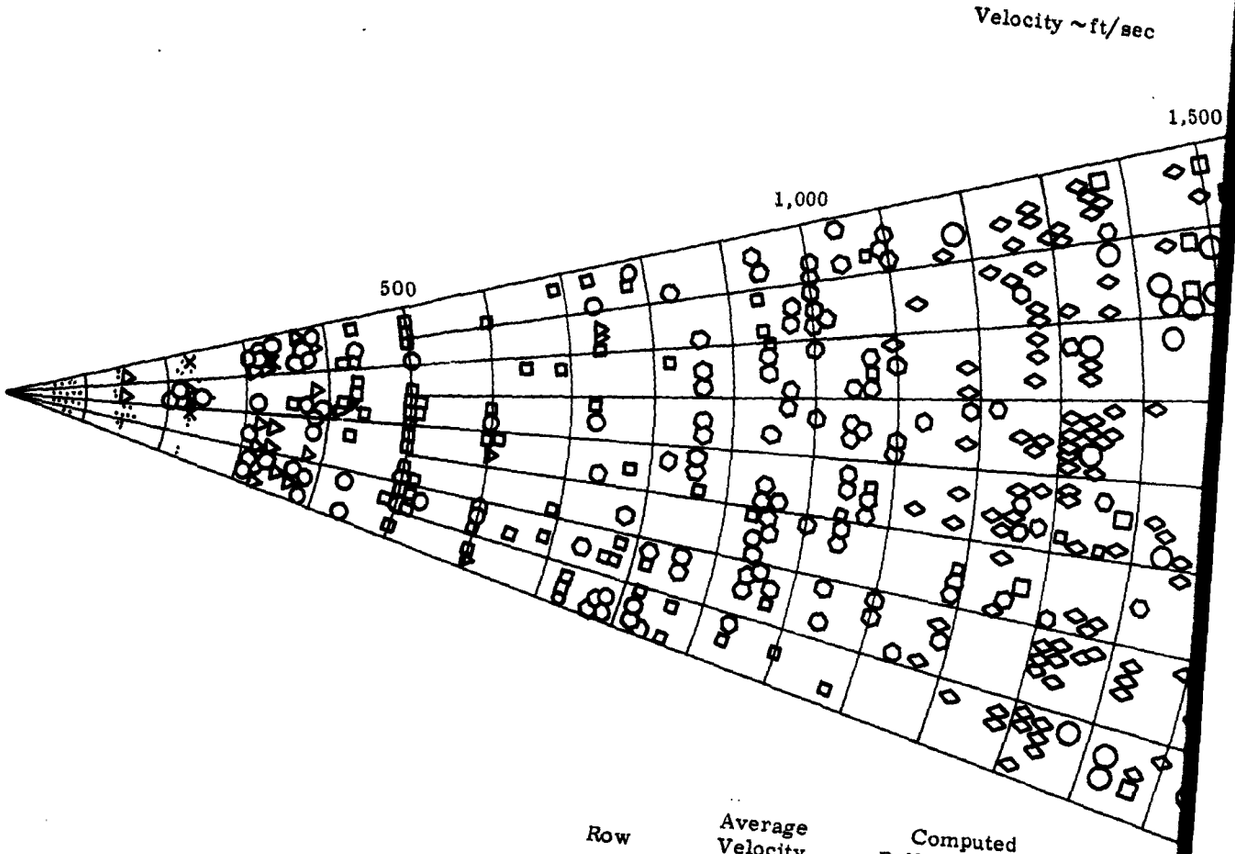


| | Row | Average Velocity | Computed Balls Available |
|---|---|---|---|
| × | 1 | | |
| △ | 2 | 318 | 25 |
| ○ | 3 | 380 | 44 |
| □ | 4 | 454 | 63 |
| ◇ | 5 | 689 | 81 |
| ○ | 6 | 1,018 | 100 |
| □ | 7 | 1,330 | 119 |
| · | 8 | 1,708 | 138 |
| | | 1,937 | 151 |

Low velocity hits not identifiable

No. H
2
4
6
9
10
13
17
4

Figure 7. Typical Eight-Layered Distribution Pattern

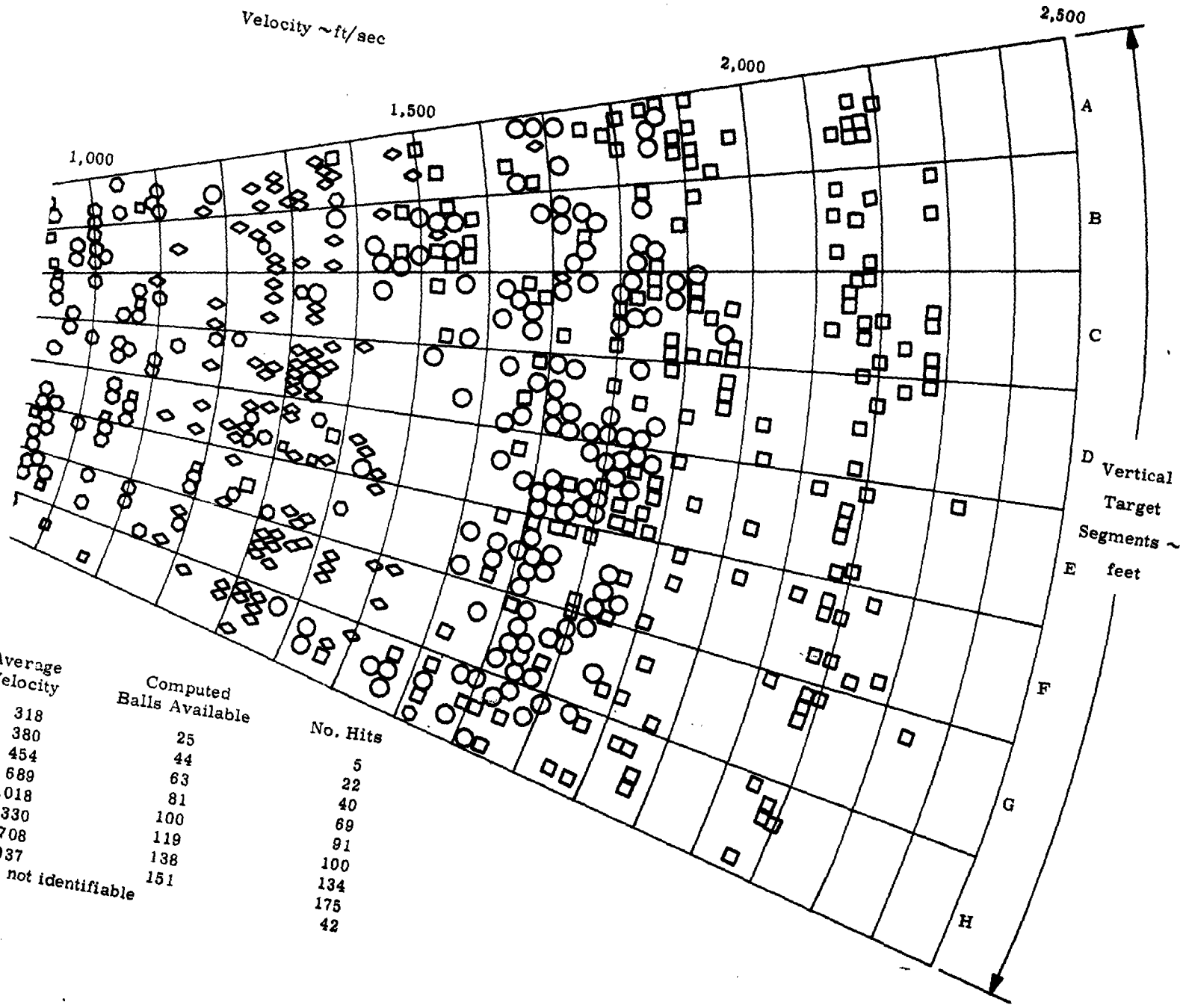


| Average Velocity | Computed Balls Available | No. Hits |
|---|---|---|
| 318 | 25 | 5 |
| 380 | 44 | 22 |
| 454 | 63 | 40 |
| 689 | 81 | 69 |
| 1,018 | 100 | 91 |
| 1,330 | 119 | 100 |
| 1,708 | 138 | 134 |
| 1,937 | 151 | 175 |
| hits not identifiable | | 42 |

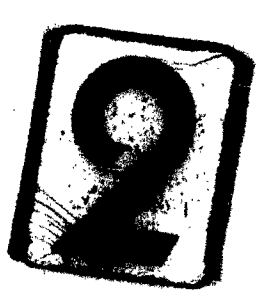

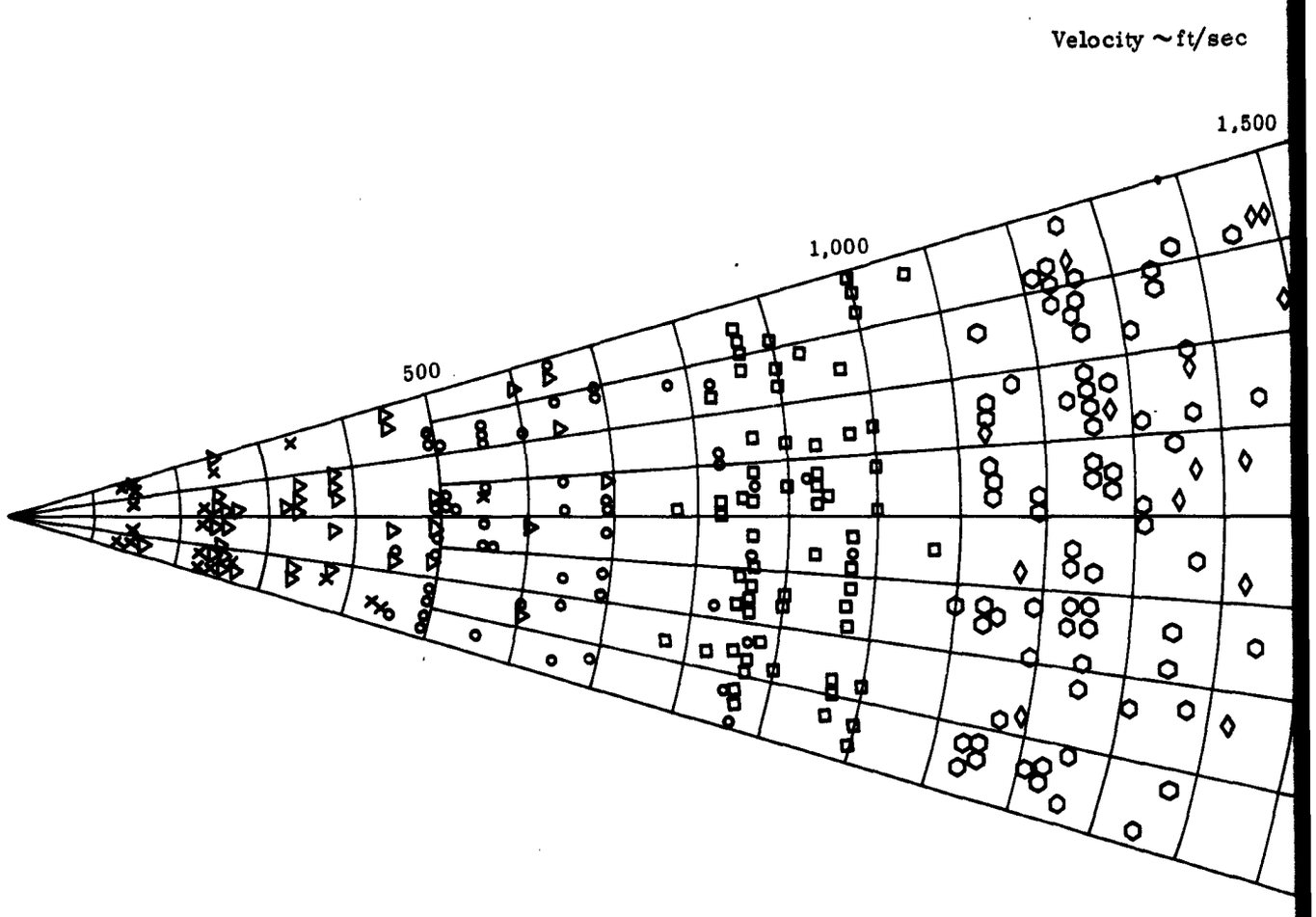


| Row | Average Velocity | Computed Balls Availa |
|---|---|---|
| × 1 | 255 | 27 |
| △ 2 | 374 | 44 |
| ○ 3 | 562 | 60 |
| □ 4 | 911 | 76 |
| ⬡ 5 | 1,265 | 92 |
| ◇ 6 | 1,648 | 108 |

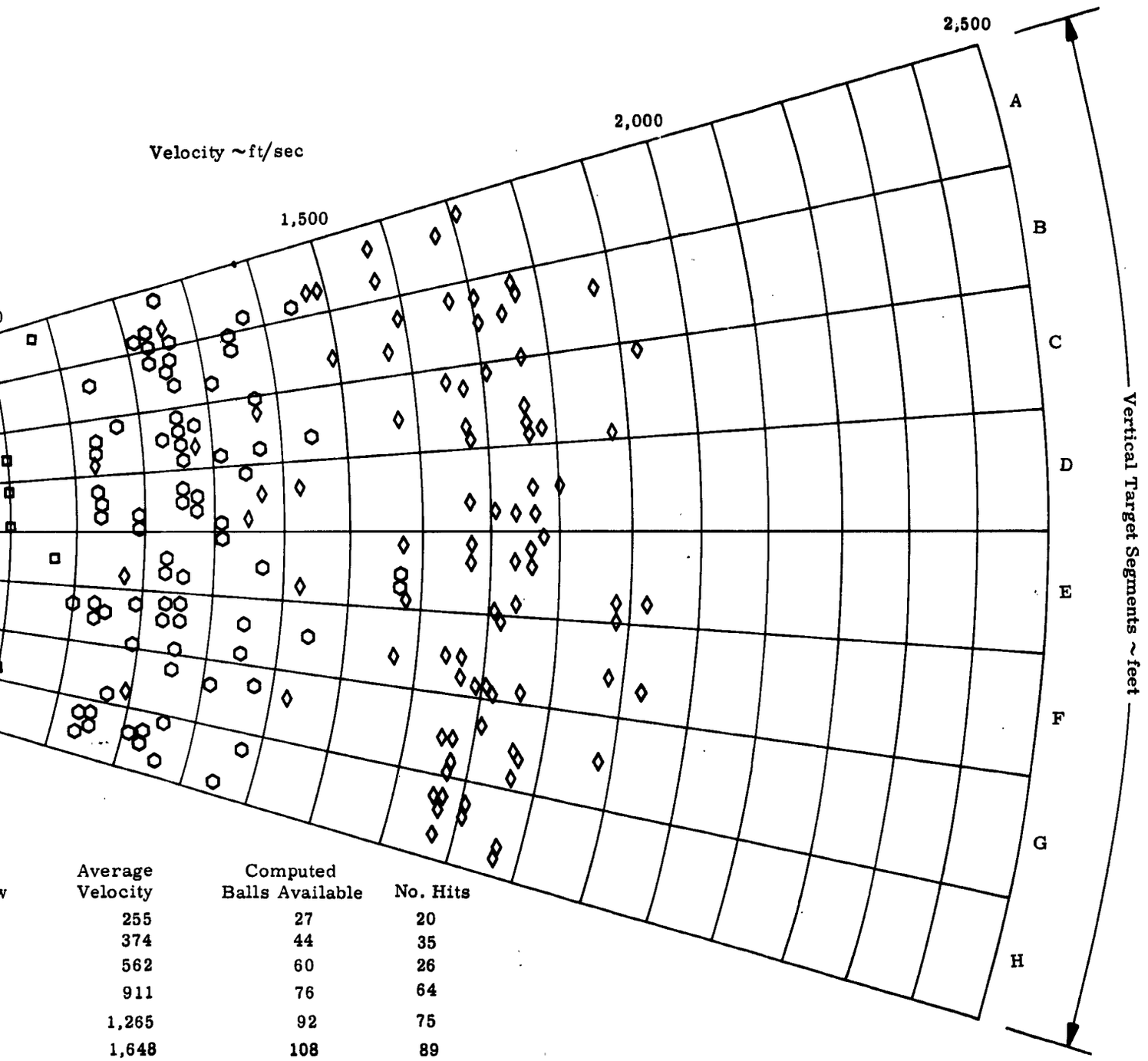


| Average Velocity | Computed Balls Available | No. Hits |
|---|---|---|
| 255 | 27 | 20 |
| 374 | 44 | 35 |
| 562 | 60 | 26 |
| 911 | 76 | 64 |
| 1,265 | 92 | 75 |
| 1,648 | 108 | 89 |

Figure 8. Typical Six-Layered Distribution Pattern

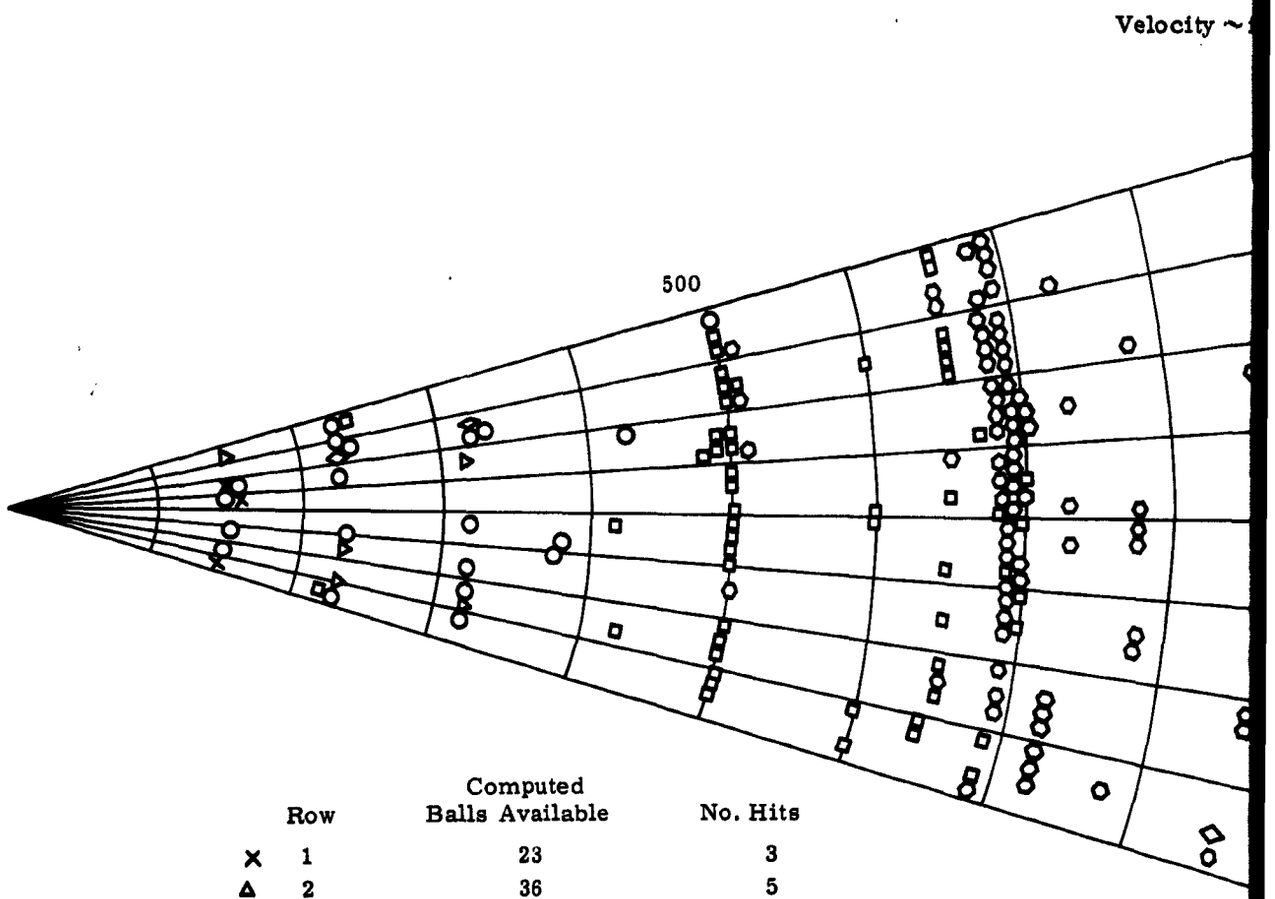


| | Row | Computed Balls Available | No. Hits |
|---|---|---|---|
| × | 1 | 23 | 3 |
| △ | 2 | 36 | 5 |
| ○ | 3 | 49 | 20 |
| □ | 4 | 63 | 54 |
| ⬡ | 5 | 76 | 79 |
| ◇ | 6 | 89 | 90 |

Figure 9. Six-Layered Distribution Pattern – Reduced Explosive Gage, Reduced Average Velocities

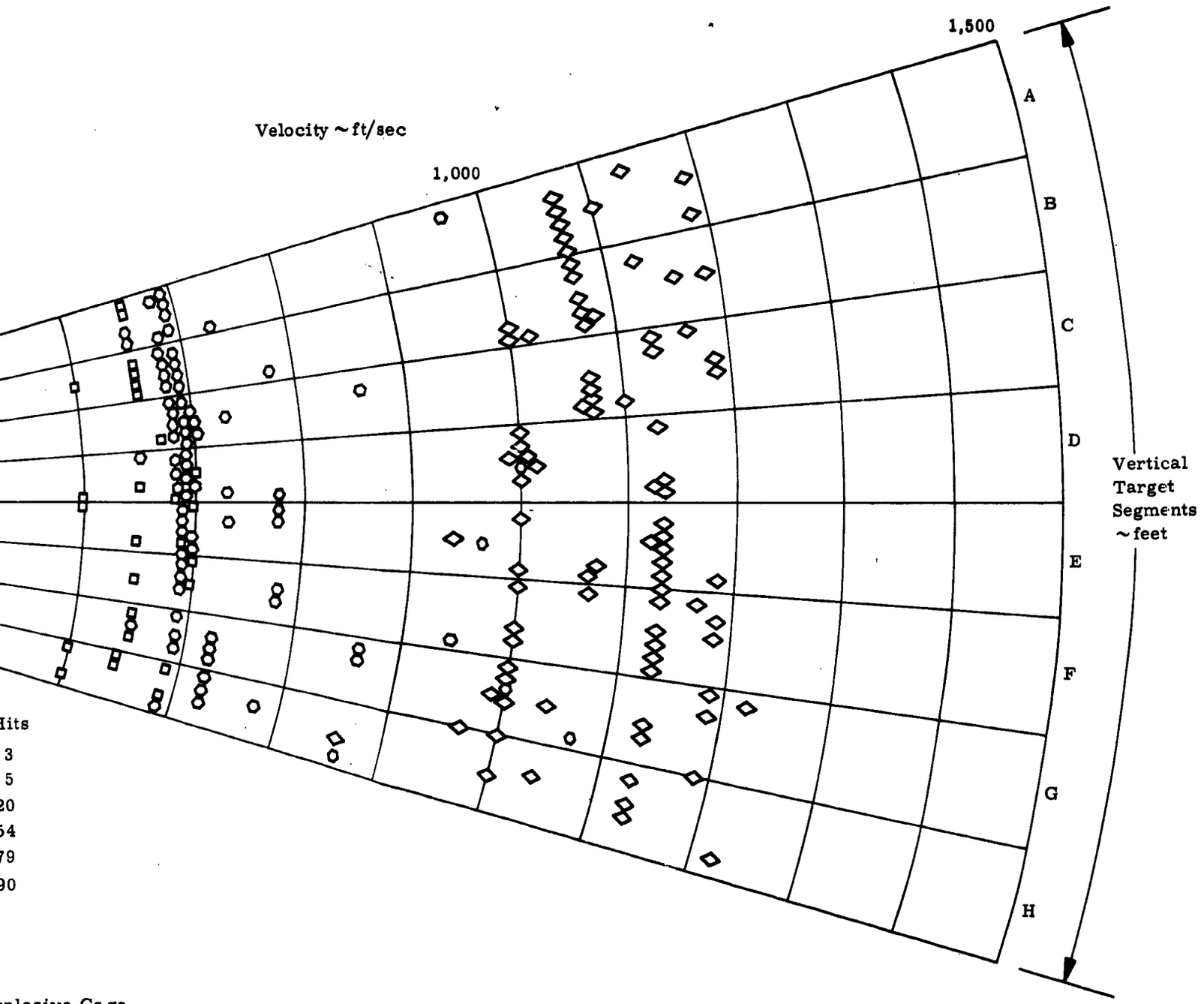


Hits
3
5
20
54
79
90

xplosive Gage,

grees or less. Subsequent experimental data utilizing explosive end confinement and hyperboloid center bursters show promise of achieving a narrow-beam spray angle without massive end confinement. Further experimentation to confirm these data is now in progress.

Further detailed discussion of results recorded during the experimental portion of this program as applicable to each basic design group is presented in paragraph G, following discussions of other items pertinent to the understanding of the overall program.

## C. BASIC WARHEAD MODEL DESIGNS

The basic model designs tested during this program are illustrated in Figure 2 and described in section A; they are further described below.

### 1. BASIC DESIGN I

This design is basic in that it comprises an intermixing of explosive and spherical fragments about a center explosive burster (Figure 10). The thin walls of the center burster tube are perforated to permit intimate contact of explosive within the burster tube with that in the interstices of the fragment package. Single-point end initiation with a Hercules J-2 blasting cap special (electric) is employed on all models of this design. Liquid explosive, nitromethane with a special activator, rather than a cast or pressed explosive, is used on all models of this design concept to minimize the potential hazard of inadvertent initiation from the numerous places where point contact could occur. Basic Design I is referred to as an explosive-filled fragment package.

### 2. BASIC DESIGN II

This design consists of an intermixing of inert filler, Laminac 4116, and spherical fragments surrounding a center explosive burster (Figure 11). Single-point end initiation is employed. The inert filler bonds individual fragments into a composite package, increases confinement, and assists in preventing fragment breakup at the time of warhead detonation (Reference 2). Basic Design II is referred to as an inert-filled fragment package.

### 3. BASIC DESIGN III

This design is a buildup of alternate layers of spherical fragments and inert buffer materials (Figure 12). Explosive projection is by an explosive-filled central burster tube initiated by a single detonator at one end. In concept, varying thicknesses of buffering materials are expected to absorb varying amounts of energy between fragment layers and produce the desired velocity gradients. The design is referred to as a buffered fragment pack.

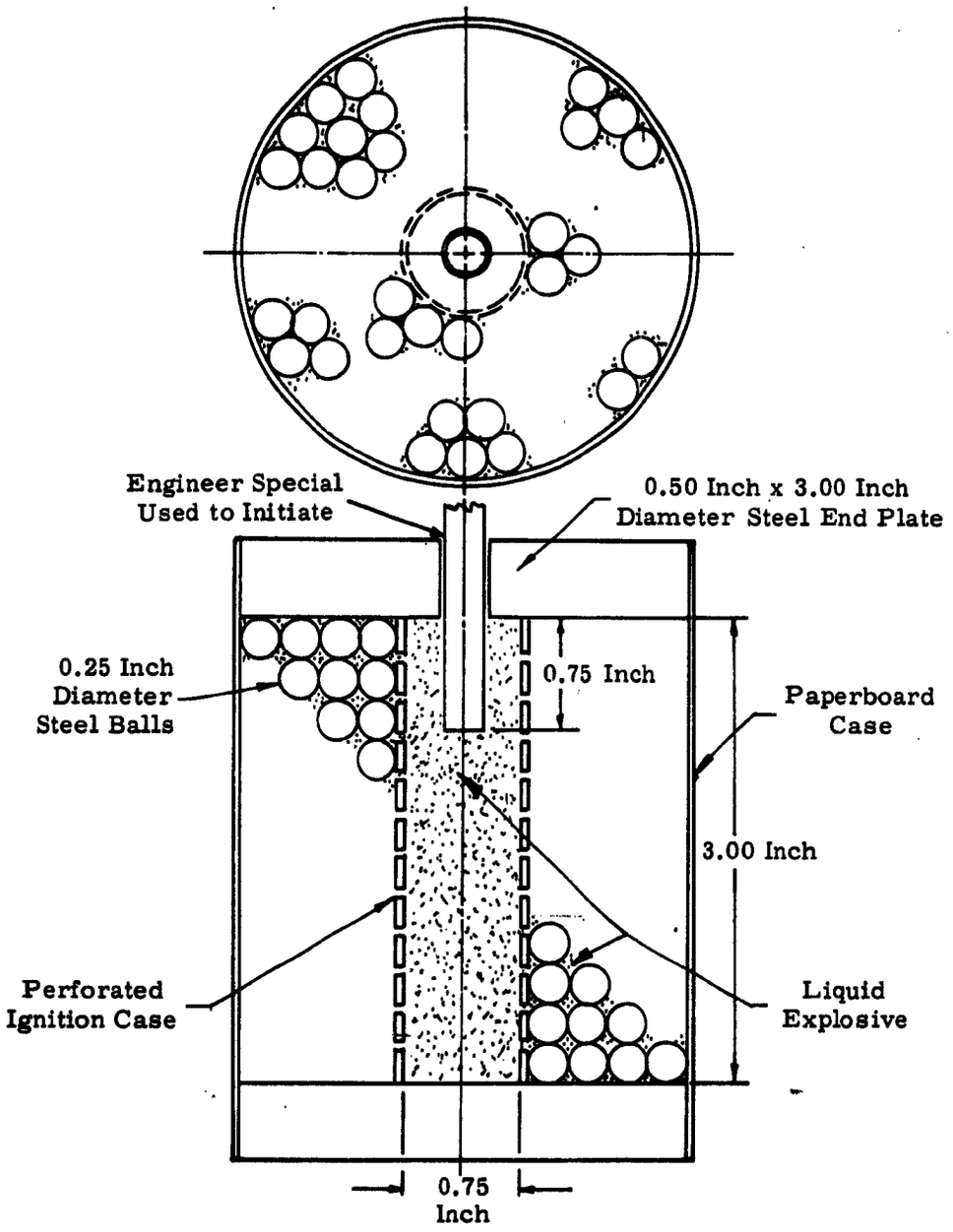


Figure 10. Basic Design I Details

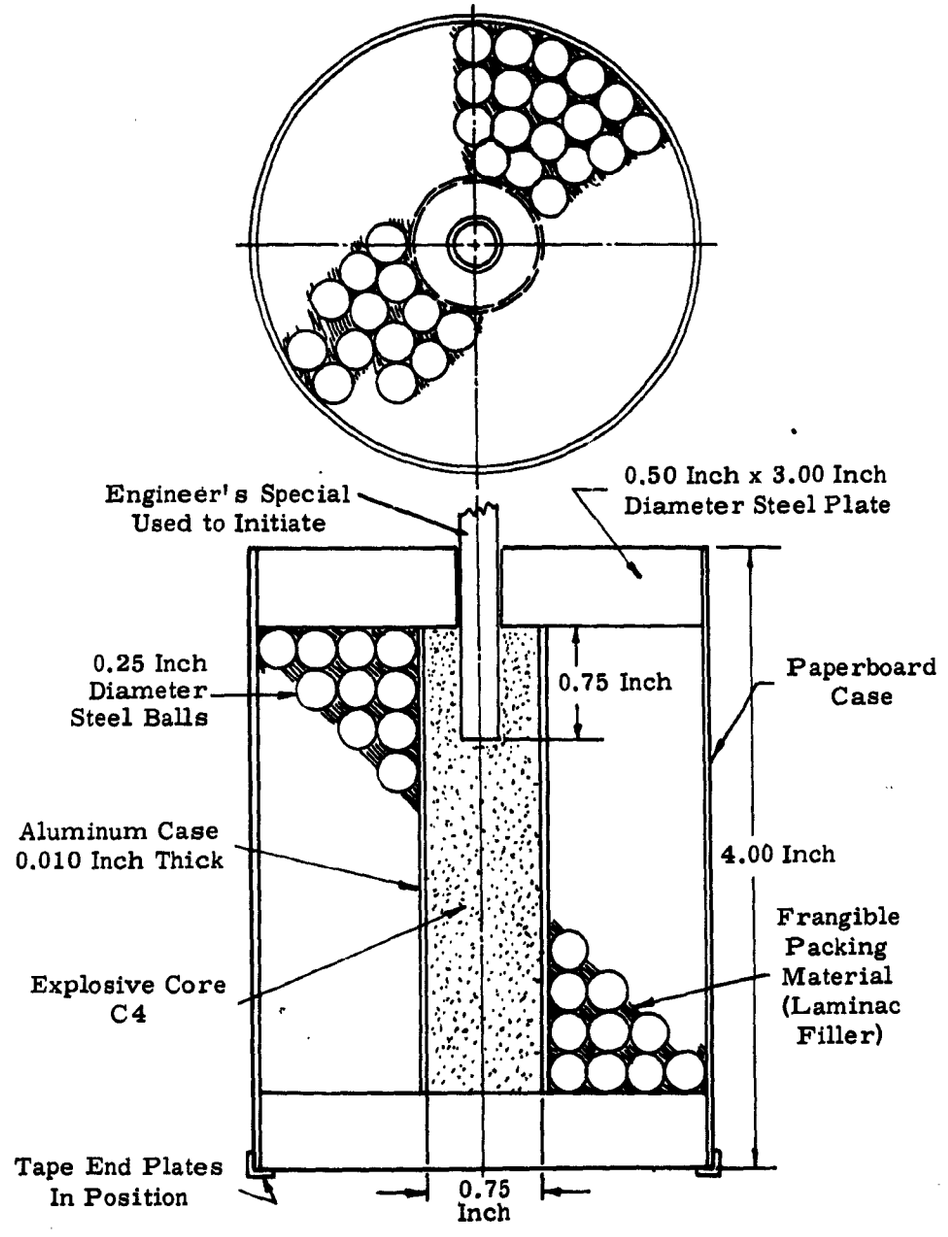


Figure 11. Basic Design II Details

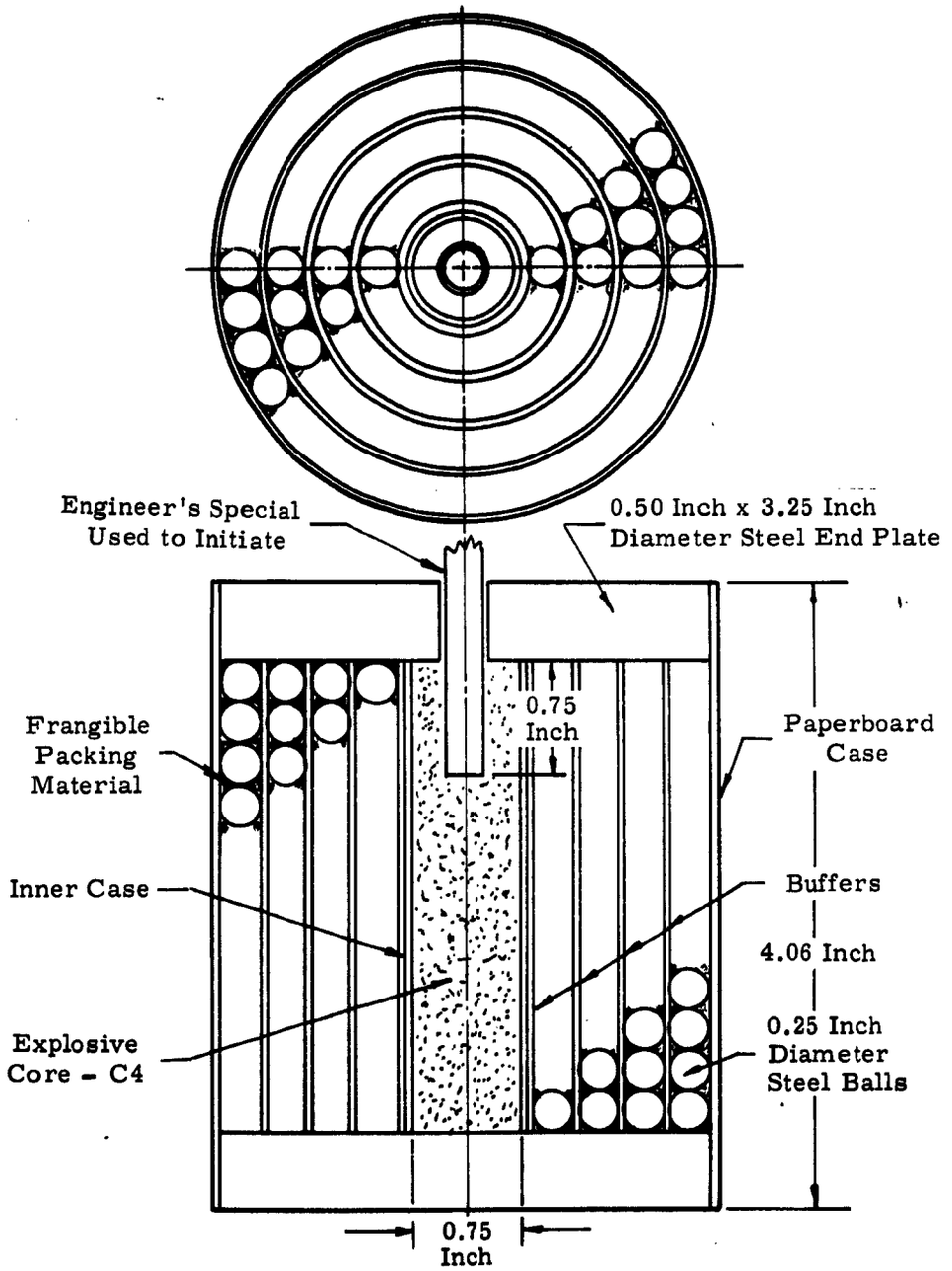


Figure 12. Basic Design III Details

4. BASIC DESIGN IV

This design is quite similar to Basic Design III except that sheet PETN explosive is used in place of buffering materials. In this concept, the velocity gradient is to be achieved by introducing energy between the various fragment layers. Single point initiation of a central explosive burster is employed. Detonations have been successfully achieved on a number of variations wherein a line wave generator is affixed to the outermost explosive layer of a spiral winding of explosive and fragments (Figure 13). This design concept is referred to as the explosive-layered fragment pack.

5. DESIGN VARIATIONS

A number of design variations on each basic concept are possible. The more significant variations that have been investigated experimentally in this program are summarized in Table 1. These variations were selected for testing parameter extremes and not for design optimization.

6. OTHER CONCEPTS

Other design concepts that have been subjected to limited testing include inert fragment packages with tapered center bursters and inert fragment packages with explosive in the end plates only, initiated at both ends simultaneously (Figure 14). In concept, the tapered burster designs are expected to project fragments in a dish type of pattern; whereas the explosive end plate design is expected to produce a sharp compressive impulse on the fragment package and result in a random distribution of low velocity fragments.

D. MODEL FABRICATION TECHNIQUES

Design drawings and descriptions of the various types of warhead models fabricated for this program are given in the appendices. Because of the wide number of variables investigated, each test model is hand made. Discussion of the more salient features pertinent to the fabrication of these devices follows.

1. FRAGMENTS

The type of fragment employed in this program includes quarter-inch diameter steel spheres (SKF 36-300, Grade 200, Polished) and quarter-inch steel (SAE-1015) cubes. Spheres are used in the major portion of the test models because of economics and ready availability. To prevent fragment breakup at the time of detonation, the spherical fragments are heat treated to a hardness of Rockwell B-85.

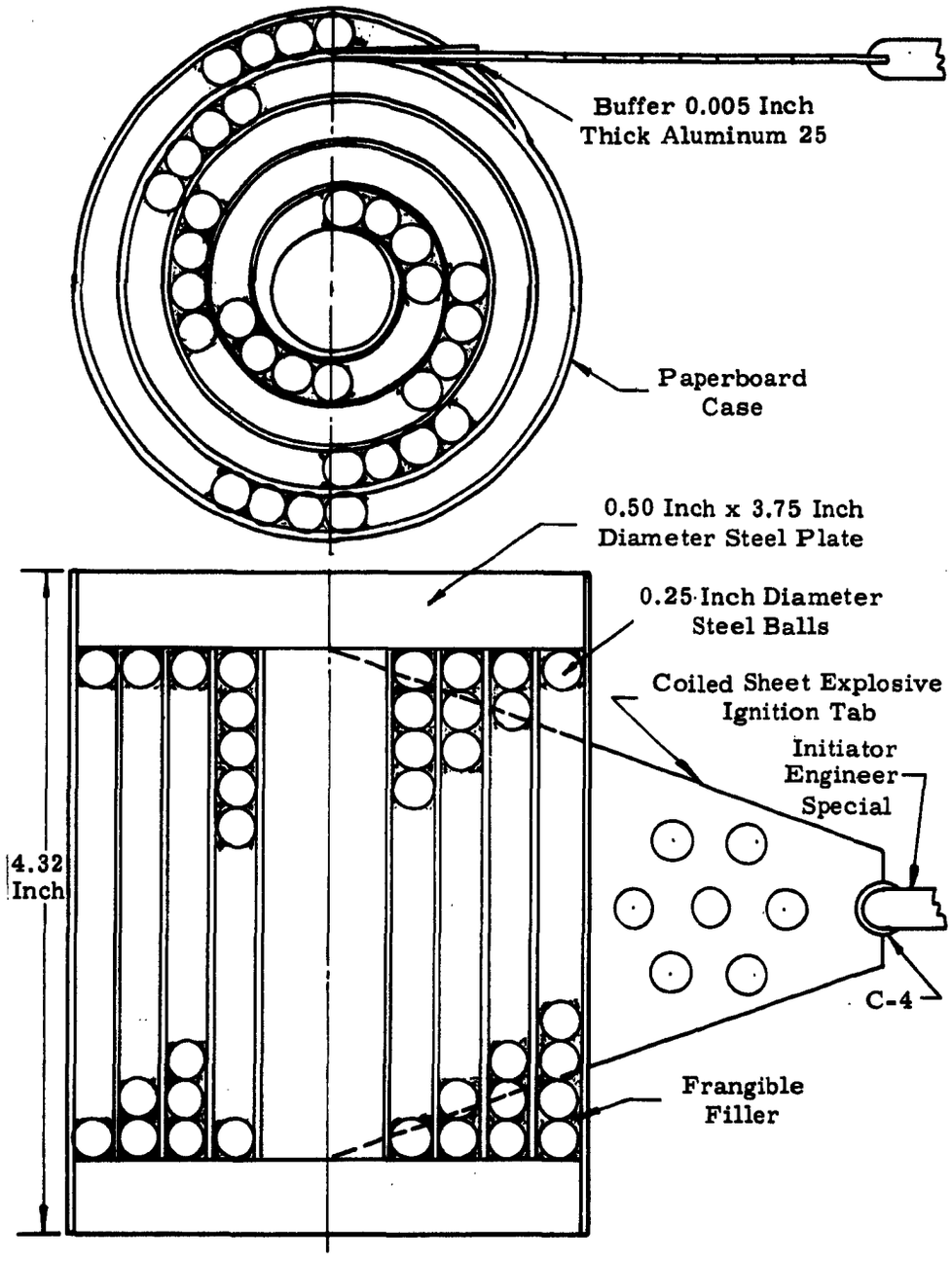


Figure 13. Basic Design IV Details

TABLE 1

Possible Projector Design Variations

| DESIGN I | DESIGN II | DESIGN III | DESIGN IV |
|---|---|---|---|
| Variation A<br>Center explosive core and explosive in interstices | Variation A<br>Buffer material between explosive and fragments | Variation A<br>Variable buffer thickness – progressive thick to thin | Variation A<br>Spiral configuration |
| Variation B<br>No center explosive burster | Variation B<br>Shaped explosive-fragment interface | Variation B<br>Variable buffer thickness – progressive thin to thick | Variation B<br>Concentric ring configuration |
| | Variation C<br>Shaped explosive-fragment interface with buffer | | Variation C<br>Varied explosive thickness, thickest outside |
| | | | Variation D<br>Reverse thickness on above |
| | | | Variation E<br>Combine inert buffer and explosive layer |

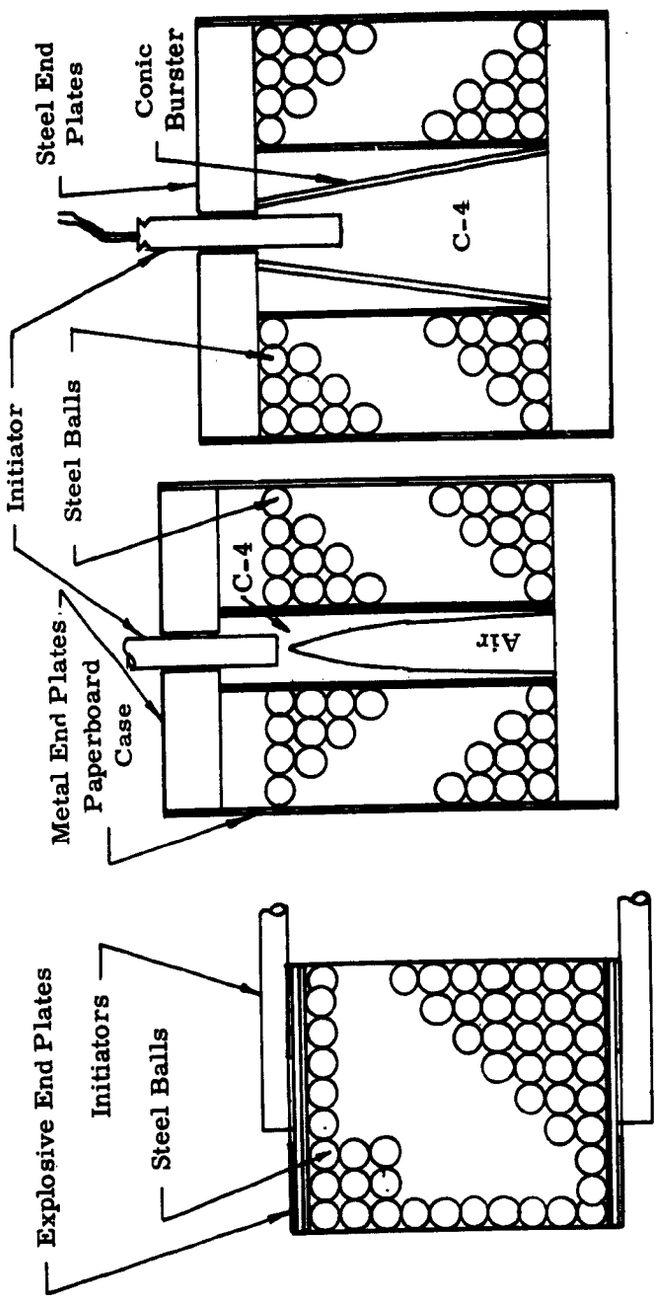


Figure 14. Additional Design Concepts

Identification marking of fragments is accomplished with a simple tooling fixture that permits a number of fragments to be marked simultaneously. Marked fragments are used only in that sector of the model where recovery is to be accomplished. Other identification processes attempted, but which proved unsatisfactory, were painting, metallic coatings, and coating with epoxy dyes where the heat of detonation and/or friction of impact obscured or removed the identifying colors.

## 2. FRAGMENT PACKAGING

The most expeditious packaging technique employed in the current program involves the use of cylindrical rods to shape the overall test model and configuration (Figures 15 and 16). As the rods are removed, fragments are fed through an assembly fixture into the voids. This process is repeated until the test model is fully packaged with fragments (Figure 17).

Another technique uses individual fragments packed in paper tubes, which are hand placed about the burster tube sequentially until the test model is complete (Figure 18). Unfortunately, experimental data indicated that the paper tubes had a slight but identifiable and reproducible effect upon fragment distribution. Figure 19 illustrates the fragment package.

For designs requiring higher-density packaging, small quantities of fragments are placed into the space between the center burster tube and outer warhead case which have been previously assembled to one end plate. This unit, in turn, is placed on a shake table and fragments added until the package is filled (Figure 20).

An alternate technique (Figure 21) is gluing fragments to paperboard wafers which, in turn, are stacked about the center burster tube.

For solid packages of cubic and hexagonal fragments, simple hand placement of individual fragments is used (Figure 22).

Figure 15. Configuration Shaping, Spiral Explosive Layering, Cubical Fragment Preparation

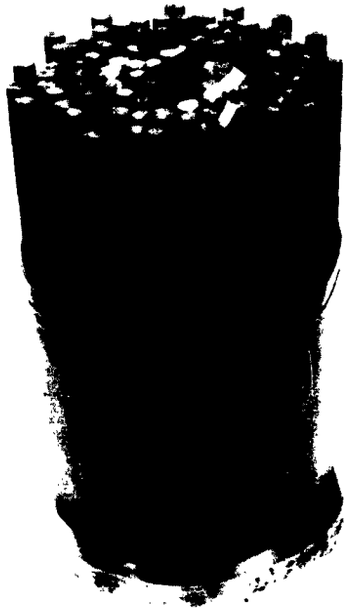

Figure 16. Configuration Shaping, Concentric Ring Explosive Layering, Spherical Fragment Preparation

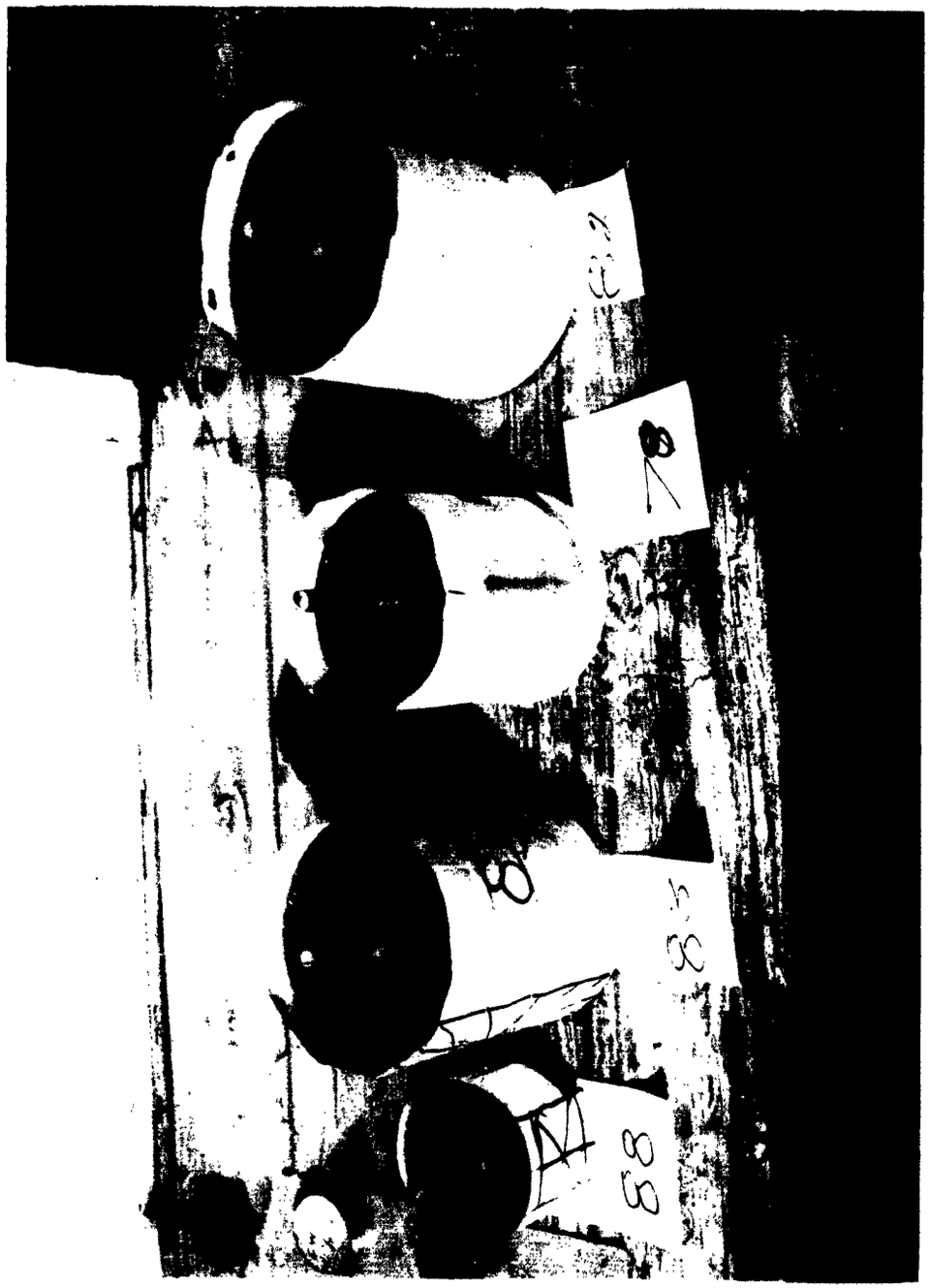

Figure 17. Typical Explosive-Layered Test Models

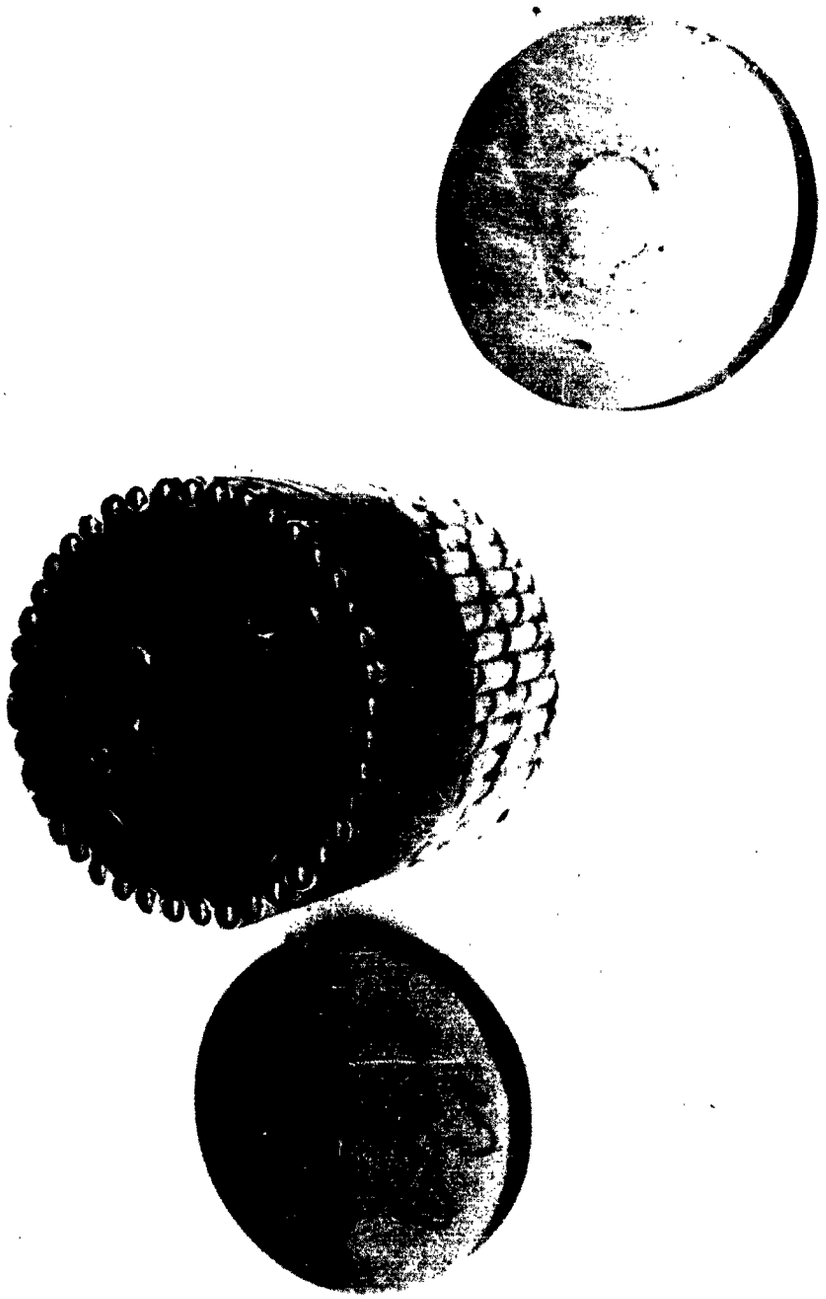

Figure 18. Tubular Fragment Packaging

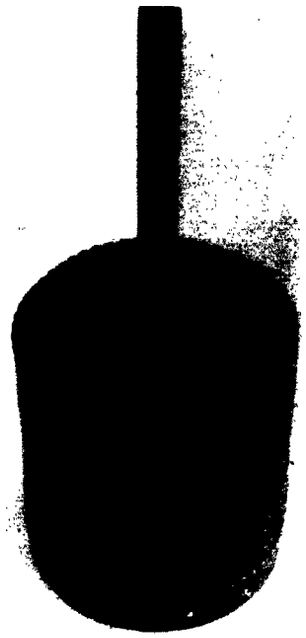

Figure 19. Hand Packaging of Fragments

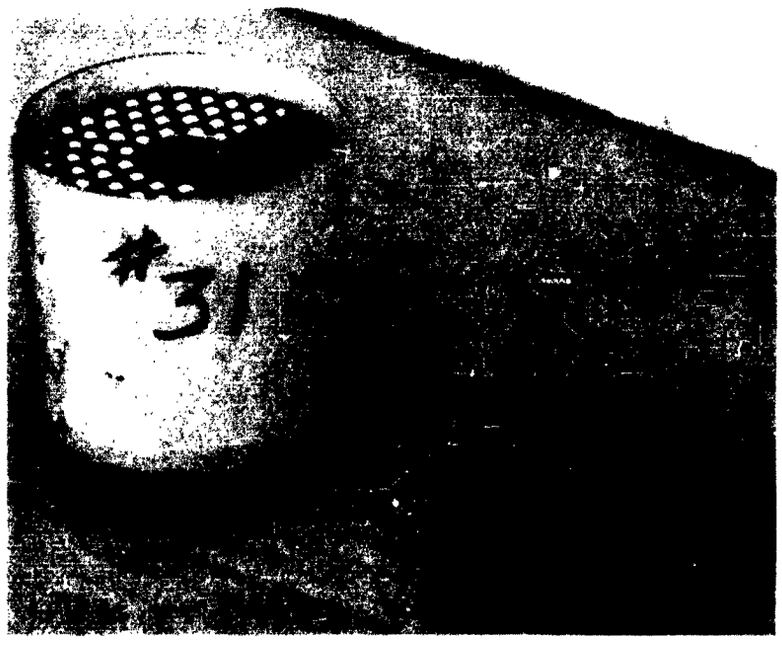


Figure 20. Interstice Fragment Package

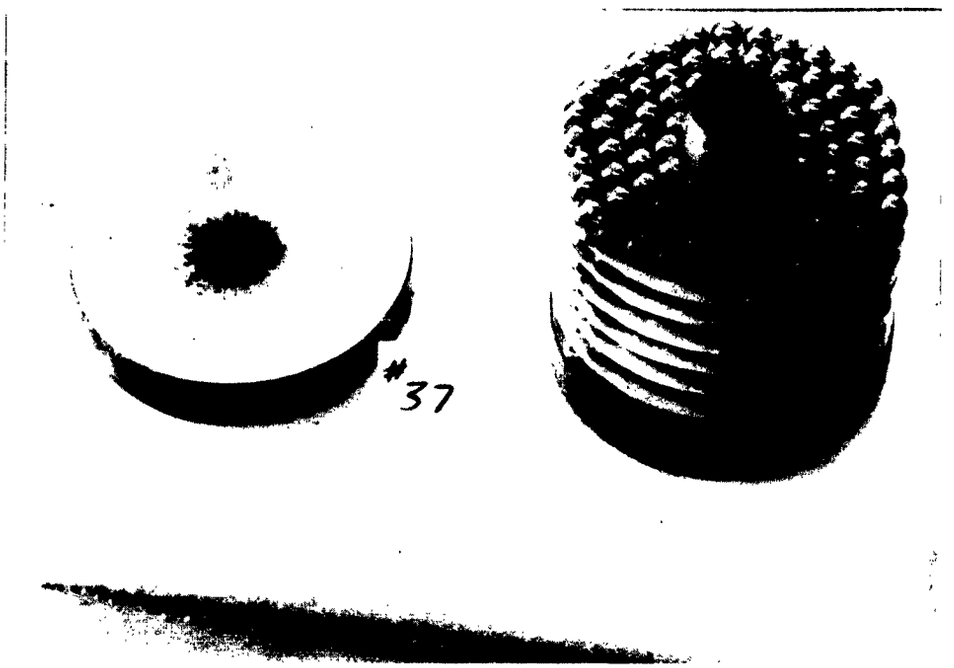


Figure 21. Wafer Packaging

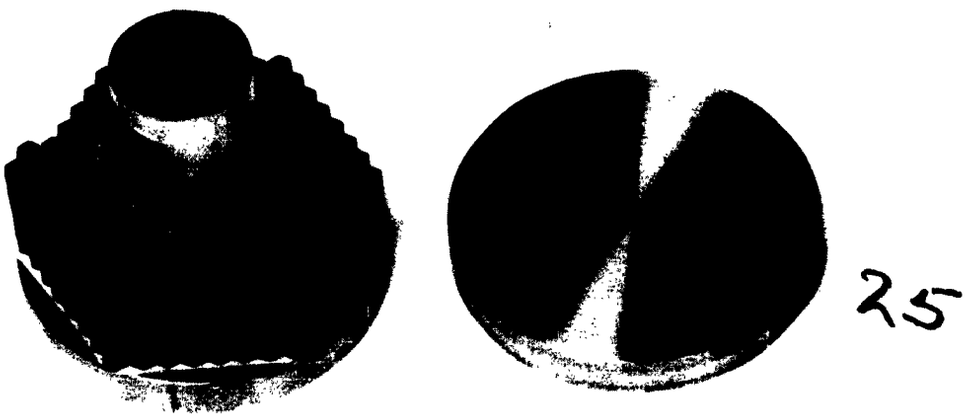


Figure 22. Solid Hexagonal Package

3. INERT FILLER

Upon completion of the fragment packaging by the various techniques previously described, the resulting package is filled with an inert material (Laminac No. 4116 with cobalt metholethelkeytone peroxide accelerator). Aside from securing the fragments firmly in place, it is believed that this filler improves energy coupling to the fragments to prevent fragment fracture.

CAUTION: When an accelerator is mixed with the Laminac resin, heat is generated during the curing process. The explosive used in layered design models is rubberized sheet PETN which decomposes rapidly at 410°F. Based on curing temperature tests, the quantity of actuator used in all Laminac mixtures was restricted to less than 3 ml for each 328 grams of resin to keep the exothermal reaction below 375°F.

4. EXPLOSIVE

Explosives used during this program include Composition C-4, Cyclonite (RDX), liquid nitromethane, and rubberized sheet PETN (DuPont No. EL-506A). Composition C-4 and RDX are used as the explosive load for center bursters in all design models except Basic Design I, which requires the liquid nitromethane. Sheet PETN is used in all explosive layered designs and for explosive end-plate experiments.

Fabrication procedures employed for those designs using sheet PETN involve cutting the explosive to the required size and covering it completely with cloth gun tape. It has been found that this tape prevents melting of the rubberizing material in the PETN during the Laminac curing process. When necessary to increase length of the explosive sheet, edges of separate sheets are feathered and spliced.

## E. TEST ARRANGEMENT AND INSTRUMENTATION

A test arena is employed throughout this program (Figure 23). In this arrangement, celotex recovery targets are used for recording fragment impact patterns and fragment penetration depths for each fragment layer. Average fragment velocities are measured with a high-speed Fastax camera Model WF-4; a Wollensak, one-millisecond, timing light, pulse generator; and an industrial timer "Goose" Model J-515. Camera framing rates vary from 5000 to 8000 frames per second depending upon the velocity anticipated for a specific test. This in turn provides data for calibration of the celotex recovery media in terms of velocity versus depth of penetration. Fragment velocities determined from a penetration calibration curve are relative measures and may differ in some small degree from absolute measurements. However, it is believed that the calibration technique is applicable to the scope of the current program and that use of more precise and expensive techniques is not warranted at this time. Care

Figure 23. Test Arrangement

has been taken to use the same type of celotex (Building Board Finish 20, Federal Specification LLL-1-535) and to pack all targets as nearly alike as possible.

The face of each recovery target is marked with a grid of one-foot squares on the face (Figure 24). Through careful correlation of fragment impact location with depth of penetration, fragment layer markings, and Fastax camera records, both fragment velocities and space distributions are determined. The sampling procedure is restricted to a recovery area of 8 feet square.

On all warhead models employing a single detonator, initiation is accomplished by a 500-volt dc supply. For test models requiring dual detonators, initiation is accomplished by a 9000-volt single-pulse unit to ensure simultaneous detonation. The basic design for this unit was obtained from the Ballistic Research Laboratories, Aberdeen Proving Ground, Maryland (Reference 3).

A diagramatic representation of the test plan followed throughout this program is illustrated by Figure 25.

## F. DATA REDUCTION PROCEDURES

Data resulting from the previously described test arrangement includes:

1 Fastax film records for velocity measurements,

2 Still photographic records of the impact patterns,

3 Fragment recovery records giving fragment layer identification and depth of penetration.

The procedures employed in utilizing these data are discussed below.

### 1. CALIBRATION CURVE

To obtain an approximation of fragment velocity, a calibration curve relating depth of penetration to velocity was prepared. These data were obtained by projecting a number of the Fastax film records (single frame technique) and correlating range data records with a large number of individual penetration versus velocity data points. These data are then plotted and fitted by the least squares technique, assuming the form $y = ax^2 + bx + c$. Figure 26 illustrates the resulting calibration curve. Although the data scatter is broad, it provides a valid basis for statistical analysis and relative fragment velocity determination.

Figure 24. Recovery Target

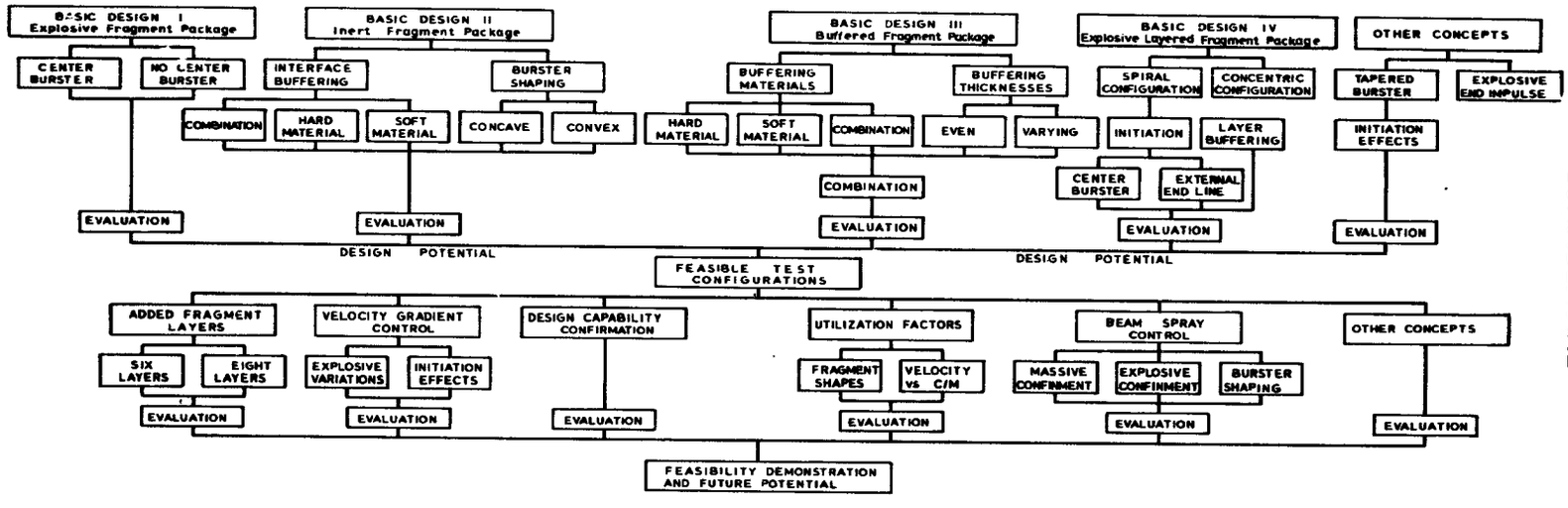


Figure 25. Test Plan Flow Chart

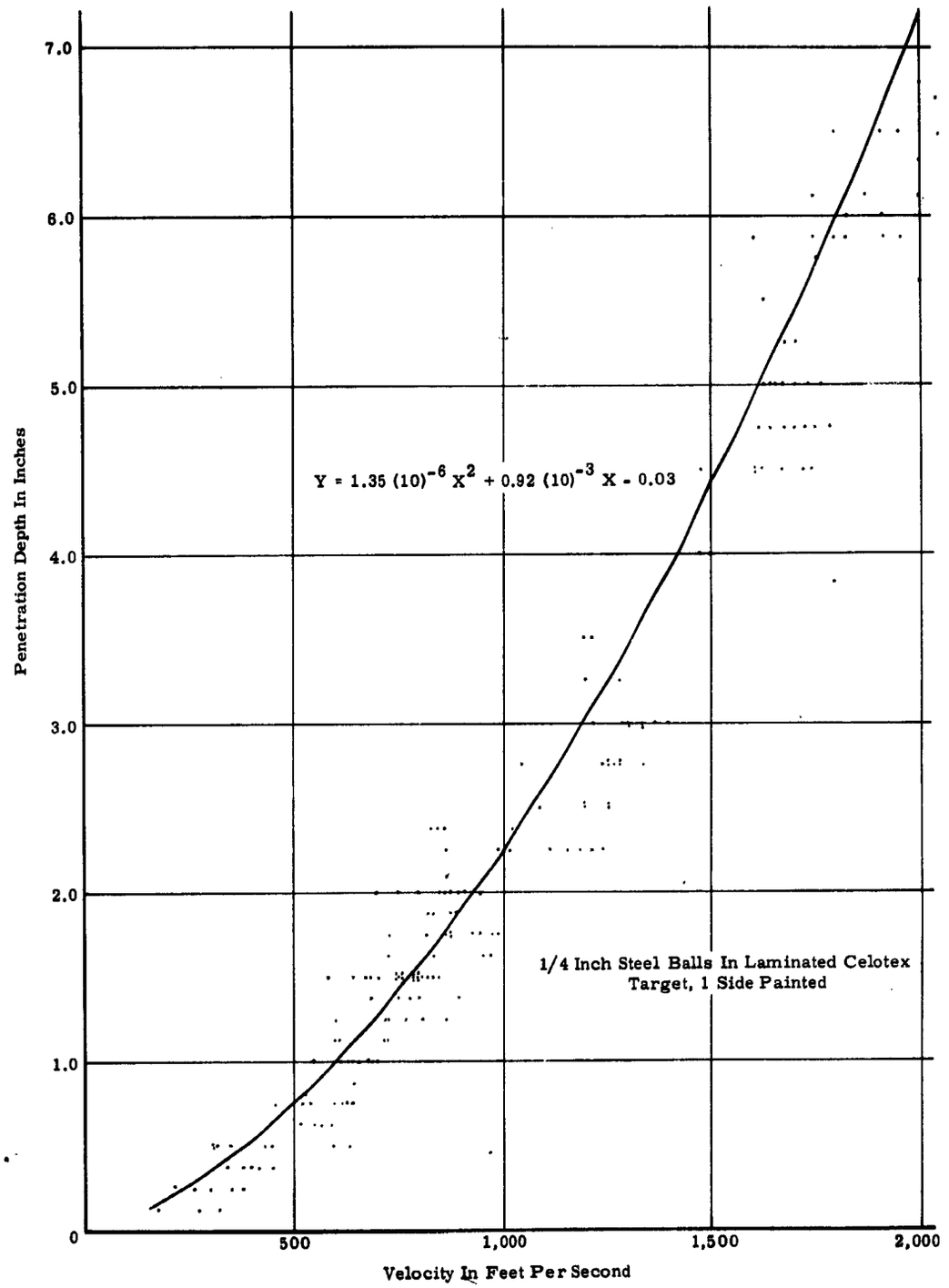


Figure 26. Penetration versus Velocity Calibration Curve

2. IMPACT PATTERNS

Following each test firing the individual fragment impact points are numbered and permanent photographic records are made (Appendices I through V). Graphic records of the impact patterns are also made with the penetration depth of each fragment recorded along with its specific impact location.

3. VELOCITY GRADIENT PLOTS

The average velocity of each layer is plotted to present graphically the velocity gradient between layers and the range of velocities for each layer. These plots are illustrated by Figure 5 and described in paragraph B. They are also presented in the appendices for each model tested.

By reviewing and comparing these gradient plots, evidence as to the performance characteristics of a given design is obtained. Ideally, a straight line slope and overlapping row dispersion is sought. The exact slope and dispersion varies according to the number of fragment layers in a particular design and the maximum velocities required.

4. POLAR DISTRIBUTION PLOTS

Polar plots (Figure 6) are prepared to illustrate thoroughly the velocity and space distribution performance of a given test model*. This presentation shows how the fragment pattern would appear to an observer viewing its formation, at a given instant, along the warhead's longitudinal axis. Average fragment velocities are plotted radially along with angular positions and fragment row location as shown by the coded data points. Velocities are determined from the previously described calibration curve and angular position from measurements of fragment impact locations on the face of the recovery target. By multiplying the fragment velocity by appropriate time factors, spatial distribution of individual fragments can be determined. The velocities recorded are calculated as the average velocity between the warhead test model and recovery target location, 14 feet. These velocities have not been corrected for air retardation. Considering the short distance involved, the error introduced by using these velocity values is approximately 1 percent less than the initial velocities within the velocity interval of interest.

*These plots are prepared only if a review of the velocity gradient plots described in paragraph 3 above shows that they are necessary.

## G. DISCUSSION OF RESULTS

The most significant results of this experimental program are discussed in paragraph B of this section and briefly summarized below:

1 Of the various design concepts investigated, the explosive layered approach offers the most potential for achieving program objectives;

2 Feasibility of the explosive layered concept to project multilayers of fragments radially into uniform patterns and at controlled velocity gradients has been confirmed with six- and eight-layered test models without fragment damage.

3 Cubic and hexagonal fragments promise improvement in coupling efficiencies and pattern distributions.

4 Reduced gage explosive or added fragment layers between explosive sheets promises a feasible means of reducing overall average fragment velocities.

5 Fragment beam spray angle can be controlled through massive end confinement. However, explosive end plates and shaped center bursters such as hyperboloid configurations promise feasible means of achieving very narrow beam spray angles without excessive parasitic weight.

Other results based on the data collected in this program, as applicable to each basic design concept, are discussed below.

### 1. BASIC DESIGN I (EXPLOSIVE FRAGMENT PACKAGE)

Fragments from these test models tend to move as a group in a torus type of pattern as though projected by the central burster only. Removal of the center burster resulted in low order detonations, very low fragment velocities, and undefinable distribution patterns. Confirmation of the low order detonation was achieved in part through color photography of the detonation process and showed very black smoke which, for this explosive, is typical of burning rather than high order detonation. Reproducible results for a similar individual test model were unsatisfactory as illustrated by the data presented in Appendix I.

### 2. BASIC DESIGN II (INERT FRAGMENT PACKAGE)

Of the interface attenuation materials tested, thick aluminum tubing resulted in the lowest overall velocities but no gradient. Rubber was effective in reducing velocities; whereas an air cavity provided the greatest gradient potential, yet was insufficient to meet program objectives. Since no significant differences were observed with any of these materials, a

combination burster tube comprised of walled aluminum and a single wrap of rubber was selected for remaining test models of this design series.

Other tests conducted included use of large diameter (1 1/2 inch) center bursters, which resulted in damage to the two innermost fragment rows, and hyperboloid center bursters, which provided reduced beam spray angles. Impact patterns indicated distinct vertical banding effects, proven to be the result of attenuation due to packaging individual fragments in paper tubes.

Because of these results and since the detailed data presented in Appendix II show the fragment layers to move essentially as a group with little to no velocity gradient between layers, further consideration of this concept was discontinued.

3. BASIC DESIGN III (BUFFERED FRAGMENT PACKAGE)

Tests of aluminum, rubber, and combinations of these materials as energy absorbers between the fragment layers resulted in the fragments being dispersed as a solid group with virtually no velocity gradients. Variations in thicknesses of materials gave essentially the same results. Based on these observations and detailed data presented in Appendix III, it was concluded that the buffered layered approach was ineffective in the control of velocity gradients.

4. BASIC DESIGN IV (EXPLOSIVE-LAYERED FRAGMENT PACKAGE)

All models of this concept that have been tested (spiral or concentric ring configurations) indicate an excellent potential for achieving the desired velocity gradient control and pattern distribution. Aside from the more significant results pertinent to this design concept, which have been described in paragraph B of this section, other applicable observations on the test performed are listed below:

1 Good gradient and pattern distributions have been achieved by both center burster and outside end-line initiation.

2 A 5/8-inch diameter C-4 explosive burster as employed in the concentric ring design models appears to be minimum for reliable detonation; 1/2-inch diameter, C-4 bursters have resulted in low order detonations and possibly deflagration of subsequent explosive layers.

3 A 1/2-inch diameter, RDX burster has been successfully employed in both six- and eight-layered test models. (To keep inner fragment row velocities to a minimum it is desirable to have a minimum explosive force in the center burster initiation concept.)

4 Removal of the center explosive burster tube and utilizing outside end-line initiation results in desirable decreased velocities of the inner fragment row as compared to designs utilizing center bursters.

5 Velocities of various fragment layers have been changed by varying the thickness of explosive associated with that particular layer.

6 In nearly all models tested, overall average fragment velocities are higher than program objectives. However, line-initiated thin-gaged explosives (0.042 and 0.025) have been utilized to reduce average velocities.

7 Spiral, explosive layered models with external end-line initiation show a tendency to distinct velocity separations between fragment layers, with small dispersions between minimum and maximum velocities for any given layer. This effect is not as pronounced with a similar center-initiated model. Indications are that center initiation may cause a "mixing" effect, probably due to collisions and energy exchange between fragments in different layers, thereby resulting in a more continuous overall velocity distribution.

Detailed data pertinent to all models tested on this concept are given in Appendix IV.

## 5. OTHER CONCEPTS

Results of all testing with the tapered burster design have resulted in the fragment package moving as a group without any gradient potential. In these designs, fragment layers are marked from top to bottom of the fragment package; whereas layer identification in the previously discussed concepts was outward from the innermost row. This concept was expected to produce a dish type of pattern with those fragments having the greatest height of explosive achieving the highest velocities. The inadequate results thus far obtained may be a function of the explosive column diameter, column shape, length-to-diameter effects, or method of initiation. Further investigations are required before conclusive results can be formulated.

Only two tests of the explosive end-impulse concept have been accomplished. Data are very sketchy but indicate a potential for achieving a random distribution with very low fragment velocities and large beam spray angles. Fragment velocities were so low that only small indentations in the recovery target were obtained. Also, large numbers of fragments were found in the ground plane between the warhead and recovery target. Again, further investigations of this concept are required to permit conclusive evaluation.

## H. CURRENT PROGRAM EXPERIMENTATION

Experimentation to devise practical means of initiating thin-gaged (0.042 and 0.025) sheet explosive is currently in progress. External end-line initiators have been effectively employed; however, attempts to initiate these thin sheet explosives with the center burster concept have resulted in deflagrations and unburned PETN as evidenced by instrumentation and fragments of PETN in the arena.

Experiments into beam spray control without massive end confinement are also in progress. Although detailed data are not available at this time, two explosive-layered test models shaped as hyperboloids have been fired; all fragments impacted within the 8-foot recovery target, indicating considerable improvement in beam spray angle.

## SECTION 3 - ANALYTICAL PROGRAM

This section describes the development of computational procedures currently used to predict fragment speeds expected during the initial firing of a test round. The objective is to arrive at this prediction by considering the design geometry of a specific model as well as the physical properties of the explosive and fabrication materials.

To meet this objective many approaches have been conceived and explored. Some of these have provided useful quantitative information and guidelines that highlighted feasible alternatives at times when it seemed that an impasse had been reached. A chronological accounting of these developments and subsequent progress follows.

### A. HYDRODYNAMIC SHOCK CONCEPT

In the beginning of this program, an attempt was made to predict the results to be expected using various combinations of layers of explosives, layers of balls, and layers of liner material. The precept forming the basis for these original predictions is demonstrated by the interaction geometry depicted in Figure 27.

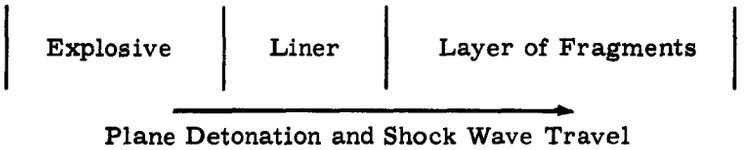


Figure 27. Interaction Geometry

The physical description of the presumed situation is as follows. The explosive liner and liner-ball layer interfaces represent contact discontinuities that separate regions of different densities and equations of state. When the detonation wave of the explosive reaches the explosive-liner boundary, an instantaneous adjustment sends a forward moving shock into the liner and a reflected wave back into the gaseous detonation products. This reflected wave constitutes a compressional shock because the shock impedance of the detonation products is less than that of the liner. When the shock in the liner reaches the layer of fragments, it is assumed that a similar adjustment occurs; however, the reflected wave in the liner can be one of either rarefaction or compression, depending on the relative magnitudes of the shock impedances of the materials of the fragments and liners.

The problem consisted of ascertaining the magnitudes of pressures, particle speeds, and shock speeds taking into account the fact that, in general, several layers of fragments would be encountered. (For computational purposes, no more than four layers of fragment were initially considered.) In undertaking the analysis, Chapman-Jouquet conditions were assumed at the detonation front, and shock attenuation was neglected.

Under the above restrictions, the conditions ahead of and behind a plane shock front are connected by Rankine-Hugoniot equations:

$$\frac{U - u_1}{V_1} = \frac{U - u_2}{V_2} = M \tag{1}$$

$$P_2 = P_1 = \frac{(u_2 - u_1)^2}{V_1 - V_2} \tag{2}$$

$$E_2 - E_1 = \frac{1}{2}(P_1 + P_2)(V_1 - V_2) \tag{3}$$

where:

$U$ = shock speed

$u$ = particle speed

$P$ = pressure

$V$ = specific volume

$E$ = specific internal energy

$M$ = mass flux across the front.

Subscript 1 refers to the region ahead of the shock.
Subscript 2 refers to the region behind the shock.

Along with these classical equations, an equation of state representing the materials at a boundary is needed. It was assumed that this equation had the form:

$$E = E(P,V) = (\gamma - 1)^{-1} PV \tag{4}$$

Upon substituting Equation (4) into Equation (3), an equation is obtained that can be used to relate $P_2$ to $V_2$ provided $P_1$ and $V_1$ are held fixed. A plot of $P_2$ versus $V_2$ generates the classical Hugoniot curve. Using the initial states denoted by the relations $P_1 = 0$, $V_1 = V_0$, and $u_1 = 0$ yields a curve that can be referred to as the (P,u) curve.

Those states (P,V) that can be reached through a backward facing wave rarefaction are known to lie on an adiabat defined by the relation:

$$\left(\frac{\partial E(P,V)}{\partial V}\right)_s = -p \qquad (5)$$

where, in general:

$$u_2 - \int_1^2 \sqrt{-\left(\frac{\partial P}{\partial V}\right)_s}\, dV = \text{a constant.} \qquad (6)$$

Hence, the locus of possible (P, u) state for the rarefaction can be obtained by eliminating V from Equations (5) and (6).

This hypothesis has been used to generate curves - available in the literature of explosive phenomena - of the type P versus u and U versus u for several combinations of materials and explosives. These curves were used to obtain preliminary estimates of the speeds of the various layers of fragments in test rounds that were fabricated and test fired. Examples and inferences based on these curves are discussed subsequently.

Using RDX explosive to approximate composition C4 explosive, P versus u and U versus u curves were used to estimate the pressures and particle speeds transmitted to single layers of steel balls through various types of plane shaped liners placed between the balls and the explosive. The results showed that changing the liner material introduced changes in the speed of the balls; however, these induced changes were too slight to provide effective control of fragment speeds through the use of different liner materials. This was confirmed through experimentation with Basic Design III.

Another example investigated toward defining feasible design models resulted in an effective possible combination. Assuming that four layers of steel fragments were adjacent to four explosive layers consisting of 70/30 tetrytol, cast composition B, RDX, and 70/23 octal, respectively, it was found that the innermost explosive layer should consist of 70/23 octal. This in turn should be followed by a layer of fragments, a layer of RDX explosive, a layer of fragments, a layer of composition B explosive, a layer of fragments, a layer of 70/30 tetrytol, and a layer of fragments in that order. It was found that the average initial speed of the layers of fragments, beginning with the outermost layer and moving inward, would be 3031, 188, 188, and 285 feet per second respectively if all explosive layers are detonated simultaneously. Although it was anticipated that these numbers would not agree with those obtained in a firing test, the solution indicated that some control over experimental results could be achieved by using layers of different types of explosives. By analogy, the idea of using different layer thicknesses of one type of explosive between the layers of fragments was conceived (Basic Design IV). Unfortunately, the available curves cannot be used easily and conveniently to conduct an experimental design program that complies with the test objectives and experimental

procedures, e.g., no motion is imparted to a fragment if the explosive in the layers ahead of or behind the fragment are the same, regardless of the magnitude of the ratio of their thicknesses. Consequently, an attempt was made to provide an alternate technique that could be expected to yield useful results. The first alternative considered was based on the spring-mass concept, and experiments to test its feasibility were incorporated into the test program. The results of this investigation are discussed in the paragraph below.

## B. SPRING-MASS SYSTEM CONCEPT

In this approach, the equation of motion for a fragment in the $i^{th}$ fragment layer of a multilayer ring fragment package is tentatively written as follows:

$$m_i \ddot{X}_i = K_i (X_i - X_{i-1}) - D_i \dot{X}_i - F_{i+1} \qquad (7)$$

where:

$m$ = mass of $i^{th}$ fragment layer

$\ddot{X}_i$ = instantaneous acceleration of $i^{th}$ fragment layer

$K_i$ = effective spring constant of $i^{th}$ fragment layer

$X_i$ = position of $i^{th}$ fragment layer

$X_{i-1}$ = position of $(i-1)^{th}$ fragment layer

$D_i$ = effective damping factor of $i^{th}$ fragment layer

$\dot{X}_i$ = instantaneous speed of $i^{th}$ fragment layer

$F_{i+1}$ = reaction force of $(i+1)^{th}$ layer.

As a basis for considering this approach it was anticipated that, given a round design having a center burster surrounded only by layered fragment rings, the succession of events following round detonation could be described in this manner. For a short time, all fragment layers would move away from the detonation center as a single unit and the inertia of the fragments reacting with the impulsive force could be used to store up compressive elastic energy between the respective rings. After the impulsive force is largely dissipated, the fragments in the rings subsequently release the stored up energy, thereby imparting a speed gradient between the successive rings. If this speed gradient is controllable and sufficient for the purposes of this study, then it seems reasonable to presume that the spring-mass concept should simulate the experimental environment adequately insofar as prediction of fragment speeds is the primary re-

quirement. To ascertain if this hypothesis were reasonable, several test rounds were fabricated and fired. The conclusions based on interpreting the test data (e.g., Test 2) were:

1 In the speed range of interest, there was no significant speed gradient between fragment rings.

2 In a higher speed range, a slight speed gradient between fragment rings is apparent.

These conclusions indicated that the spring-mass system concept does not apply in the speed range of interest. Again, it seemed that the most obvious means of controlling speed gradients would be to include explosive layers between the fragment rings. That the spring-mass system analogy reasonably simulates the interaction phenomena in the detonation of explosive layered rounds was considered to be extremely doubtful; consequently, this concept was discarded and has not been used to test results.

## C. SEMIEMPERICAL APPROACH

The method of analysis eventually used has been referred to as a semiempirical approach. It utilizes both simple empirical and hypothetical concepts to obtain useful design criteria. In general, the inputs include as many physical properties of the model design as feasible such as explosive detonation properties, loading density, round design geometry, fragment material and fragment shape and experimental data to compute measures of empirical constants. These constants account for variations in round-to-round performance, day-to-day effects, initiation energy, and other factors too complex to be accounted for in a more systematic manner.

As an introduction to the semiempirical approach, let the unbalanced force appearing at the mass center of a fragment in the $i^{th}$ layer be defined as shown in Figure 28.

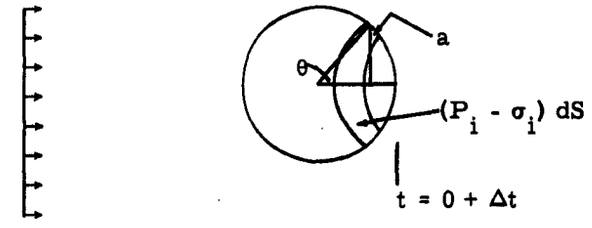


Figure 28. Detonation Products and Medium Interaction with Spherical Fragment

Considering Figure 28, the unbalanced force appearing at the mass center of the fragment and caused by the pressure on the element of area dS can be written:

$$dF_i = (P_i - \sigma_i)\, dS \cos\theta = (P_i - \sigma_i)\, \pi\, da d\theta = \frac{\pi d^2}{2} (P_i - \sigma_i) \cos\theta \sin\theta\, d\theta .$$

The total unbalanced force, $F_i$ can then be written:

$$F_i = \frac{\pi d^2}{2} (P_i - \sigma_i) \int_0^{2\pi} \sin\theta \cos\theta\, d\theta = \pi d^2 (P_i - \sigma_i) \qquad (8)$$

where:

$P_i$ = the pressure on the surface of a fragment in the $i^{th}$ layer caused by $i^{th}$ explosive layer detonations

$\sigma_i$ = the reaction pressure due to the medium properties of inertia and elasticity

$d$ = the fragment (sphere) diameter (0.25 in.)

Under the assumptions that $\sigma_i << P_i$ and $P_i$ is defined by the relation:

$$P_i = \frac{\rho_i D_i^2}{g}, \qquad (9)$$

the unbalanced force becomes

$$F_i = \pi d^2 \rho_i D_i^2 g^{-1} \qquad (10)$$

where:

$g$ = 32.2 ft/sec$^2$

$\rho_i$ = packing density of $i^{th}$ explosive layer

$D_i$ = detonation rate of explosive in $i^{th}$ layer.

To extend this analysis to a multilayer round, a four-layer configuration is used for demonstration purposes. The static geometry and unbalanced force interactions during the explosive process are depicted in Figure 29.

$F_1$, $F_2$, $F_3$, and $F_4$ are the forces exerted on the fragments by the respective explosive columns.

$r_1$, $r_2$, $r_3$, and $r_4$ are the distances from the round center line to the outermost edge of the respective explosive columns.

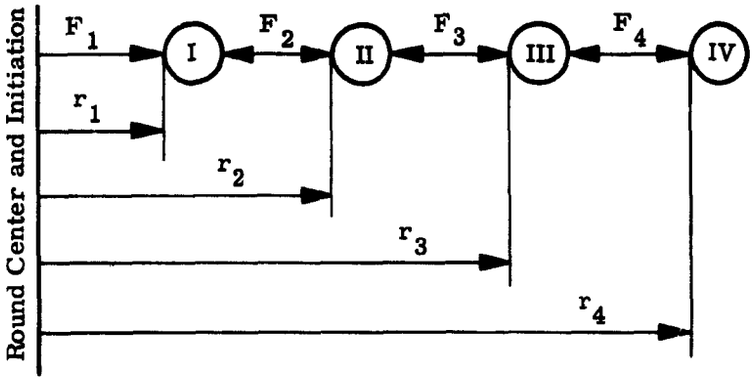


Figure 29. Static Geometry and Unbalanced Force Interaction

Rings I, II, III, and IV denote the rings of the respective fragments.

Let $G_I$, $G_{II}$, $G_{III}$, and $G_{IV}$ be the unbalanced forces on the fragment appearing in each of the respective rings. Then, by definition, the following set of equations apply:

$$\begin{aligned} G_I &= K_1F_1 - K_2F_2 - K_3F_3 - K_4F_4 = m_I\ddot{X}_I \\ G_{II} &= K_1F_1 + K_2F_2 - K_3F_3 - K_4F_4 = m_{II}\ddot{X}_{II} \\ G_{III} &= K_1F_1 + K_2F_2 + K_3F_3 - K_4F_4 = m_{III}\ddot{X}_{III} \\ G_{IV} &= K_1F_1 + K_2F_2 + K_3F_3 + K_4F_4 = m_{IV}\ddot{X}_{IV} \end{aligned} \qquad \text{(Set 1)}$$

where: $K_1$, $K_2$, $K_3$, and $K_4$ are constants to be computed from experimental data.

$m_I$, $m_{II}$, $m_{III}$, and $m_{IV}$ are the masses of the fragment in the respective ring columns provided all fragments have the same mass. (In the experimental program all fragments in all ring columns were made of steel and all had the same dimensions. Consequently, $m_I$, $m_{II}$, $m_{III}$, and $m_{IV}$ can each be replaced with a common mass denoted by the symbol m.)

Replacing all the m factors appearing in the equations of Set 1 with the common symbol m, defining m by the relation:

$$m = \frac{\pi d^3 \rho}{6g}$$

substituting Equation (10) into Set 1, and then integrating the resultant set with respect to time leads to the equations of Set 2

$$\begin{aligned}
\dot{X}_I &= 6\,(\rho d)^{-1}\,(K_1\rho_1\dot{D}_1^{\,2} - K_2\rho_2\dot{D}_2^{\,2} - K_3\rho_3\dot{D}_3^{\,2} - K_4\rho_4\dot{D}_4^{\,2})\,\Delta t'_I \\
\dot{X}_{II} &= 6\,(\rho d)^{-1}\,(K_1\rho_1\dot{D}_1^{\,2} + K_2\rho_2\dot{D}_2^{\,2} - K_3\rho_3\dot{D}_3^{\,2} - K_4\rho_4\dot{D}_4^{\,2})\,\Delta t'_{II} \\
\dot{X}_{III} &= 6\,(\rho d)^{-1}\,(K_1\rho_1\dot{D}_1^{\,2} + K_2\rho_2\dot{D}_2^{\,2} + K_3\rho_3\dot{D}_3^{\,2} - K_4\rho_4\dot{D}_4^{\,2})\,\Delta t'_{III} \\
\dot{X}_{IV} &= 6\,(\rho d)^{-1}\,(K_1\rho_1\dot{D}_1^{\,2} + K_2\rho_2\dot{D}_2^{\,2} + K_3\rho_3\dot{D}_3^{\,2} + K_4\rho_4\dot{D}_4^{\,2})\,\Delta t'_{IV}
\end{aligned} \qquad \text{(Set 2)}$$

where:

$\dot{X}_I$, $\dot{X}_{II}$, $\dot{X}_{III}$, and $X_{IV}$ represent speeds of the fragments in respective ring columns.

$\Delta t'_I$, $\Delta t'_{II}$, $\Delta t'_{III}$, and $\Delta t'_{IV}$ are the effective impulsive loading times influencing the motion of the fragment in respective ring columns.

$\rho$ is the fragment density. (In this study, $\rho$ = 7.85 gm/cc).

Introducing the assumptions that:

1. The impulsive loading times are all equal and proportional to $d\Delta t/D_i$ ($\Delta t$ = a constant),

2. Pressure exerted on a fragment is proportional to the amount of explosive in a layer of thickness d,

3. Speeds are proportional to the dimensionless constant $(c/m)^b$ leads to the computability equation listed as Set 3.

$$\begin{aligned}
K_1\rho_1\dot{D}_1 - K_2\rho_2\dot{D}_2 - K_3\rho_3\dot{D}_3 - K_4\rho_4\dot{D}_4 &= (\rho/6)\,U_I \\
K_1\rho_1\dot{D}_1 + K_2\rho_2\dot{D}_2 - K_3\rho_3\dot{D}_3 - K_4\rho_4\dot{D}_4 &= (\rho/6)\,U_{II} \\
K_1\rho_1\dot{D}_1 + K_2\rho_2\dot{D}_2 + K_3\rho_3\dot{D}_3 - K_4\rho_4\dot{D}_4 &= (\rho/6)\,U_{III} \\
K_1\rho_1\dot{D}_1 + K_2\rho_2\dot{D}_2 + K_3\rho_3\dot{D}_3 + K_4\rho_4\dot{D}_4 &= (\rho/6)\,U_{IV}
\end{aligned} \qquad \text{(Set 3)}$$

where:

$$U_j = \dot{X}_j \left(\frac{M}{C}\right)_j^b .$$

Solving these equations for the constants gives the following results:

$$K_1 = \frac{\rho^*(U_I^* + U_{IV}^*)}{12\,\rho_1^*\,\dot{D}_1^*} \qquad K_3 = \frac{\rho^*(U_{III}^* - U_{II}^*)}{12\,\rho_1^*\,\dot{D}_1^*}$$

$$K_2 = \frac{\rho^*(U_{II}^* - U_I^*)}{12\,\rho_2^*\,\dot{D}_2^*} \qquad K_4 = \frac{\rho^*(U_{IV}^* - U_{III}^*)}{12\,\rho_4^*\,\dot{D}_4^*}$$

and $$U_j^* = \dot{X}_j^* \left(\frac{M^*}{C^*}\right)_j^b .$$

All starred values represent actual design and experimental results that have been observed in fabricating and firing four layered test models.

Using Round No. 34 as a normalizing round and using a value of unity for b, these equations were used to predict fragment speeds to be expected in firing Round No. 35, 38, and 43. The results are shown in Table 2 and the results of an error analysis and their computations are shown in Tables 3 and 4. Comparing the entries leads to the following conclusions:

TABLE 2

Speed Performance Comparison

(Explosive Layered Design - Concentric Ring Type)

| Round No. | Condition | Average Speed (feet per second) Ring 1 | Ring 2 | Ring 3 | Ring 4 |
|---|---|---|---|---|---|
| 35 | Predicted | 431 | 878 | 1,315 | 1,674 |
| | Experimental | 140 | 1,080 | 1,250 | 1,840 |
| 38 | Predicted | 268 | 530 | 1,008 | 2,373 |
| | Experimental | 333 | 484 | 882 | 1,781 |
| 43 | Predicted | 212 | 389 | 775 | 1,567 |
| | Experimental | 267 | 336 | 1,189 | 1,863 |

TABLE 3

Speed Differences

| Round No. | Average Experimental Speed Minus Predicted Speed | | | |
|---|---|---|---|---|
| | Ring 1 | Ring 2 | Ring 3 | Ring 4 |
| 35 | -281 | 202 | -65 | 166 |
| 38 | 65 | -46 | -126 | -592 |
| 43 | 55 | -53 | 414 | 286 |

TABLE 4

Standard Deviations

| Round No. | Standard Deviations (feet per second) in Predicted Values | | | |
|---|---|---|---|---|
| | Ring 1 | Ring 2 | Ring 3 | Ring 4 |
| 35 | 67 | 232 | 454 | 753 |
| 38 | 71 | 140 | 348 | 1,067 |
| 43 | 33 | 102 | 268 | 704 |

1 Nine of the predicted values lie within one standard deviation of the computed error.

2 Two of the remaining predicted values lie within two standard deviations of the computed error.

3 Only one fragment was recovered from layer one of Round No. 35; hence, a comparison of predicted and experimental results for this layer is meaningless.

The equations used to compute the dimensionless constant C/M in performing this analysis are:

$$\left(\frac{C}{M}\right)_I = \frac{6\,\rho_1\,r_1^{\,2}\,L_1}{\rho\,d^2\sum_{i=1}^{4} n_i + 6\,(\rho_{A\ell}\,\ell_1 + \rho_R\,\ell_2)} \qquad (11)$$

$$\left(\frac{C}{M}\right)_{II} = \left(\frac{C}{M}\right)_I + \frac{6\,\rho_2\,L_2}{\rho\,d^2\sum_{i=2}^{4} n_i} \qquad (12)$$

$$\left(\frac{C}{M}\right)_{III} = \left(\frac{C}{M}\right)_{II} + \frac{6\,\rho_3\,L_3}{\rho\,d^2 \sum_{i=3}^{4} n_i} \qquad (13)$$

$$\left(\frac{C}{M}\right)_{IV} = \left(\frac{C}{M}\right)_{III} + \frac{6\,\rho_4\,L_4}{\rho\,d^2\,n_4} \qquad (14)$$

where:

$L_1 = 1$

$L_2 = r_2^2 - (r_1 + d + 0.065)^2$

$L_3 = r_3^2 - (r_2\ A\ d)^2$

$L_4 = r_4^2 - (r_3 + d)^2$

$\ell_1 = (r_1 + 0.005) - r_1^2$

$\ell_2 = (r_1 + 0.065)^2 - (r_1 + 0.005)^2$

$\rho_{AL}$ = density of aluminum liner (2.699 gm/cc)

$\rho_R$ = density of rubber lining (1.507 gm/cc)

$N_i$ = number of fragment in $i^{th}$ ring.

A list of constants peculiar to Round No. 34 follows:

| | | | |
|---|---|---|---|
| $\rho_1^*$ | = 1.66 gm/cc | $X_{II}^*$ | = 557 ft/sec |
| $\rho_2^* = \rho_3^* = \rho_4^*$ | = 1.5 gm/cc | $\dot{X}_{III}^*$ | = 785 ft/sec |
| $r_1$ | = 0.375 in. | $\dot{X}_{IV}^*$ | = 1,252 ft/sec |
| $r_2$ | = 0.78 in. | $n_1$ | = 14 |
| $r_3$ | = 1.11 in. | $n_2$ | = 22 |
| $r_4$ | = 1.44 in. | $n_3$ | = 31 |
| $\dot{X}_I^*$ | = 475 ft/sec | $n_4$ | = 39 |

Although the results given by this procedure are encouraging, a major deficiency exists. Neither the results nor the procedure can be used to predict the experimental speeds to be expected in firing a round fabricated with more than four different ring layers of fragments. Before the procedure can be used to predict fragment speeds generated by exploding a round fabricated with five different ring layers, a five- ring layered round must be fabricated and fired. Because of this shortcoming, an attempt was made to modify the analysis to provide a procedure that could be used to predict fragment speeds for any hypothesized number of ring layers without fabricating and firing a test round. This extension was based on the following considerations. Assuming a normal distribution holds for the experimental observations given in Table 2, the probability that a better comparison is achieved by chance, between the experimental and predicted values is approximately 0.06. This means there is insufficient reason for rejecting the null hypothesis defined by the statement: The means of both the experimental and predicted values are equal. This result implies that the form of the equations used gives reasonable agreement with test data. This conclusion led to a decision to use the least squares method and fit the data to a general equation having the form

$$X_j = U_j \left(\frac{C}{M}\right)_j^b .$$

Because $U_j$ and b are constants and a general equation relating speed to (C/M) was deemed necessary, the equation actually used (note notational change) in this latter phase was

$$V = A\left(\frac{C}{M}\right)^b \qquad (15)$$

where:

V = the average fragment speed in feet per second

$\frac{C}{M}$ = dimensionless quantity analogue to the conventional charge-to-mass ratio concept

A,b = constants to be computed using observed test results.

To compute the quantities A and b, it is first necessary to compute C/M values. Because two types of rounds (i.e., rounds incorporating either concentric rings or a spiral design) were under test, two procedures for computing C/M values were needed. Those used are described in paragraphs 1 and 2 below.

1. CONCENTRIC RING PROCEDURE

Figure 30 depicts a cross sectional sketch of this design concept and consists of a central explosive burster surrounded by alternate rings of

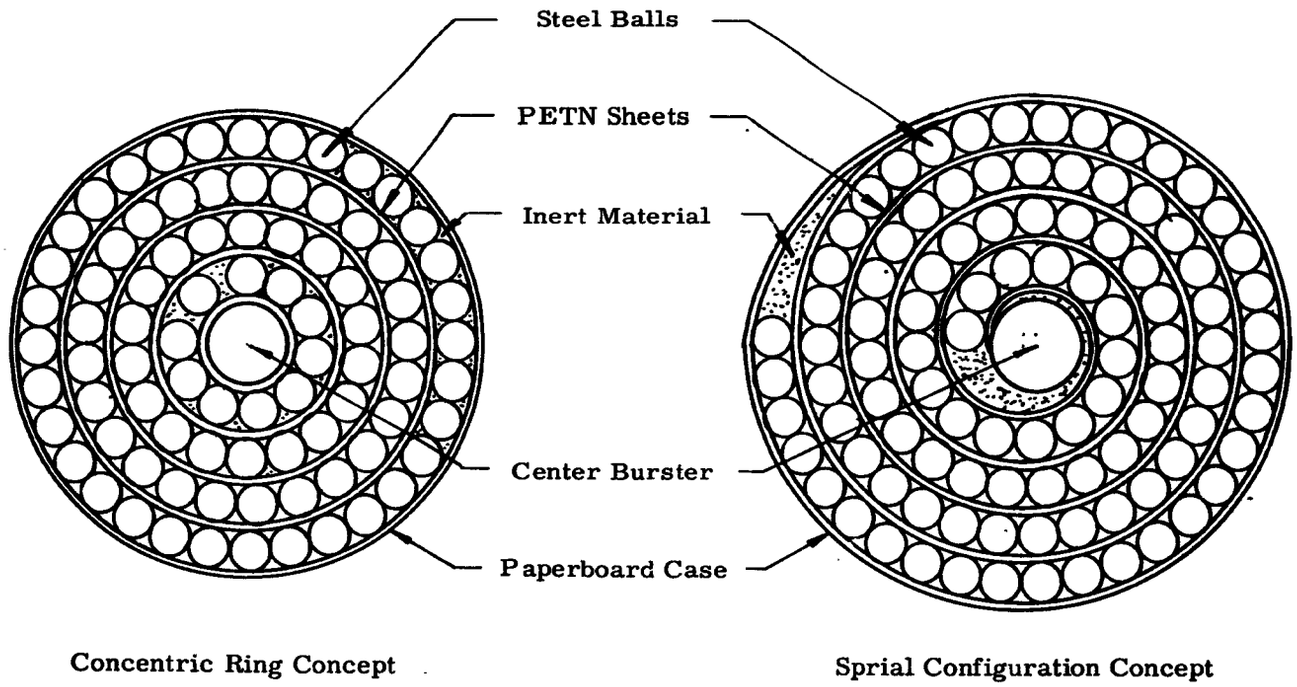


Figure 30. Cross Sections of Explosive Layered Concepts

steel balls and PETN explosive. The innermost ring of balls is designed as Ring 1, its C/M as $(C/M)_1$, the next ring of balls encountered in moving away from the center is designated as Ring 2, its C/M as $(C/M)_2$, . . ., etc. Equations used to compute values for these parameters are essentially the same as Equations (11) through (14). (As the forms used are slightly different, they are included herein to ensure completeness.)

$$\left(\frac{C}{M}\right)_1 = 6\,\rho_{CB}\,r_1^2/d\,\rho\sum_{j=1}^{\ell} n_j \tag{16}$$

and, in general, for i ranging from 2 to $\ell$:

$$\left(\frac{C}{M}\right)_i = \left(\frac{C}{M}\right)_{i-1} + \frac{6\,\rho_P\left[r_i - (r_i - T_i)^2\right]}{d^2\,\rho\sum_{j=1}^{\ell} n_j} \tag{17}$$

where:

$r_i$ = distance from round centerline to outer edge of $i^{th}$ layer of PETN shut (in.)

$r_1$ = radius of center burster (in.)

$T_i$ = width of $i^{th}$ layer PETN sheet (in.)

$\rho_{CB}$ = density of center burster (gm/cc)

$\rho_P$ = density of PETN (gm/cc)

$\rho$ = density of steel (gm/cc)

d = steel ball diameter (in.)

$\ell$ = number of rings in round

$N_i$ = number of balls in $j^{th}$ ring (e.g., $N_j = 2\,\pi\,r_{Bj}/d$)

## 2. SPIRAL CONFIGURATION PROCEDURE

This configuration is also illustrated in Figure 30. It consists of an explosive center burster, a continuous sheet of PETN explosive, and ball shaped fragments, which are wound about the center burster to form a spiral. The same basic computational procedure is used for spiral rounds as for concentric rounds. The principal difference is in the equations used to compute C/M values. For spiral rounds, these assume the form:

$$\left(\frac{C}{M}\right)_1 = \frac{6\, r_1^{\,2}\, \rho_{CB}}{L_B\, d\, \rho} + \frac{6\, L_{C_i}\, T_1\, \rho_P}{L_B\, d\, \rho} \tag{18}$$

and, in general, for i ranging from 2 to

$$\left(\frac{C}{M}\right)_i = \left(\frac{C}{M}\right)_{i-1} + \frac{6\, L_{C_i}\, T_1\, \rho_P}{\pi\, d\, \rho\, (L_B - L_{B_1} - \ldots - L_{B_{i-1}})} \tag{19}$$

where:

$r_1$, $T_i$, $\rho_{CB}$, $\rho_P$, $\rho$, d, and $\ell$ are defined in the concentric ring procedure section.

$L_{C_i}$ = length of $i^{th}$ loop of the PETN spiral

$L_{B_i}$ = length of $i^{th}$ loop of the fragment spiral

$L_B$ = length of the fragment spiral.

If the PETN thickness is uniform (i.e., $T_1 = T_2 = \ldots = T_i = T$), then the following equations can be used to compute measures of $L_{C_i}$ $L_{B_i}$ and $L_B$.

$$L_{C_i} = \frac{1}{a} \int_{r_C}^{(r_C + 2\pi ia)} (r_2^{\,2} + a^2)^{\frac{1}{2}}\, dr - \sum_{k=1}^{i-1} L_{C_k}$$

$$\frac{1}{2a}\, r^2 \Big|_{r_C}^{r_C + 2\pi ia} - \sum_{k=1}^{i-1} L_{C_K} \tag{20}$$

$$L_{B_i} = \frac{1}{a} \int_{r_B}^{(r_B + 2\pi ia)} (r^2 + a^2)^{\frac{1}{2}}\, dr - \sum_{k=1}^{i-1} L_{B_k} \simeq$$

$$\frac{r^2}{2a} \Big|_{r_B}^{r_B + 2\pi ia} - \sum_{k=1}^{i-1} L_{B_k} \tag{21}$$

$$L_B = \sum_{i=1}^{\ell} L_{B_i} \tag{22}$$

where:

$$a = \frac{(d + T)}{2\pi} \tag{23}$$

$$r_C = r_1 + \frac{T}{2} \tag{24}$$

$$r_B = r_1 + T + \frac{d}{2} \tag{25}$$

If the thickness of PETN varies from loop to loop in the PETN spiral, the length of each loop must be computed separately using the relations:

$$L_{C_i} = \frac{1}{a_i} \int_{r_{C_i}}^{(r_{C_i}+2\pi a_i)} (r^2 + a^2)^{\frac{1}{2}}\, dr \simeq \frac{1}{2a_i}\, r^2 \Bigg|_{r_{C_i}}^{r_{C_i}+2\pi a_i} \tag{26}$$

$$L_{B_i} = \frac{1}{a_i} \int_{r_{B_i}}^{(r_{B_i}+2\pi a_i)} (r^2 + a^2)^{\frac{1}{2}}\, dr \simeq \frac{1}{2a_i}\, r^2 \Bigg|_{r_{B_i}}^{r_{B_i}+2\pi a_i} \tag{27}$$

where:

$r_{C_i}$ is the distance from the center burster centerline to the center of the PETN sheet at the origin of the $i^{th}$ loop in the spiral;

$r_{B_i}$ is the distance from the center burster centerline to the center of the balls at the origin of the $i^{th}$ loop in the spiral;

$$a_i = \frac{(d + T_i)}{2} . \tag{28}$$

This completes the description of the procedures to be used in computing values of C/M to be used in obtaining estimates of the constants A and b of Equation (15). To perform this latter operation, Equation (15) is transformed to:

$$\log V = \log A + b \log \left(\frac{C}{M}\right). \tag{29}$$

Whence, the normalizing equation defining A and b are:

$$\sum_{s=1}^{w} \log V_s = w \log A + b \sum_{s=1}^{w} \log \left(\frac{C}{M}\right)_s \tag{30}$$

$$\sum_{s=1}^{w} (\log V_s) \log \left(\frac{C}{M}\right)_s = (\log A) \sum_{s=1}^{w} \log \left(\frac{C}{M}\right)_s + b \sum_{s=1}^{w} \log \left(\frac{C}{M}\right)_s^2 \tag{31}$$

where w is the total number of rings for all rounds. Introducing observed speeds and corresponding values of C/M into Equations (30) and (31), values A and b were computed for both the concentric ring type round and the spiral type round. Substituting these numbers into Equation (15) yields, as the respective prediction equations, the following:

$$\text{Concentric round:} \quad V = 3240 \left(\frac{C}{M}\right)^{0.579} \tag{32}$$

$$\text{Spiral round:} \quad V = 6320 \left(\frac{C}{M}\right)^{0.733} \tag{33}$$

Figure 31 shows the locus of these equations and has been used to provide the comparative values shown in Table 5. Because a statistical analysis of the goodness of fit between predicted and experimental observations has not yet been conducted, no statement concerning the validity of the results can be made at this time. The following observation is made without recourse to statistical analysis. From the experimental data, the fragment speeds within layers can be expected to vary over a range of 200 feet per second. If subsequent analysis and testing confirm that a difference of 200 feet per second between prediction and experiment is acceptable, the number of acceptable comparisons is greater than the number of non-acceptable comparisons. If a difference of 250 feet per second is proven acceptable, the number of acceptable comparisons exceeds the non-acceptable comparisons by a ratio of about three to one. This is sufficient to indicate that the semiempirical approach is a useful basis for the design of test rounds and the prediction of fragment layer speeds.

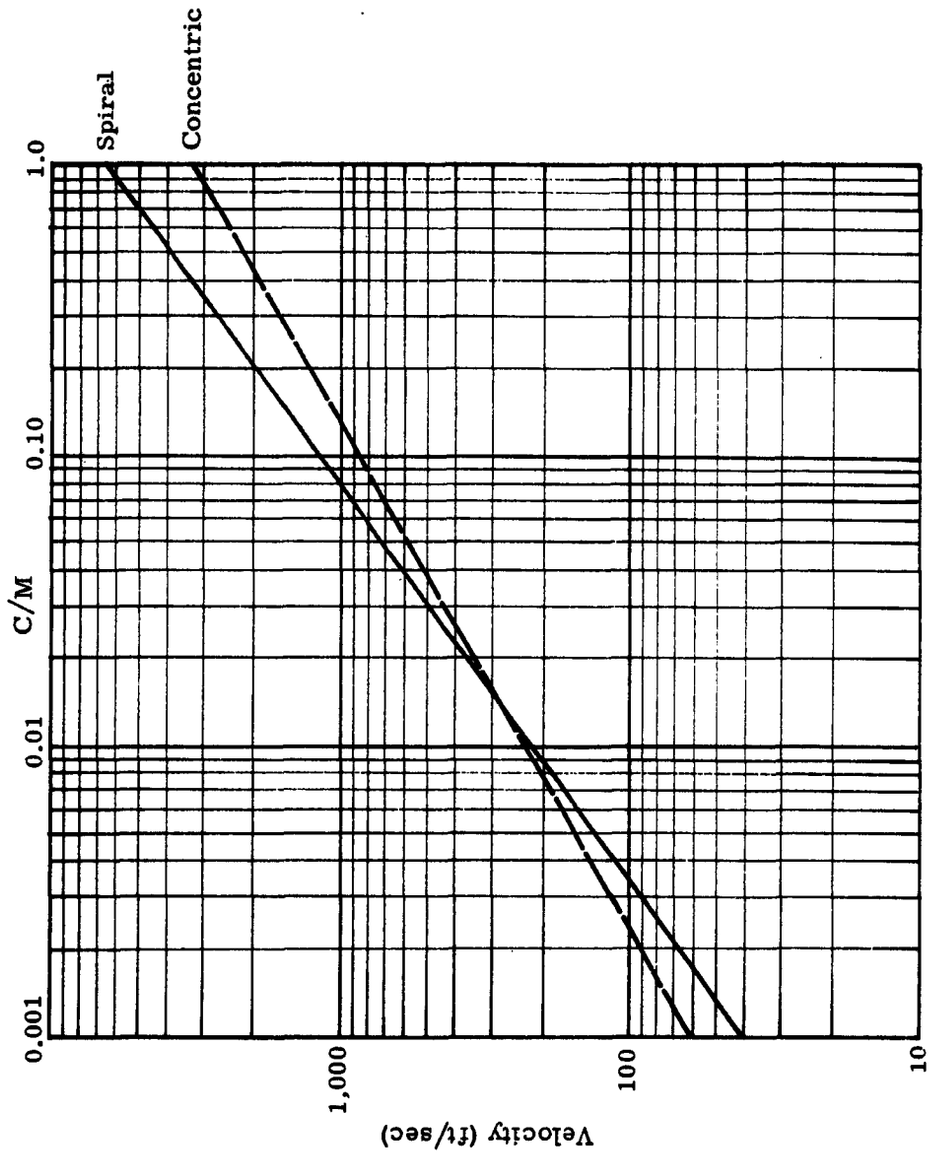


Figure 31. Equation Locus

TABLE 5

Results Comparison

| Round No. | Condition | Average Fragment Velocities (Feet per Second) Layer 1 | Layer 2 | Layer 3 | Layer 4 | Layer 5 | Layer 6 | Layer 7 | Layer 8 |
|---|---|---|---|---|---|---|---|---|---|
| 30 | Experimental | No hits | 380 | 820 | 1800 | | | | |
| | Predicted | 330 | 640 | 1250 | 2400 | | | | |
| 48 | Experimental | 259 | 429 | 1038 | 1575 | | | | |
| | Predicted | 345 | 640 | 1075 | 1925 | | | | |
| 56 | Experimental | 320 | 332 | 534 | 886 | 1221 | 1605 | | |
| | Predicted | 210 | 340 | 500 | 680 | 950 | 1450 | | |
| 60 | Experimental | No hits | 203 | 879 | 2294 | | | | |
| | Predicted | 360 | 550 | 1050 | 1750 | | | | |
| 63 | Experimental | 255 | 374 | 562 | 911 | 1265 | 1688 | | |
| | Predicted | 210 | 380 | 600 | 900 | 1350 | 2150 | | |
| 65 | Experimental | 258 | 278 | 372 | 595 | 943 | 1266 | 1636 | 2700 |
| | Predicted | 150 | 260 | 400 | 590 | 820 | 1125 | 1600 | 2400 |
| 70 | Experimental | 494 | 573 | 677 | 731 | | | | |
| | Predicted | 290 | 390 | 560 | 890 | | | | |
| 71 | Experimental | 546 | 714 | 813 | 851 | | | | |
| | Predicted | 290 | 390 | 560 | 890 | | | | |
| 77 | Experimental | 150 | 250 | 280 | 560 | 722 | 1068 | | |
| | Predicted | 95 | 210 | 360 | 590 | 1000 | 1950 | | |
| 81 | Experimental | 325 | 426 | 565 | 943 | 1288 | 1566 | | |
| | Predicted | 210 | 380 | 600 | 900 | 1350 | 2150 | | |


CONFIDENTIAL

TABLE 5 (Cont)

| Round No. | Condition | Average Fragment Velocities (Feet per Second) Layer 1 | Layer 2 | Layer 3 | Layer 4 | Layer 5 | Layer 6 | Layer 7 | Layer 8 |
|---|---|---|---|---|---|---|---|---|---|
| 82 | Experimental | 318 | 380 | 454 | 689 | 1018 | 1330 | 1708 | 1937 |
| | Predicted | 150 | 260 | 410 | 600 | 810 | 1120 | 1550 | 1550 |
| 83 | Experimental | 385 | 377 | 401 | 436 | 439 | 440 | 425 | 449 |
| | Predicted | 100 | 170 | 250 | 360 | 490 | 690 | 940 | 1400 |
| 84 | Experimental | 402 | 391 | 382 | 410 | 459 | 467 | | |
| | Predicted | 180 | 250 | 340 | 470 | 640 | 950 | | |
| 85 | Experimental | 317 | 367 | 353 | 359 | 376 | 378 | | |
| | Predicted | 130 | 195 | 330 | 510 | 790 | 1100 | | |
| 88 | Experimental | 354 | 456 | 819 | 1168 | | | | |
| | Predicted | 265 | 400 | 720 | 1200 | | | | |
| 89 | Experimental | 394 | 646 | 681 | 706 | | | | |
| | Predicted | 265 | 400 | 720 | 1200 | | | | |


CONFIDENTIAL

## SECTION 4 - CONCLUSIONS

The following major conclusions are based on the data resulting from this study:

1 Multiple layers of fragments (four, six, and eight) can be explosively projected into radially expanding patterns by a warhead design concept utilizing alternate layers of fragments and sheet PETN explosive.

2 It is feasible to achieve multilayer fragment projection with either spiral or concentric ring configurations of the explosive layered concept.

3 Fragment radial velocities can be controlled to obtain uniform radial growth patterns by varying the gage thickness of explosive between fragment layers.

4 The explosive layered design promises the desired pattern and velocity distributions for charge-to-metal ratios of 0.080 or less.

5 Cubic and hexagonal fragments promise further improvement in packaging and energy coupling efficiencies than that currently obtained with spherical fragments.

6 Fragment beam spray angles can be confined to an order of 25 or 30 degrees with massive end confinement. Alternate concepts such as explosive end plates, shaped center bursters combined with light metal end plates, and hyperboloid configurations offer means of achieving the same or improved spray angle control without excessive parasitic weight.

7 A semiempirical procedure utilizing equations of the form $V = A(C/M)^b$ and experimental data permits analytical prediction of warhead design parameters and fragment velocity performance.

8 Problem areas currently under investigation and requiring further experimental data for resolution include further reduction of fragment velocity and beam spray angle.

## SECTION 5 - RECOMMENDATIONS

Recommendations for future work leading to successful prototype test devices are as follows:

1. Continue the experimental program with emphasis on projection of up to 14 or more layers of fragments.

2. Expand the analytical effort to include additional physical parameters associated with design, and investigate alternate analytical procedures for predicting the behavior of multilayer fragment packages.

3. Continue investigations into alternate means of controlling beam spray angles without excessive parasitic weight such as explosive end plates, hyperboloid configurations, and shaped center bursters.

4. Define the feasibility of combining multilayer radial projectors with multilayer end projectors to maintain high-density fragment distribution near the centerline.

5. Determine a practical means of initiating thin explosive layers such as end line initiation, cast explosives, manifolding techniques, and voids in fragment package.

6. Investigate the effect of different fragment materials such as nickel and tungsten.

7. Establish fragment size scaling effects.

8. Determine practical and economical fabrication techniques considering serrated cylinders or wire, cast explosives, and tape placement of preformed fragments.

9. Establish safety requirements and/or hazard possibilities.

10. Investigate methods of projecting in a space environment to determine the effect on the explosive-to-fragment coupling.

11. Conduct prototype feasibility demonstrations including static firings and dynamic pattern formations.

## REFERENCES

1. "R&D Exhibit No. ASQW 62-48," 6 June 1963, Detachment 4, ASD, Eglin Air Force Base, Florida, Confidential.

2. Ballistic Research Laboratories Report No. 614, "Experiments with Shrapnel and Wire Wound Model Warheads," N. Share, 1946, Confidential.

3. Technical Note No. 1470, Ballistic Research Laboratories, "Simultaneity of Explosion Times of Engineers Special Detonators," E. Bonner L. Bryant, J. Trimble, August 1962, Unclassified.

# APPENDICES

These appendices present detailed data on all warhead models that have been test fired. Each appendix is organized to present data pertinent to that particular design concept and, where possible, to show the results of a particular design variable change. Round numbers are not sequential and serve only as an identifier for data record files.

# APPENDIX I

## BASIC DESIGN I DATA

This appendix summarizes design and test data pertinent to all Basic Design I warhead models.

TABLE 6

Basic Design I Data Summary

| Round No. | Round Description | | | | | | | | | Parameter Varied | Test Objectives |
|---|---|---|---|---|---|---|---|---|---|---|---|
| | Expl Mass (grams) | Frag Mass (grams) | End Plate Mass (grams) | C/M | Type | Cent. Burst Type | Cent. Burst Diam (in.) | Over Dim. Ht (in.) | Over Dim. Diam (in.) | | |
| 11 | 90.4 | 778.7 | 445<br>454 | 0.116 | Fig. 32 | Liquid Nitro-Methane | 0.75 | 3.5 | 3.0 | Liquid explosive in center burster and in fragmentation package interstices | Pattern/velocity gradient check for fragment breakup |
| 12 | 84.8 | 778.7 | 447<br>455 | 0.108 | Fig. 32 | Liquid Nitro-Methane | 0.75 | 3.5 | 3.0 | Same as 11 | Same as 11 |
| 37 | 117.5 | 814.3 | 790.5 | 0.134 | Fig. 32 | Liquid Nitro-Methane | 0.75 | 3.5 | 3.0 | Same as 11 | Same as 11 |
| 39 | 124.3 | 1253.0 | 894.8 | 0.061 | Fig. 33 | None | None | 3.5 | 3.0 | Same as 11 with void center | Same as 11 |
| 42 | 124.3 | 1247.0 | 856.0 | 0.095 | Fig. 33 | None | None | 3.5 | 3.0 | Same as 39 | Same as 11 |

TABLE 6

Basic Design I Data Summary

| | Over Dim. | | | | Results | | | | |
|---|---|---|---|---|---|---|---|---|---|
| m .) | Ht (in.) | Diam (in.) | Parameter Varied | Test Objectives | Impact Pattern | Beam Spray Angle | Velocity Gradient | Polar Plot | Conclusions and Comments |
| 5 | 3.5 | 3.0 | Liquid explosive in center burster and in fragmentation package interstices | Pattern/velocity gradient check for fragment breakup | Fig. 37 | 16 Deg | 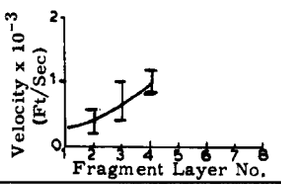  | Fig. 34 | Retest scheduled<br>Good gradient potential |
| 5 | 3.5 | 3.0 | Same as 11 | Same as 11 | Similar to Round 11 | 24 Deg | 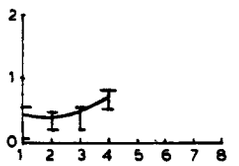  | Fig. 35 | Gradient reproducibility unsatisfactory<br>Retest scheduled<br>Fragments move as a group |
| 5 | 3.5 | 3.0 | Same as 11 | Same as 11 | Fig. 38 | 21 Deg | 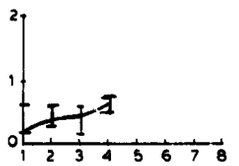  | Fig. 36 | Small gradient<br>Poor reproducibility<br>Fragments move as a group |
| e | 3.5 | 3.0 | Same as 11 with void center | Same as 11 | Velocity too low to penetrate target | Not available | 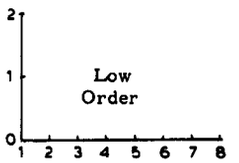  | | Low order detonation<br>No velocity gradient |
| e | 3.5 | 3.0 | Same as 39 | Same as 11 | Same as Round 39 | 31 Deg | 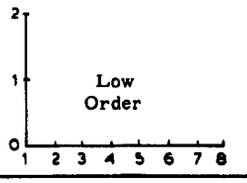  | | Same as 39<br>No further tests of design planned |

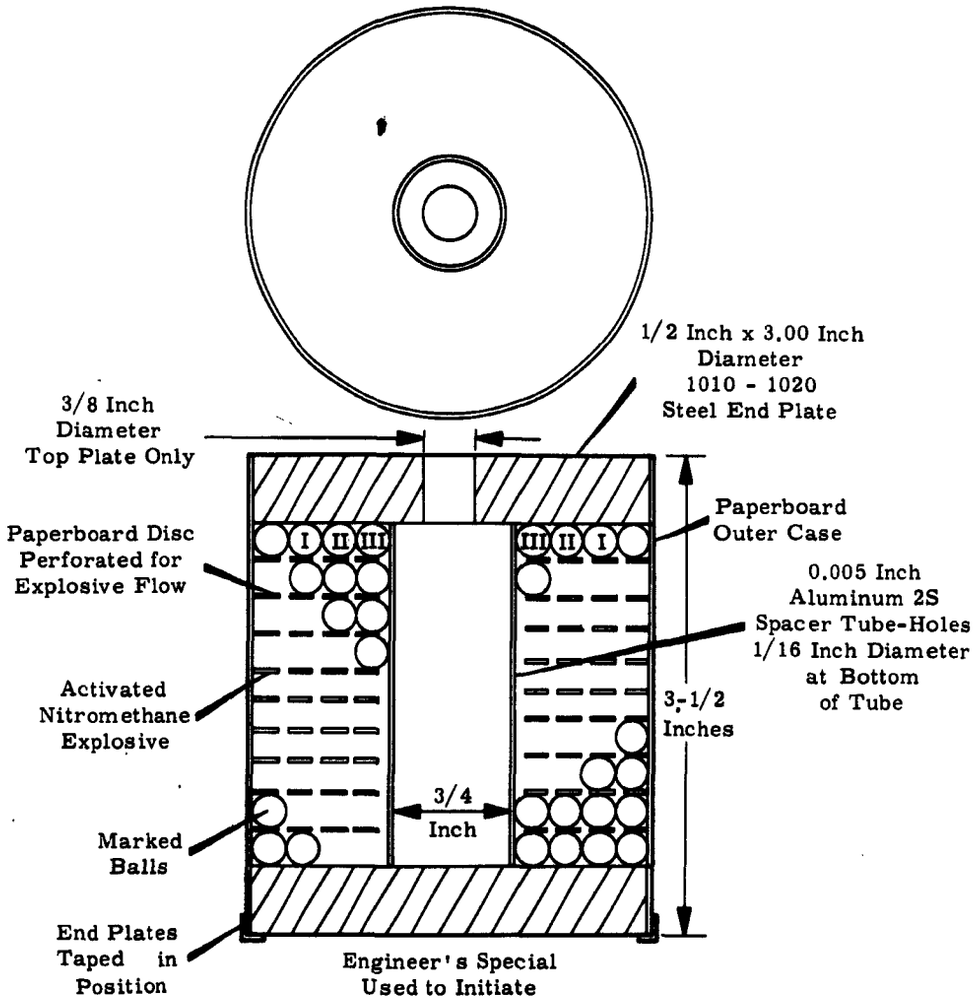


Figure 32. Test Model Design, Round No. 11 and 12

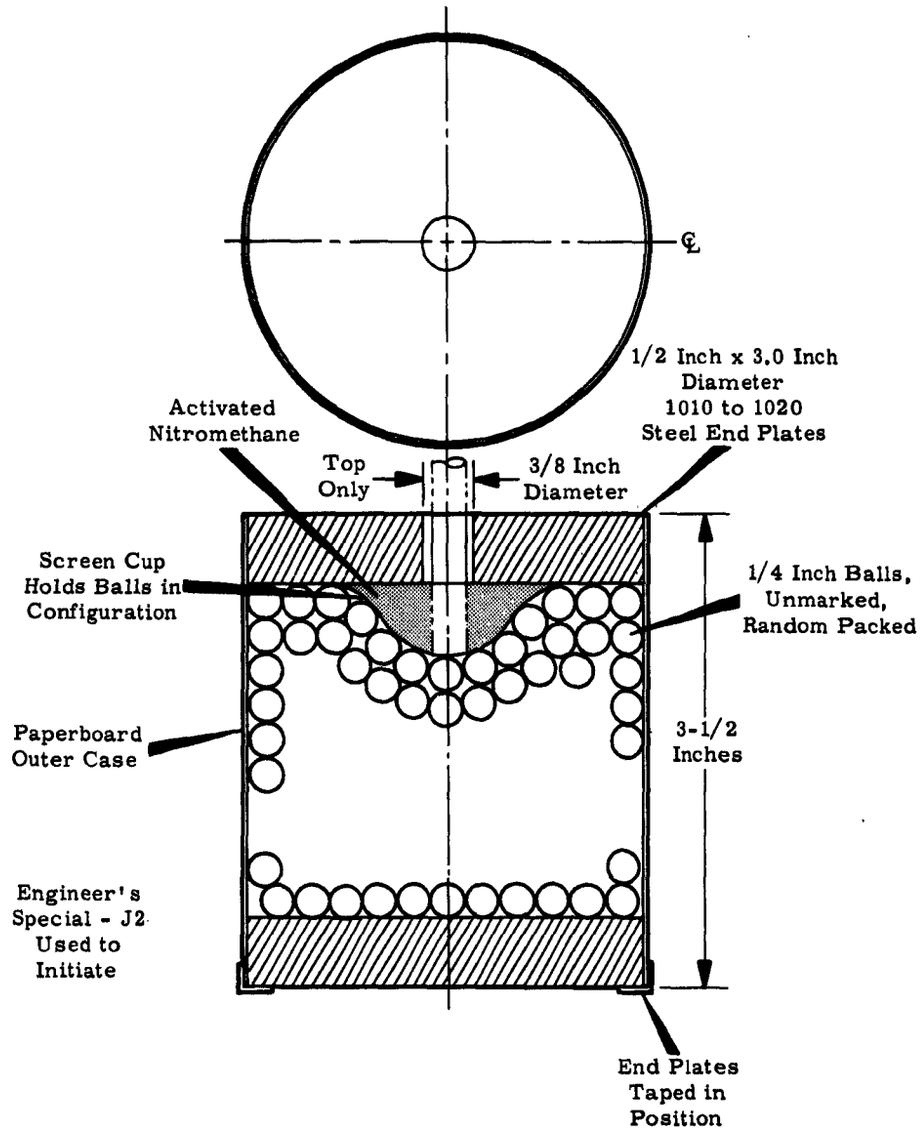


Figure 33. Test Model Design, Round No. 39 and 42

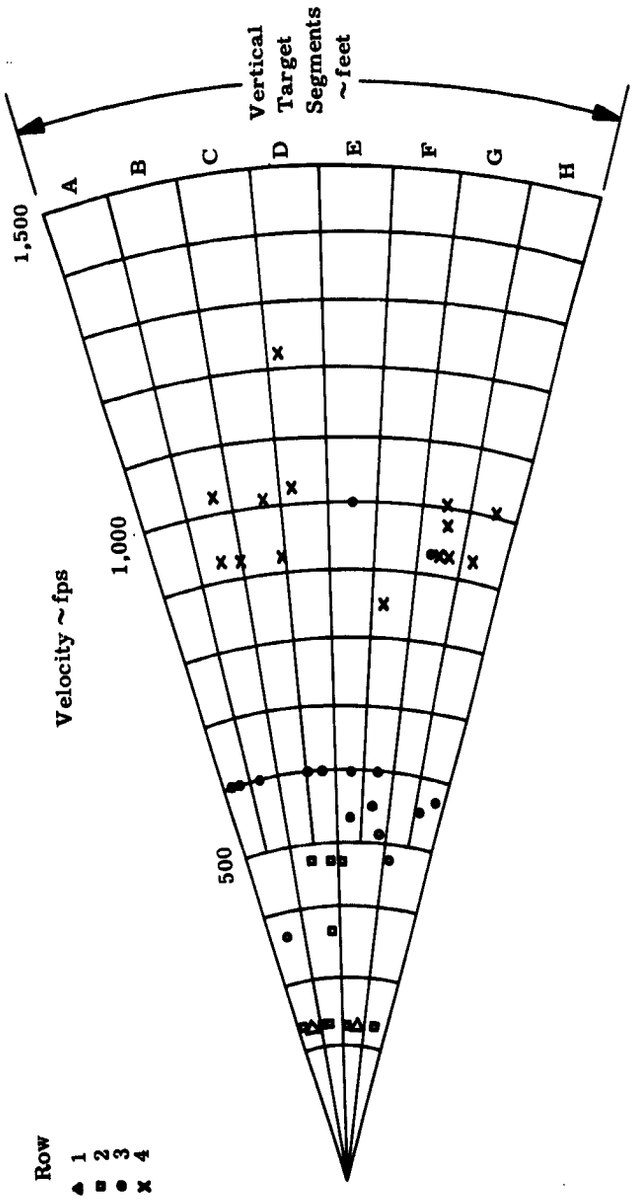


Figure 34. Velocity versus Radial Distribution, Round No. 11

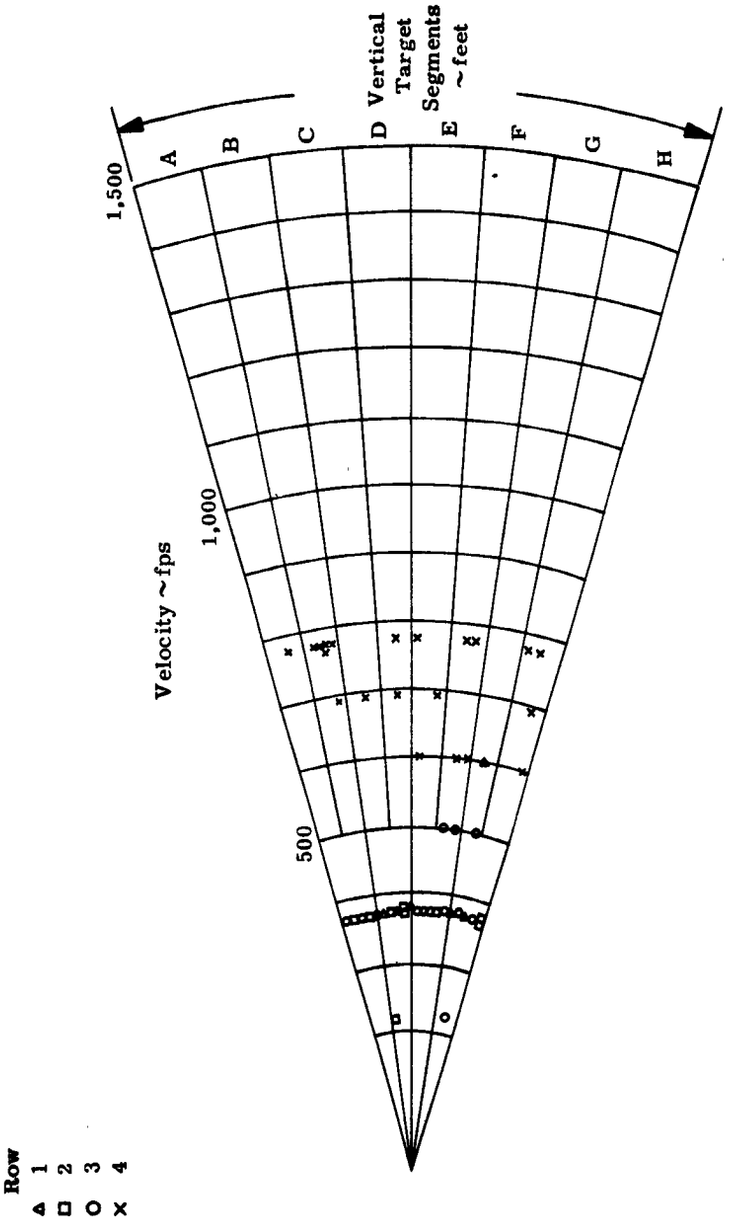


Figure 35. Velocity versus Radial Distribution, Round No. 12

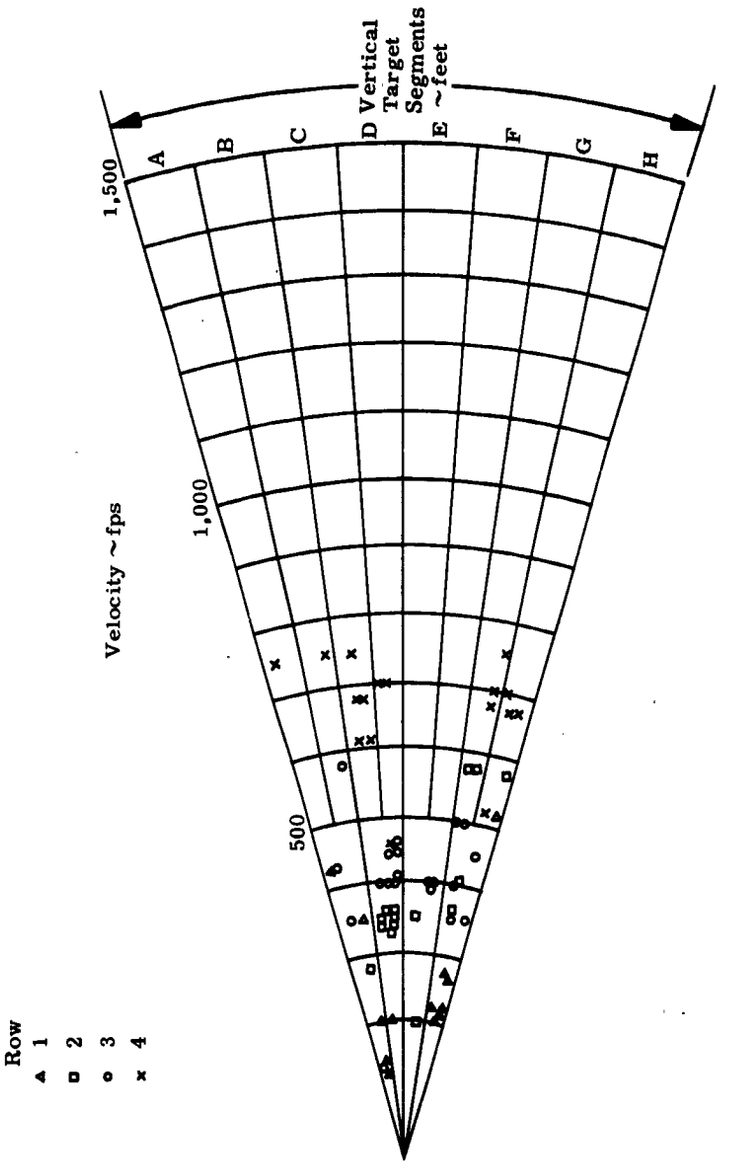


Figure 36. Velocity versus Radial Distribution, Round No. 37

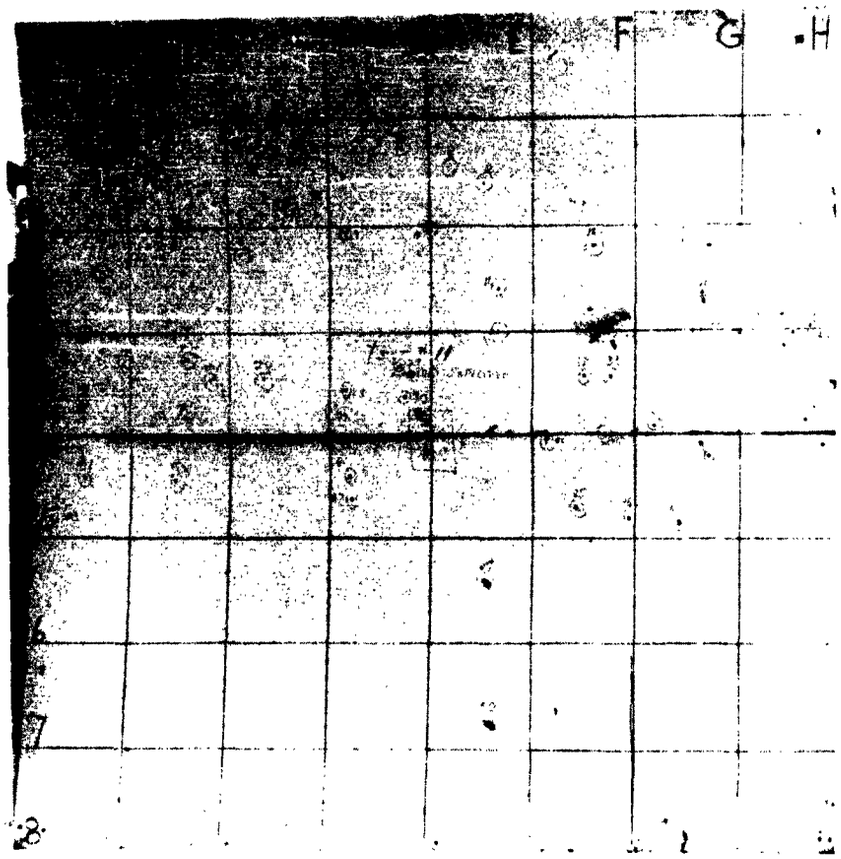


Figure 37. Impact Pattern, Round No. 11

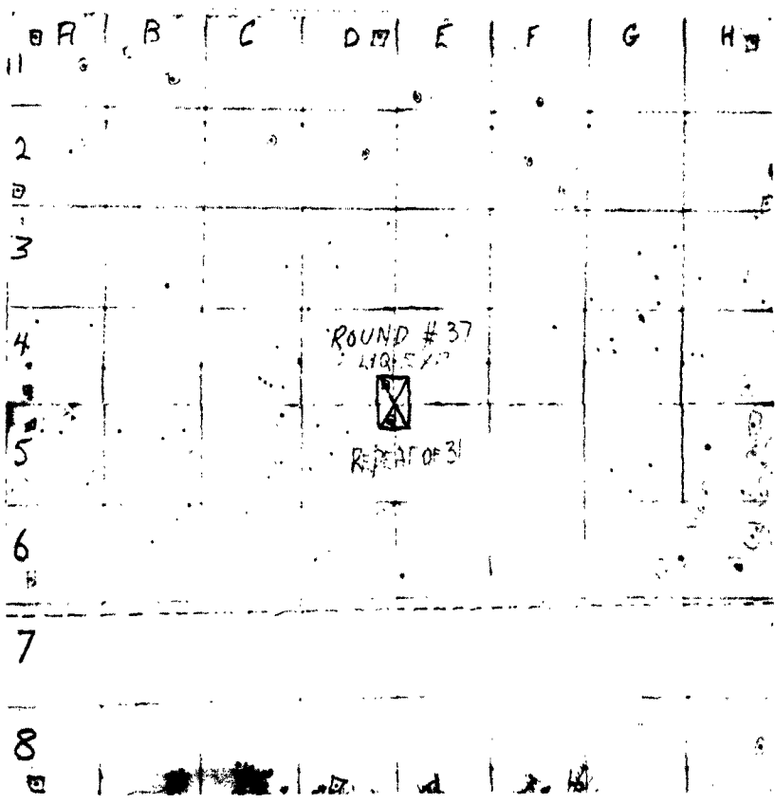


Figure 38. Impact Pattern, Round No. 37

# APPENDIX II

## BASIC DESIGN II DATA

This appendix summarizes design and test data pertinent to all Basic Design II warhead models.

TABLE 7

Basic Design II Data Summa

| Round No. | Round Description | | | | | | | | | Parameter Varied | Test Objectives |
|---|---|---|---|---|---|---|---|---|---|---|---|
| | Expl Mass (grams) | Frag Mass (grams) | End Plate Mass (grams) | C/M | Type | Cent. Burst Type | Cent. Burst Diam (in.) | Over Dim. Ht (in.) | Over Dim. Diam (in.) | | |
| 2 | 29.4 | 1366.0 | | 0.021 | Fig. 39 | C-4 | 0.75 | 3.5 | 2.8 | Basic design | Velocity gradient sphere breakup |
| 26 | 27.1 | 1984.0 | 445<br>457 | 0.014 | Fig. 39 | C-4 | 0.75 | 3.5 | 3.03 | 0.75 inch burster; Fragments packaged in paper tubes | Effect of tubes on pattern velocity gradient |
| 7 | 26.4 | 927.0 | 486<br>435 | 0.028 | Fig. 39 | C-4 | 0.75 | 3.5 | 3.03 | Center burster tube | Test effect of aluminum center burster tube |
| 8 | 26.4 | 927.0 | 467<br>495 | 0.028 | Fig. 39 | C-4 | 0.75 | 3.5 | 3.03 | Same as 7 | Same as 7 |
| 3 | 104.1 | 1573.0 | 748<br>750 | 0.071 | Fig. 39 | C-4 | 1.5 | 3.5 | 3.8 | Larger center burster | Higher fragment velocities |

## TABLE 7

## Basic Design II Data Summary

| Over Dim. | | Parameter Varied | Test Objectives | Results | | | | Conclusions and Comments |
|---|---|---|---|---|---|---|---|---|
| Ht (in.) | Diam (in.) | | | Impact Pattern | Beam Spy Angle | Velocity Gradient | Polar Plot | |
| 3.5 | 2.8 | Basic design | Velocity gradient sphere breakup | Fig. 50 | 40 Deg | 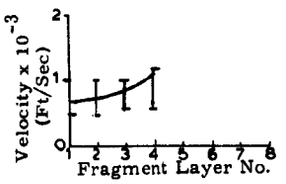  | Fig. 41 | Excessive beam spray; no sphere breakup; fragments move as a group |
| 3.5 | 3.03 | 0.75 inch burster; Fragments packaged in paper tubes | Effect of tubes on pattern velocity gradient | Fig. 51 | | 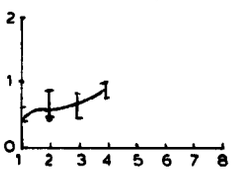  | Fig. 42 | Angular banding due to tube pack packaging; fragments move as a group |
| 3.5 | 3.03 | Center burster tube | Test effect of aluminum center burster tube | Fig. 52 | 17 Deg |   | Fig. 43 | No sphere breakup<br>Fragments move as a group<br>Slight reduction in velocity |
| 3.5 | 3.03 | Same as 7 | Same as 7 | | 16 Deg | 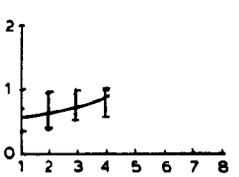  | Similar to Round 7 | Same as 7 |
| 3.5 | 3.8 | Larger center burster | Higher fragment velocities | Fig. 53 | 20 Deg | 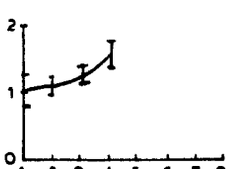  | Fig. 44 | Two inner fragment layers damaged<br>Higher velocities on outer rows achieved<br>Fragments move as a group |



TABLE 7 (Cont)

| Round No. | Round Description | | | | | | | | | Parameter Varied | Test Objectives | |
|---|---|---|---|---|---|---|---|---|---|---|---|---|
| | Expl Mass (grams) | Frag Mass (grams) | End Plate Mass (grams) | C/M | Type | Cent. Burst Type | Cent. Burst Diam (in.) | Over Dim. Ht (in.) | Over Dim. Diam (in.) | | | |
| 4 | 97.0 | 2267.0 | 734<br>750 | .042 | Fig. 39 | C-4 | 1.5 | 3.5 | 3.8 | Same as Round 3 | Same as Round 3 | |
| 27 | 155.8 | 4280.0 | 790<br>792 | 0.037 | Fig. 39 | C-4 | | | | Aluminum burster tube | Check results of Round 3 | |
| 13 | 42.0 | 1638.0 | 605<br>606 | 0.026 | Fig. 40 | C-4 | 1.37 | 2.5 | 3.5 | Shaped burster<br>Laminac buffer<br>Wafer fragment pack construction | Effect on beam spray Pattern<br>Velocity | |
| 14 | 43.8 | 1665.0 | 601<br>607 | 0.026 | Fig. 40 | C-4 | 1.37 | 2.5 | 3.5 | Same as 13 | Same as 13 | |
| 17 | 34.0 | 1219.0 | 607<br>611 | 0.025 | Fig. 40 | C-4 | 1.37 | 2.5 | 3.5 | Shaped burster<br>Laminac buffer<br>Tubular fragment pack | Observe effects of fragment packaging as compared to Round 13 | |

TABLE 7 (Cont)

| Parameter Varied | Test Objectives | Results | | | | Conclusions and Comments |
|---|---|---|---|---|---|---|
| | | Impact Pattern | Beam Spy Angle | Velocity Gradient | Polar Plot | |
| Same as Round 3 | Same as Round 3 | Fig. 54 | 35 Deg | 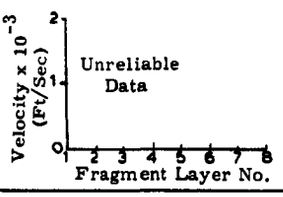  | | Unreliable data |
| Aluminum burster tube | Check results of Round 3 | Fig. 55 | | 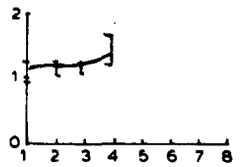 | Fig. 45 | Slight reduction in outer row fragment velocity Fragments move as a group |
| Shaped burster Laminac buffer Wafer fragment pack construction | Effect on beam spray Pattern Velocity | Fig. 56 | 14 Deg |  | Fig. 46 | Good beam spray Small gradient |
| Same as 13 | Same as 13 | Fig. 57 | 10 Deg | 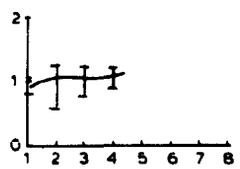 | Fig. 47 | Good beam spray Higher outer row velocities |
| Shaped burster Laminac buffer Tubular fragment pack | Observe effects of fragment packaging as compared to Round 13 | Fig. 58 | 16 Deg | 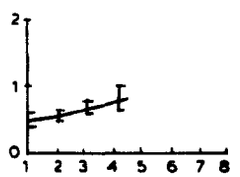 | Fig. 48 | Good beam spray Packaging technique may result in lower velocities |

TABLE 7 (Cont)

| Round No. | Round Description | | | | | | | | | Parameter Varied | Test Objectives |
|---|---|---|---|---|---|---|---|---|---|---|---|
| | Expl Mass (grams) | Frag Mass (grams) | End Plate Mass (grams) | C/M | Type | Cent. Burst Type | Cent. Burst Diam (in.) | Over Dim. Ht (in.) | Over Dim. Diam (in.) | | |
| 18 | 41.2 | 1233.0 | 604<br>612 | 0.032 | Fig. 40 | C-4 | 1.37 | 2.5 | 3.5 | Shaped burster<br>Air interface buffer<br>Tubular fragment pack | Effects of different interface buffer |
| 28 | 28.5 | 336.6<br>Rods<br>1048.0<br>1384.6 | 785.0 | 0.0171 | Fig. 39 | C-4 | 0.75 | 3.5 | 2.873 | Hexagonal fragments | Velocity gradient Pattern |
| 29 | 36.9 | 646<br>Rods<br>1307<br>1953 | 1406 | 0.0174 | Fig. 40 | C-4 | 1.37 to 0.5 to 1.37 Hyper-boloid | 3.5 | 3.8 | Hexagonal fragments<br>Shaped burster | Same as 28 |
| 32 | 30.5 | 1780 | 900 | 0.053 | Fig. 39 | C-4 | 0.75 | 3.5 | 3.1 | Cubic fragments | Same as 28 |
| 33 | 40.5 | 2160 | 1174 | 0.0795 | Fig. 40 | C-4 | 1.37 to 0.5 to 1.37 Hyper-boloid | 3.5 | 3.6 | Cubic fragments<br>Shaped burster | Same as 28 |

TABLE 7 (Cont)

| irst Diam (in.) | Over Dim. Ht (in.) | Over Dim. Diam (in.) | Parameter Varied | Test Objectives | Results: Impact Pattern | Results: Beam Spy Angle | Results: Velocity Gradient | Results: Polar Plot | Conclusions and Comments |
|---|---|---|---|---|---|---|---|---|---|
| 1.37 | 2.5 | 3.5 | Shaped burster<br>Air interface buffer<br>Tubular fragment pack | Effects of different interface buffer | Fig. 59 | 18 Deg | 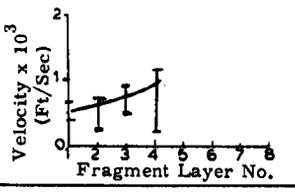 | Fig. 49 | Good gradient potential |
| 0.75 | 3.5 | 2.873 | Hexagonal fragments | Velocity gradient Pattern | Fig. 60 | 16 Deg | 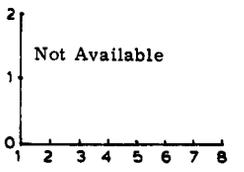 | Not available | Apparent high average velocities<br>Good beam spray |
| 1.37 to 0.5 to 1.37 Hyper-boloid | 3.5 | 3.8 | Hexagonal fragments<br>Shaped burster | Same as 28 | Fig. 61 | 12 Deg | 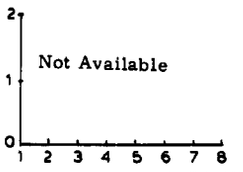 | Not available | Same as 28 |
| 0.75 | 3.5 | 3.1 | Cubic fragments | Same as 28 | Fig. 62 | 20 Deg | 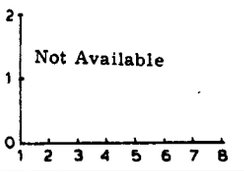 | Not available | Same as 28 |
| 1.37 to 0.5 to 1.37 Hyper-boloid | 3.5 | 3.6 | Cubic fragments<br>Shaped burster | Same as 28 | Fig. 63 | 16 Deg | 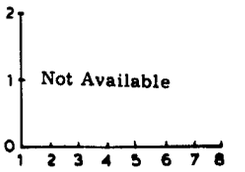 | Not available | Same as 28 |

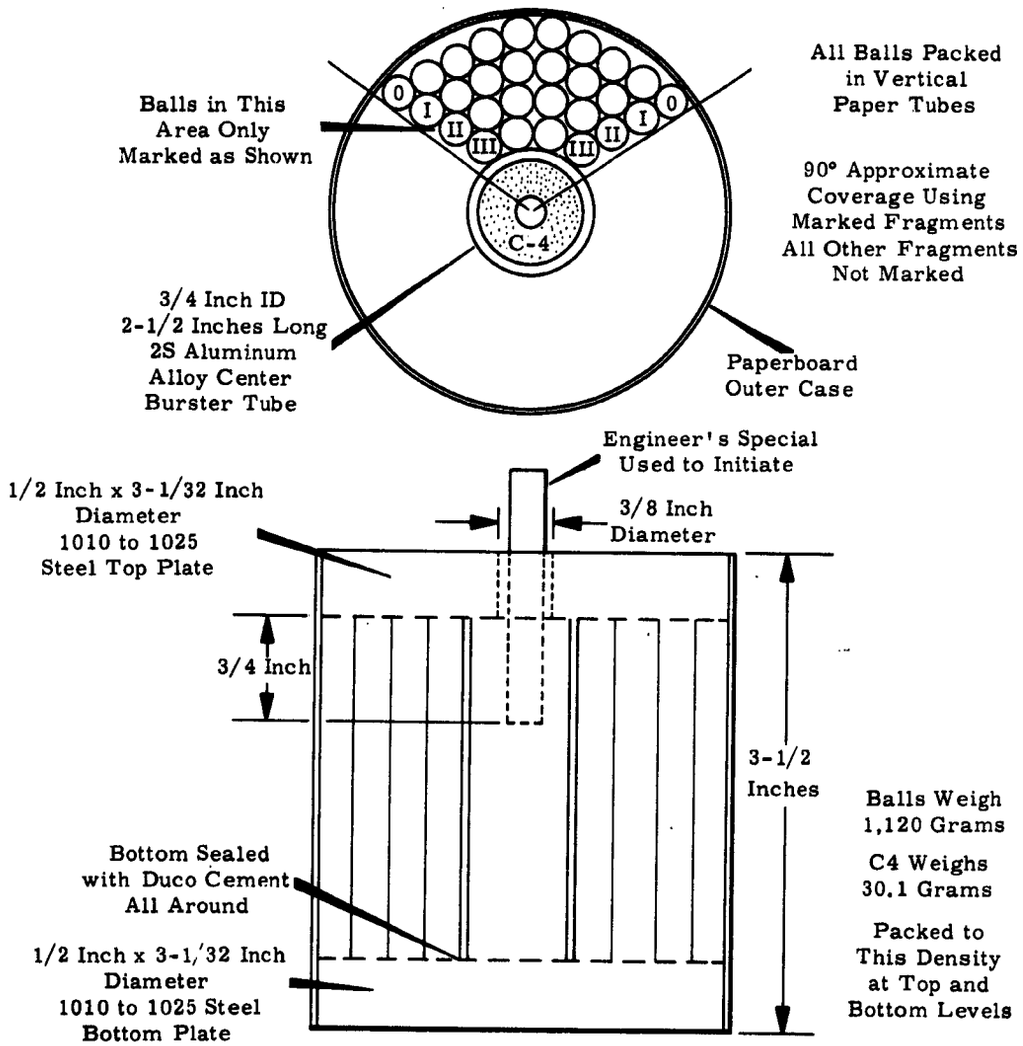


Figure 39. Test Model Design Rounds No. 7 and 8

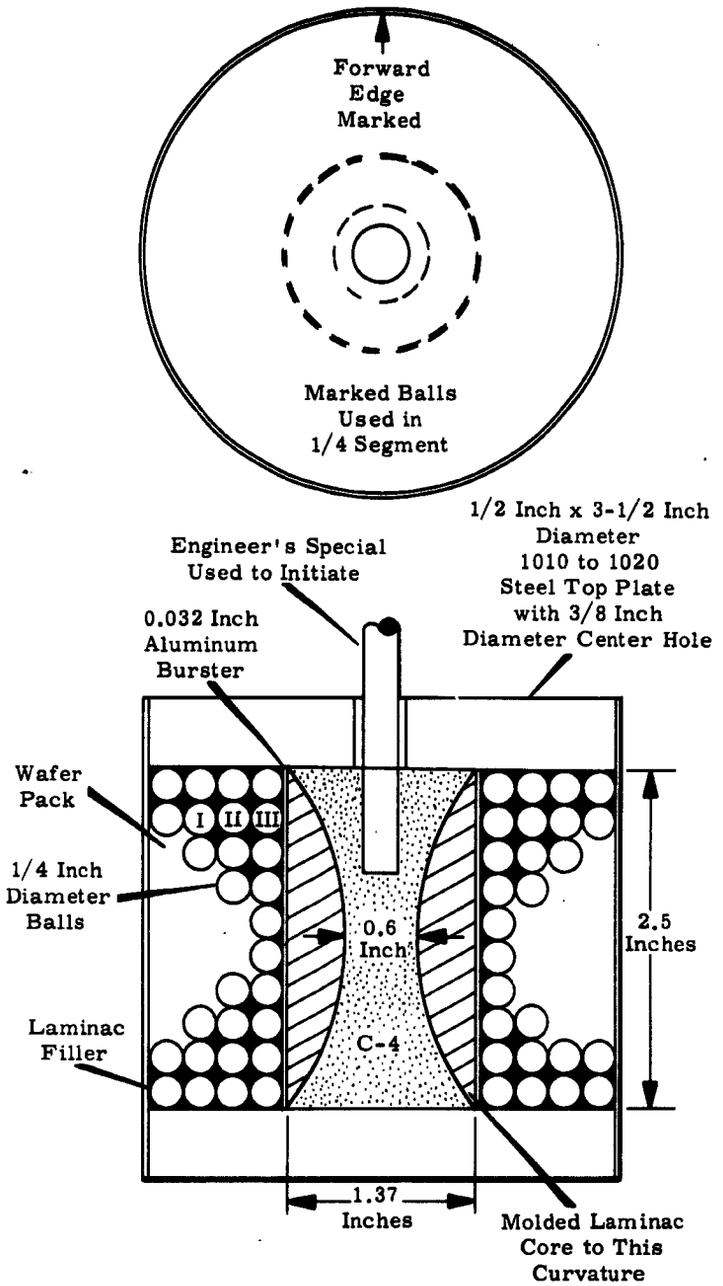


Figure 40. Test Model Design Rounds No. 13 and 14

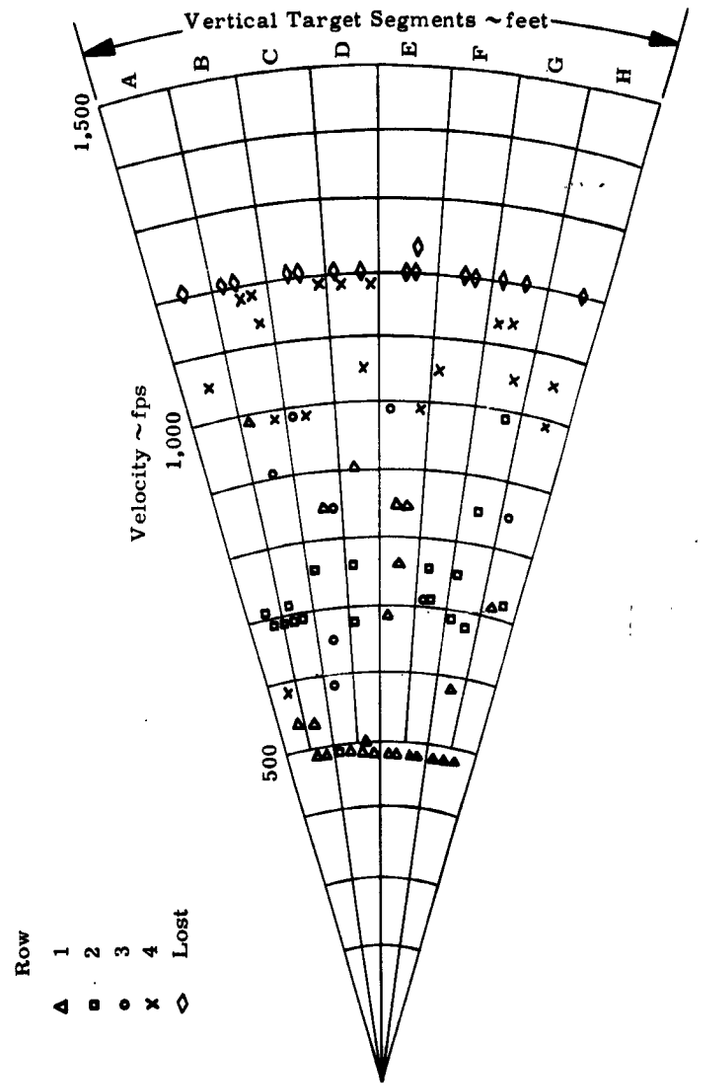


Figure 41. Velocity versus Radial Distribution, Round No. 2

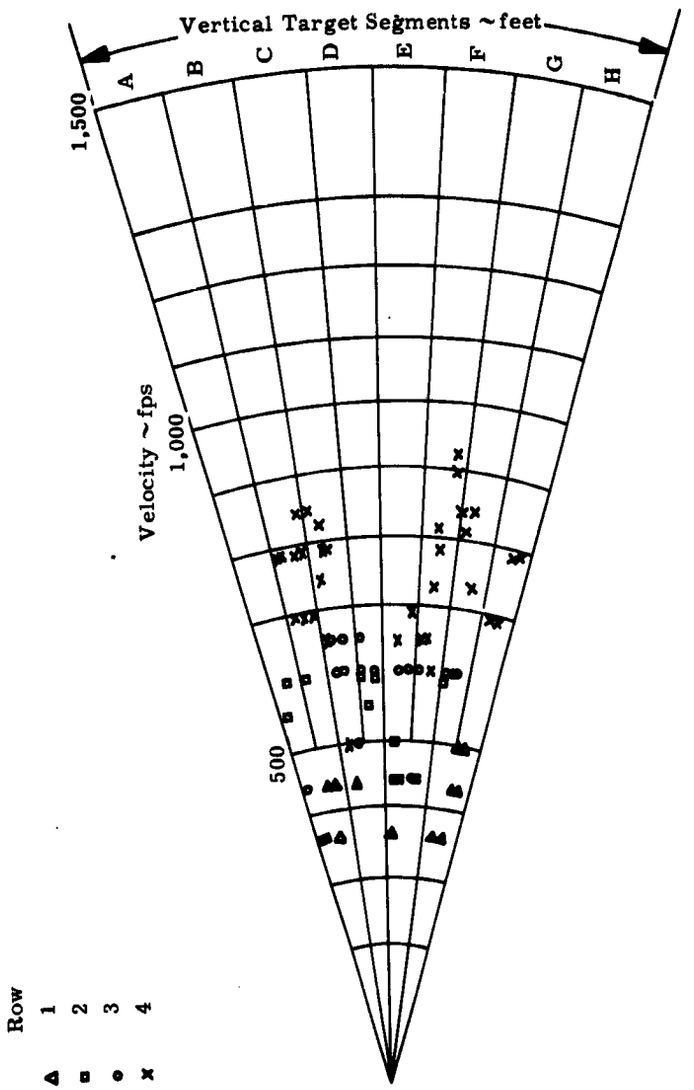


Figure 42. Velocity versus Radial Distribution, Round No. 26

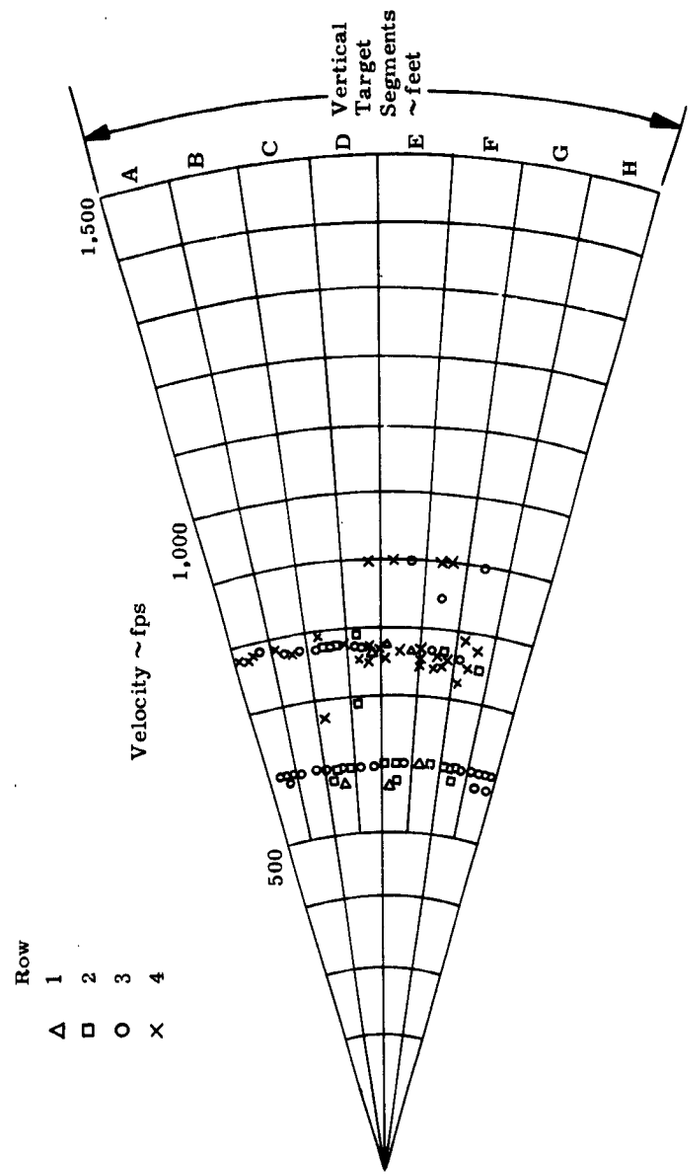


Figure 43. Velocity versus Radial Distribution, Round No. 7

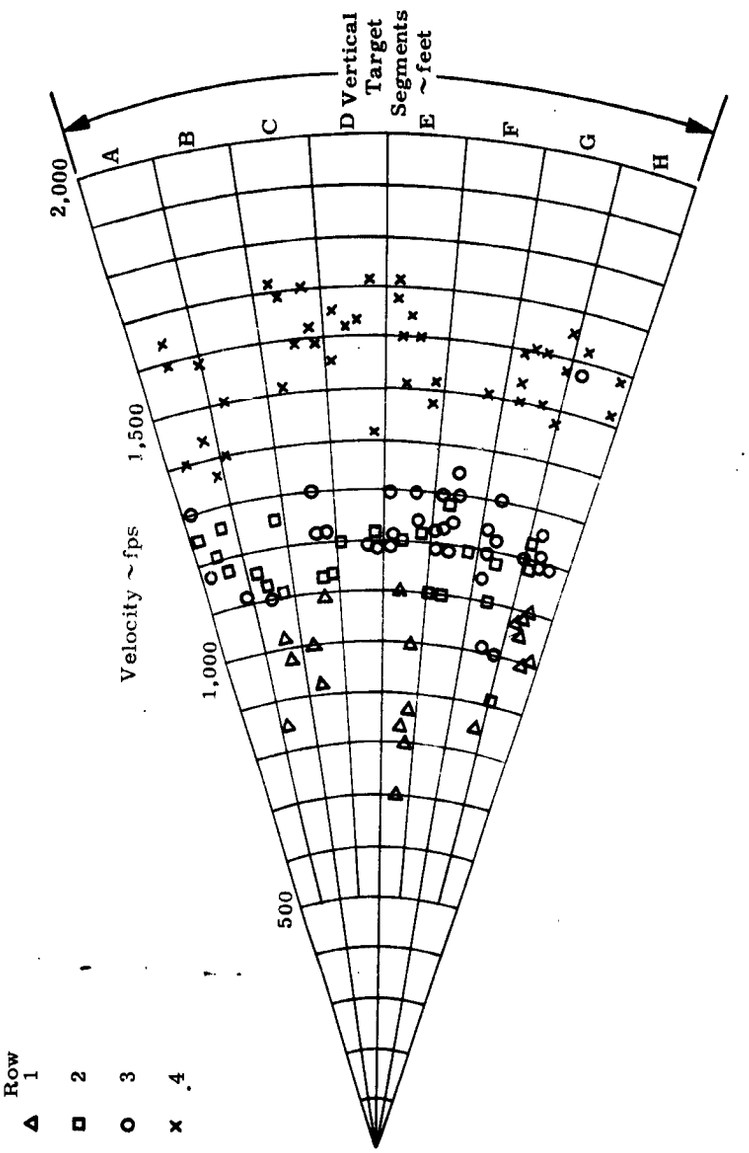


**Figure 44.** Velocity versus Radial Distribution, Round No. 3

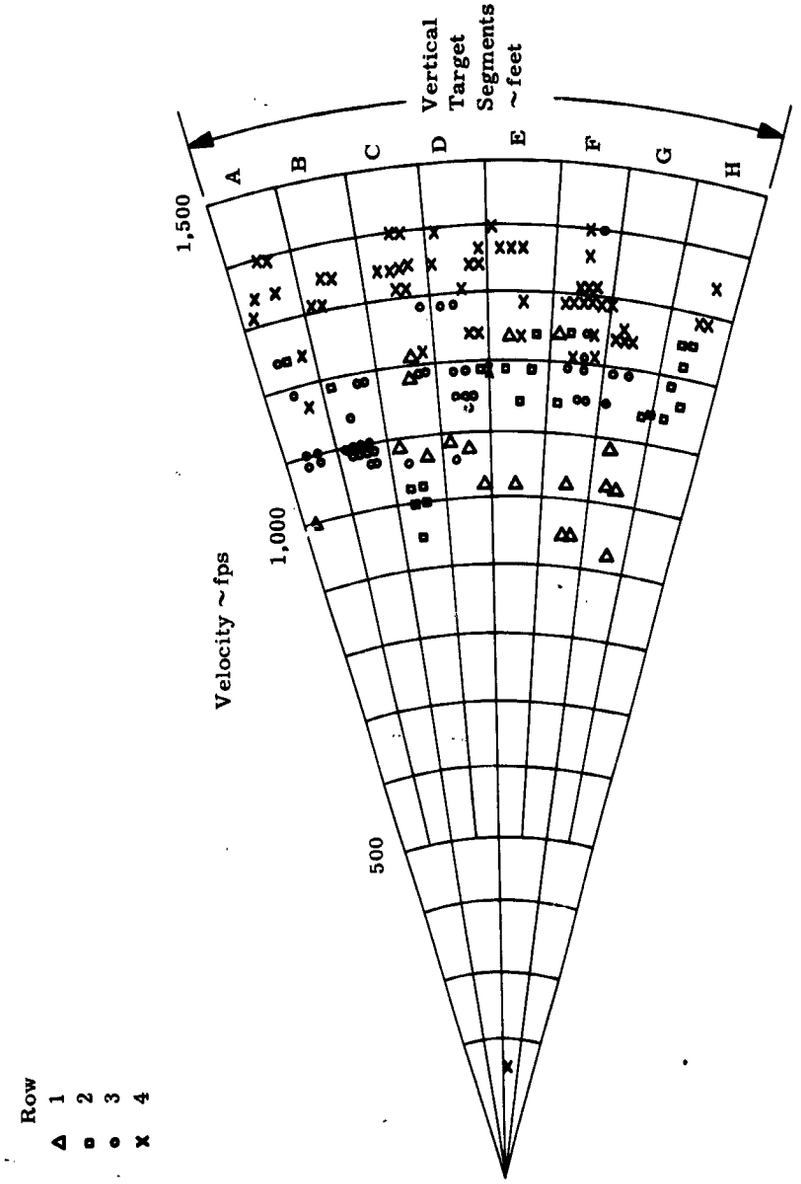


Figure 45. Velocity versus Radial Distribution, Round No. 27

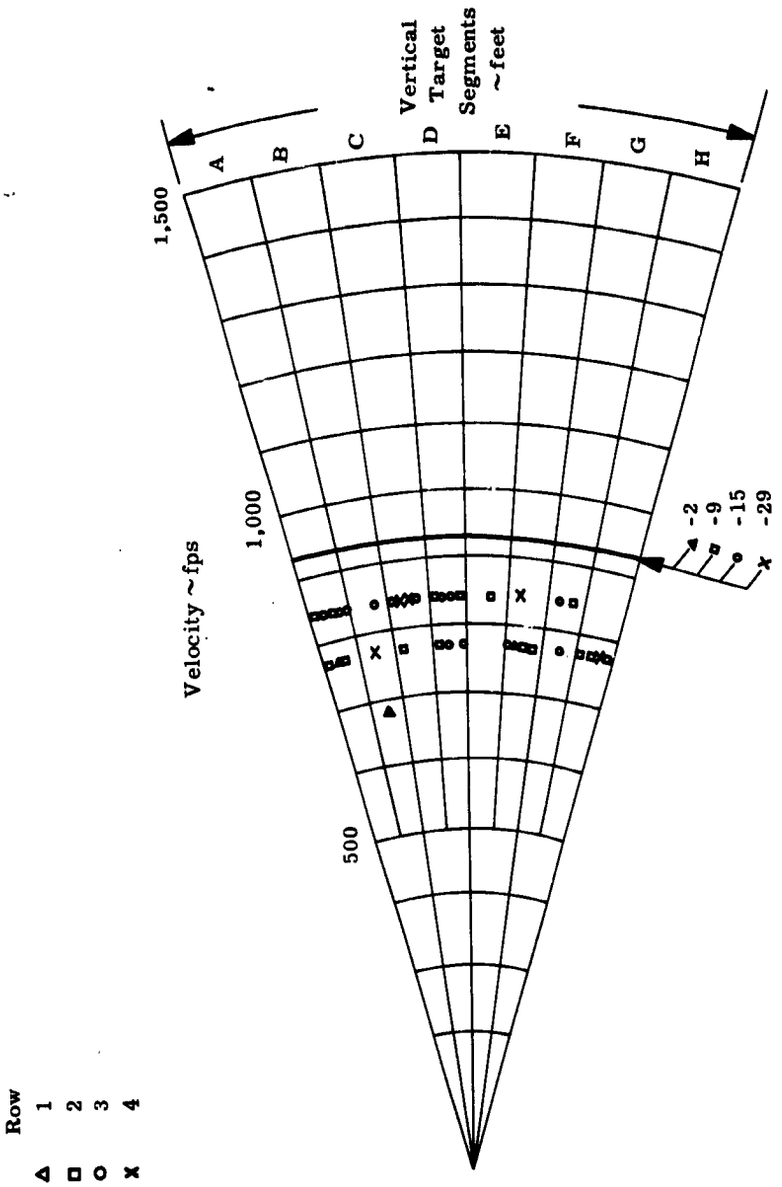


Figure 46. Velocity versus Radial Distribution, Round No. 13

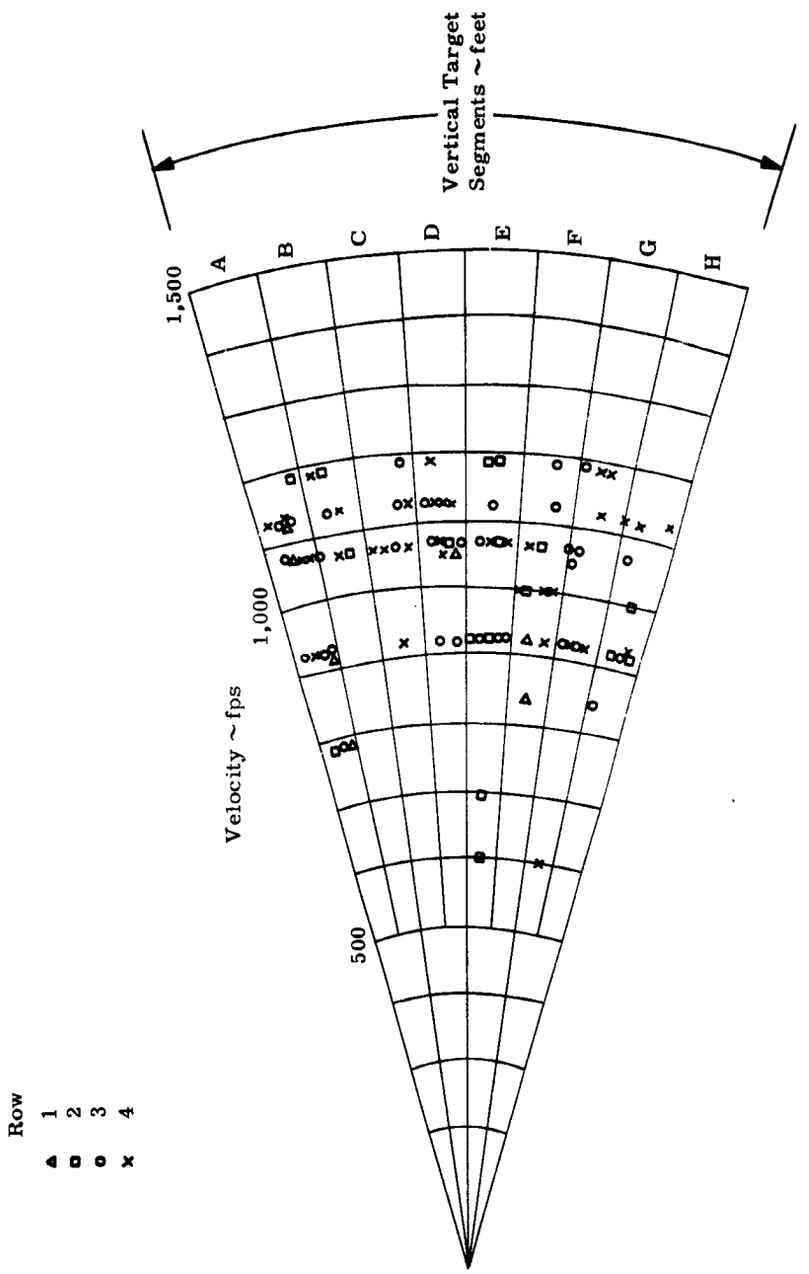


Figure 47. Velocity versus Radial Distribution, Round No. 14

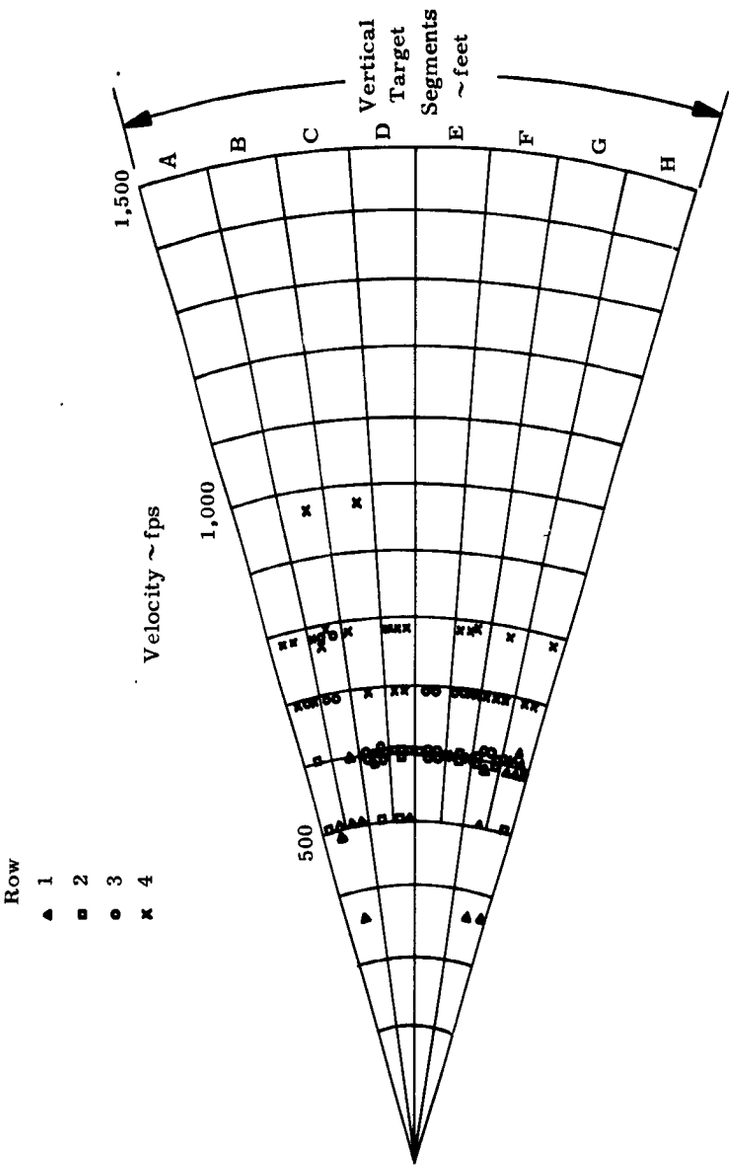


Figure 48. Velocity versus Radial Distribution, Round No. 17

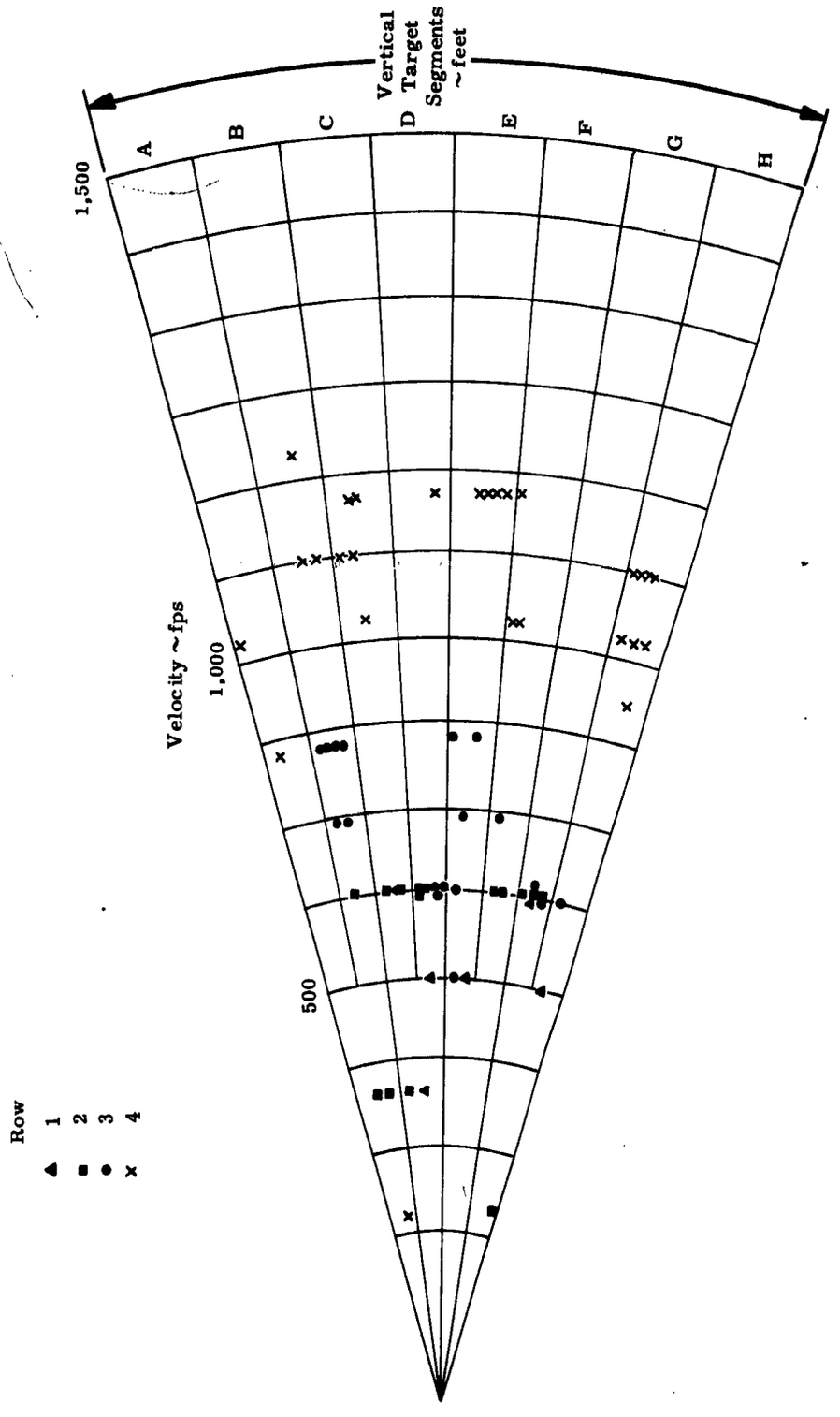


Figure 49. Velocity versus Radial Distribution, Round No. 18

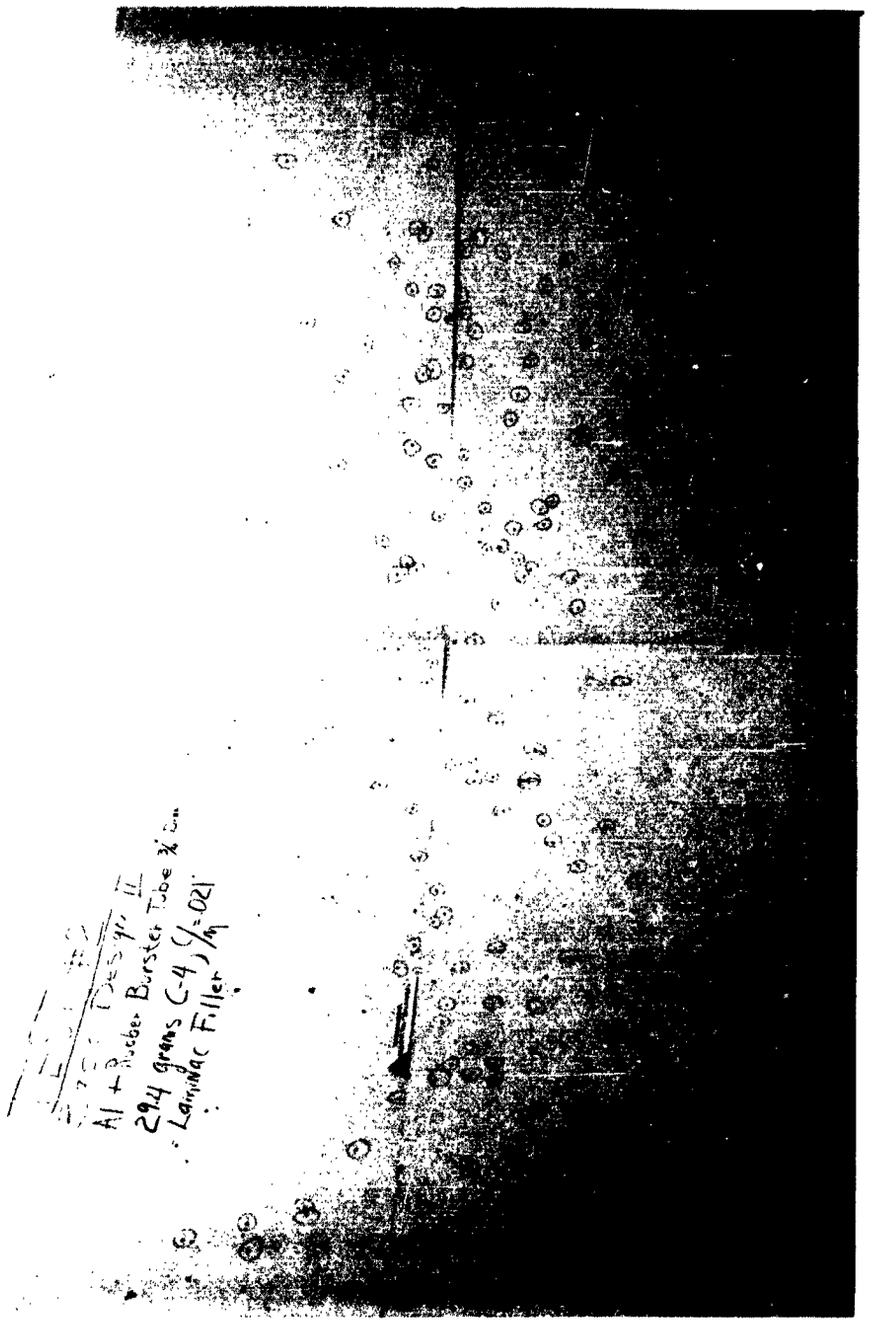


Figure 50. Impact Pattern Round No. 2

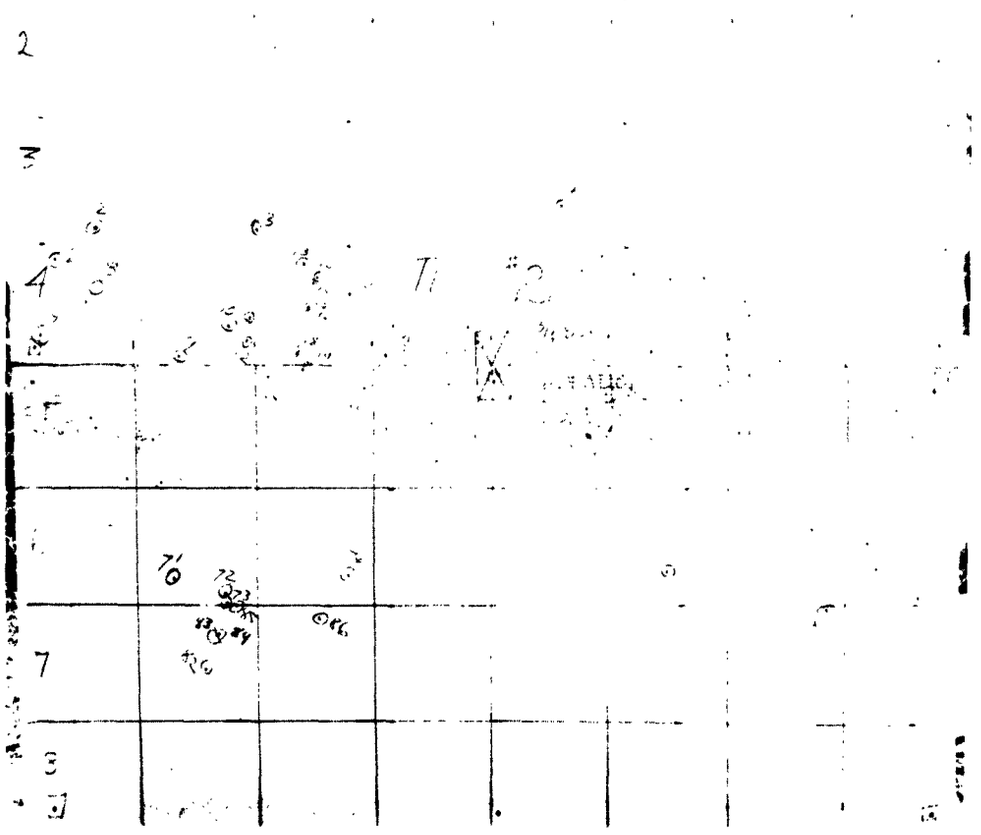

Figure 51. Impact Pattern Round No. 26

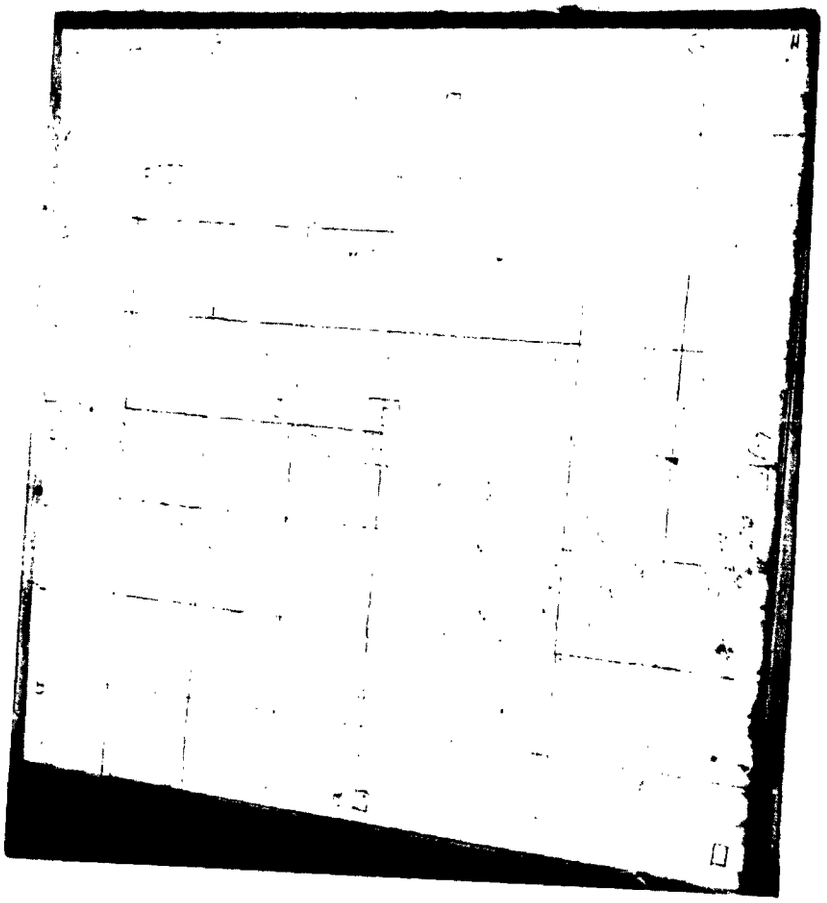

Figure 52. Impact Pattern Round No. 7

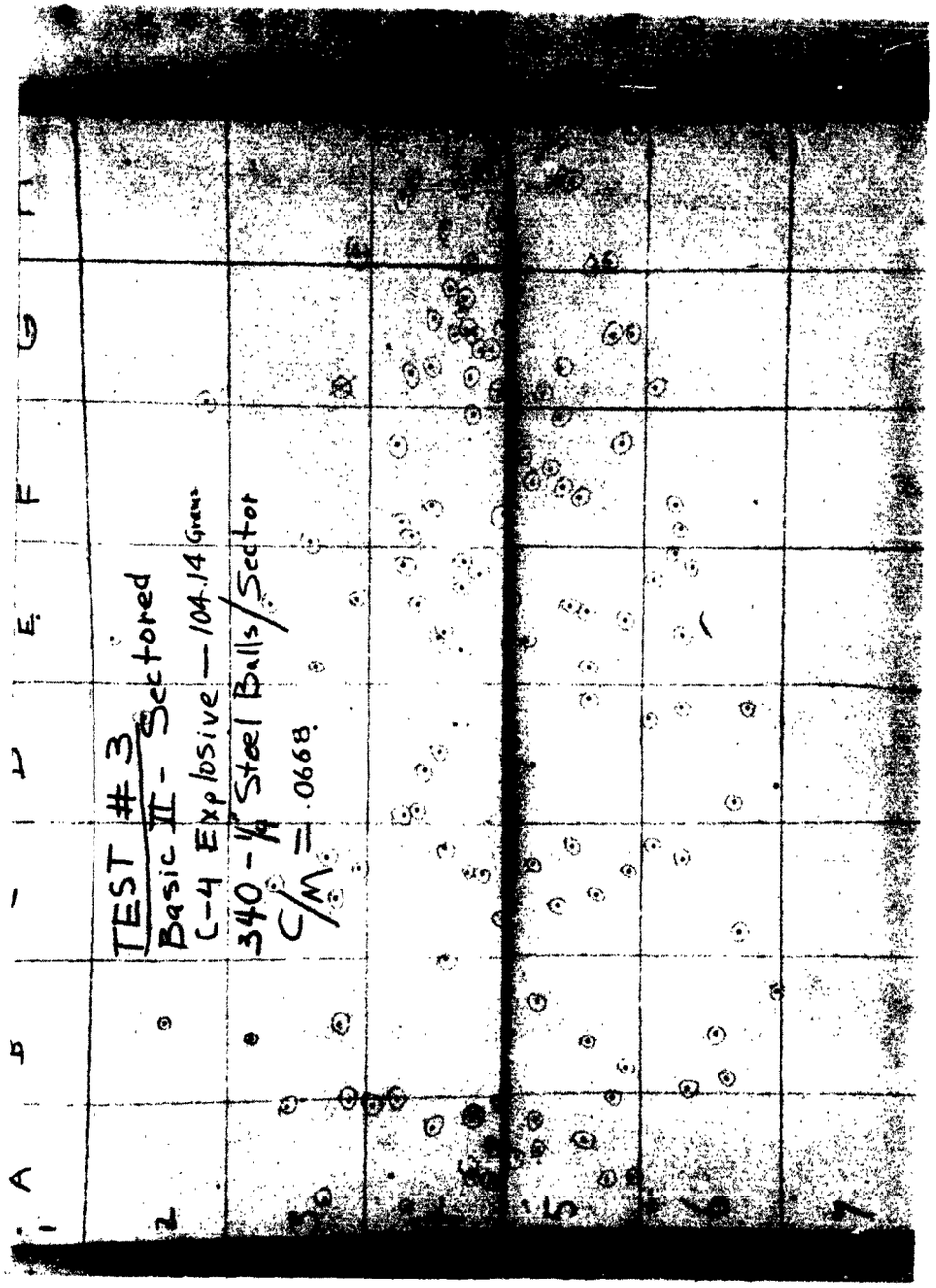


Figure 53. Impact Pattern Round No. 3

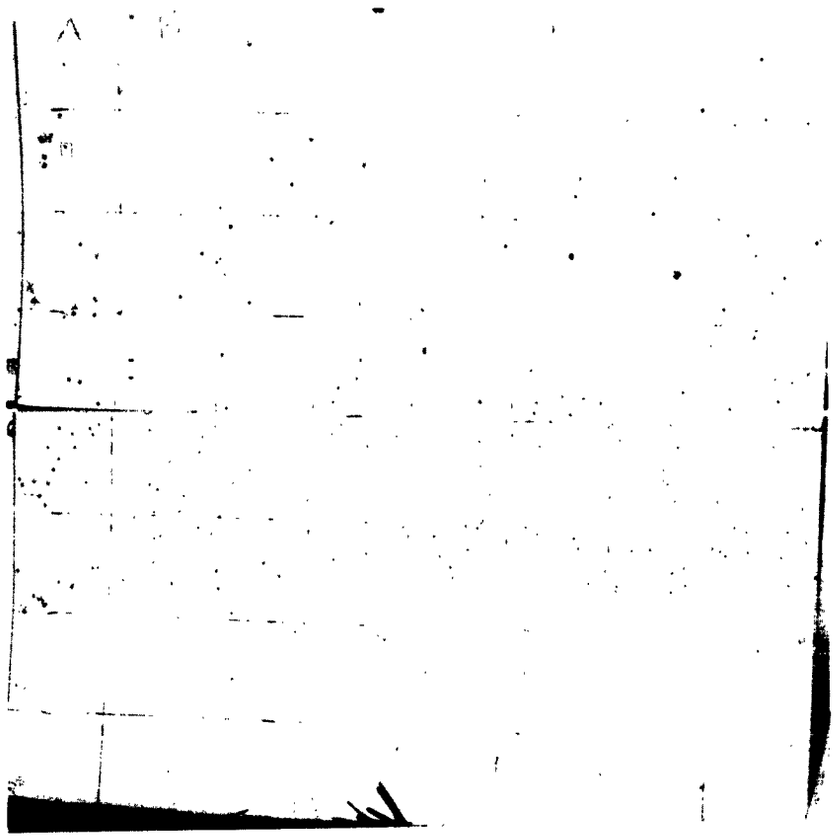

Figure 54. Impact Pattern Round No. 4

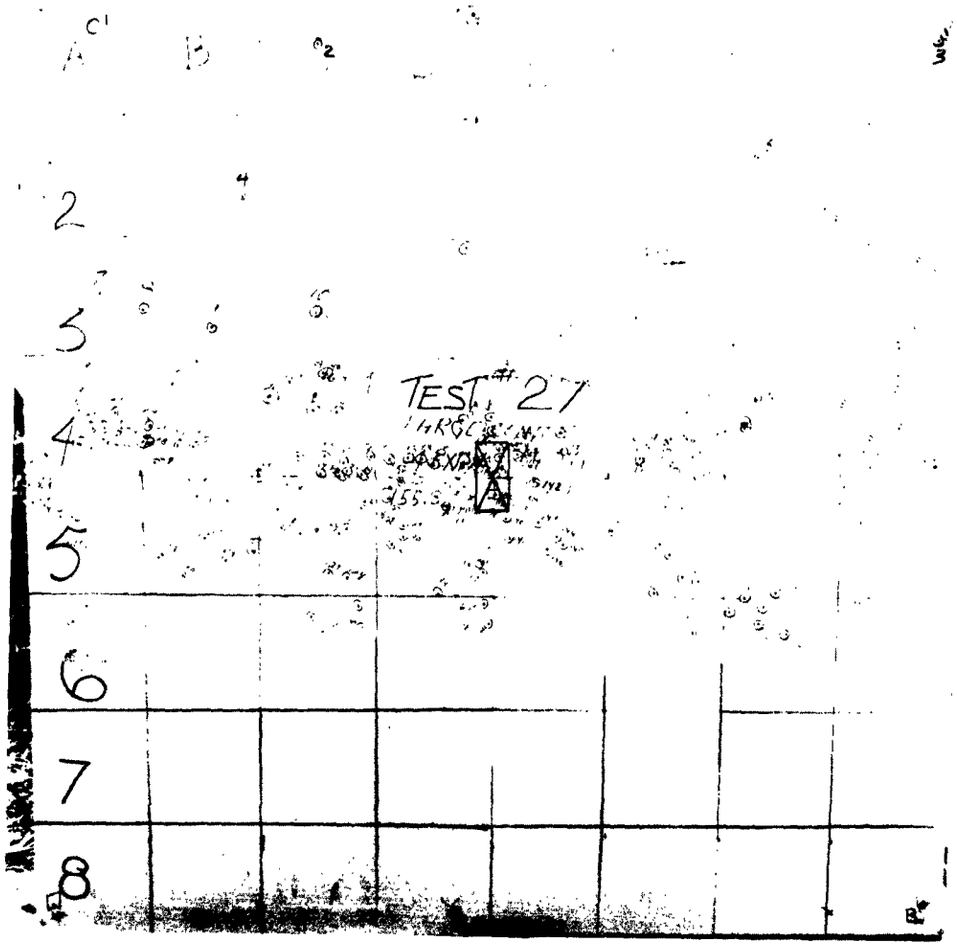


Figure 55. Impact Pattern Round No. 27

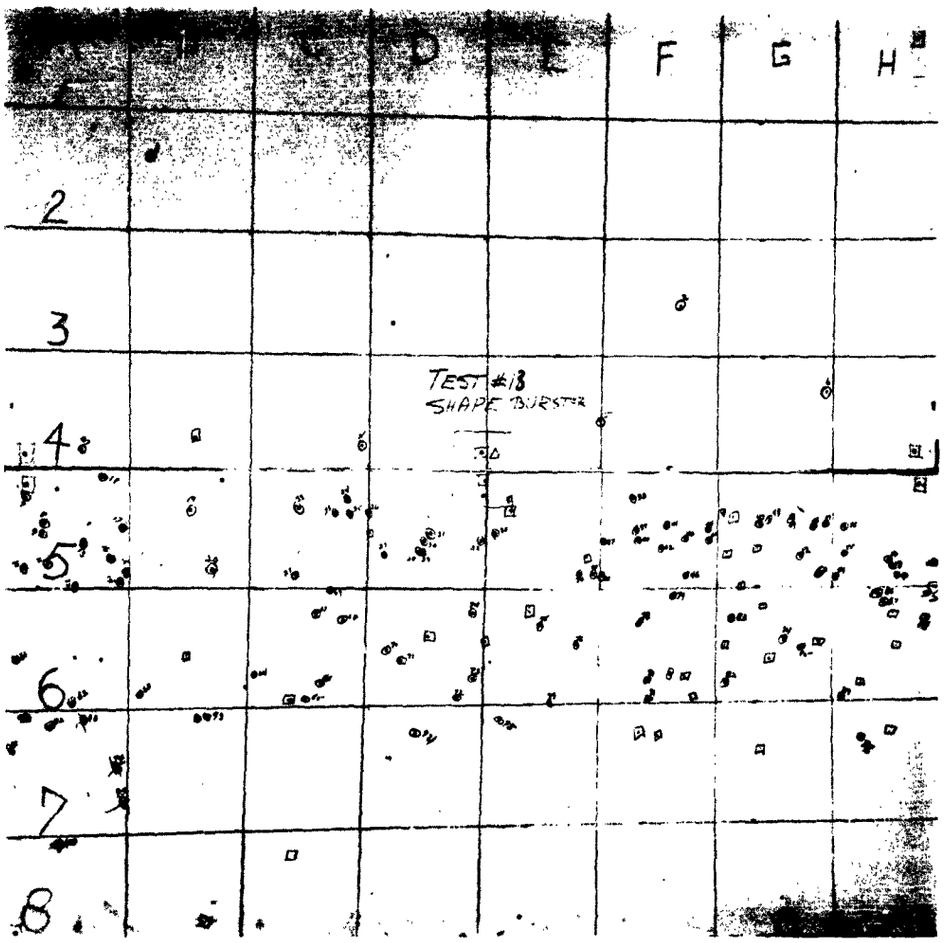


Figure 56. Impact Pattern Round No. 13

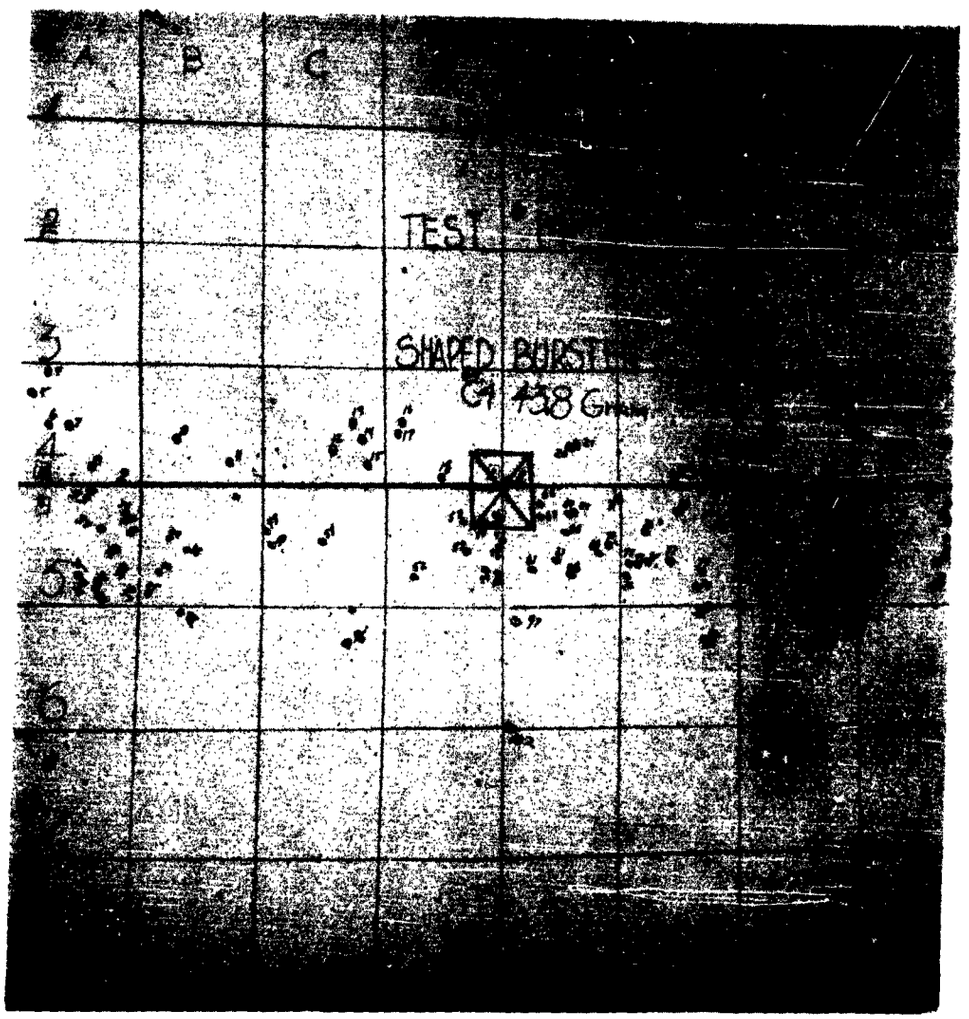


Figure 57. Impact Pattern Round No. 14

Figure 58. Impact Pattern Round No. 17

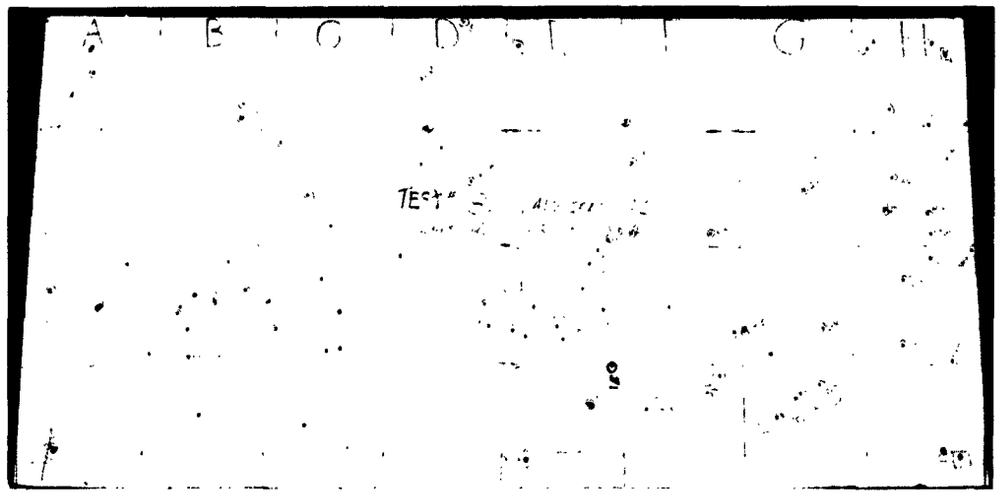


Figure 59. Impact Pattern Round No. 18

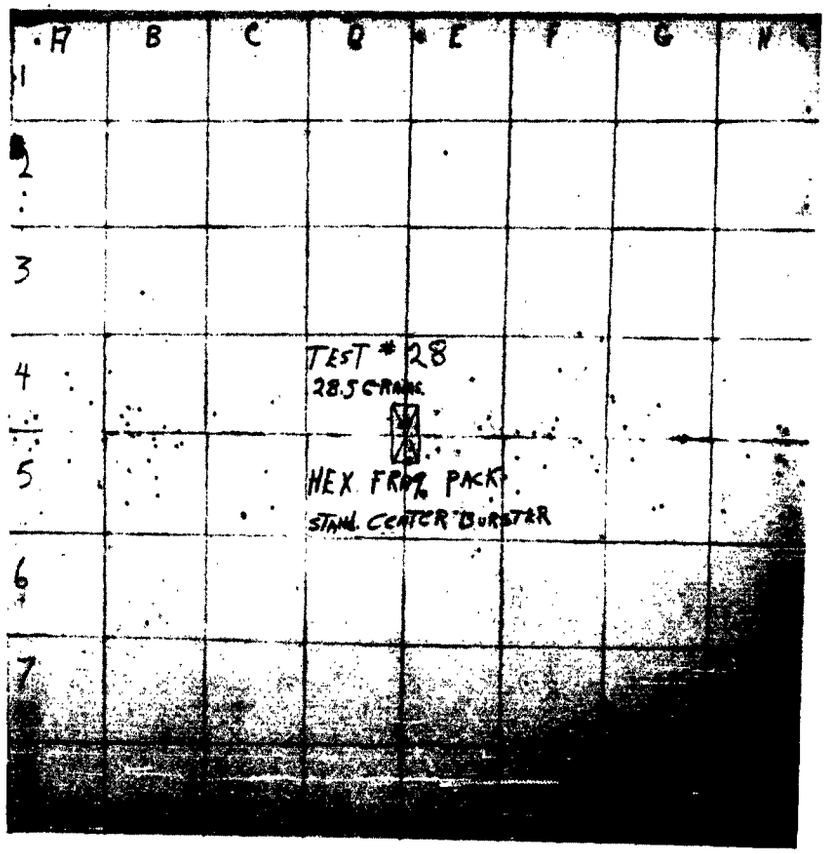


Figure 60. Impact Pattern Round No. 28

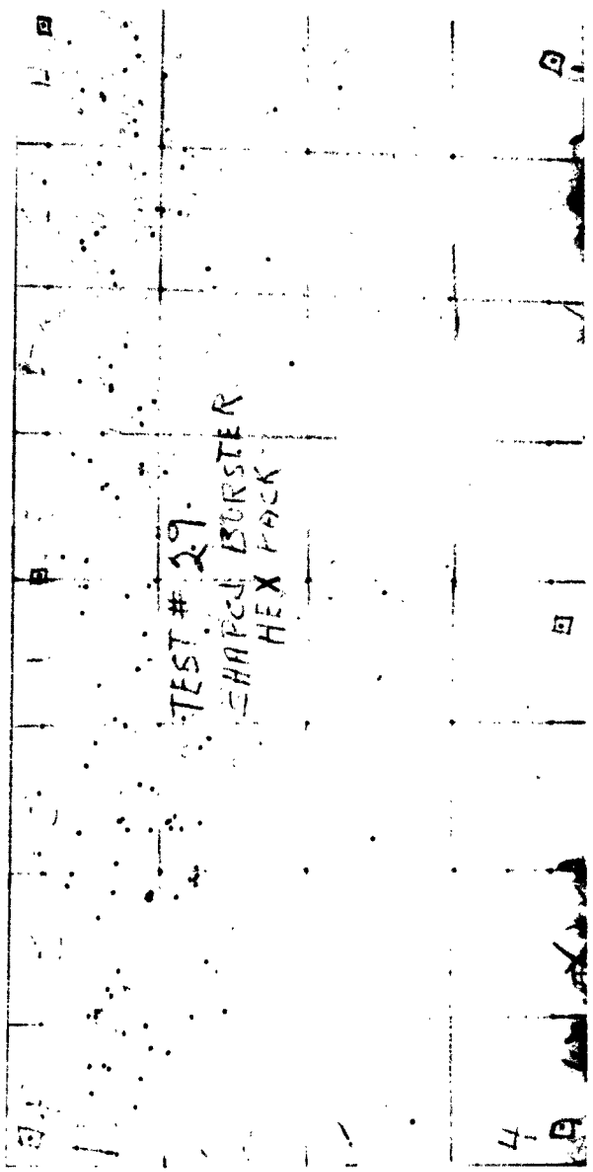


Figure 61. Impact Pattern Round No. 29

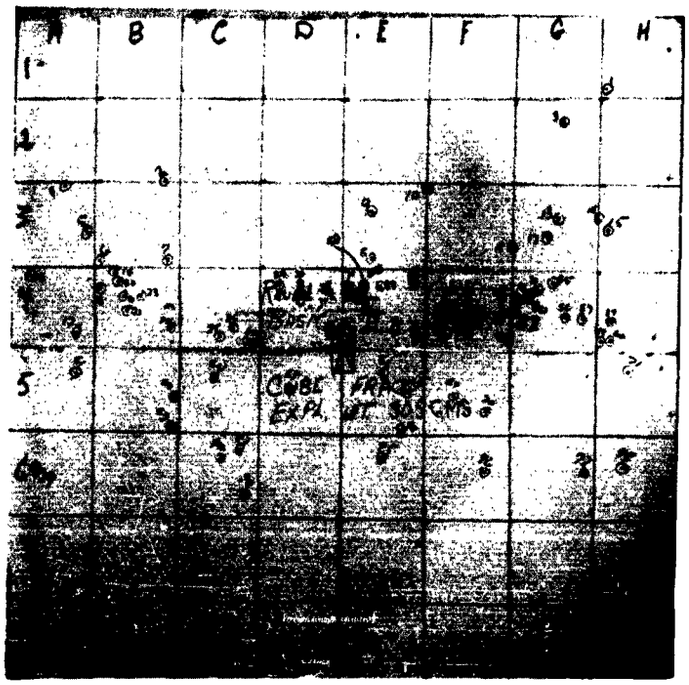


Figure 62. Impact Pattern Round No. 32

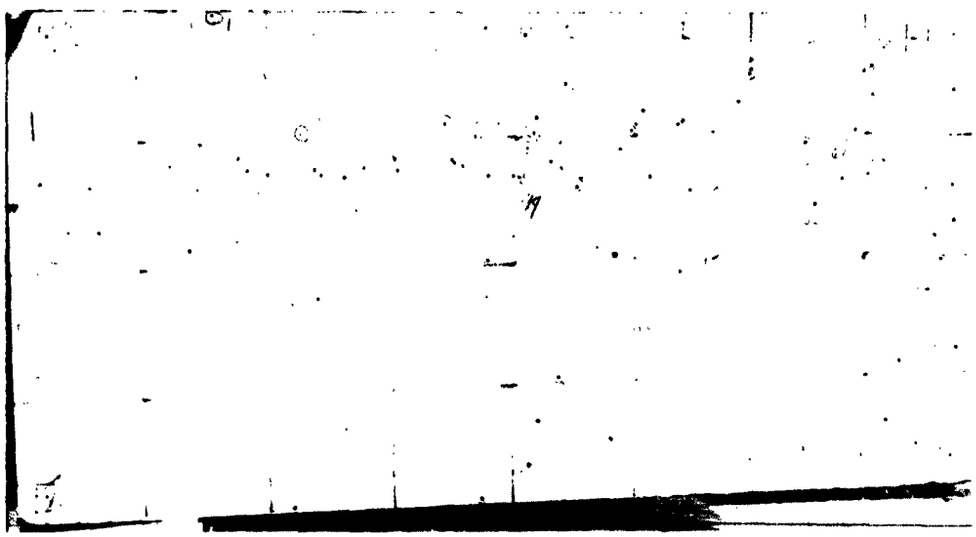

Figure 63. Impact Pattern Round No. 33

# APPENDIX III

## BASIC DESIGN III DATA

This appendix summarizes design and test data pertinent to all Basic Design III warhead models.

## TABLE 8

### Basic Design III Data Summary

| Round No. | Round Description | | | | | | | | | Parameter Varied | Test Objectives |
|---|---|---|---|---|---|---|---|---|---|---|---|
| | Expl Mass (grams) | Frag Mass (grams) | End Plate Mass (grams) | C/M | Type | Cent. Burst Type | Cent. Burst Diam (in.) | Over Dim. Ht (in.) | Over Dim. Diam (in.) | | |
| 9 | 45.7 | 1390 | 526 | 0.033 | Fig. 64 | C-4 | 0.75 | 3.5 | 3.25 | Thin aluminum buffers between fragment layers | Check pattern, velocity gradient, and fragment breakup for Basic Design III |
| 10 | 44.1 | 1419 | 532<br>539 | 0.031 | Fig. 64 | C-4 | 0.75 | 3.5 | 3.25 | Same as round 9 | |
| 15 | 38.6 | 1680 | 607<br>613 | 0.021 | Fig. 65 | C-4 | 0.75 | 3.5 | 3.5 | Variable thickness buffers of aluminum and rubber<br>Fragments in paper tubes | Buffering effects on velocity and pattern |
| 16 | 42.3 | 1872 | 608<br>613 | 0.022 | Fig. 65 | C-4 | 0.75 | 3.5 | 3.5 | Same as round 15 except fragments not in tubes | Same as 15 |
| 21 | 42.0 | 4025 | | 0.010 | Fig. 66 | C-4 | 1.37 | 2.5 | 4.38 | Shaped burster (hyperboloid) | Same as 15 |
| 22 | 42.0 | 4110 | | 0.009 | | C-4 | 1.37 | 2.5 | 4.38 | 21 aluminum and rubber buffers and 36 aluminum buffers used | |
| 36 | 26.8 | 3742 | | 0.007 | | C-4 | 1.37 | 2.5 | 4.38 | Paper tubes used in packing | |

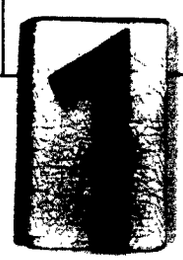

## TABLE 8

### Basic Design III Data Summary

| Burst Diam (in.) | Over Dim. Ht (in.) | Over Dim. Diam (in.) | Parameter Varied | Test Objectives | Results: Impact Pattern | Results: Beam Spy Angle | Results: Velocity Gradient | Results: Polar Plot | Conclusions and Comments |
|---|---|---|---|---|---|---|---|---|---|
| 0.75 | 3.5 | 3.25 | Thin aluminum buffers between fragment layers | Check pattern, velocity gradient, and fragment breakup for Basic Design III | | 16 Deg | 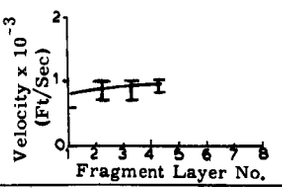  | Fig. 67 | No fragment breakup, good beam spray<br>Fragments move as a group<br>Very small velocity gradient |
| 0.75 | 3.5 | 3.25 | Same as round 9 | | | 16 Deg |   | Fig. 68 | Same as round 9 |
| 0.75 | 3.5 | 3.5 | Variable thickness buffers of aluminum and rubber<br>Fragments in paper tubes | Buffering effects on velocity and pattern | Fig. 74 | 20 Deg | 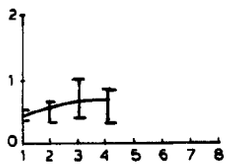  | Fig. 69 | No velocity gradient<br>Fragments move as a group<br>Apparently no significant effects caused by difference in buffering material and thickness variations |
| 0.75 | 3.5 | 3.5 | Same as round 15 except fragments not in tubes | Same as 15 | Fig. 75 | | 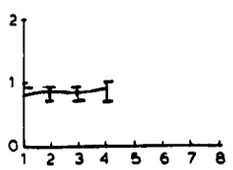  | Fig. 70 | Slight gradient improvement<br>Fragments still move as a solid group |
| 1.37 | 2.5 | 4.38 | Shaped burster (hyperboloid) | Same as 15 | Fig. 76 | 14 Deg | 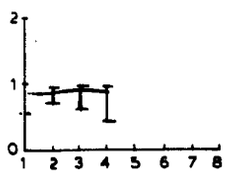  | Fig. 71 | No significant difference in three rounds |
| 1.37 | 2.5 | 4.38 | 21 aluminum and rubber buffers and 36 aluminum buffers used | | Fig. 77 | 15 Deg | | Fig. 72 | Small gradient<br>Angular banding due to tube pack |
| 1.37 | 2.5 | 4.38 | Paper tubes used in packing | | Fig. 78 | 11 Deg | | Fig. 73 | Good beam spray control<br>No noticeable difference in buffering materials |

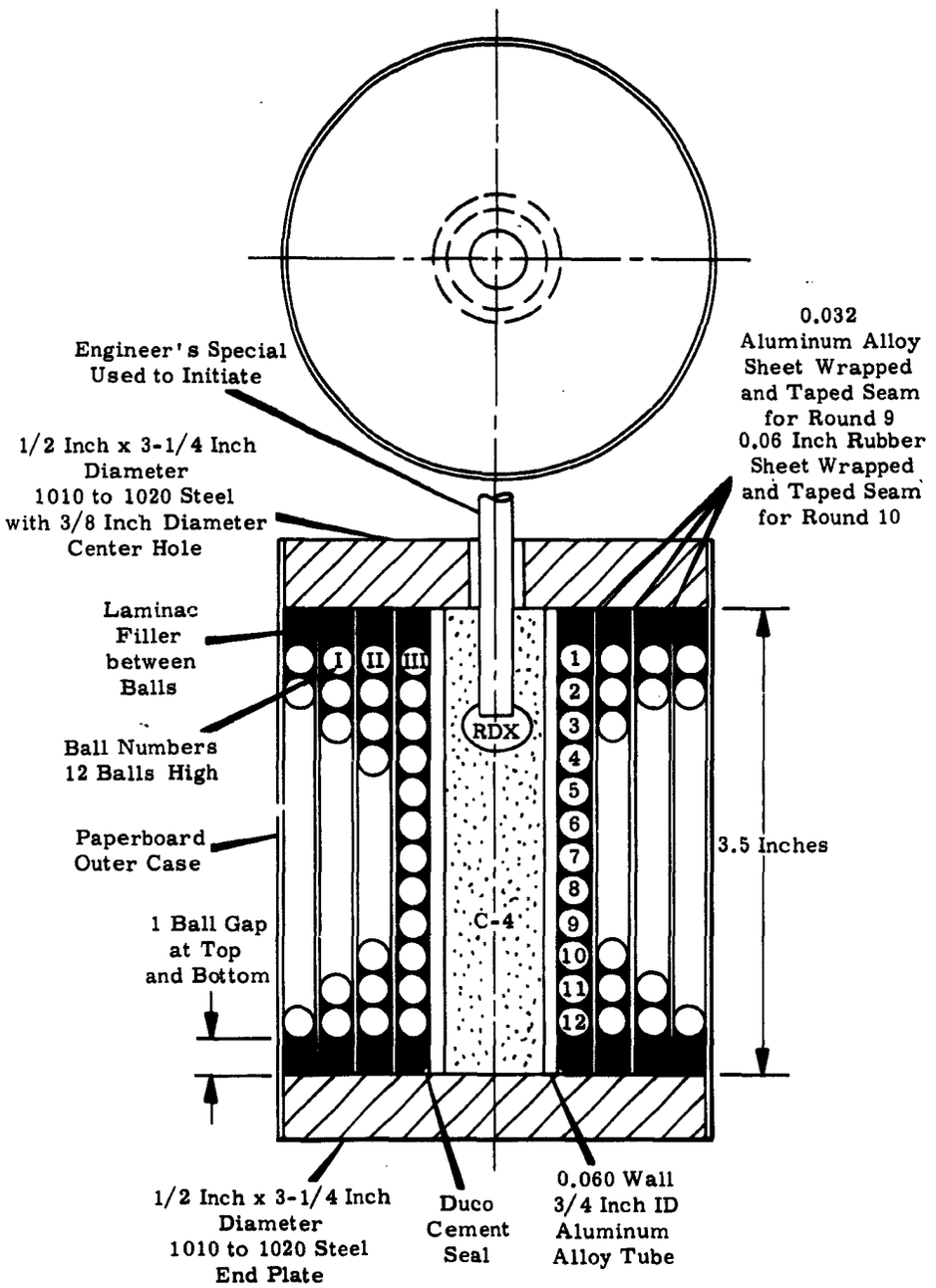


Figure 64. Test Model Design, Rounds No. 9 and 10

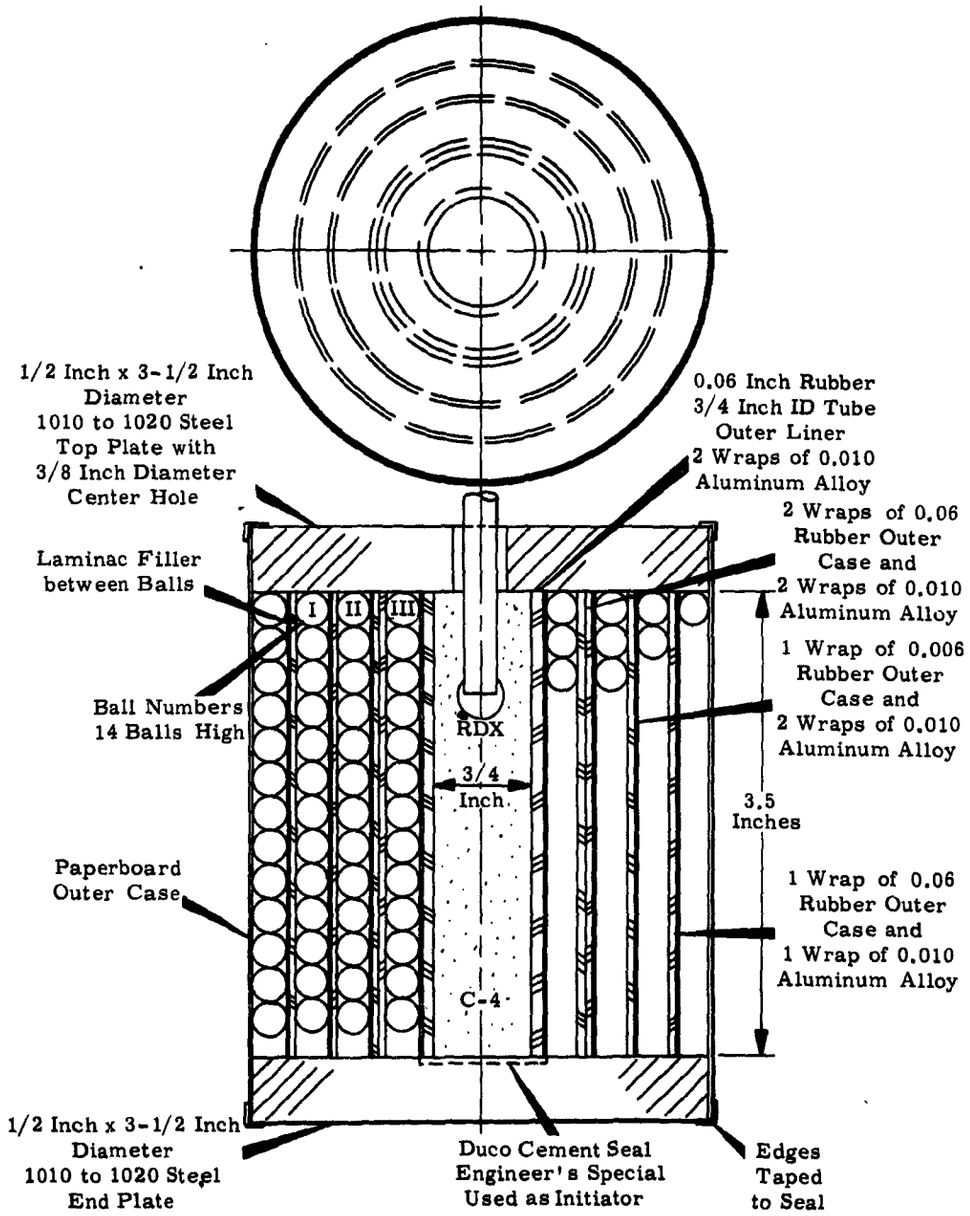


Figure 65. Test Model Design, Rounds No. 15 and 16

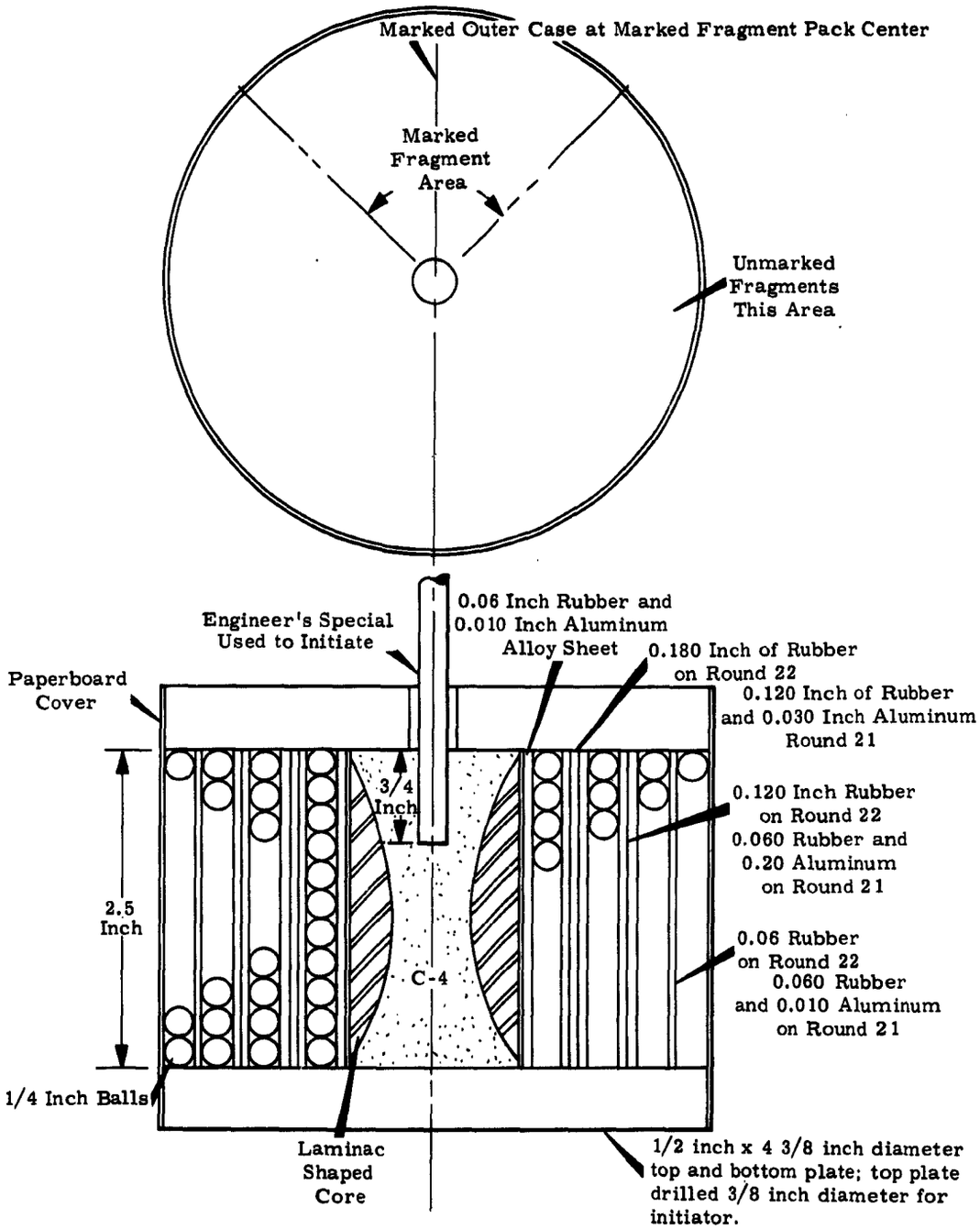


Figure 66. Test Model Design, Rounds No. 21 and 22

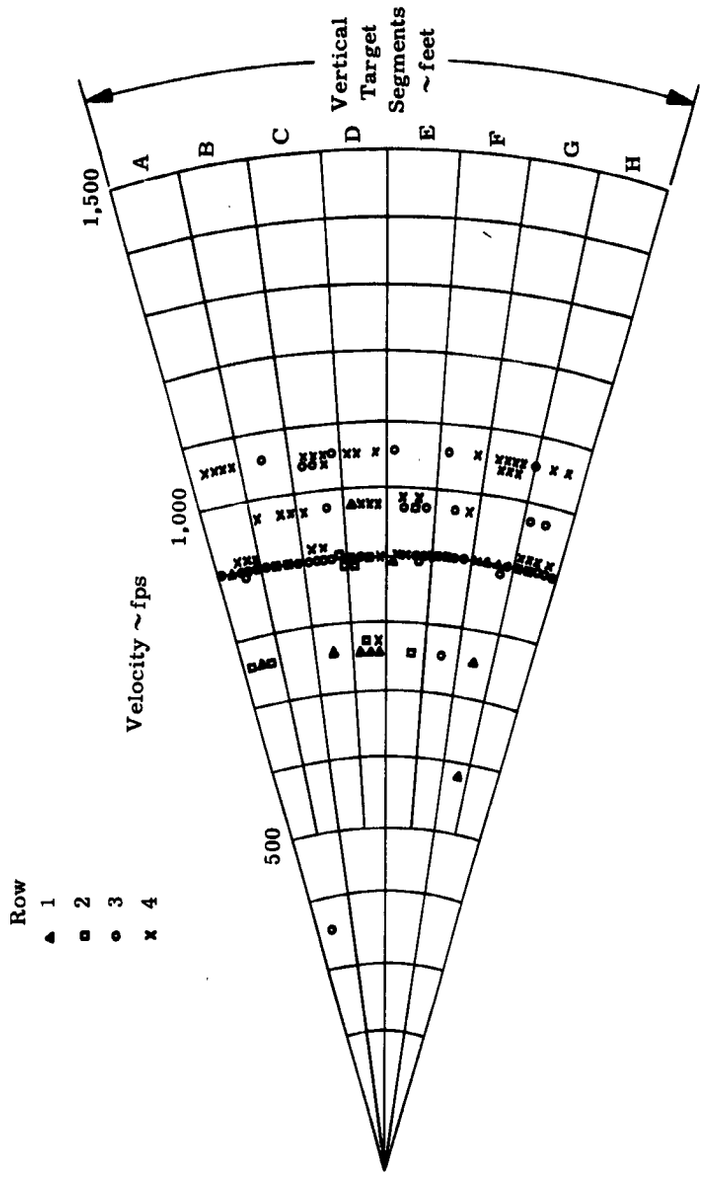


Figure 67. Velocity versus Radial Distribution, Round No. 9

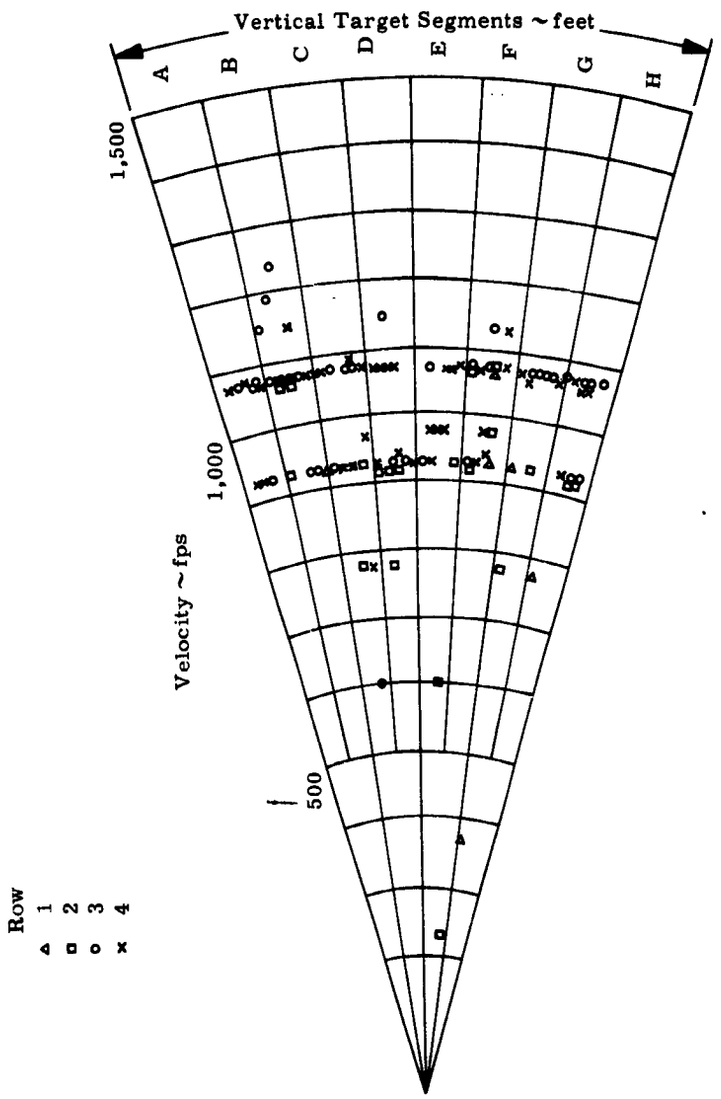


Figure 68. Velocity versus Radial Distribution, Round No. 10

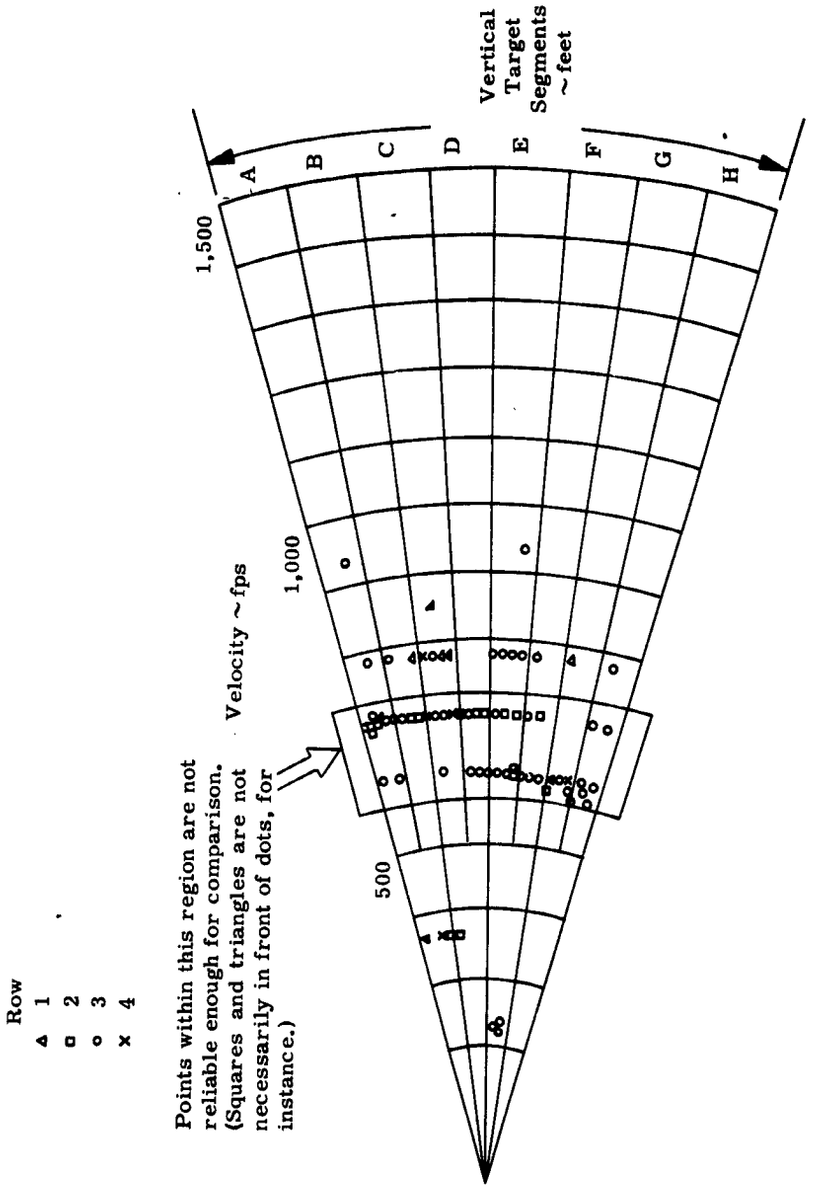


Figure 69. Velocity versus Radial Distribution, Round No. 15

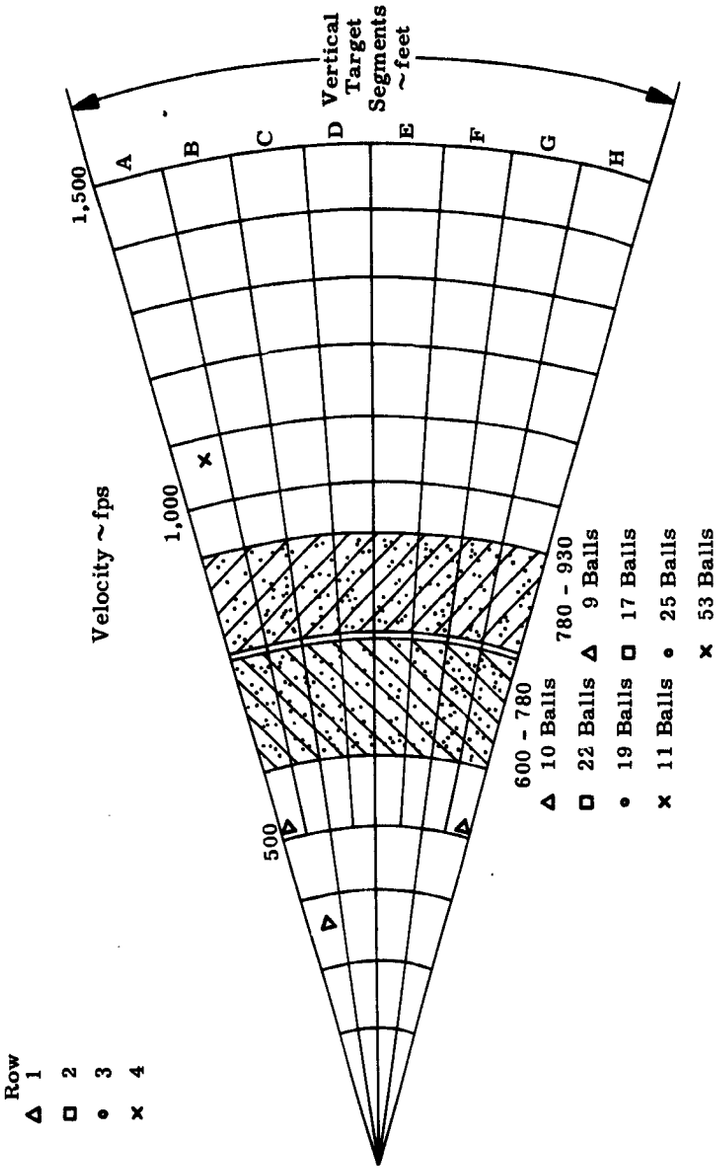


Figure 70. Velocity versus Radial Distribution, Round No. 16

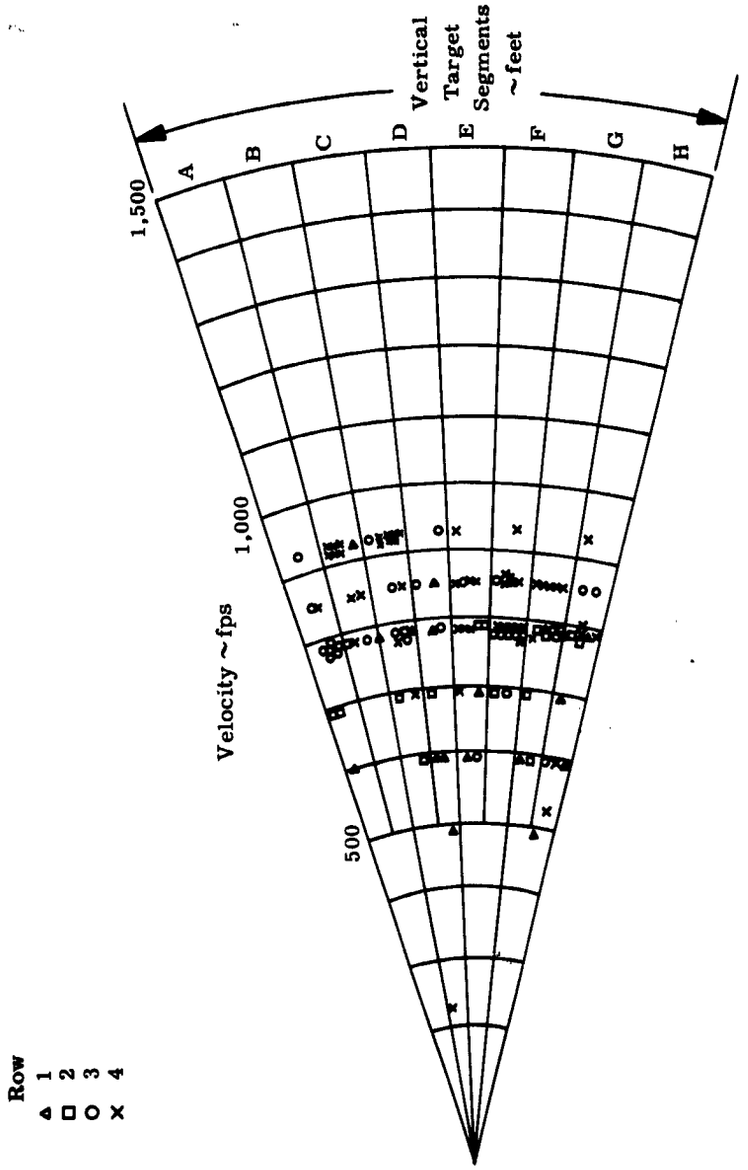


Figure 71. Velocity versus Radial Distribution, Round No. 21

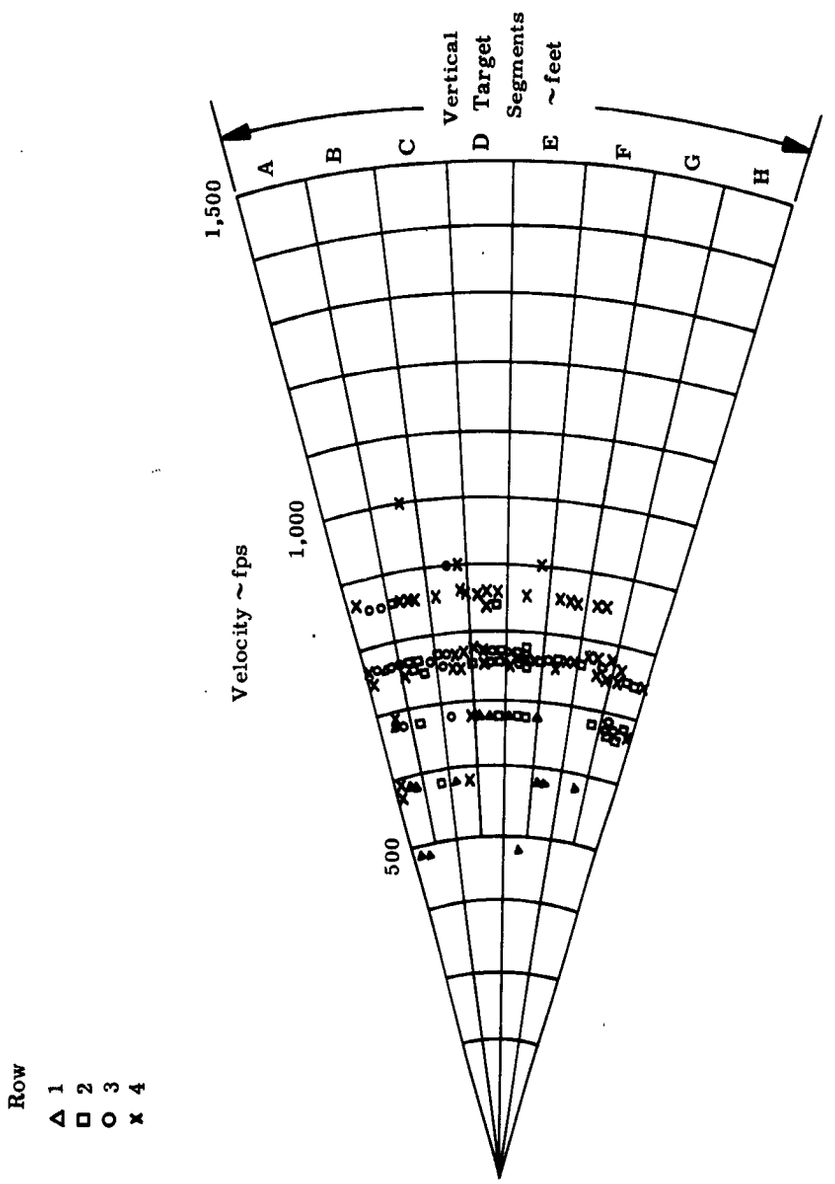


Figure 72. Velocity versus Radial Distribution, Round No. 22

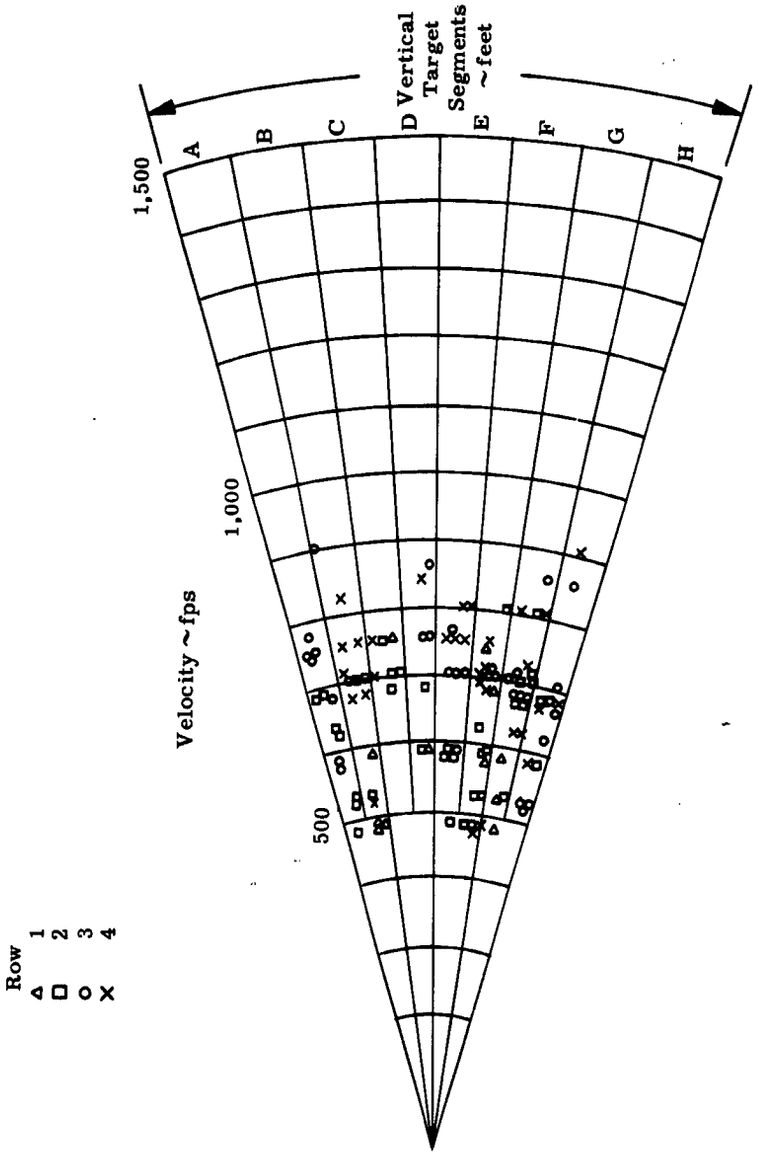


Figure 73. Velocity versus Radial Distribution, Round No. 36

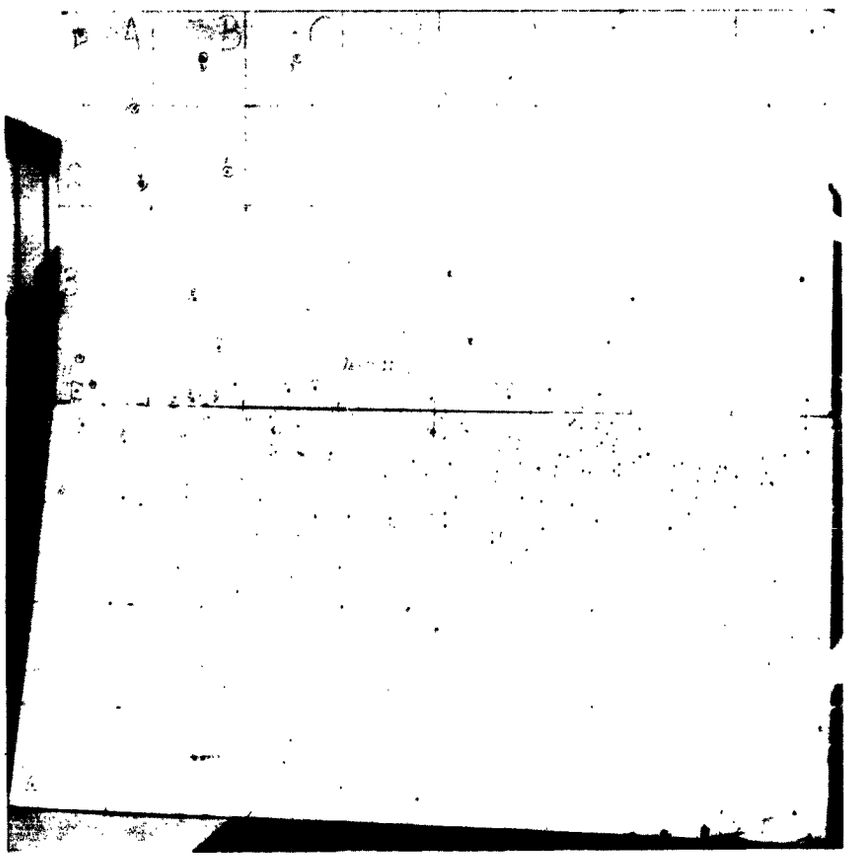

Figure 74. Impact Pattern, Round No. 15

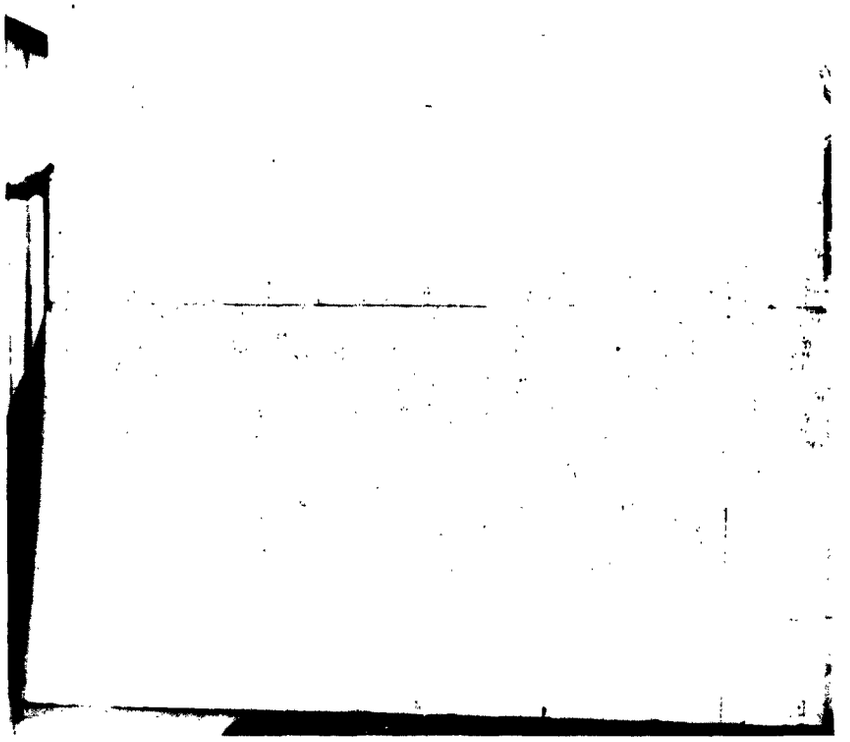

Figure 75. Impact Pattern, Round No. 16

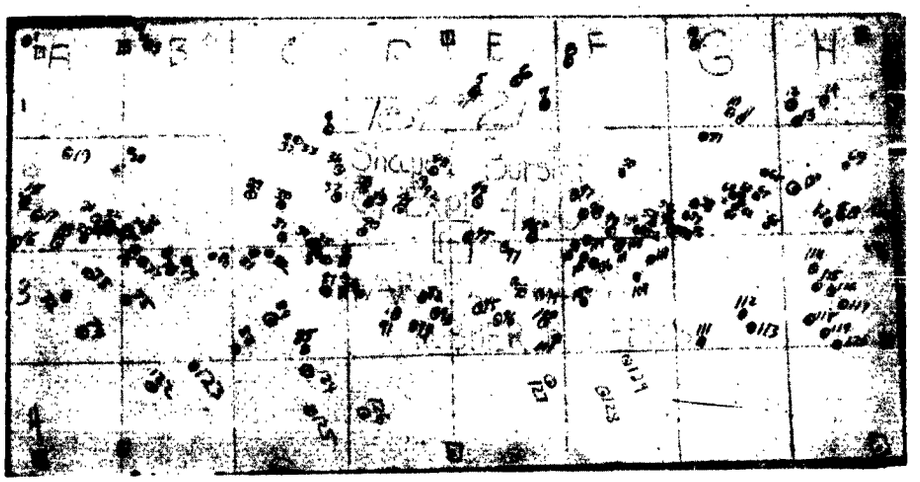

Figure 76. Impact Pattern, Round No. 21


Figure 77. Impact Pattern, Round No. 22

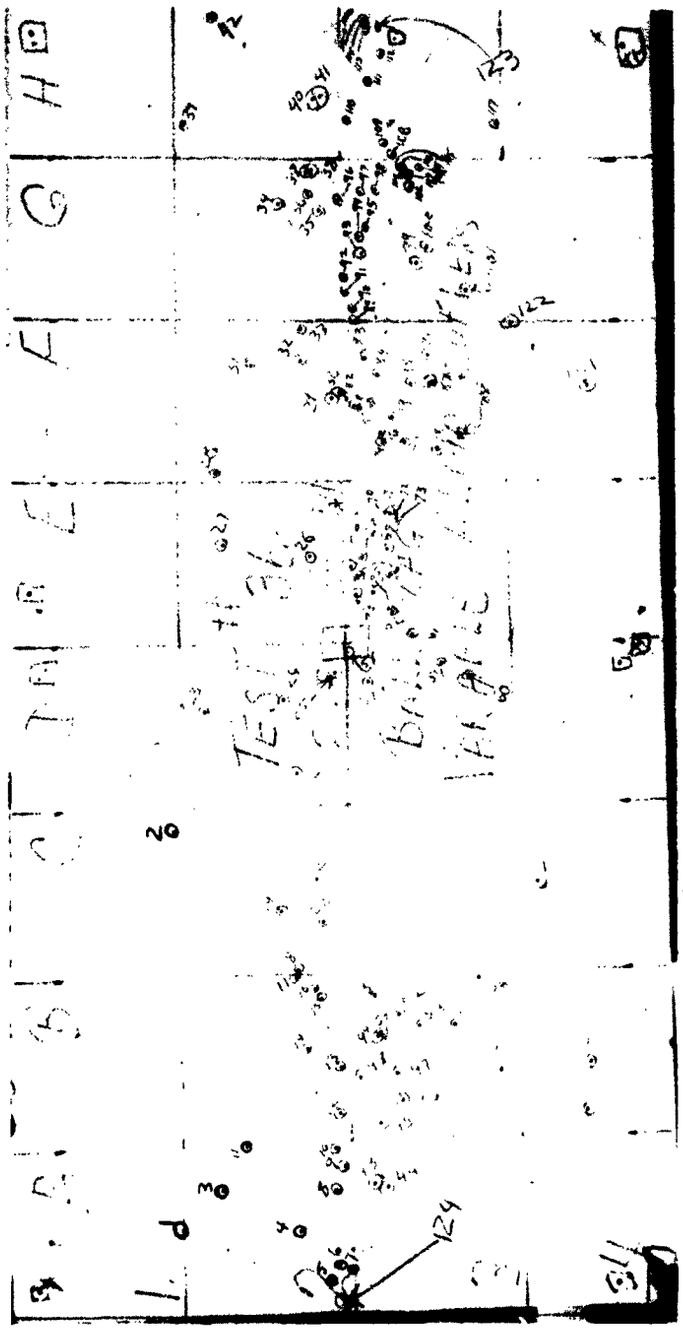

Figure 78. Impact Pattern, Round No. 36

# APPENDIX IV

## BASIC DESIGN IV DATA

This appendix summarizes design and test data pertinent to all Basic Design IV warhead models.

## TABLE 9

### Basic Design IV Data Summary

| Round No. | Round Description | | | | | | | | | Parameter Varied | Test Objectives | Impa Patte |
|---|---|---|---|---|---|---|---|---|---|---|---|---|
| | Expl Mass (grams) | Frag Mass (grams) | End Plate Mass (grams) | C/M | Type | Cent. Burst Type | Cent. Burst Diam (in.) | Over Dim. Ht (in.) | Over Dim. Diam (in.) | | | |
| 5 | 292.0 | 1399 | 1119 | 0.017 | Figs. 79 and 80 | None | None | 5.0 | 3.37 | Basic design | Velocity gradient | Fig. 123 |
| 6 | 301.4 | 1399 | 1140 | 0.021 | Figs. 79 and 80 | None | None | 5.0 | 3.37 | Same as 5 | Same as 5 | Fig. 124 |
| 19 | 347.4 | 1193 | 1213 | 0.193 | Figs. 79 and 80 | None | None | 5.0 | 3.5 | Same as 5 except center burster removed | Effects of center burster on velocity gradient | Fig. 125 |
| 20 | 361. | 1193 | 1213 | 0.193 | Figs. 79 and 80 | None | None | 5.0 | 3.5 | Same as 19 except thin aluminum sheet covering PETN sheets | Buffering effects | Fig. 126 |
| 30 | 390.1 | 1193 | 1224 | 0.283 | Figs. 79 and 80 | None | None | 5.0 | 3.5 | Thin sheet explosive wrapped in gun tape | Same as 20 | |

TABLE 9

Basic Design IV Data Summary

| Dim. Diam (in.) | Parameter Varied | Test Objectives | Results | | | | Conclusions and Comments |
|---|---|---|---|---|---|---|---|
| | | | Impact Pattern | Beam Spy Angle | Velocity Gradient | Polar Plot | |
| 3.37 | Basic design | Velocity gradient | Fig. 123 | 35 Deg | 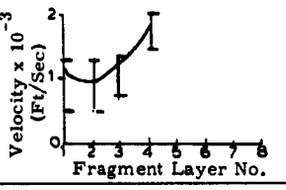  | Fig. 89 | Good gradient potential<br>Angular banding from fragment packaging technique |
| 3.37 | Same as 5 | Same as 5 | Fig. 124 | 35 Deg | 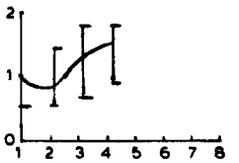  | Fig. 90 | Same as 5 |
| 3.5 | Same as 5 except center burster removed | Effects of center burster on velocity gradient | Fig. 125 | 30 Deg |   | Fig. 91 | Reduced inner row velocity<br>Good gradient potential |
| 3.5 | Same as 19 except thin aluminum sheet covering PETN sheets | Buffering effects | Fig. 126 | 30 Deg | 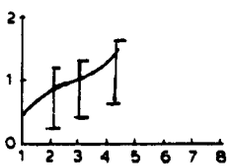  | Fig. 92 | Slightly reduced average velocities<br>Large pieces of buffering material recovered<br>Good gradient potential |
| 3.5 | Thin sheet explosive wrapped in gun tape | Same as 20 | | 30 Deg | 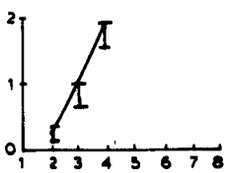  | Fig. 93 | Outer layer velocities very high<br>Increased outer row velocity<br>Good gradient potential |



TABLE 9 (Cont)

| Round No. | Round Description | | | | | | | | | Parameter Varied | Test Objectives | Impact Pattern |
|---|---|---|---|---|---|---|---|---|---|---|---|---|
| | Expl Mass (grams) | Frag Mass (grams) | End Plate Mass (grams) | C/M | Type | Cent. Burst Type | Cent. Burst Diam (in.) | Over Dim. Ht (in.) | Over Dim. Diam (in.) | | | |
| 34 | 121.7 | 1102 | 1247 | 0.092 | Fig. 81 | C-4 | 0.75 | 3.5 | 3.375 | C-4 center burster<br>Concentric PETN rings | Determine mode of propagation of shock waves | Fig. 127 |
| 35 | 258.6 | 1331 | 1460 | 0.032 | Fig. 81 | C-4 | 0.75 | 3.5 | 3.8 | C-4 center burster<br>Concentric PETN layers<br>Thick inside to thin outside | Determine effect of variable layered PETN | Fig. 128 |
| 38 | 289.4 | 1185 | 1602 | 0.148 | Fig. 81 | C-4 | 0.75 | 3.5 | 3.8 | Same as 35 but with thin inside to thick outside | Same as 35 | Fig. 129 |
| 41 | 185.6 | 1081 | 1346 | | Fig. 81 | C-4 | 0.5 | 3.5 | 3.6 | 0.5 inch C-4 center burster<br>Concentric PETN layers | Velocity gradient and pattern | Not available |
| 43<br>43X | 207.4 | 1378 | 1537 | 0.115 | Fig. 81 | C-4 | 0.5 | 3.5 | 3.6 | Variable explosive layer<br>Small diameter center burster thicknesses | Shock initiation of PETN with small center burster<br>Pattern/velocity gradient | Fig. 130 |

TABLE 9 (Cont)

| Over Dim. Ht (in.) | Over Dim. Diam (in.) | Parameter Varied | Test Objectives | Results: Impact Pattern | Results: Beam Spy Angle | Results: Velocity Gradient | Results: Polar Plot | Conclusions and Comments |
|---|---|---|---|---|---|---|---|---|
| 3.5 | 3.375 | C-4 center burster<br>Concentric PETN rings | Determine mode of propagation of shock waves | Fig. 127 | 24 Deg | 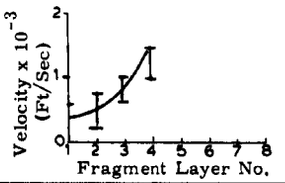 | Fig. 94 | Fair gradient<br>All explosive layers detonated |
| 3.5 | 3.8 | C-4 center burster<br>Concentric PETN layers<br>Thick inside to thin outside | Determine effect of variable layered PETN | Fig. 128 | 27 Deg | 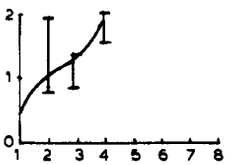 | Fig. 95 | Fair gradient<br>Row two velocities as high as those in rows three and four |
| 3.5 | 3.8 | Same as 35 but with thin inside to thick outside | Same as 35 | Fig. 129 | 30 Deg | 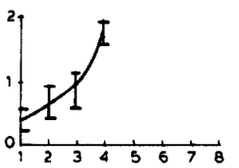 | Fig. 96 | Possible means of controlling velocity gradient |
| 3.5 | 3.6 | 0.5 inch C-4 center burster<br>Concentric PETN layers | Velocity gradient and pattern | Not available | 30 Deg | 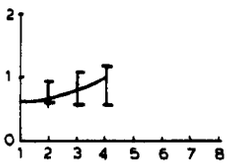 | Fig. 97 | Incomplete detonation of PETN; suspected due to small diameter center burster |
| 3.5 | 3.6 | Variable explosive layer<br>Small diameter center burster thicknesses | Shock initiation of PETN with small center burster<br>Pattern/velocity gradient | Fig. 130 | 30 Deg | 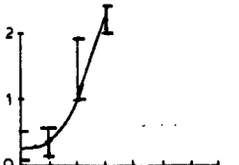 | Fig. 98 | Same as 41 |

TABLE 9 (Cont)

| Round No. | Round Description | | | | | | | | | Parameter Varied | Test Objectives | Im Pa |
|---|---|---|---|---|---|---|---|---|---|---|---|---|
| | Expl Mass (grams) | Frag Mass (grams) | End Plate Mass (grams) | C/M | Type | Cent. Burst Type | Cent. Burst Diam (in.) | Over Dim. Ht (in.) | Over Dim. Diam (in.) | | | |
| 48 | 230.9 | 1229 | 1176 | 0.116 | Fig. 84 | RDX | 0.5 | 4.5 | 3.5 | Explosive layering, spiral configuration<br>Center initiation | Compare effects of center initiation | Fi 13 |
| 49X | 188.2 | 1790 | 1432 | 0.085 | Fig. 84 | RDX | 0.5 | 4.5 | 3.5 | Same as 48 | Same as 48 | Fi 13 |
| 52X | 299.1 | 1435 | 39.9 | 0.272 | Fig. 82 | C-4 | 0.75 | 2.5 | 3.8 | C-4 burster<br>PETN rings<br>PETN end plates<br>Dual initiation | Check of explosive end plate potential and dual initiation | Fi 13 |
| 53 | 276.4 | 1441 | 32.0 | 0.157 including end plate mass and end plate expl. | Fig. 82 | C-4 | 0.75 | 2.5 | 3.8 | Same as 52 | Same as 52 | Fig 134 |
| 54 | 194.8 | 1320 | 1601 | 0.111 | Fig. 81 | C-4 | 0.625 | 3.5 | 3.725 | Increased burster size<br>Four layer concentric PETN | Increased reliability of initiation<br>Pattern/velocity distribution | Not ava abl |

TABLE 9 (Cont)

| t am ı.) | Over Dim. Ht (in.) | Over Dim. Diam (in.) | Parameter Varied | Test Objectives | Results: Impact Pattern | Results: Beam Spy Angle | Results: Velocity Gradient | Results: Polar Plot | Conclusions and Comments |
|---|---|---|---|---|---|---|---|---|---|
| | 4.5 | 3.5 | Explosive layering, spiral configuration<br>Center initiation | Compare effects of center initiation | Fig. 131 | 24 Deg | 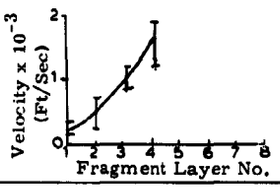 | Fig. 99 | Good gradient<br>Reasonable pattern<br>Center initiation appears effective and possibly provides improved distribution patterns over those obtained with external end-line initiation |
| | 4.5 | 3.5 | Same as 48 | Same as 48 | Fig. 132 | 24 Deg | 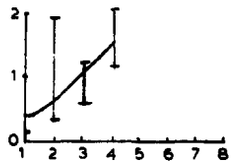 | Fig. 100 | Same as 48<br>Good reproducibility |
| 5 | 2.5 | 3.8 | C-4 burster<br>PETN rings<br>PETN end plates<br>Dual initiation | Check of explosive end plate potential and dual initiation | Fig. 133 | |  | | Many balls deformed<br>First and second layers lost<br>Poor recovery percentage |
| 5 | 2.5 | 3.8 | Same as 52 | Same as 52 | Fig. 134 | 24 Deg | 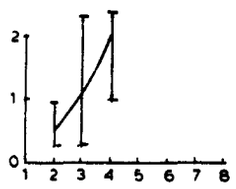 | Fig. 102 | Inner row lost<br>Poor recovery percentage |
| 25 | 3.5 | 3.725 | Increased burster size<br>Four layer concentric PETN | Increased reliability of initiation<br>Pattern/velocity distribution | Not available | 24 Deg | 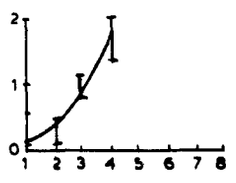 | Fig. 103 | Pattern good<br>Velocity excessive<br>Reliable initiation |



TABLE 9 (Cont)

| Round No. | Round Description | | | | | | | | | Parameter Varied | Test Objectives | |
|---|---|---|---|---|---|---|---|---|---|---|---|---|
| | Expl Mass (grams) | Frag Mass (grams) | End Plate Mass (grams) | C/M | Type | Cent. Burst Type | Cent. Burst Diam (in.) | Over Dim. Ht (in.) | Over Dim. Diam (in.) | | | |
| 55 | 197.0 | 1320 | 1595 | 0.117 | Fig. 81 | C-4 | 0.625 | 3.5 | 3.725 | Same as 54 | Same as 54 | F 1 |
| 56 | 412.9 | 4540 | 1816 | 0.073 | Fig. 83 | C-4 | 0.625 | 5.5 | 4.26 | Six layer concentric PETN<br>5/8 inch center burster | Pattern/velocity check for additional fragment layers | F 1 |
| 57 | 457.5 | 4650 | 1810 | 0.086 | Fig. 83 | C-4 | 0.625 | 5.5 | 4.26 | Same as 56 | Same as 56 | F 1 |
| 60 | | 1400 | 49.1 | 0.061 | Fig. 82 | C-4 | 0.75 | 2.5 | 3.8 | Increased PETN end confinement<br>PETN concentric layers<br>C-4 center burster | Check concept feasibility to control beam spray | F 1 |
| 61 | | 1425 | 48.8 | | Fig. 82 | C-4 | 0.75 | 2.5 | 3.8 | Same as 60 | Same as 60 | F 1 |

TABLE 9 (Cont)

| Burst | Over Dim. | | | | Results | | | | |
|---|---|---|---|---|---|---|---|---|---|
| Diam (in.) | Ht (in.) | Diam (in.) | Parameter Varied | Test Objectives | Impact Pattern | Beam Spy Angle | Velocity Gradient | Polar Plot | Conclusions and Comments |
| 0.625 | 3.5 | 3.725 | Same as 54 | Same as 54 | Fig. 135 | 24 Deg | 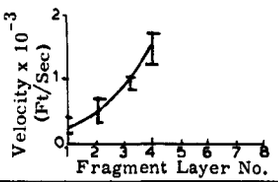  | Fig. 104 | Same as 54<br>Good reproducibility |
| 0.625 | 5.5 | 4.26 | Six layer concentric PETN<br>5/8 inch center burster | Pattern/velocity check for additional fragment layers | Fig. 136 | 28 Deg | 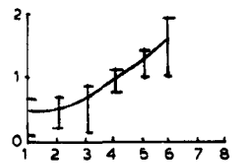 | Figs. 105 and 106 | Good pattern<br>High velocities<br>Velocities of rows one and two essentially the same |
| 0.625 | 5.5 | 4.26 | Same as 56 | Same as 56 | Fig. 137 | 28 Deg | 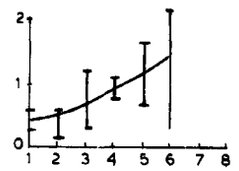 | Fig. 107 | Same as 56<br>Good reproducibility |
| 0.75 | 2.5 | 3.8 | Increased PETN end confinement<br>PETN concentric layers<br>C-4 center burster | Check concept feasibility to control beam spray | Fig. 138 | 24 Deg | 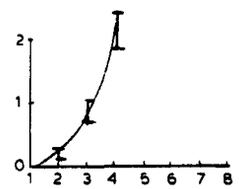 | Fig. 108 | 16 mm film indicates mixing of fragments in flight<br>Top velocities excessive<br>Poor recovery percentage |
| 0.75 | 2.5 | 3.8 | Same as 60 | Same as 60 | Fig. 139 | 24 Deg | 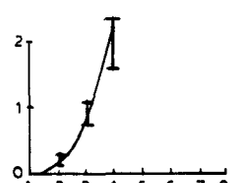 | Fig. 109 | Same as 60 |

TABLE 9 (Cont)

| Round No. | Round Description | | | | | | | | | Parameter Varied | Test Objectives |
|---|---|---|---|---|---|---|---|---|---|---|---|
| | Expl Mass (grams) | Frag Mass (grams) | End Plate Mass (grams) | C/M | Type | Cent. Burst Type | Cent. Burst Diam (in.) | Over Dim. Ht (in.) | Over Dim. Diam (in.) | | |
| 62 | 454.2 | 4685 | 2264 | 0.083 | Fig. 85 | RDX | 0.5 | 5.25 | 4.25 | Six layer spiral RDX center initiated | Pattern/velocity distribution |
| 63 | 464.6 | 4805 | 2278 | 0.080 | Fig. 85 | RDX | 0.5 | 5.25 | 4.25 | Same as 62 | Same as 62 |
| 64 | 1019 | 9880 | 3043 | 0.085 | Fig. 85 | RDX | 0.5 | 6.5 | 5.5 | Same as 62, with 8 fragment layers | Same as 62 |
| 65 | 1014 | 9880 | 3035 | 0.085 | Fig. 85 | RDX | 0.5 | 6.5 | 5.5 | Same as 64 | Same as 64 |
| 66 | 331.8 | 1816 | 42.6 | 0.155 | Fig. 82 | C-4 | 0.5 | 3.75 | 3.7 | Four layer spiral C-4 center burster Domed explosive end plates | Explosive confinement of beam spray |

TABLE 9 (Cont)

| st am n.) | Over Dim. Ht (in.) | Over Dim. Diam (in.) | Parameter Varied | Test Objectives | Results: Impact Pattern | Results: Beam Spy Angle | Results: Velocity Gradient | Results: Polar Plot | Conclusions and Comments |
|---|---|---|---|---|---|---|---|---|---|
| 5 | 5.25 | 4.25 | Six layer spiral RDX center initiated | Pattern/velocity distribution | Fig. 140 | 32 Deg | 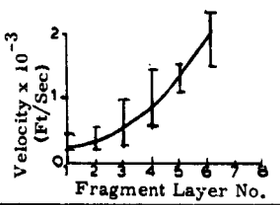  | Fig. 110 | Excellent velocity gradient<br>Excessive velocities<br>Good pattern |
| 5 | 5.25 | 4.25 | Same as 62 | Same as 62 | Fig. 141 | 32 Deg | 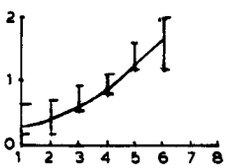  | Figs. 111 and 112 | Same as 62<br>Excellent reproducibility |
| 5 | 6.5 | 5.5 | Same as 62, with 8 fragment layers | Same as 62 | Fig. 142 | 32 Deg | 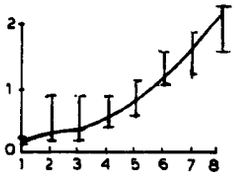  | Figs. 113 and 114 | Eighth row velocity excessive<br>Velocity gradient good<br>Good pattern |
| 5 | 6.5 | 5.5 | Same as 64 | Same as 64 | Fig. 143 | 32 Deg | 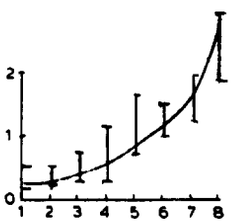  | Fig. 115 | Same as 64<br>Excellent reproducibility |
| 5 | 3.75 | 3.7 | Four layer spiral<br>C-4 center burster<br>Domed explosive end plates | Explosive confinement of beam spray | Not available | Excessive | 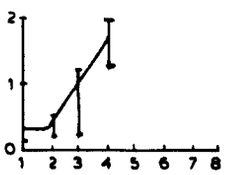  | Not available | Indications of high velocities in outer layer<br>Large number of fragments in ground ripple board indicate possible crossing of fragments |



TABLE 9 (Cont)

| Round No. | Round Description | | | | | | | | | Parameter Varied | Test Objectives | Im Pa |
|---|---|---|---|---|---|---|---|---|---|---|---|---|
| | Expl Mass (grams) | Frag Mass (grams) | End Plate Mass (grams) | C/M | Type | Cent. Burst Type | Cent. Burst Diam (in.) | Over Dim. Ht (in.) | Over Dim. Diam (in.) | | | |
| 67 | 306 | 1405 | 43.5 | 0.186 | Fig. 82 | C-4 | 0.75 | 2.75 | 3.8 | Same as 66 | Same as 66 | No Av ab |
| 68 | 244.6 | 2442 | 1409 | 0.077 | Figs. 79 and 80 | None | None | 4.0 | 3.5 | Four layer spiral; outside line initiation | Check effects of initiation point | Fi 14 |
| 69 | 144.3 | 2861 | 1411 | 0.047 | Fig. 84 | RDX | 0.5 | 4.5 | 3.5 | Four layer spiral, center initiated, using 1/4 inch cubic fragments | Pattern/velocity for cubic fragments | No Av ab |
| 70 | 63.1 | 1208 | 922.6 | 0.033 | Fig. 84 | C-4 | 0.5 | 4.5 | 3.7 | Four layer spiral, center initiated, using 0.025 gage PETN sheet | Reduction of overall velocities | Fi 14 |
| 71 | 62.0 | 1482 | 921.6 | 0.034 | Fig. 84 | C-4 | 0.5 | 4.5 | 3.7 | Same as 70 | Same as 70 | No Av ab |

TABLE 9 (Cont)

| Over Dim. Ht (in.) | Over Dim. Diam (in.) | Parameter Varied | Test Objectives | Results: Impact Pattern | Results: Beam Spy Angle | Results: Velocity Gradient | Results: Polar Plot | Conclusions and Comments |
|---|---|---|---|---|---|---|---|---|
| 2.75 | 3.8 | Same as 66 | Same as 66 | Not Available | Excessive | 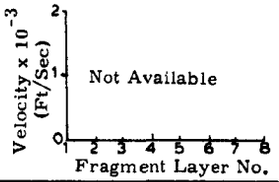  | Not available | Loss of two inner layers of fragments, possibly due to non-simultaneous end plate initiation |
| 4.0 | 3.5 | Four layer spiral; outside line initiation | Check effects of initiation point | Fig. 144 | 24 Deg | 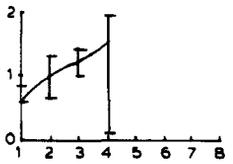 | Not available | Heavy concentration of fragments in inner 12 degrees<br>Indication of velocity banding possibly resulting from end-line initiation |
| 4.5 | 3.5 | Four layer spiral, center initiated, using 1/4 inch cubic fragments | Pattern/velocity for cubic fragments | Not Available | 16 Deg | 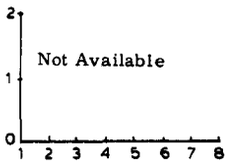  | Not available | Malassembly of model; retest scheduled |
| 4.5 | 3.7 | Four layer spiral, center initiated, using 0.025 gage PETN sheet | Reduction of overall velocities | Fig. 145 | 20 Deg | 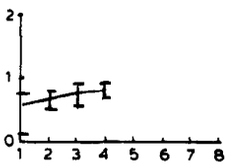 | Fig. 116 | Reduced velocities<br>Fragments moved as a group<br>Possible initiation problem with thin gaged explosive |
| 4.5 | 3.7 | Same as 70 | Same as 70 | Not Available | 20 Deg | 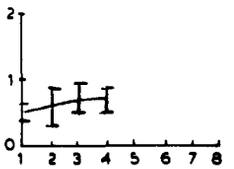 | Fig. 117 | Same as 70 |

TABLE 9 (Cont)

| Round No. | Round Description | | | | | | | | | Parameter Varied | Test Objectives |
|---|---|---|---|---|---|---|---|---|---|---|---|
| | Expl Mass (grams) | Frag Mass (grams) | End Plate Mass (grams) | C/M | Type | Cent. Burst Type | Cent. Burst Diam (in.) | Over Dim. Ht (in.) | Over Dim. Diam (in.) | | |
| 76 | 302.1 | 1262 | 42.7 | 0.194 | Fig. 81 | C-4 | 0.625 | 2.5 | 3.8 | Four layer concentric, flat explosive end plates, center initiated | Explosive control of beam spray Pattern/velocity gradient |
| 77 | 228.9 | 3975 | 2051 | 0.050 | Figs. 86 and 87 | Kept clear | Kept clear | 5.25 | 4.25 | Six layer spiral, outside initiation | Pattern/velocity distribution |
| 78 | 508.2 | 6419 | 2753 | 0.065 | Fig. 85 | RDX | 0.5 | 5.25 | 4.25 | Six layer spiral 1/4 inch cubic fragments 1/2 inch RDX center burster, end initiated | Velocity/pattern distribution for cubic fragments Compares with Round 62 |
| 79 | 509.1 | 4563 | 2737 | 0.075 | Fig. 85 | RDX | 0.5 | 5.25 | 4.25 | Same as 78 except with hexagonal fragments | Same as 78 |
| 80 | 446.3 | 4381 | 2304 | 0.085 | Fig. 85 | RDX | 0.5 | 5.25 | 4.25 | Six layer spiral 1/2 inch steel balls 1/2 inch RDX burster Identical to Round 62 Round suspended from scaffold for firing | Test effects of firing fixture on beam spray and velocity gradient |

TABLE 9 (Cont)

| rst Diam (in.) | Over Dim. Ht (in.) | Over Dim. Diam (in.) | Parameter Varied | Test Objectives | Results: Impact Pattern | Results: Beam Spy Angle | Results: Velocity Gradient | Results: Plot | Conclusions and Comments |
|---|---|---|---|---|---|---|---|---|---|
| 0.625 | 2.5 | 3.8 | Four layer concentric, flat explosive end plates, center initiated | Explosive control of beam spray<br>Pattern/velocity gradient | Not available | | 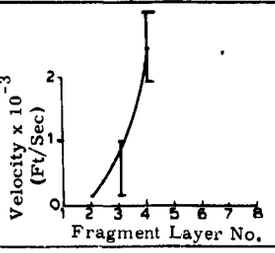 | Fig. 118 | Vague pattern, similar to Round 67<br>Two inner fragment layers lost |
| Kept clear | 5.25 | 4.25 | Six layer spiral, outside initiation | Pattern/velocity distribution | Fig. 146 | 24 Deg | 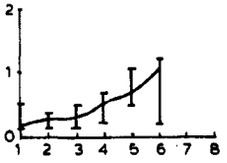 | Fig. 119 | Velocity gradient shows some signs of velocity banding |
| 0.5 | 5.25 | 4.25 | Six layer spiral<br>1/4 inch cubic fragments<br>1/2 inch RDX center burster, end initiated | Velocity/pattern distribution for cubic fragments<br>Compares with Round 62 | Fig. 147 | 20 Deg | 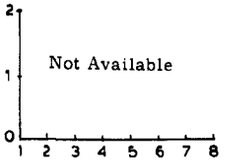 | Not available | Appears to produce higher velocities than identical ball round and comparable gradient<br>Probably improved coupling efficiency |
| 0.5 | 5.25 | 4.25 | Same as 78 except with hexagonal fragments | Same as 78 | Fig. 148 | 20 Deg | 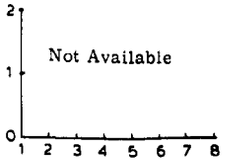 | Not available | Same as 78 |
| 0.5 | 5.25 | 4.25 | Six layer spiral<br>1/2 inch steel balls<br>1/2 inch RDX burster<br>Identical to Round 62<br>Round suspended from scaffold for firing | Test effects of firing fixture on beam spray and velocity gradient | Not available | 120 Deg | 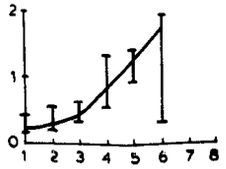 | Not available | Velocities and gradient comparable to Round 62<br>Beam spray excessive |



TABLE 9 (Cont)

| Round No. | Round Description | | | | | | | | | Parameter Varied | Test Objectives |
|---|---|---|---|---|---|---|---|---|---|---|---|
| | Expl Mass (grams) | Frag Mass (grams) | End Plate Mass (grams) | C/M | Type | Cent. Burst Type | Cent. Burst Diam (in.) | Over Dim. Ht (in.) | Over Dim. Diam (in.) | | |
| 81 | 497.5 | 3960 | 2320 | 0.100 | Fig. 85 | RDX | 0.5 | 5.25 | 4.25 | Same as 80 | Same as 80 |
| 82 | 876.4 | 8800 | 3876 | 0.082 | Fig. 88 | RDX | 0.5 | 6.5 | 6.0 | Eight layer spiral with PETN between each row of balls except for two outer rows<br>1/2 inch RDX center burster | Reduce gradient and dispersion in outer layers of fragments |
| 83 | 509.8 | 8430 | 3552 | 0.052 | Fig. 88 | RDX | 0.5 | 6.5 | 5.5 | Eight layer spiral with 0.042 PETN instead of 0.084<br>1/2 inch RDX center burster | Show feasibility of reducing all fragment velocities in eight layer configuration |
| 84 | 154.2 | 3019 | 2041 | 0.039 | Fig. 84 | C-4 | 0.5 | 4.76 | 4.25 | Six layer concentric<br>1/2 inch C-4 center burster<br>First 4 rings PETN 0.042<br>Last ring 0.025 | Investigate ability to predict design in accordance with desired performance |
| 85 | 311.2 | 3465 | 2060 | 0.102 | Fig. 84 | RDX | 0.5 | 4.76 | 4.25 | Six layer concentric<br>First two rings 0.025 PETN<br>Next three rings 0.042 PETN<br>Last ring 0.025 PETN | Same as 84 |

TABLE 9 (Cont)

| urst Diam (in.) | Over Dim. Ht (in.) | Over Dim. Diam (in.) | Parameter Varied | Test Objectives | Results: Impact Pattern | Results: Beam Spy Angle | Results: Velocity Gradient | Results: Polar Plot | Conclusions and Comments |
|---|---|---|---|---|---|---|---|---|---|
| 0.5 | 5.25 | 4.25 | Same as 80 | Same as 80 | Not available | 120 Deg | 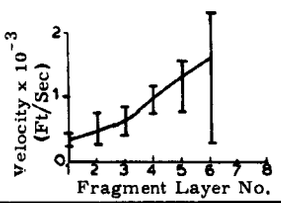  | Not available | Same as 80 |
| 0.5 | 6.5 | 6.0 | Eight layer spiral with PETN between each row of balls except for two outer rows<br>1/2 inch RDX center burster | Reduce gradient and dispersion in outer layers of fragments | Fig. 149 | 32 Deg | 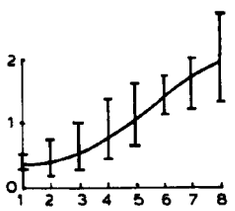  | Fig. 120 | Definite reduction in gradient dispersion between outermost rows<br>Good overall gradient control |
| 0.5 | 6.5 | 5.5 | Eight layer spiral with 0.042 PETN instead of 0.084<br>1/2 inch RDX center burster | Show feasibility of reducing all fragment velocities in eight layer configuration | Fig. 150 | 14 Deg | 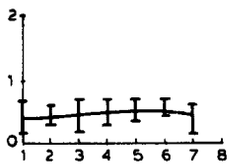  | Not available | Narrow beam spray possibly misleading due to low order detonation; no gradients, probable initiation problem<br>Unburned PETN recovered |
| 0.5 | 4.76 | 4.25 | Six layer concentric<br>1/2 inch C-4 center burster<br>First 4 rings PETN 0.042<br>Last ring 0.025 | Investigate ability to predict design in accordance with desired performance | Not available | 12 Deg | 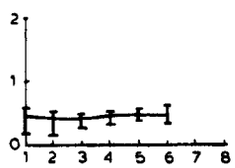  | Not available | Same as 83 |
| 0.5 | 4.76 | 4.25 | Six layer concentric<br>First two rings 0.025 PETN<br>Next three rings 0.042 PETN<br>Last ring 0.025 PETN | Same as 84 | Not available | 8 Deg | 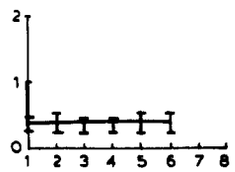  | Not available | Same as 83 |

TABLE 9 (Cont)

| Round No. | Round Description | | | | | | | | | Parameter Varied | Test Objectives |
|---|---|---|---|---|---|---|---|---|---|---|---|
| | Expl Mass (grams) | Frag Mass (grams) | End Plate Mass (grams) | C/M | Type | Cent. Burst Type | Cent. Burst Diam (in.) | Over Dim. Ht (in.) | Over Dim. Diam (in.) | | |
| 86 | 216.1 | 1505 | 28.2 | 0.108 | Fig. 81 | C-4 0.375 at each end | 0.625 | 2.5 | 3.8 | Four layer concentric with explosive end plates and 3/8 inch deep, 5/8 inch diameter C-4 at each end<br>Rest of center is air space<br>Dual end initiated, suspended from scaffold | Investigate mode of detonation Propagation |
| 87 | 229.7 | 1378 | 28.25 | 0.129 | Fig. 81 | C-4 0.375 at each end | 0.625 | 2.5 | 3.8 | Same as 86 | Same as 86 |
| 88 | 160.8 | 1344 | 1744 | None available | Fig. 81 | C-4 | 1.37 to 0.5 to 1.37 | 3.5 | 4.0 | Four layer concentric shaped C-4 burster (hyperboloid)<br>Varying thickness PETN rings<br>Dual end initiation<br>Suspended from scaffold<br>1/2 inch steel end plates | Investigate shaped burster effects on beam spray control |
| 89 | 107.8 | 1791 | 3606 | None available | Fig. 81 | C-4 | 1.37 to 0.5 to 1.37 | 3.5 | 4.0 | Same as 88 except 1 inch thick end plates<br>Suspended from scaffold | Same as 86 |

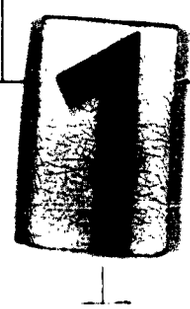

TABLE 9 (Cont)

| | Over Dim. | | Parameter Varied | Test Objectives | Results | | | | Conclusions and Comments |
|---|---|---|---|---|---|---|---|---|---|
| | Ht (in.) | Diam (in.) | | | Impact Pattern | Beam Spy Angle | Velocity Gradient | Polar Plot | |
| 5 | 2.5 | 3.8 | Four layer concentric with explosive end plates and 3/8 inch deep, 5/8 inch diameter C-4 at each end<br>Rest of center is air space<br>Dual end initiated, suspended from scaffold | Investigate mode of detonation<br>Propagation | Not available | Not available | 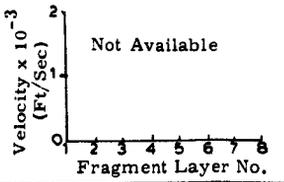 | Not available | Low order detonation; probable initiation problem<br>Much unburned PETN recovered |
| 5 | 2.5 | 3.8 | Same as 86 | Same as 86 | Not available | Not available | 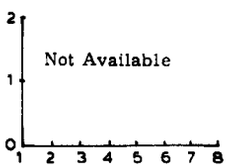 | Not available | Same as 86 |
| | 3.5 | 4.0 | Four layer concentric shaped C-4 burster (hyperboloid)<br>Varying thickness PETN rings<br>Dual end initiation<br>Suspended from scaffold<br>1/2 inch steel end plates | Investigate shaped burster effects on beam spray control | Not available | 75 Deg | 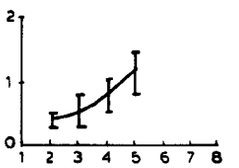 | Not available | Good velocity gradient<br>Excessive beam spray |
| | 3.5 | 4.0 | Same as 88 except 1 inch thick end plates<br>Suspended from scaffold | Same as 86 | Fig. 151 | 25 Deg | 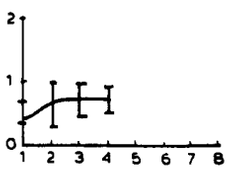 | Figs. 121 and 122 | Improved beam spray<br>Fragment layers intermixed<br>Probable fabrication error<br>Retest scheduled |
| | | | | | | | | | |

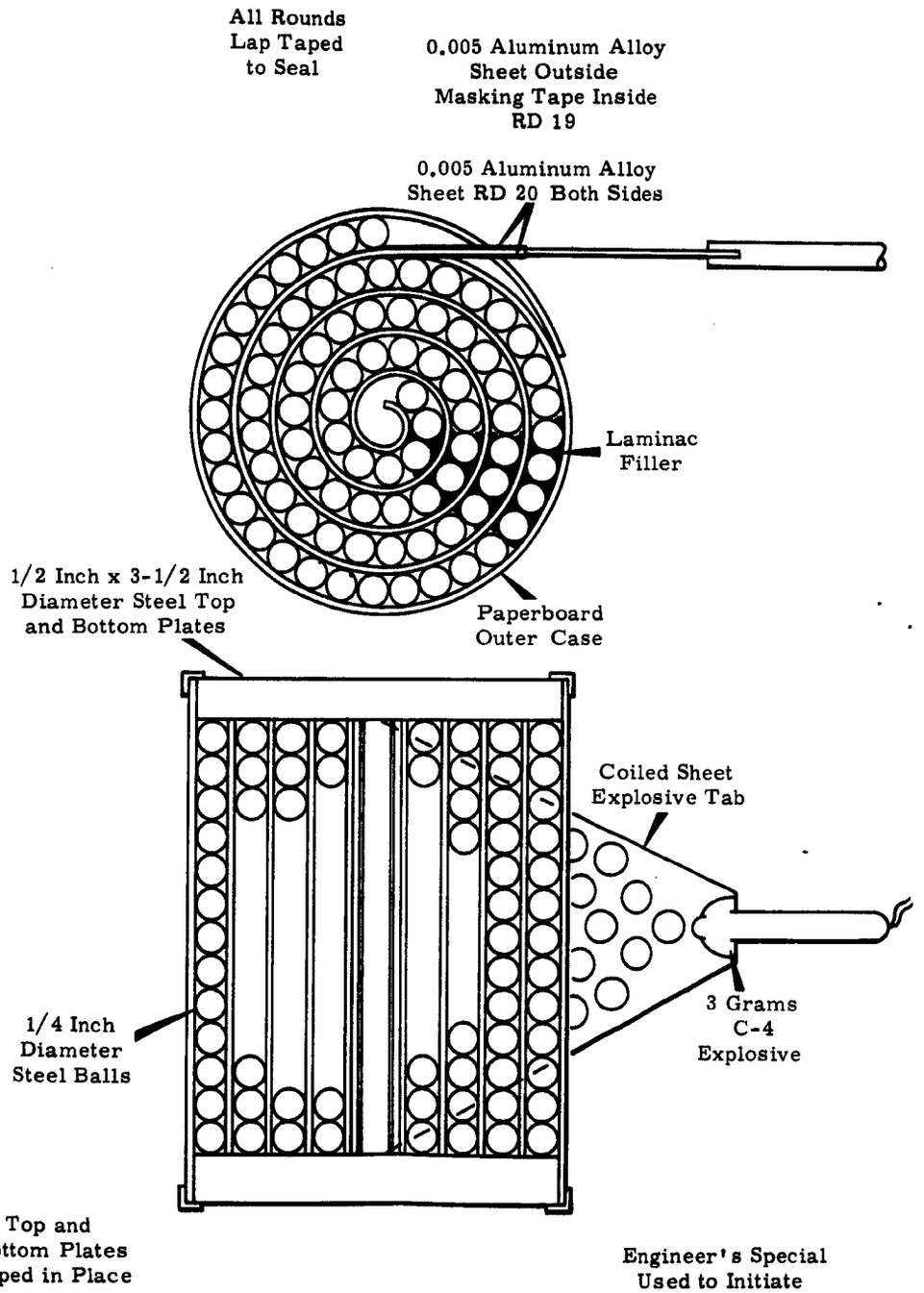


Figure 79. Test Model Design, Round No. 19 and 20

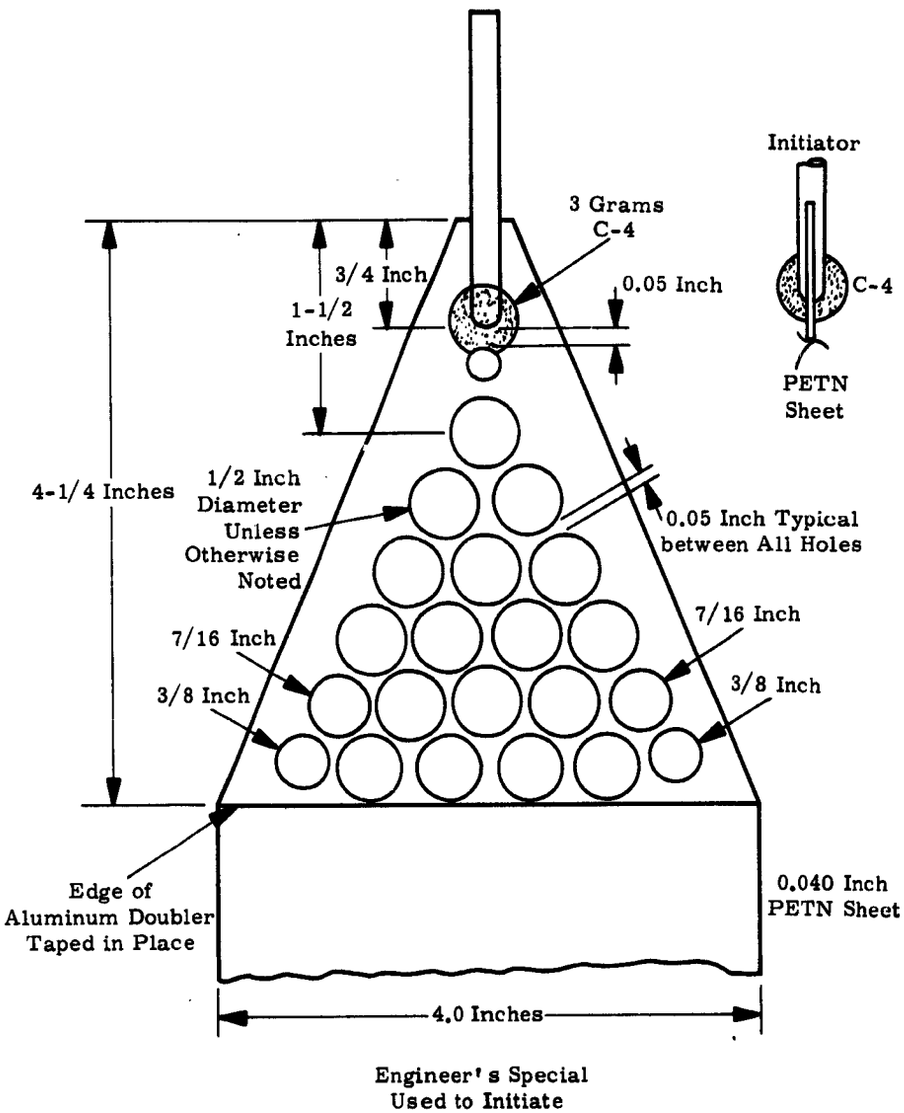


Figure 80. Test Model Design, Round No. 19 and 20 End-Line Initiator

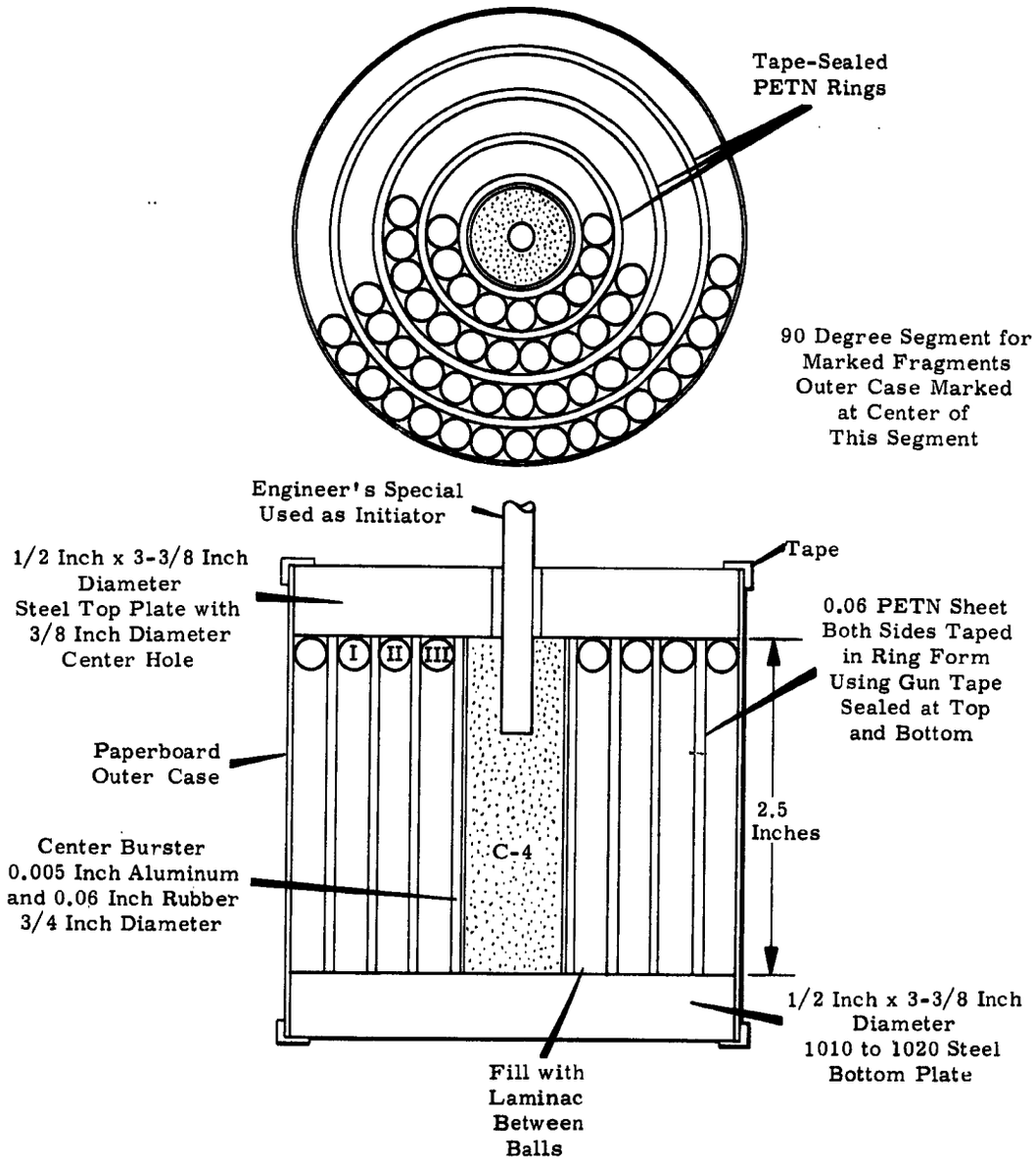


Figure 81. Test Model Design, Round No. 34

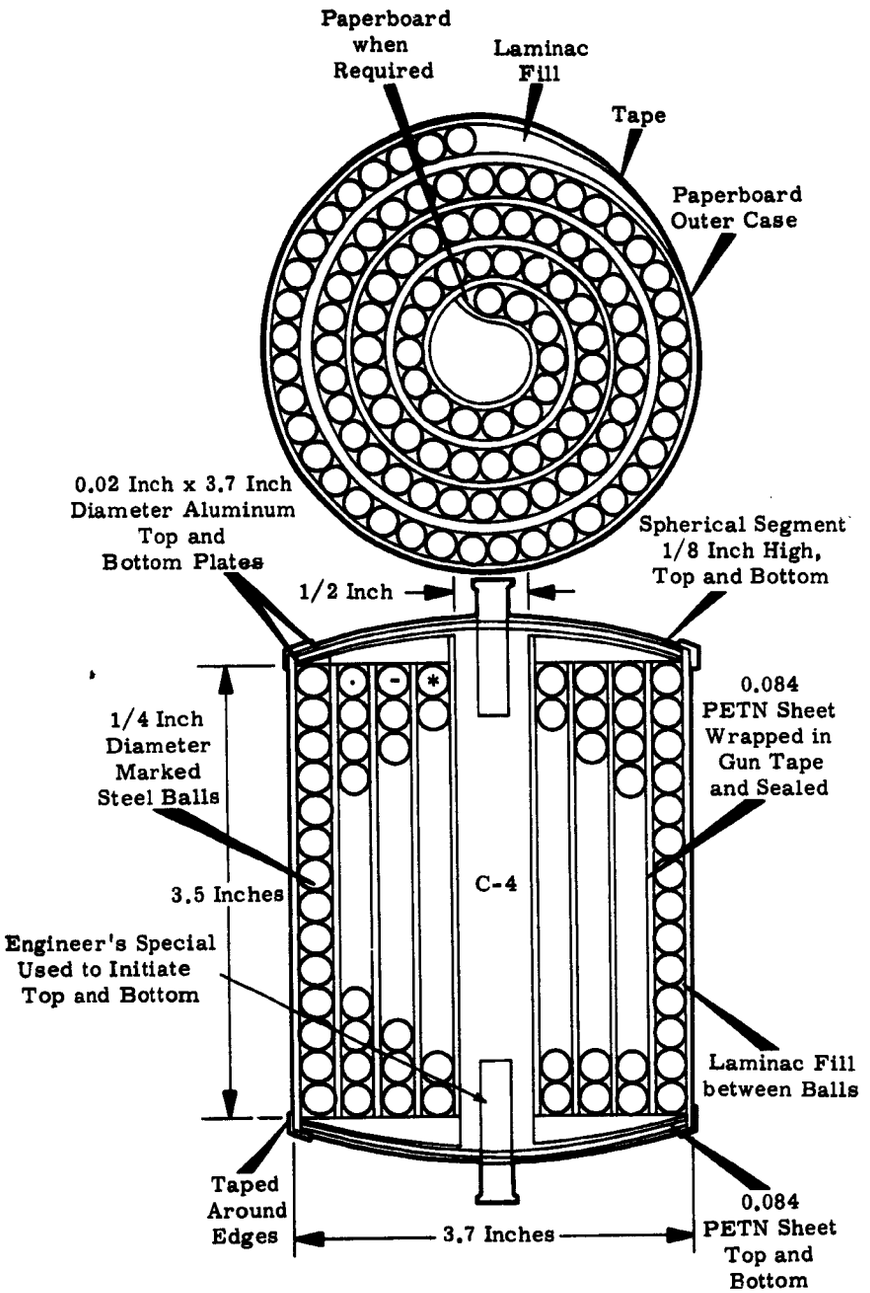


Figure 82. Test Model Design, Round No. 66

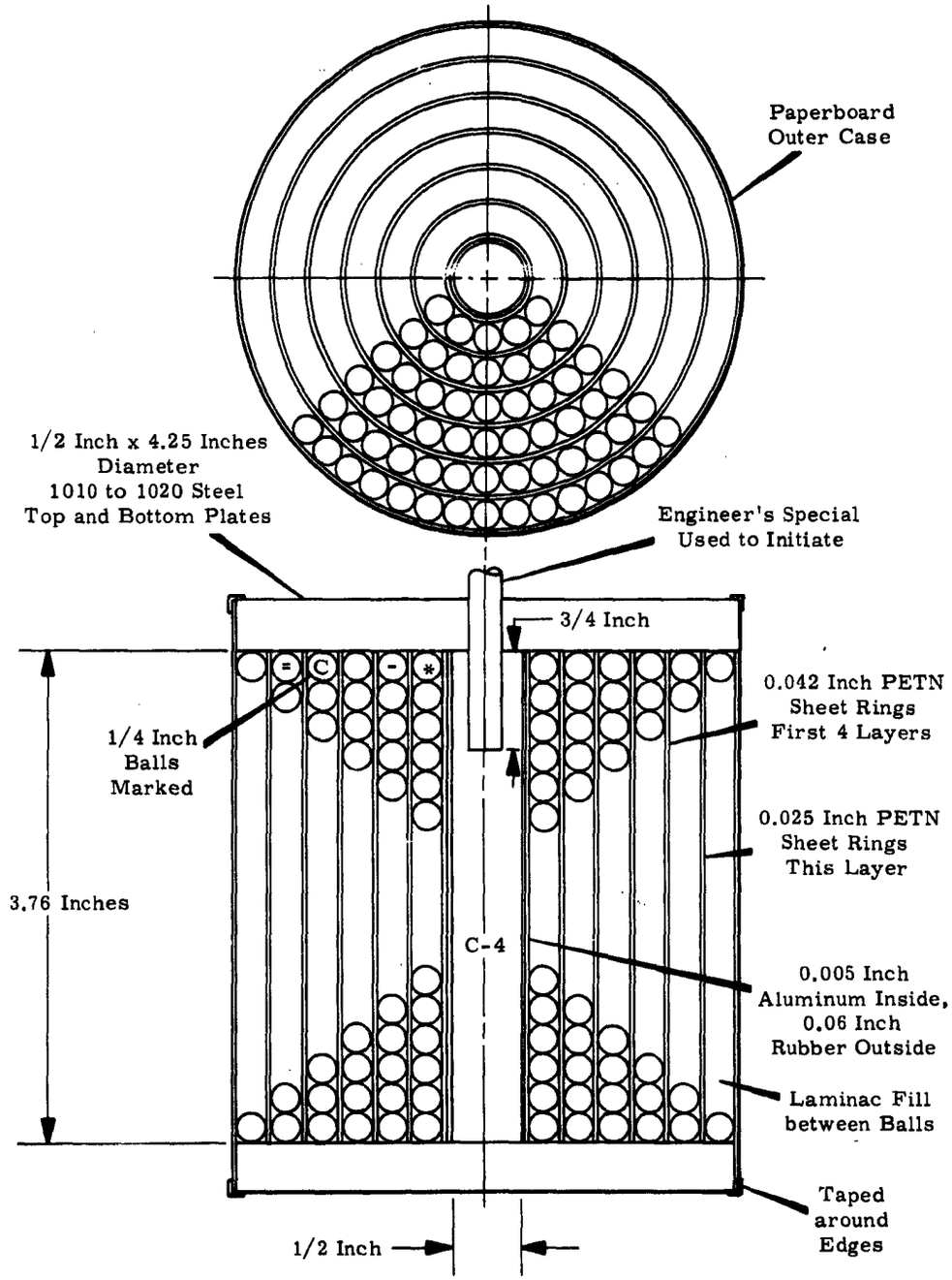


Figure 83. Test Model Design, Round No. 84

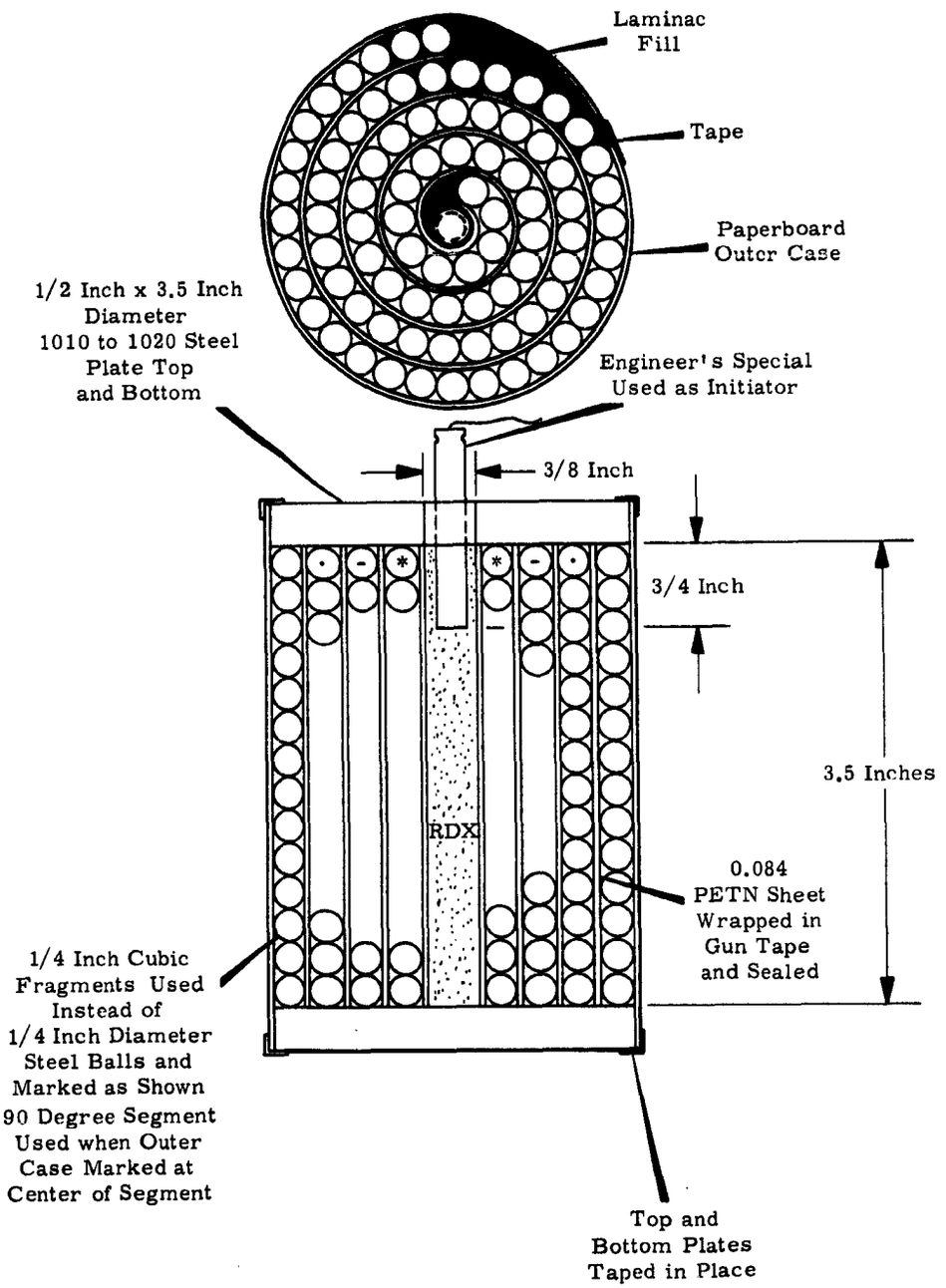


Figure 84. Test Model Design, Round No. 48 and 49

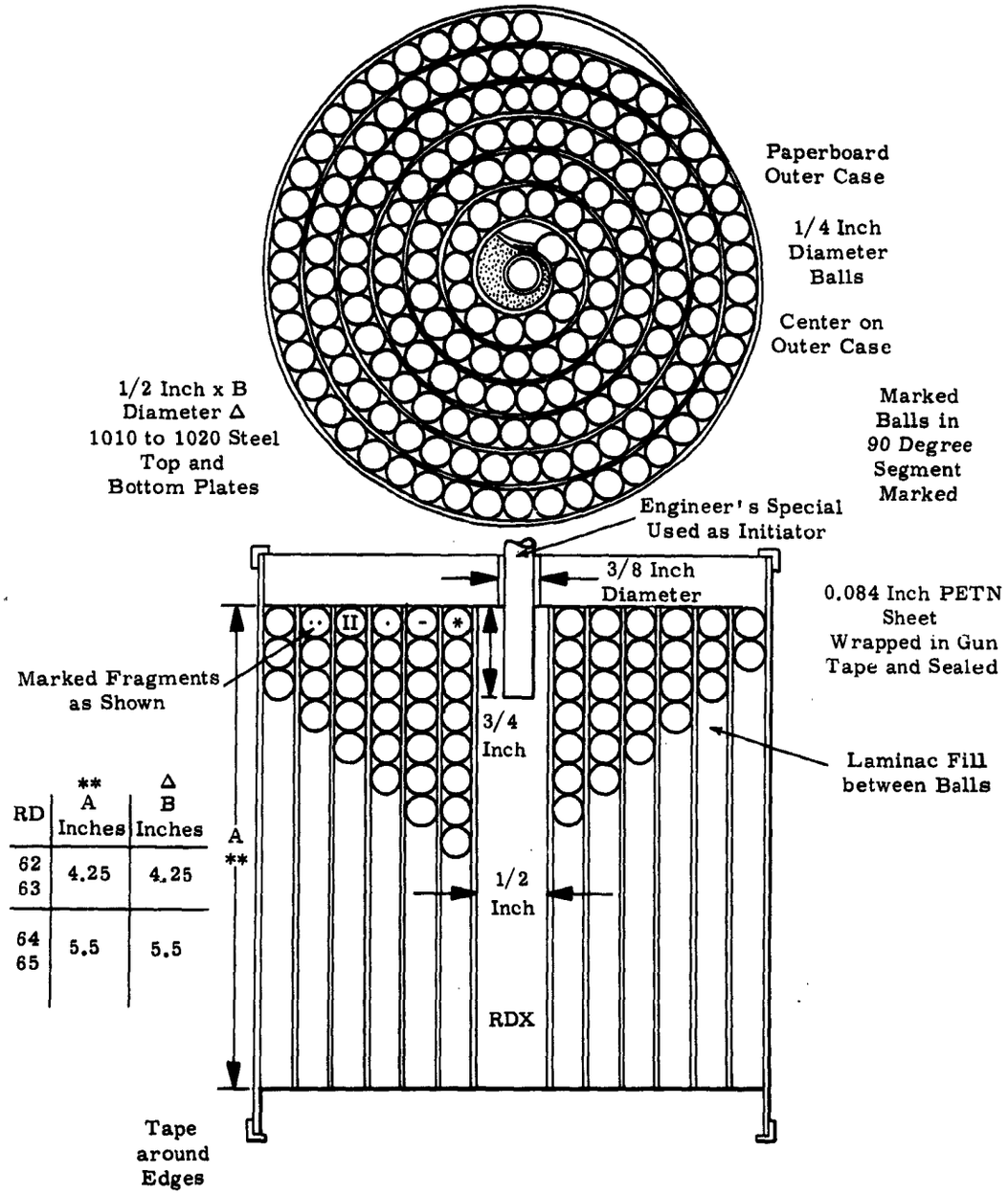


| RD | ** A Inches | Δ B Inches |
|---|---|---|
| 62 63 | 4.25 | 4.25 |
| 64 65 | 5.5 | 5.5 |

Figure 85. Test Model Design, Rounds No. 62 Through 65, 80, 81, and 83

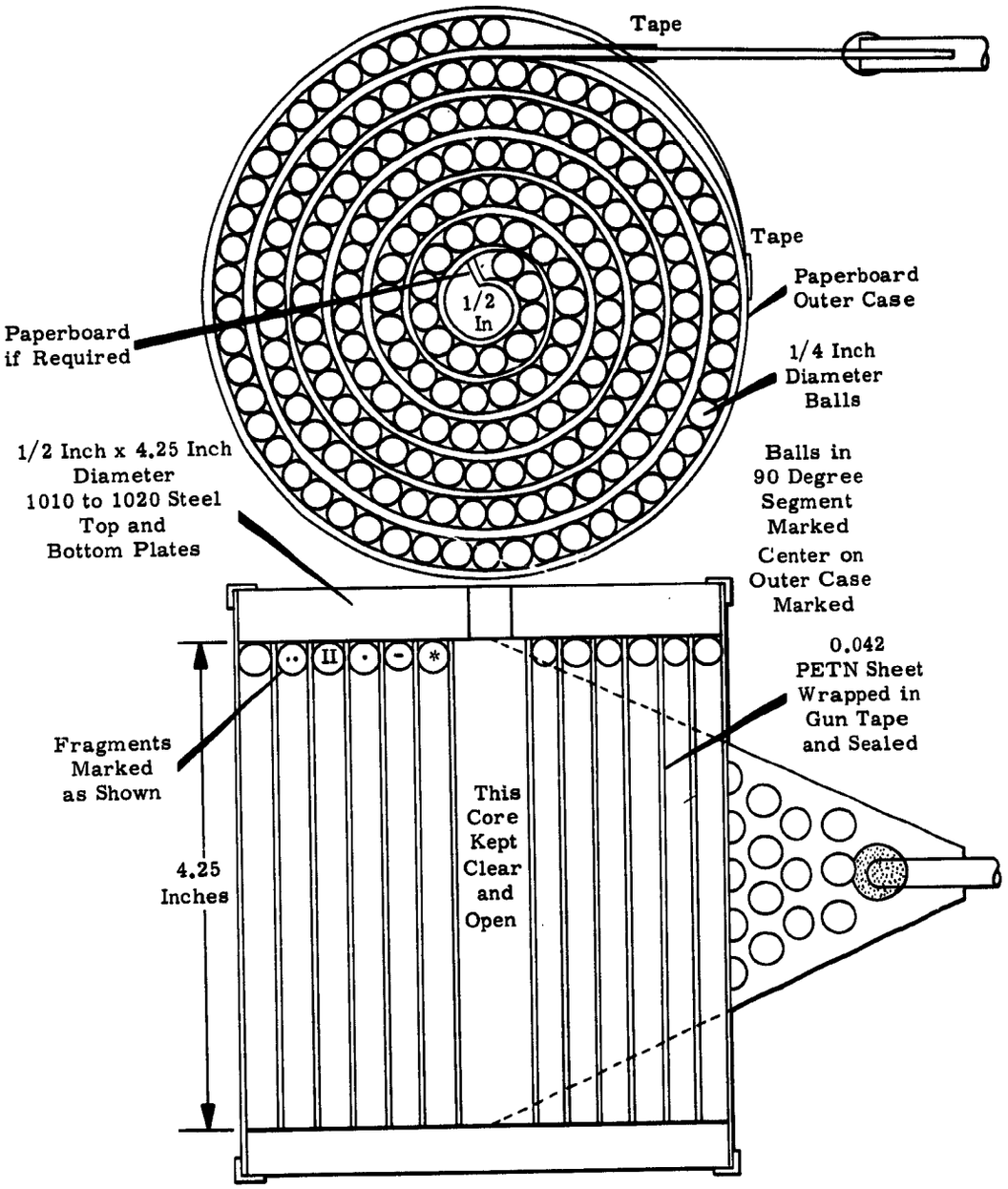


Figure 86. Test Model Design, Round No. 77

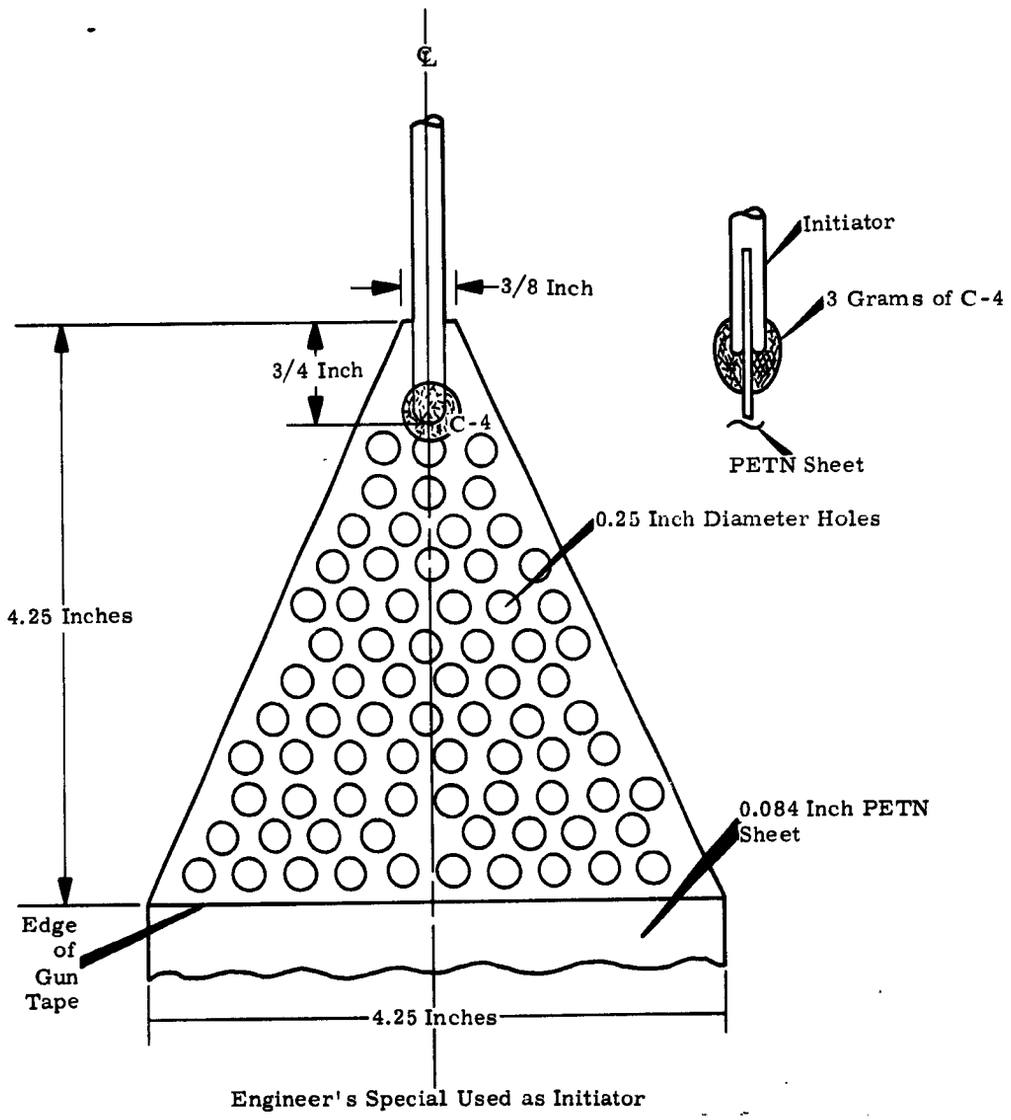


Figure 87. Test Model Design, End-Line Initiator, Round No. 77

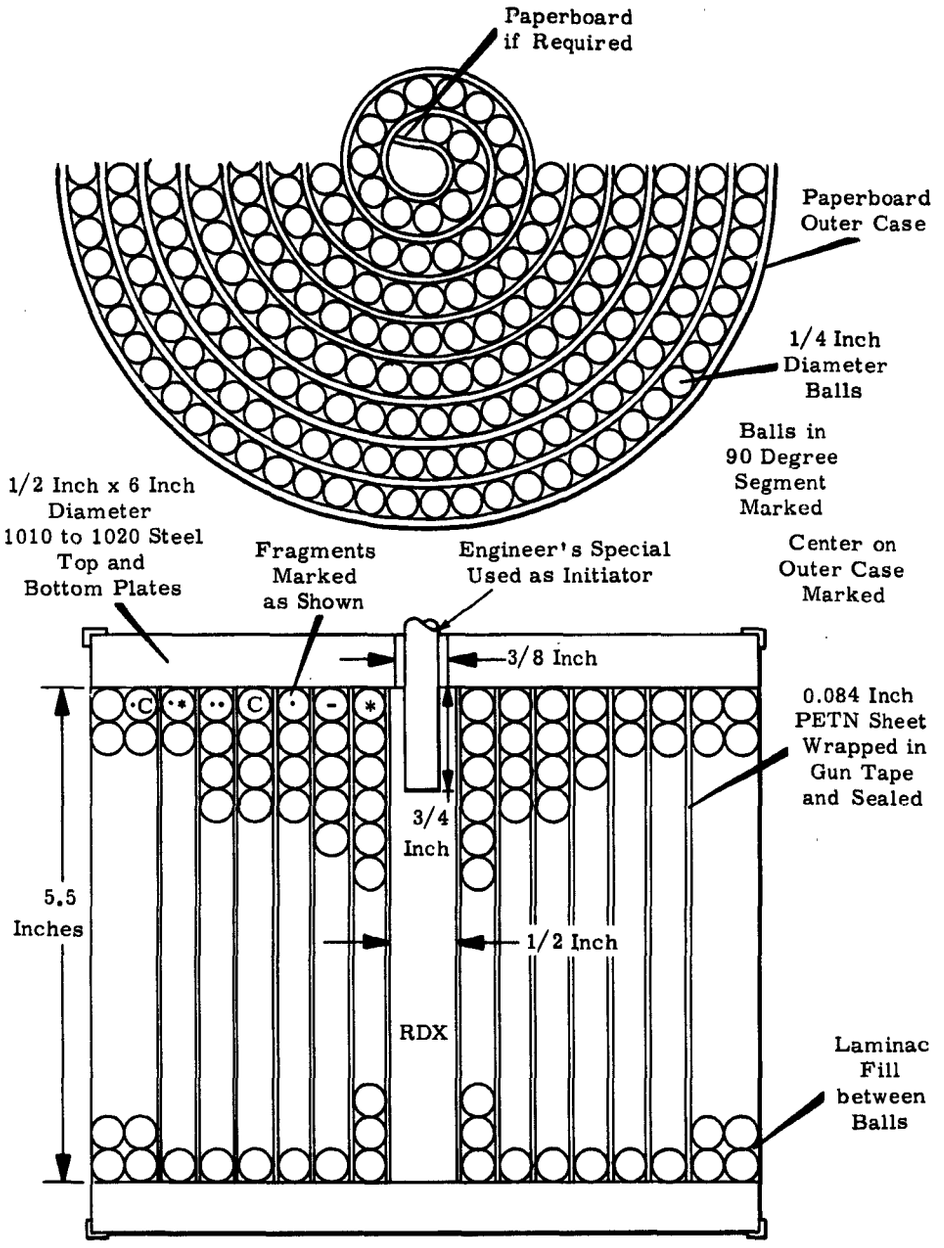


Figure 88. Test Model Design, Round No. 82

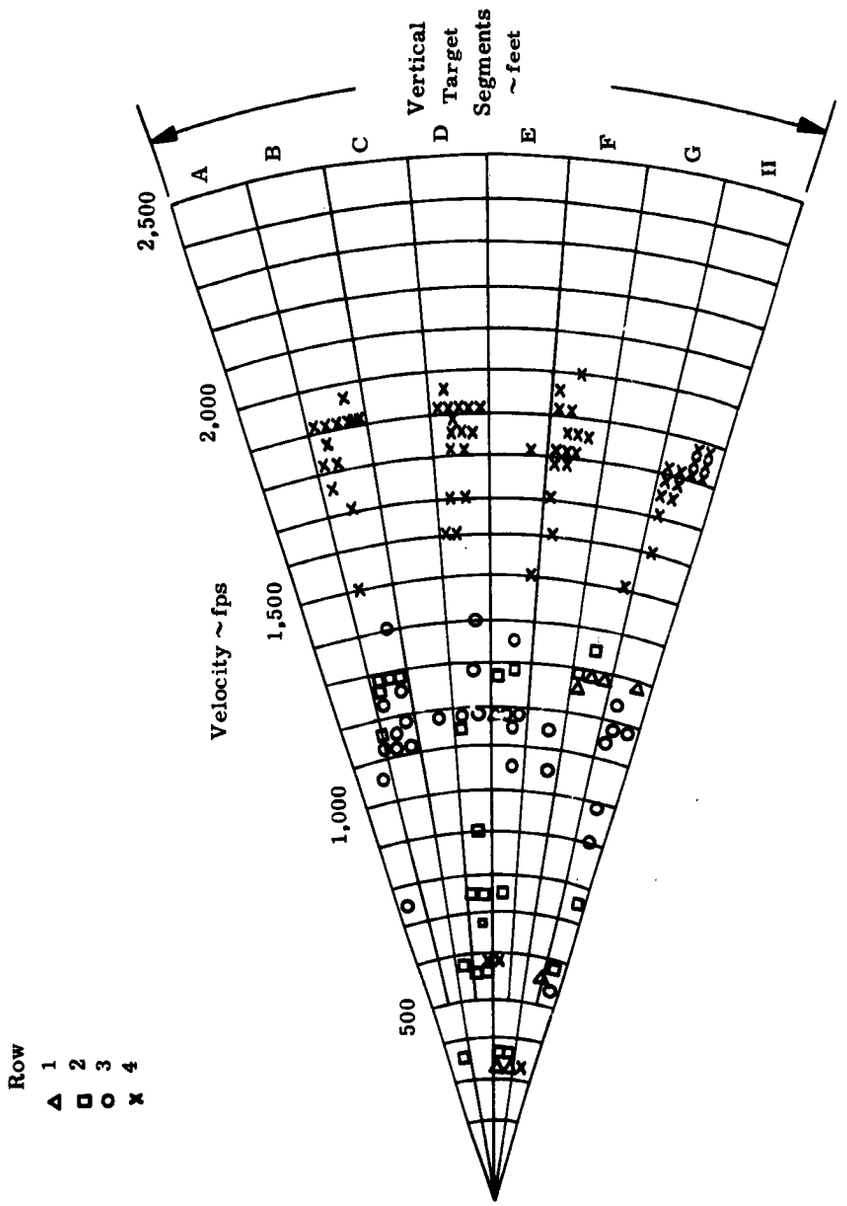


Figure 89. Velocity versus Radial Distribution, Round No. 5

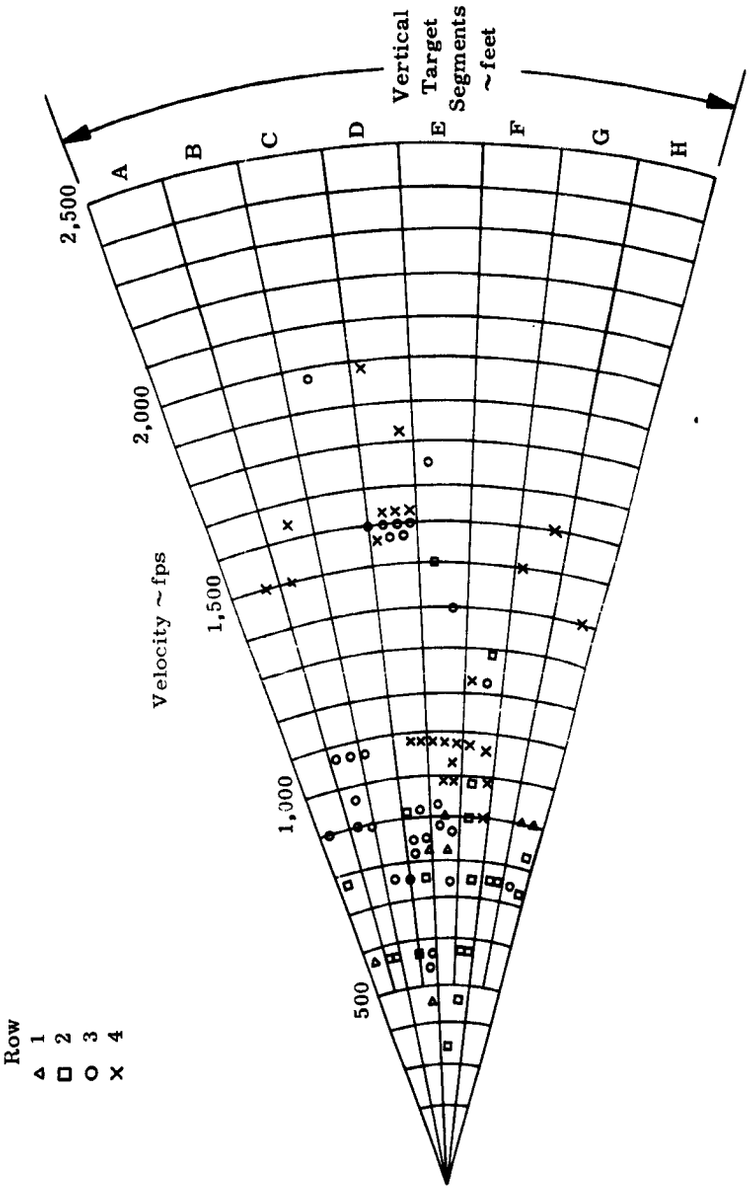


Figure 90. Velocity versus Radial Distribution, Round No. 6

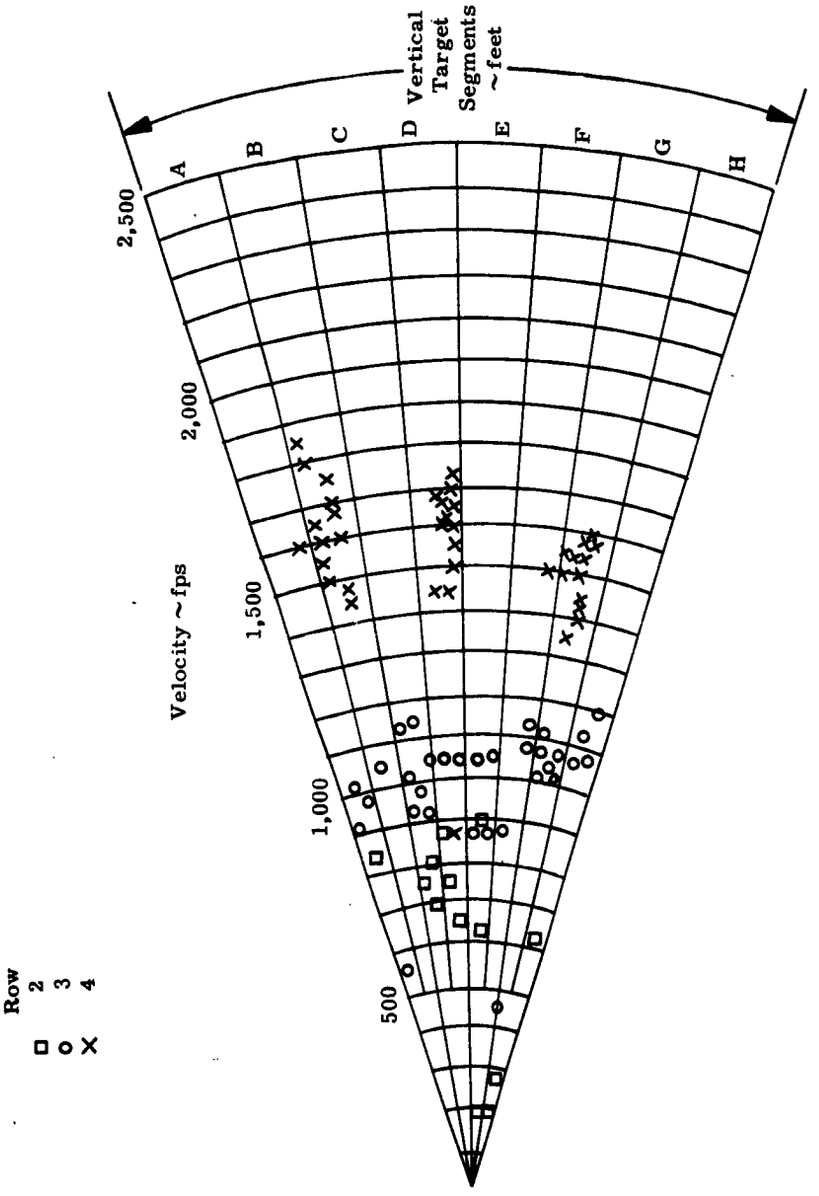


Figure 91. Velocity versus Radial Distribution, Round No. 19

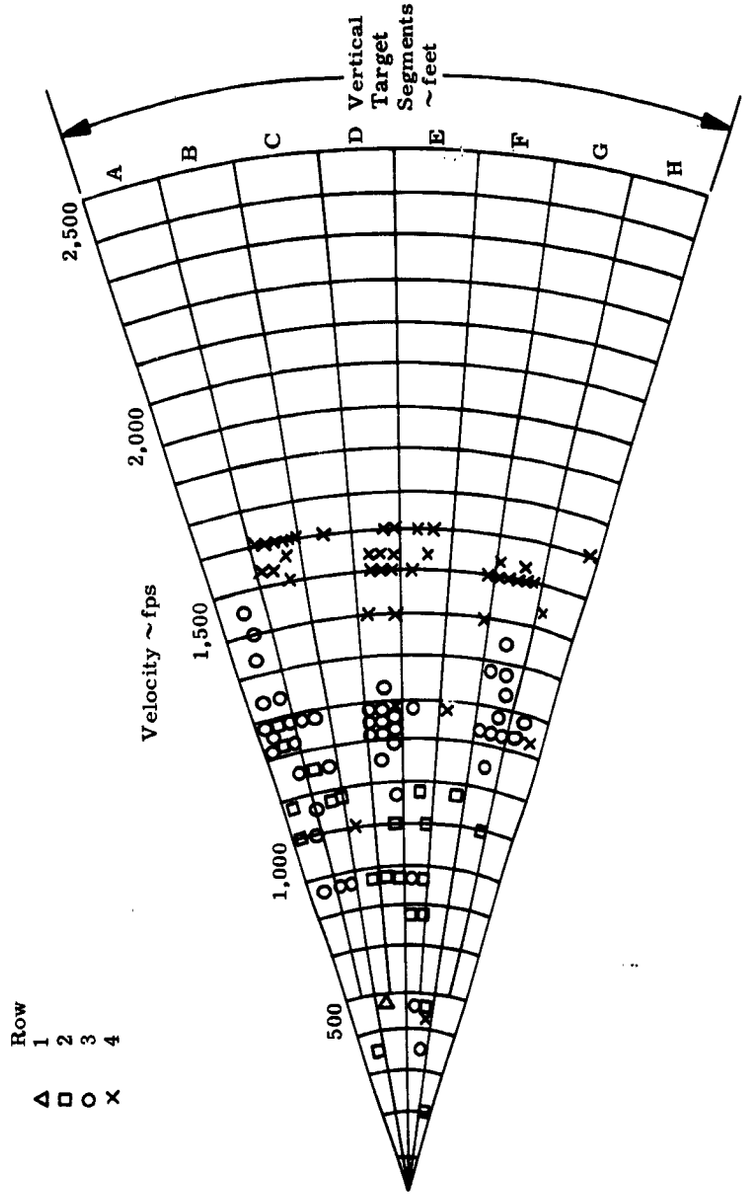


Figure 92. Velocity versus Radial Distribution, Round No. 20

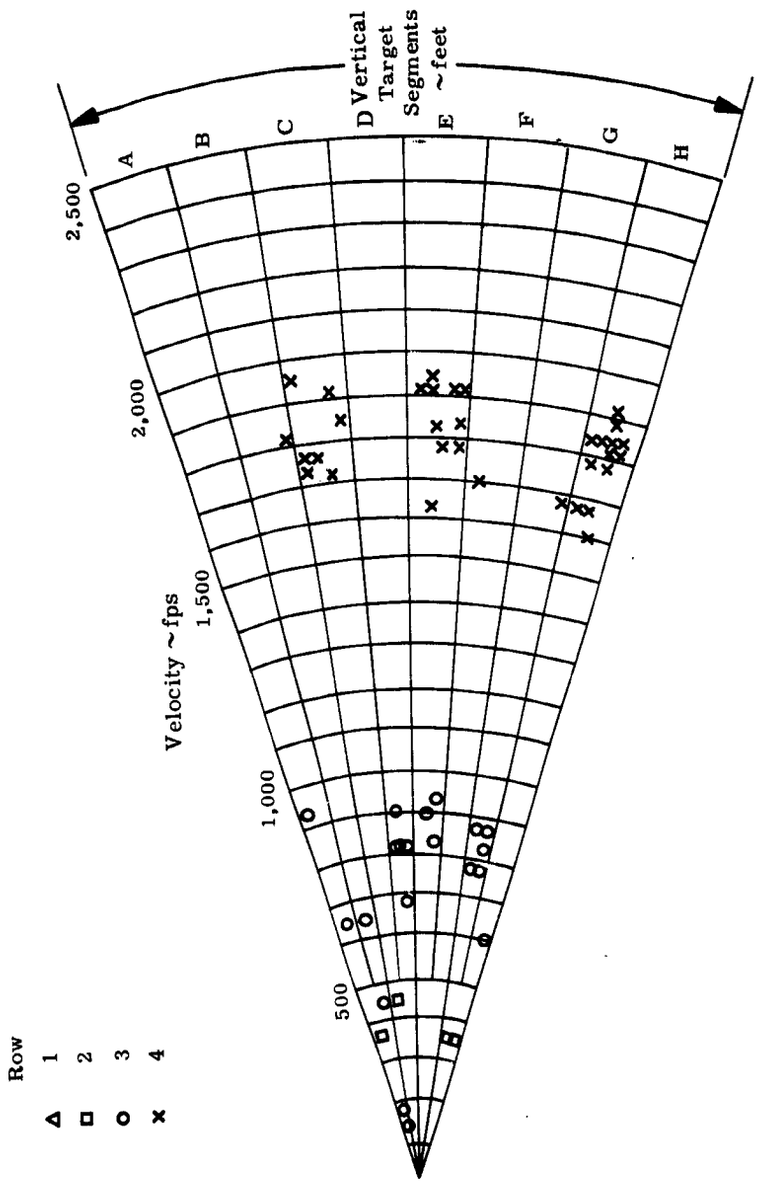


Figure 93. Velocity versus Radial Distribution, Round No. 30

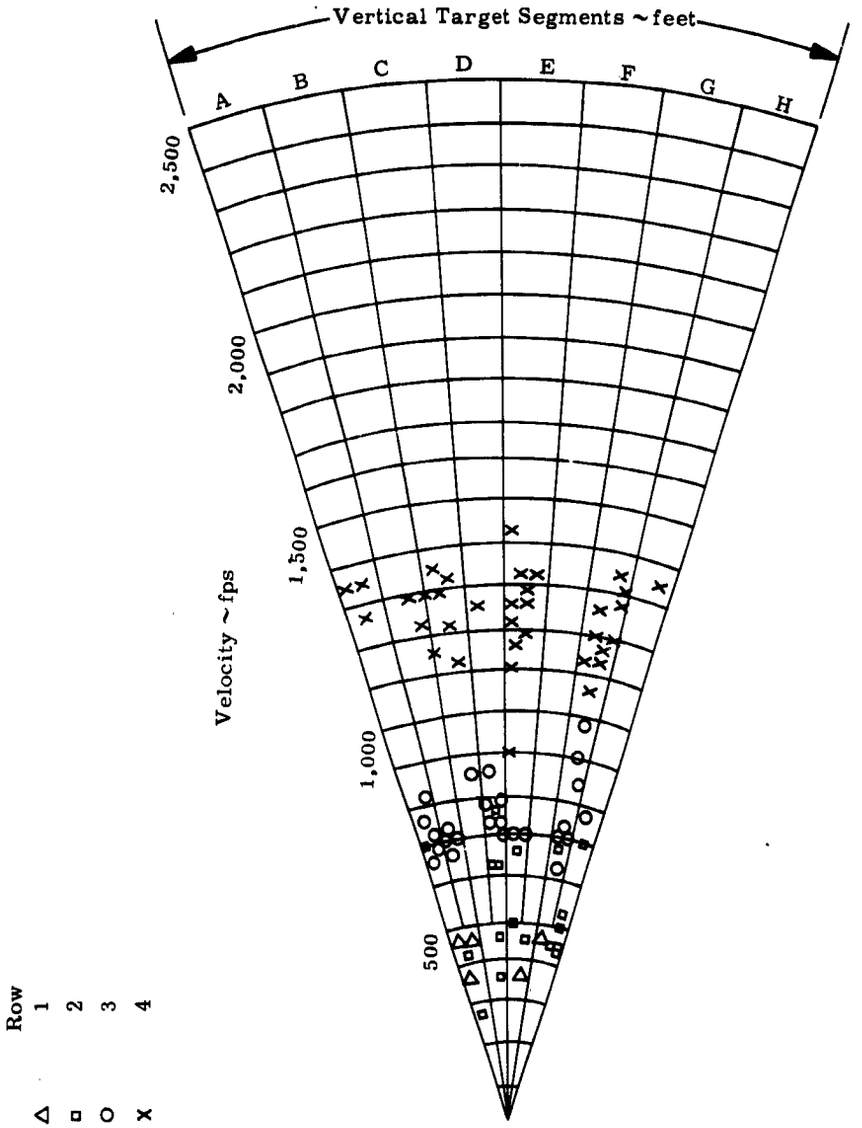


Figure 94. Velocity versus Radial Distribution, Round No. 34

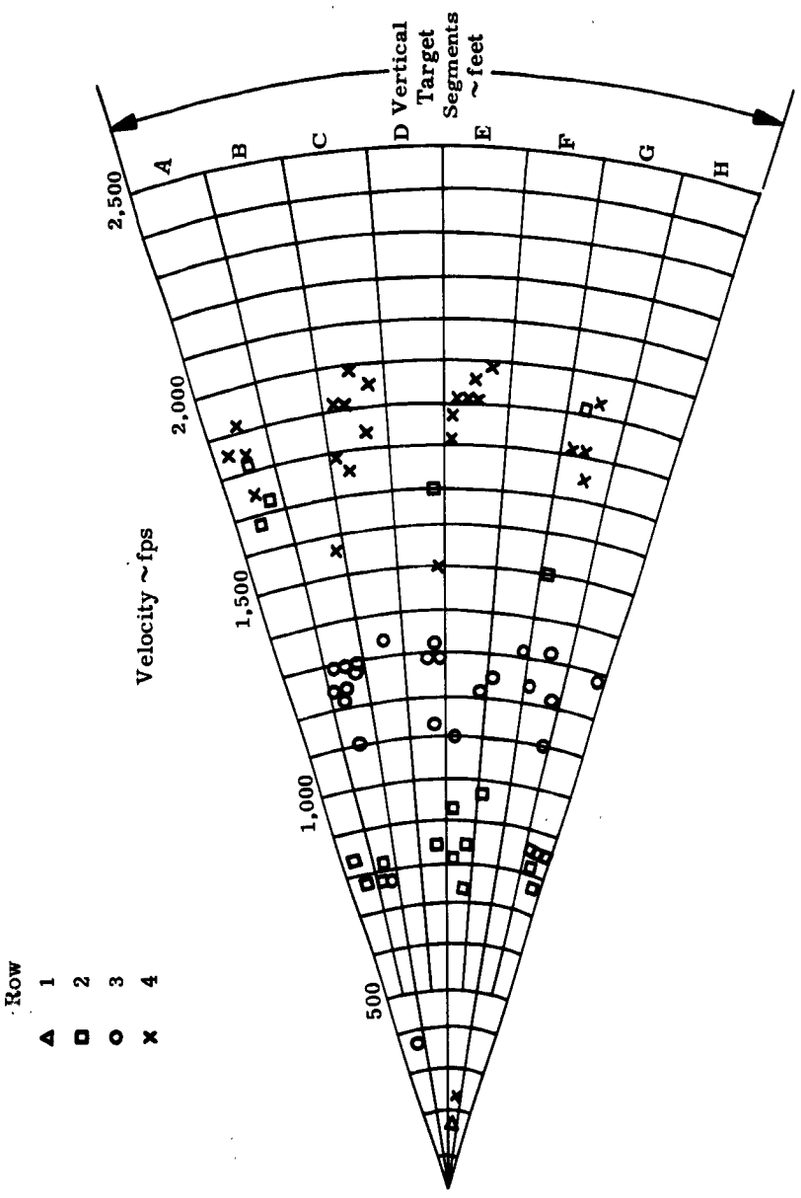


Figure 95. Velocity versus Radial Distribution, Round No. 35

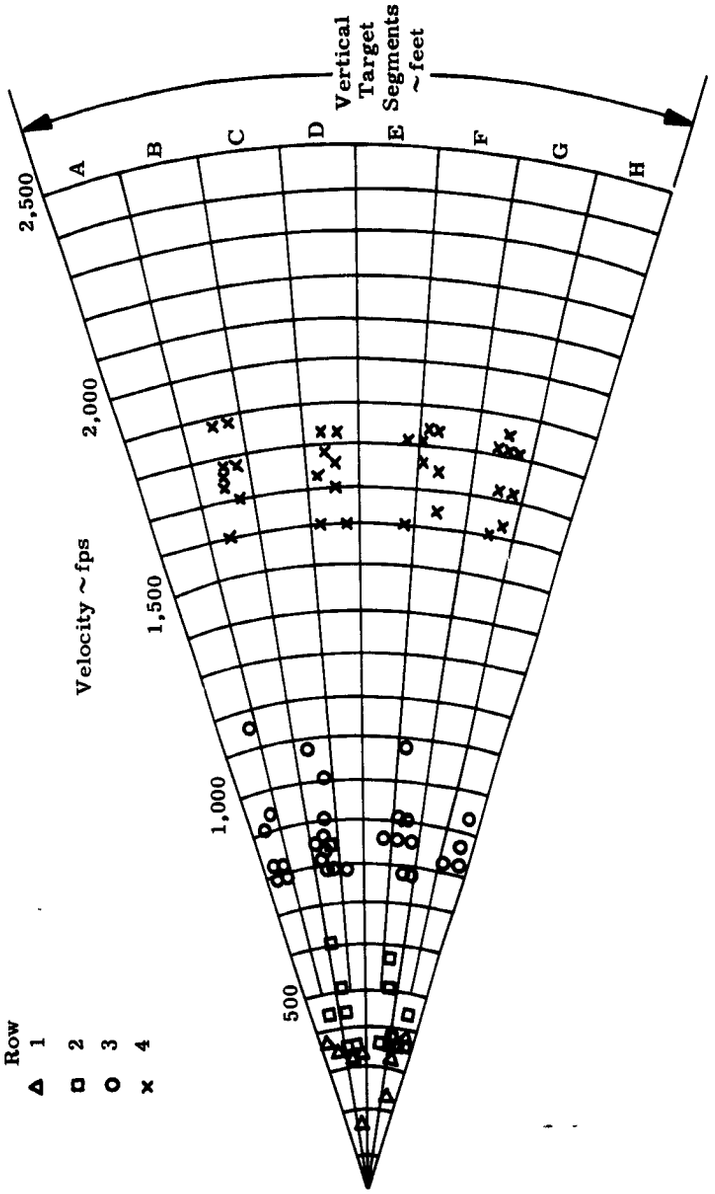


Figure 96. Velocity versus Radial Distribution, Round No. 38

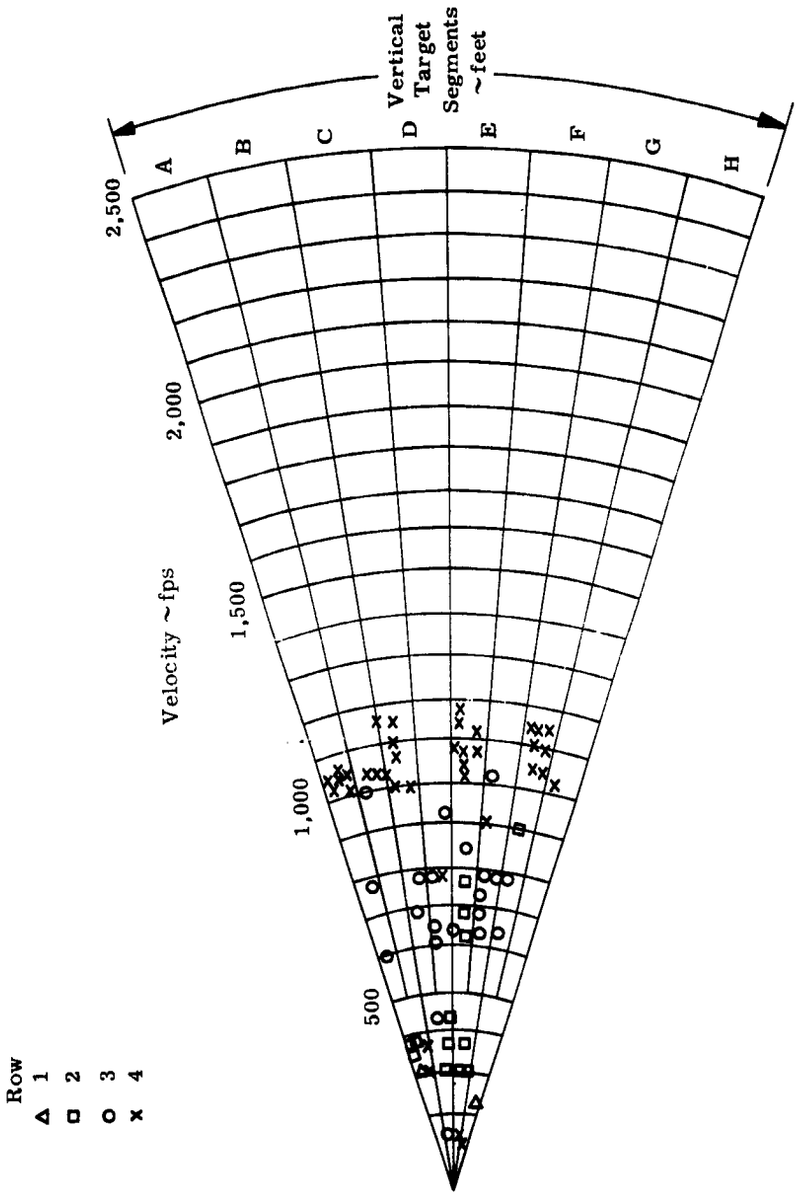


Figure 97. Velocity versus Radial Distribution, Round No. 41

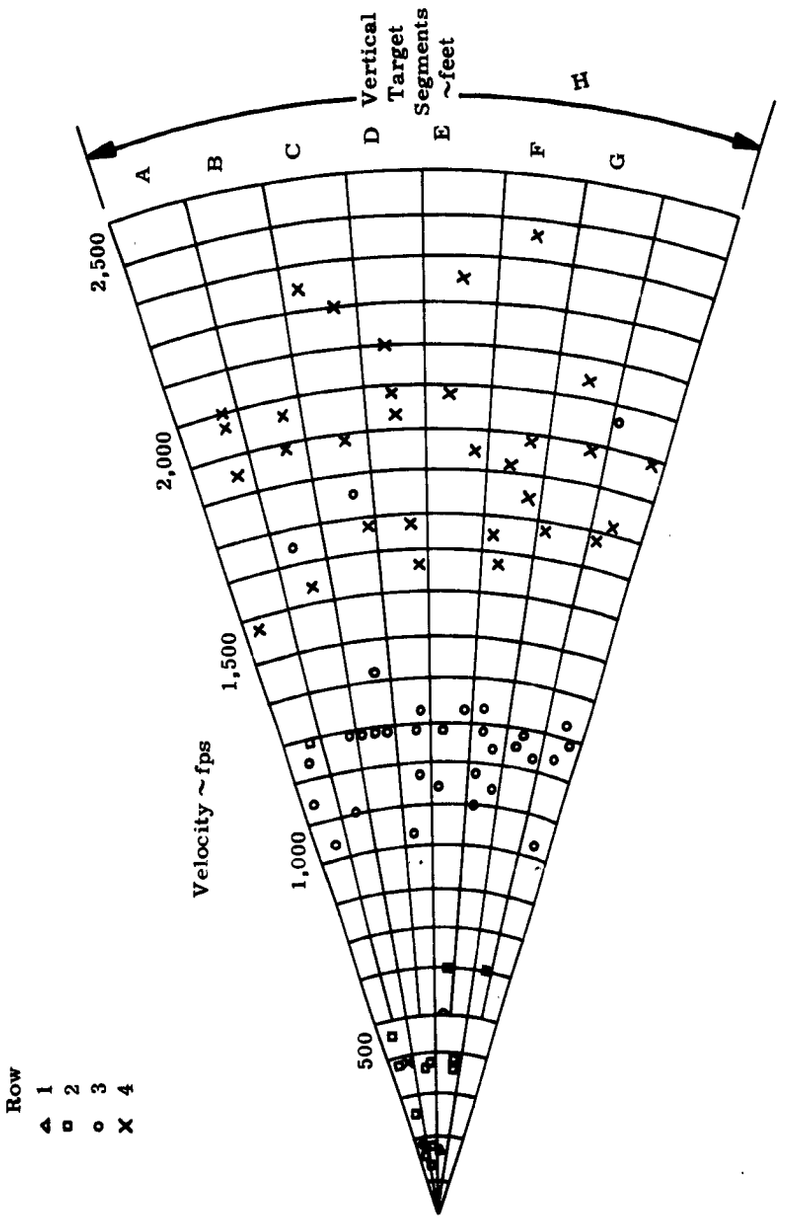


Figure 98. Velocity versus Radial Distribution, Round No. 43X

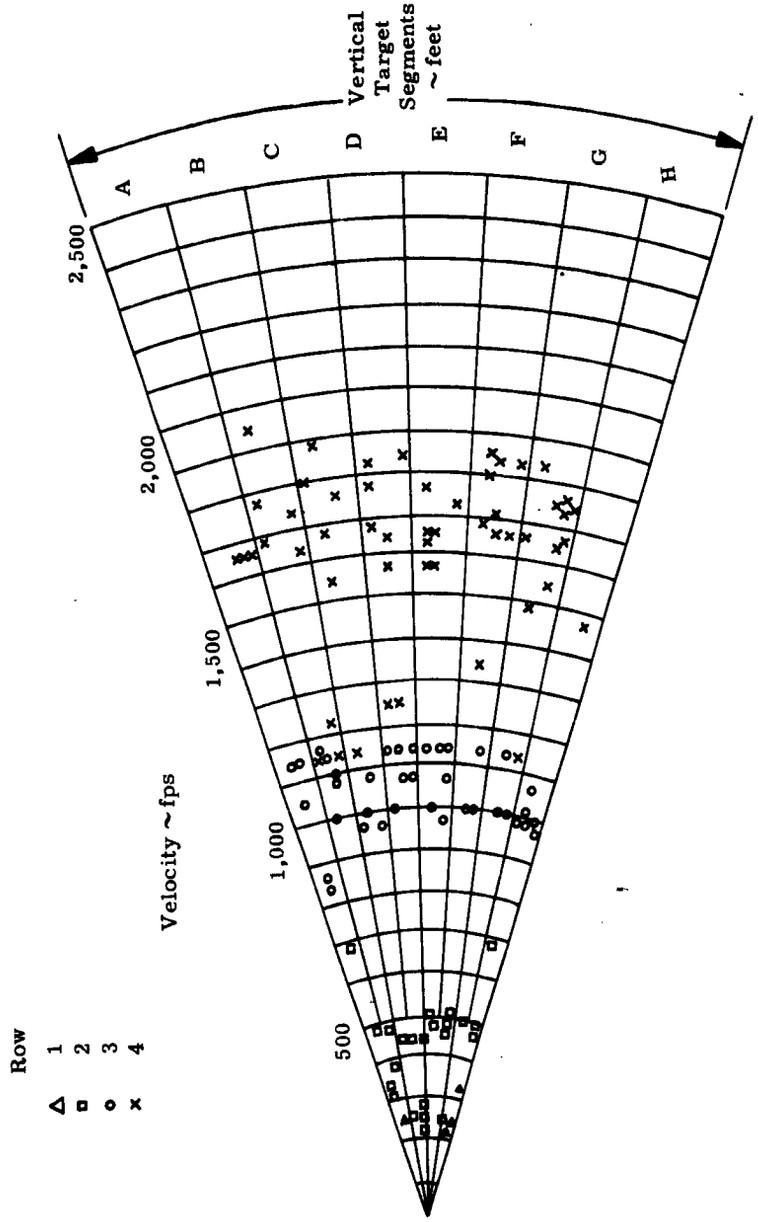


Figure 99. Velocity versus Radial Distribution, Round No. 48

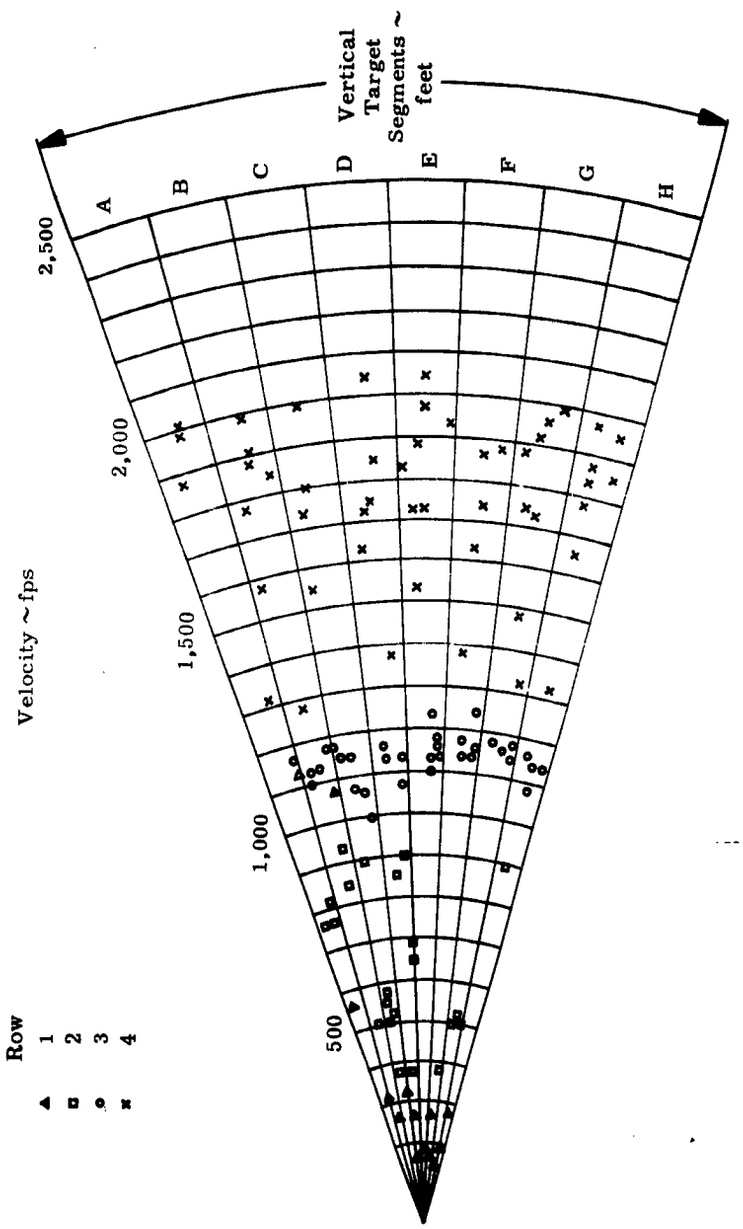


Figure 100. Velocity versus Radial Distribution, Round No. 49X

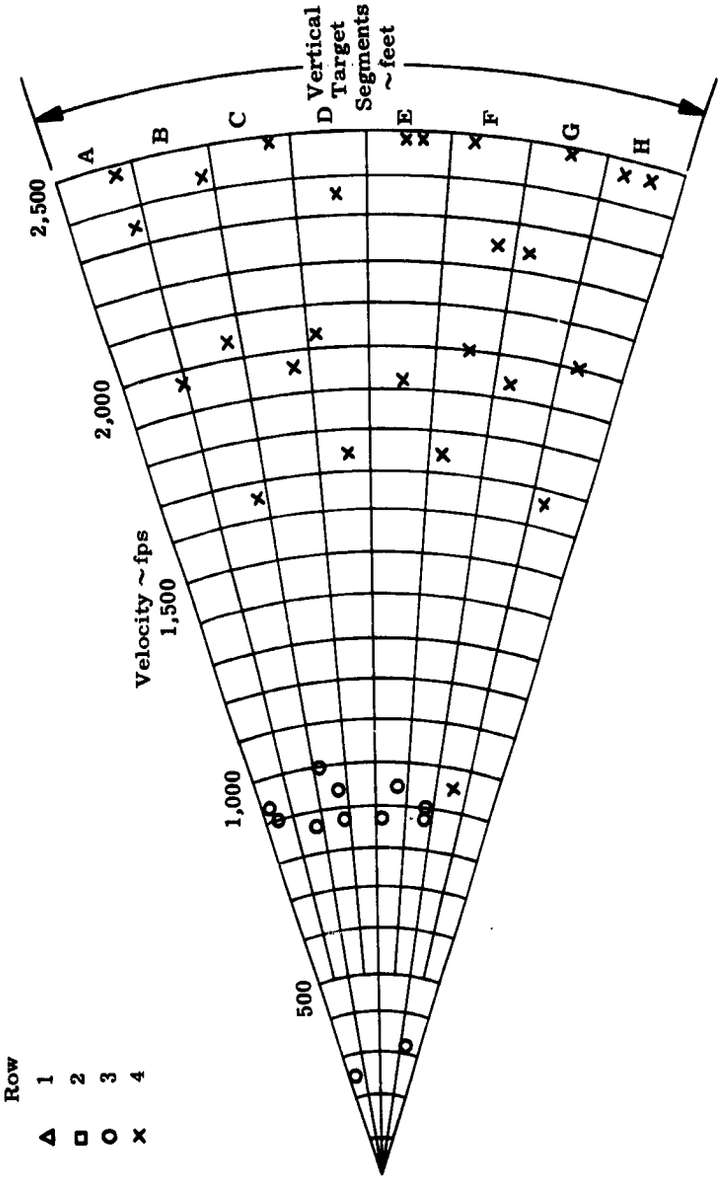


Figure 101. Velocity versus Radial Distribution, Round No. 52X

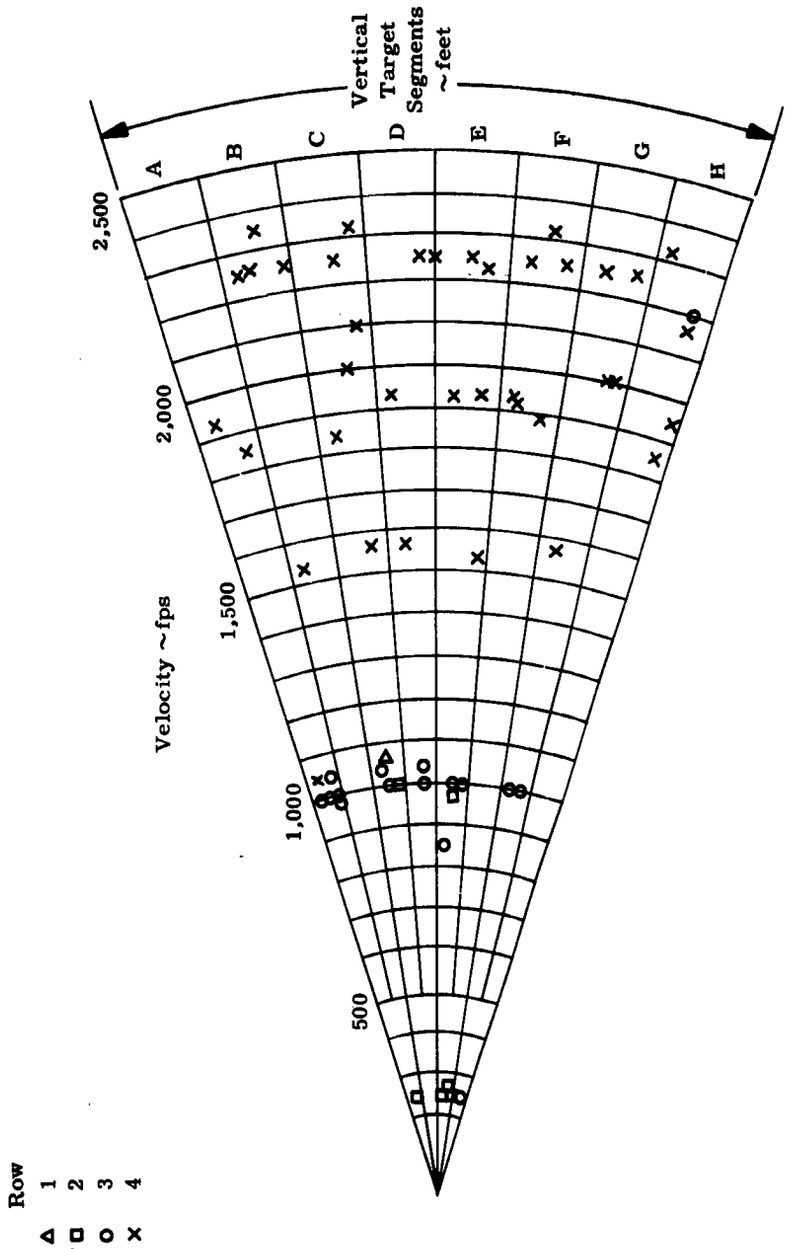


Figure 102. Velocity versus Radial Distribution, Round No. 53

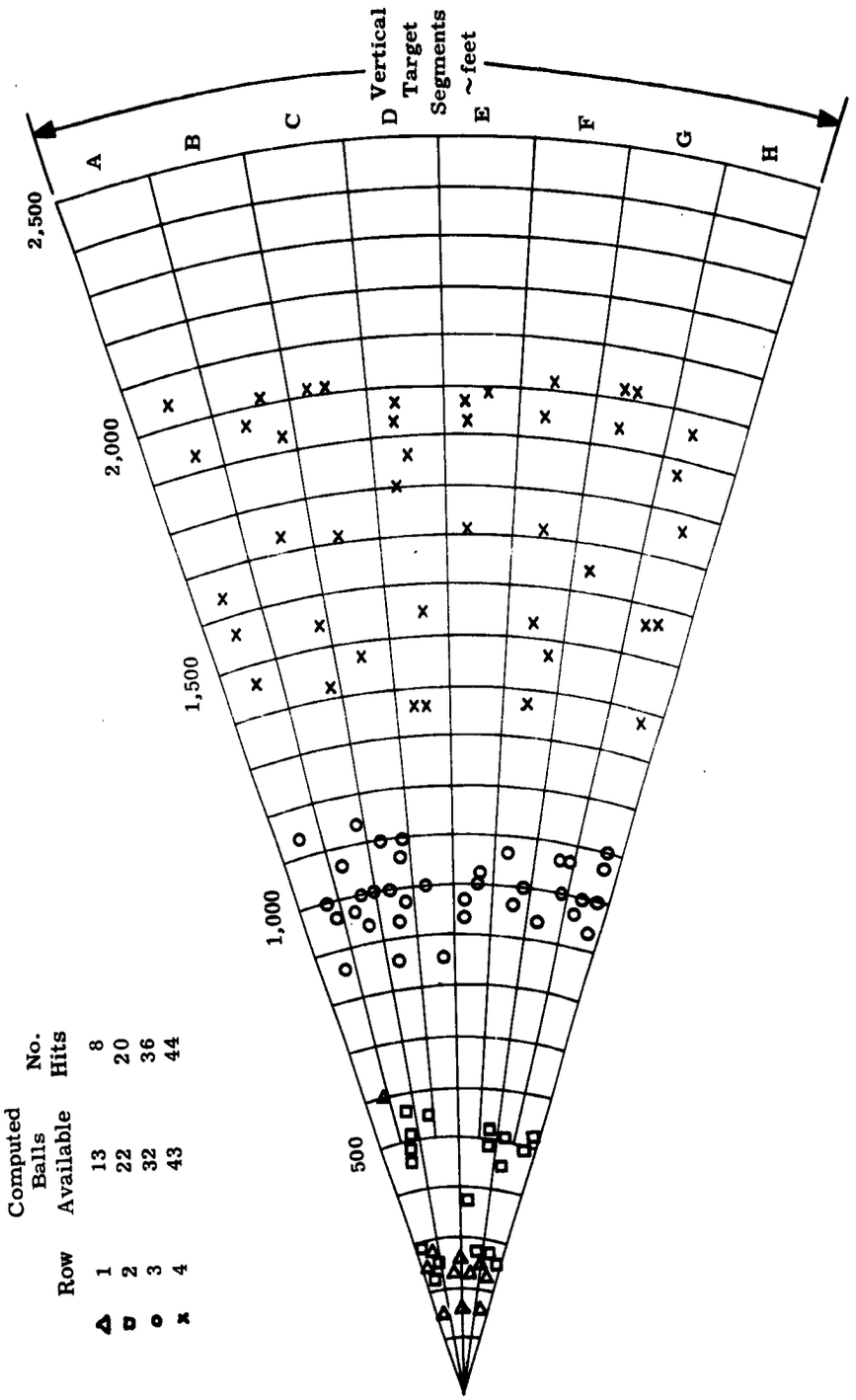


Figure 103. Velocity versus Radial Distribution, Round No. 54

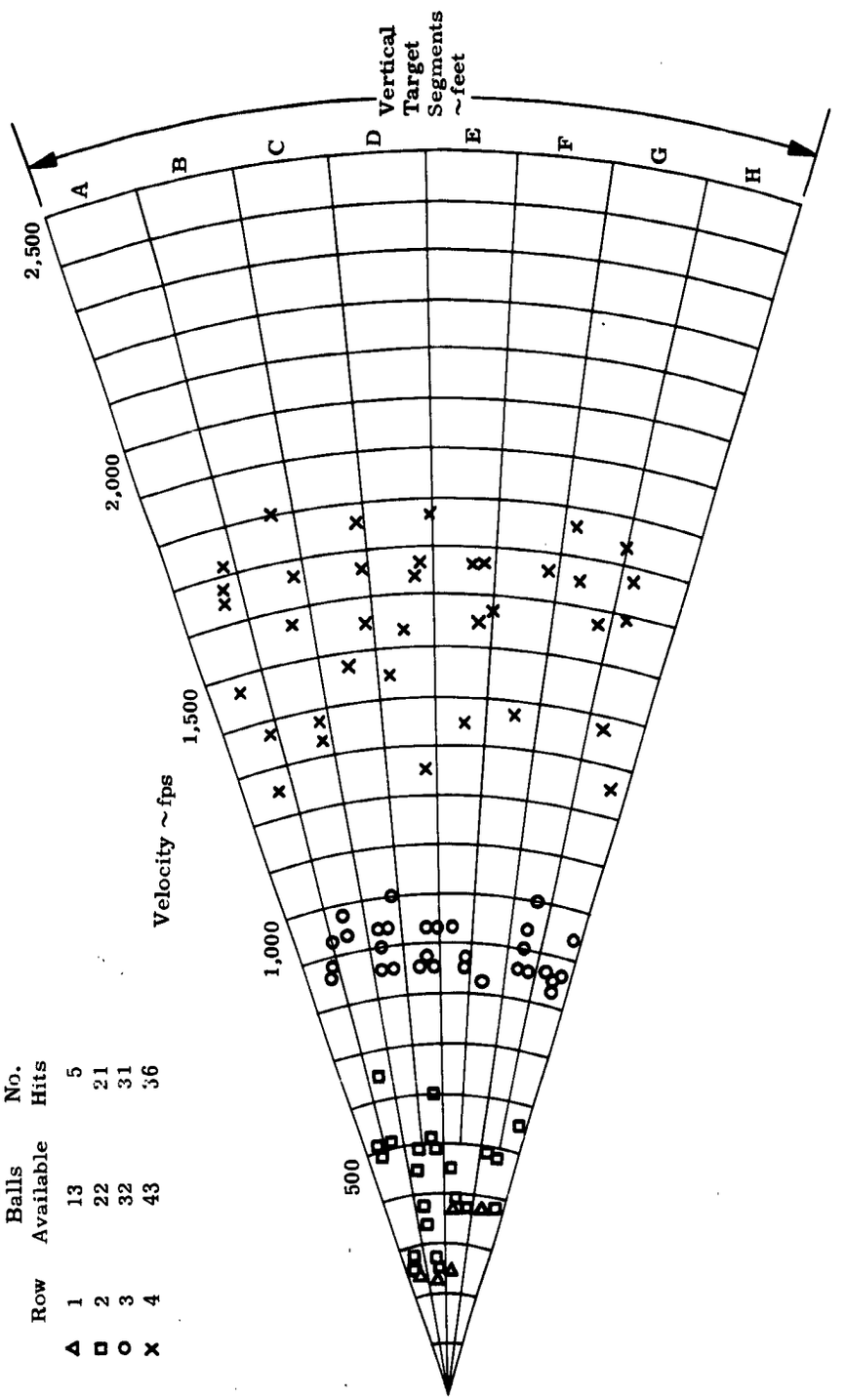


Figure 104. Velocity versus Radial Distribution, Round No. 55

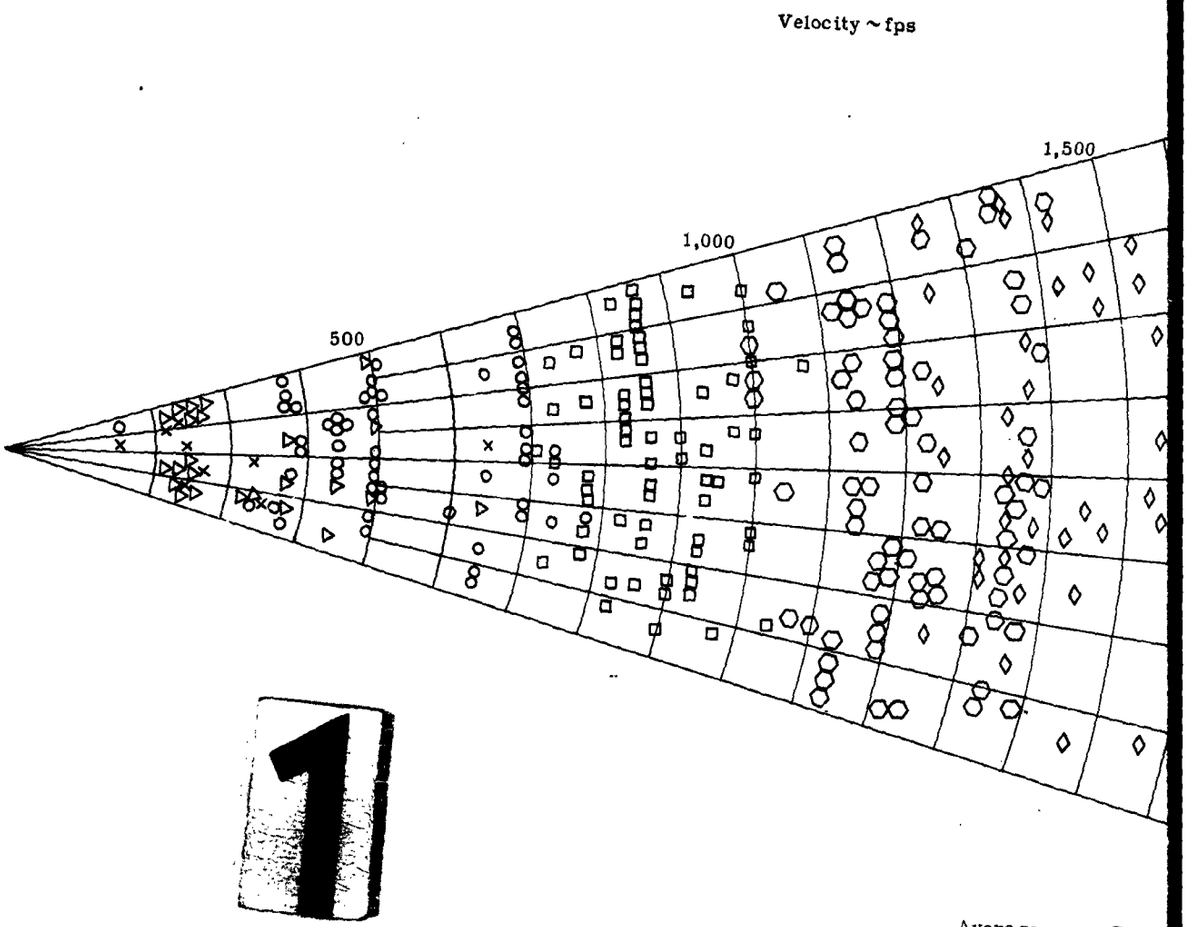




| Row | | Average Velocity fps | Comp Ball Avail |
|---|---|---|---|
| × | 1 | 320 | 24 |
| △ | 2 | 332 | 40 |
| ○ | 3 | 534 | 56 |
| □ | 4 | 886 | 72 |
| ⬡ | 5 | 1,221 | 88 |
| ◇ | 6 | 1,605 | 104 |

Figure 105. Velocity versus Radial Distribution, Round No. 56

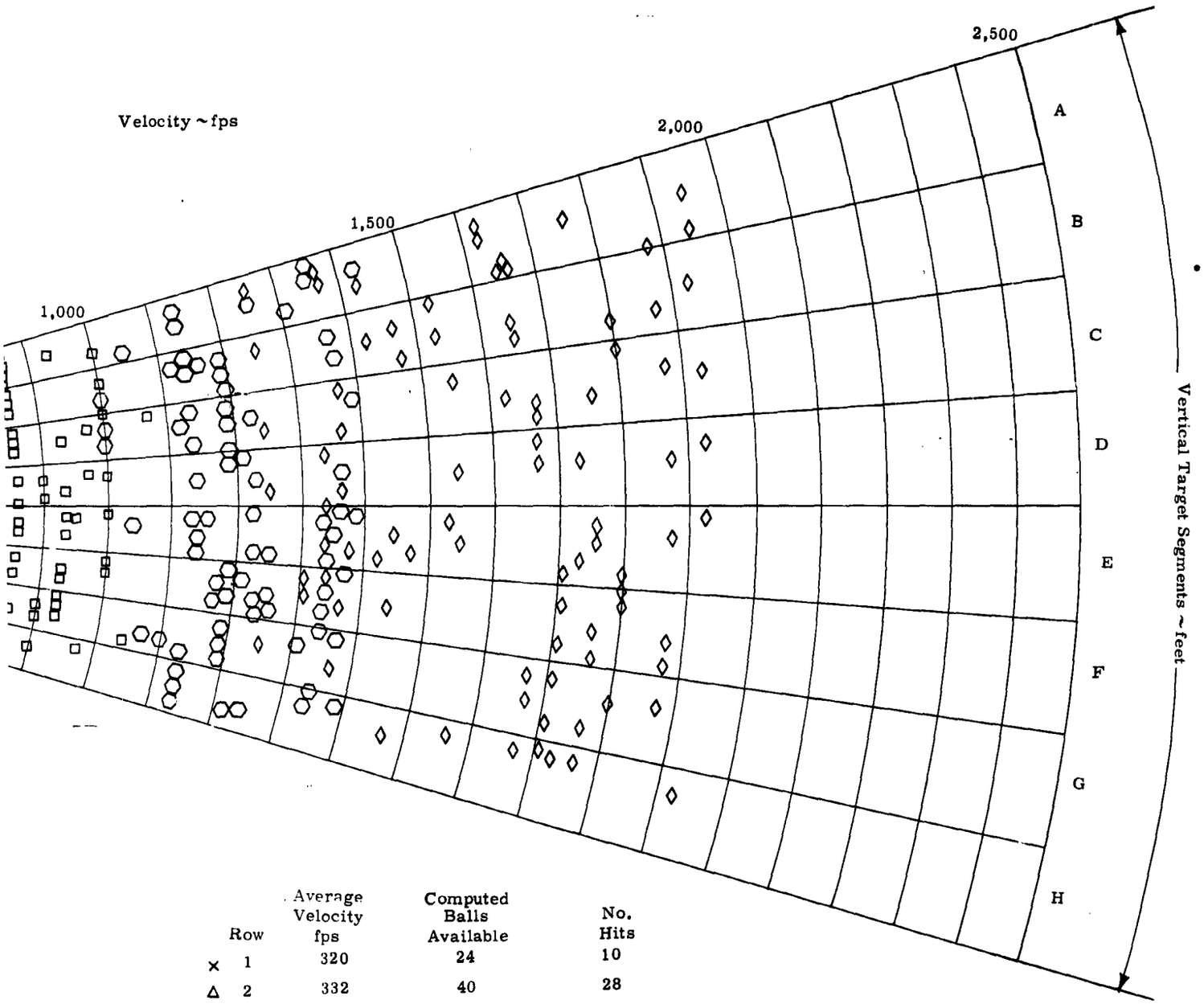


| Row | Average Velocity fps | Computed Balls Available | No. Hits |
|---|---|---|---|
| × 1 | 320 | 24 | 10 |
| △ 2 | 332 | 40 | 28 |
| ○ 3 | 534 | 56 | 53 |
| □ 4 | 886 | 72 | 70 |
| ⬡ 5 | 1,221 | 88 | 77 |
| ◇ 6 | 1,605 | 104 | 87 |

Round No. 56

2

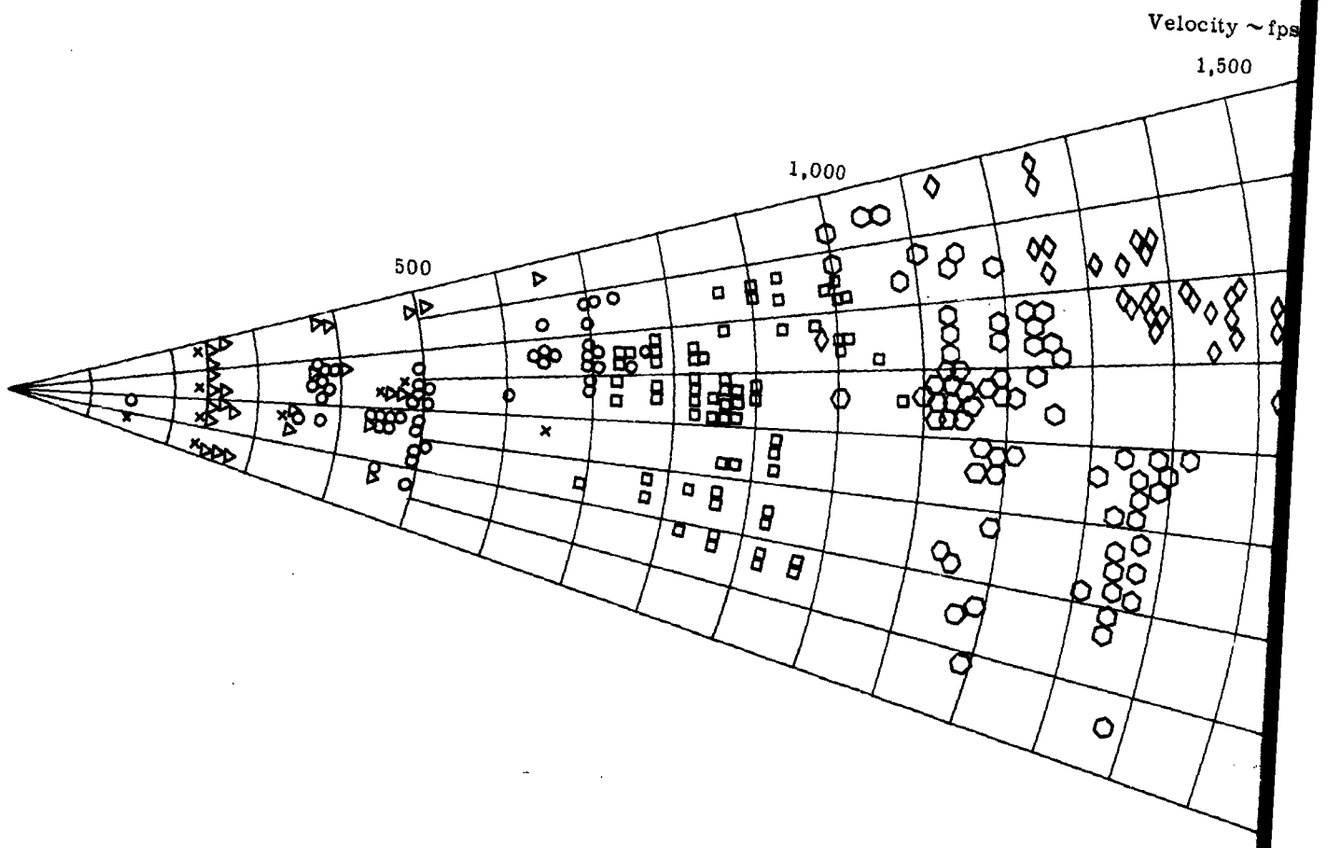
Velocity ~ fps
1,500
1,000
500

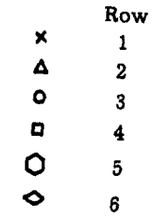
Row
1
2
3
4
5
6

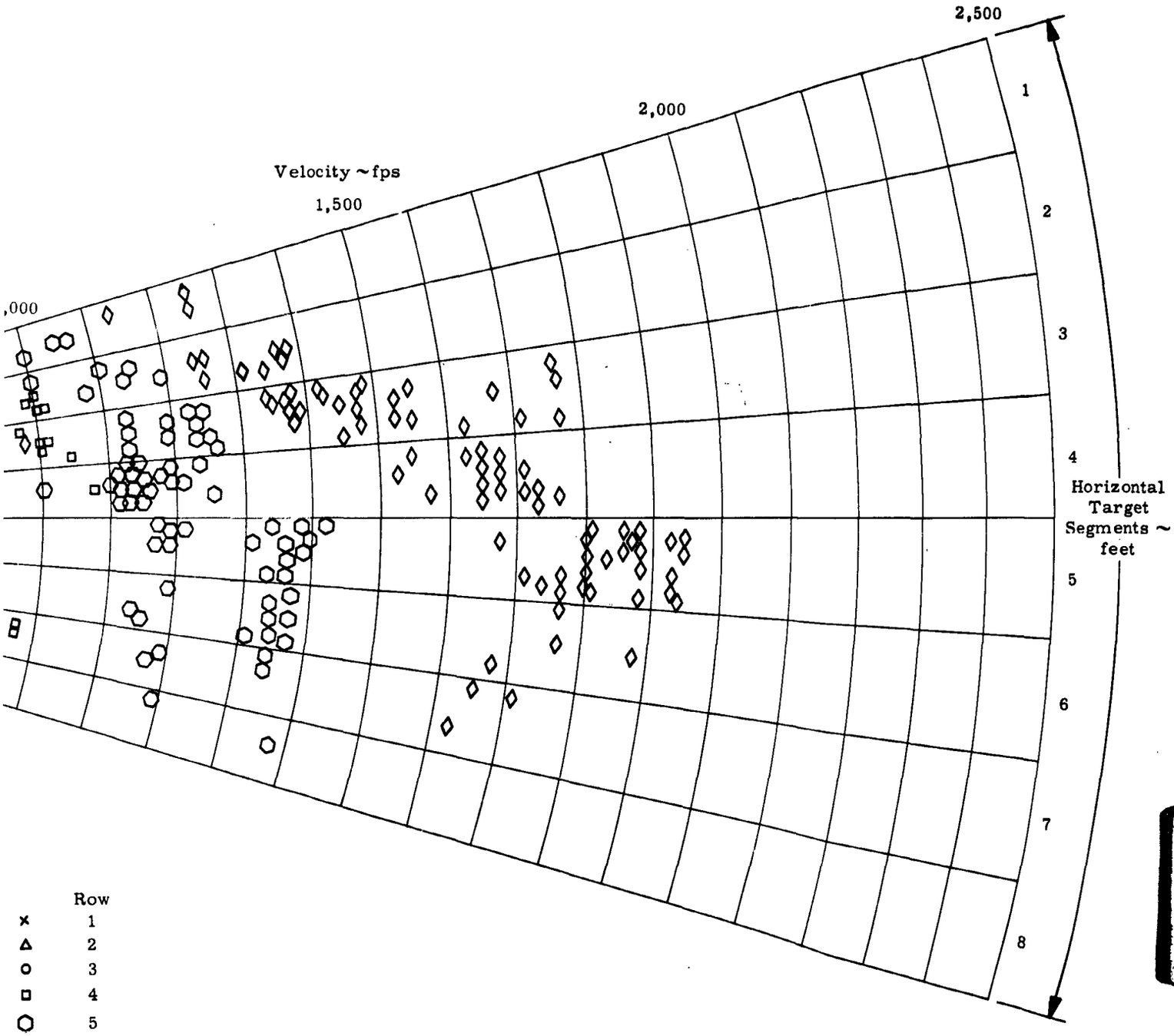


Figure 106. Velocity versus Radial Distribution, Round No. 56 (Side Cut)

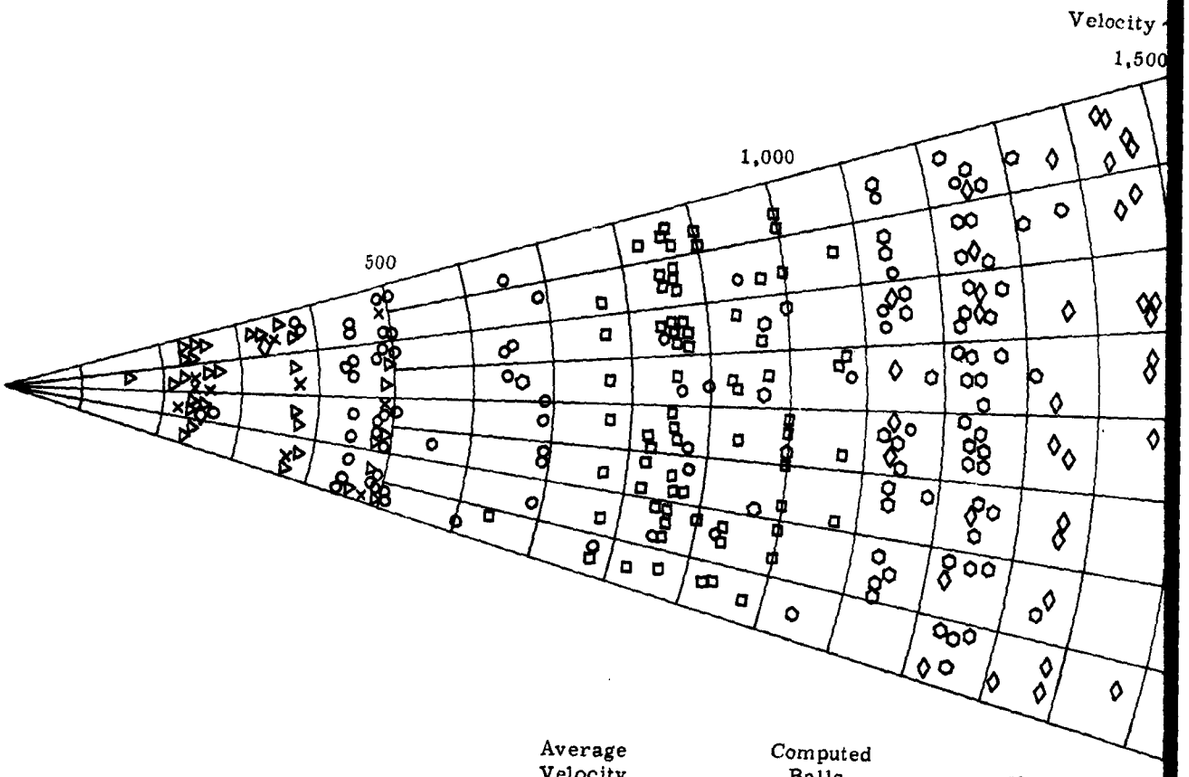


| | Row | Average Velocity fps | Computed Balls Available | No. Hits |
|---|---|---|---|---|
| × | 1 | 343 | 25 | 11 |
| △ | 2 | 346 | 41 | 32 |
| ○ | 3 | 633 | 57 | 56 |
| □ | 4 | 896 | 74 | 72 |
| ⬡ | 5 | 1,192 | 90 | 62 |
| ◇ | 6 | 1,540 | 106 | 95 |

Figure 107. Velocity versus Radial Distribution, Round No. 57

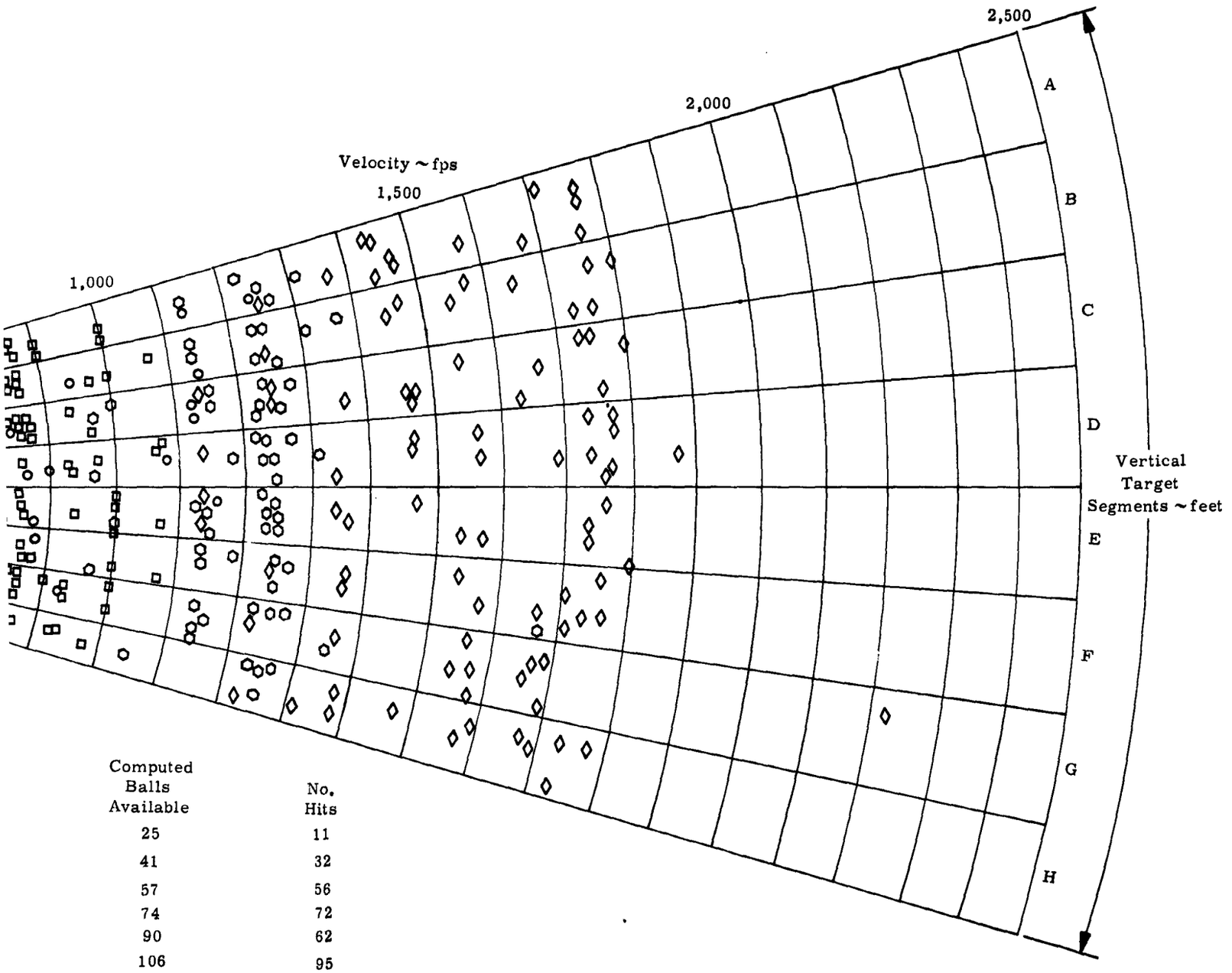


| Computed Balls Available | No. Hits |
|---|---|
| 25 | 11 |
| 41 | 32 |
| 57 | 56 |
| 74 | 72 |
| 90 | 62 |
| 106 | 95 |



2

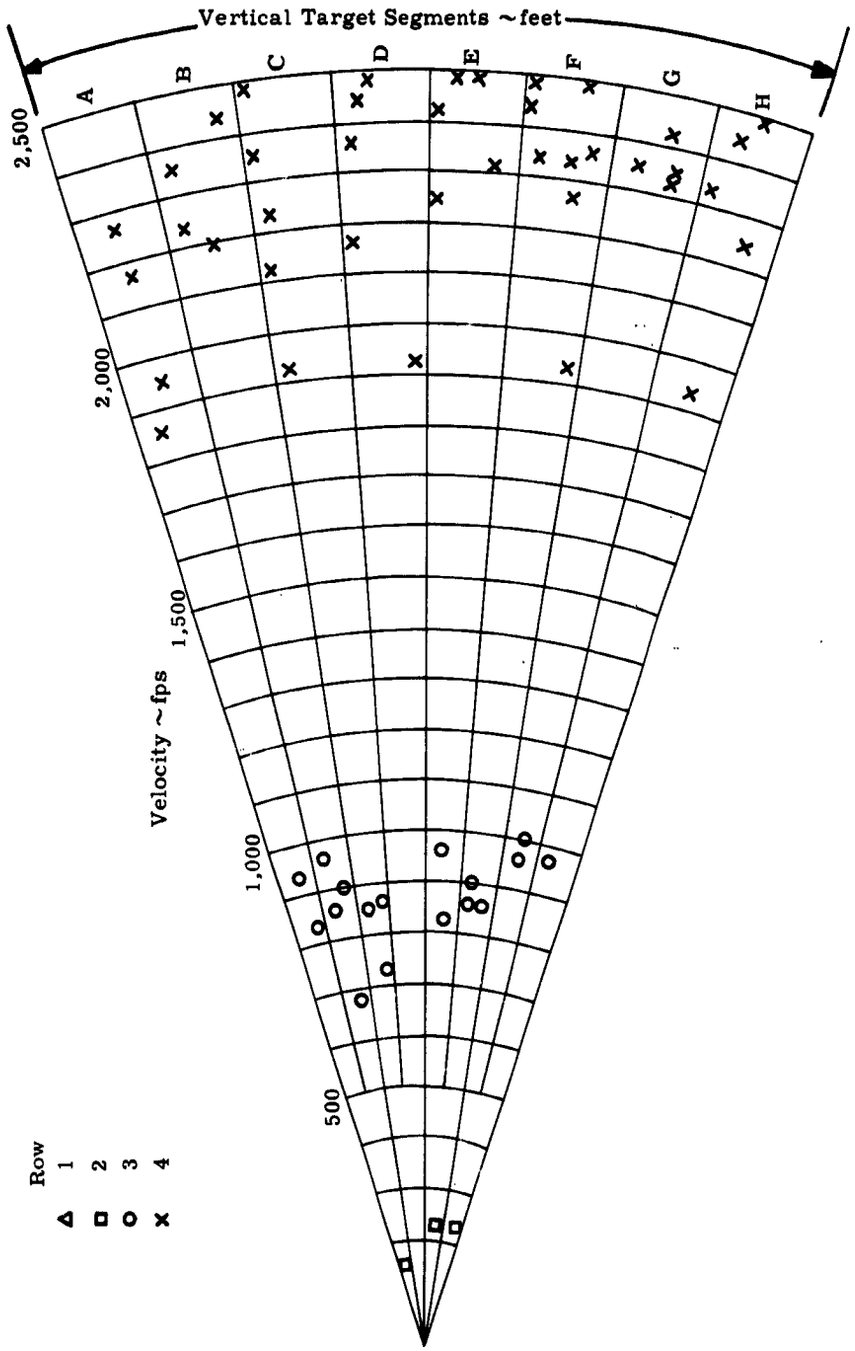


Figure 108. Velocity versus Radial Distribution, Round No. 60

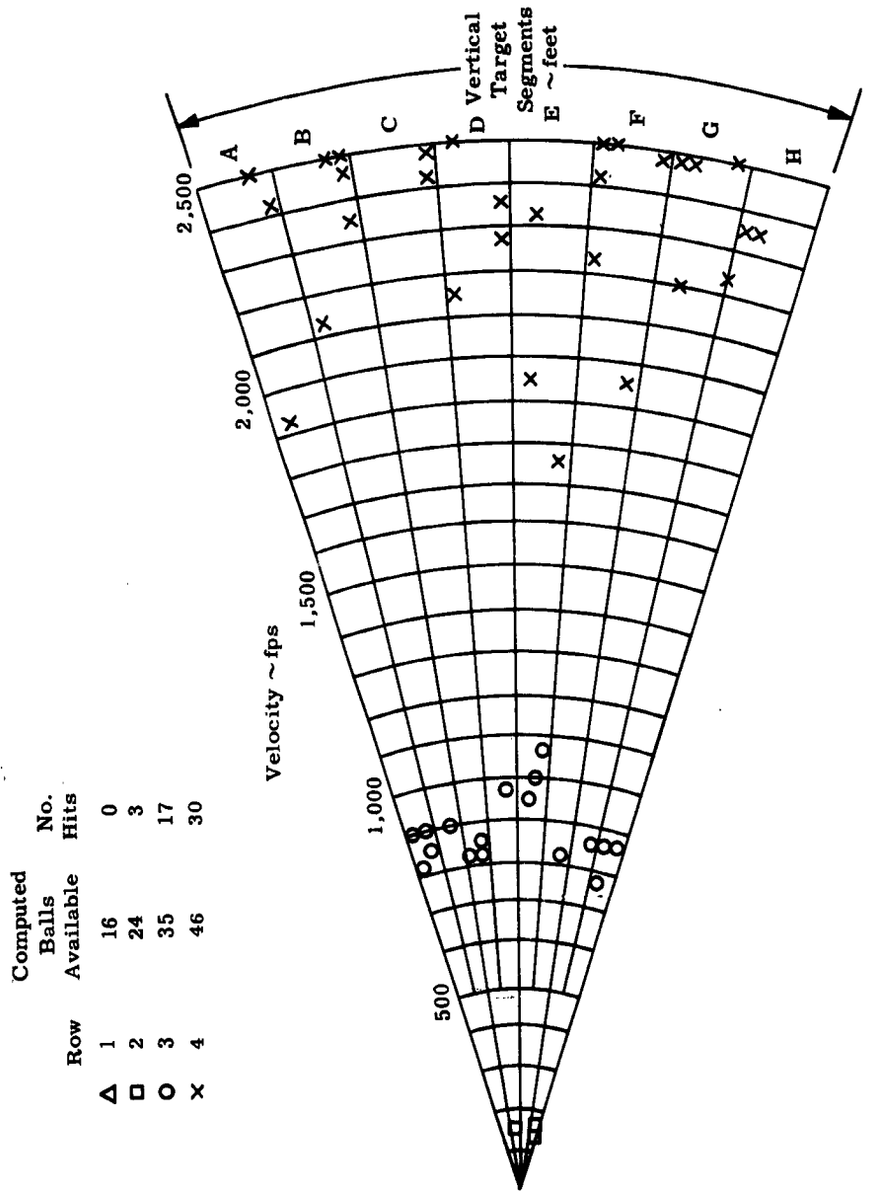


Figure 109. Velocity versus Radial Distribution, Round No. 61

Velocity ~ f

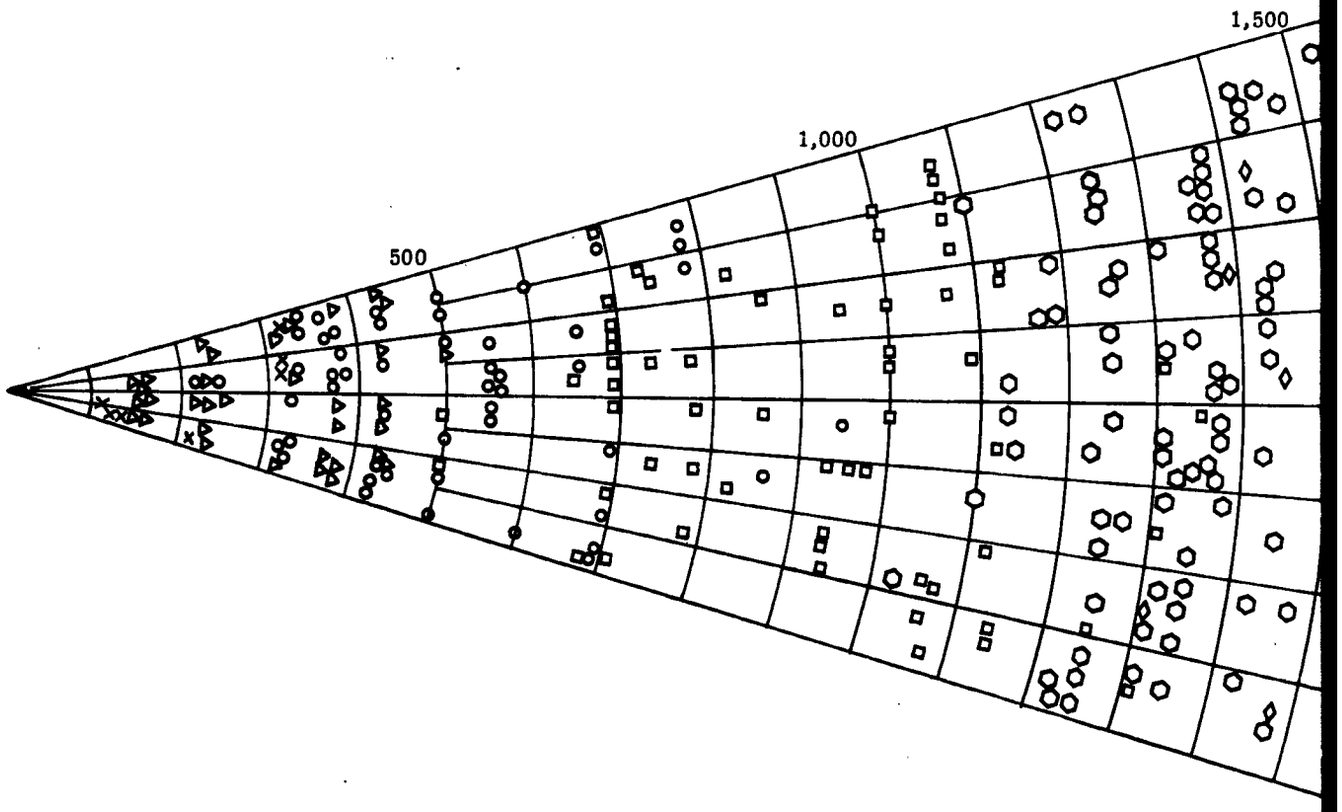


| | Row | Average Velocity | Computed Balls Available | No |
|---|---|---|---|---|
| × | 1 | 234 | 27 | |
| △ | 2 | 300 | 44 | |
| ○ | 3 | 507 | 60 | |
| □ | 4 | 925 | 76 | |
| ⬡ | 5 | 1,331 | 92 | |
| ◇ | 6 | 1,919 | 108 | |

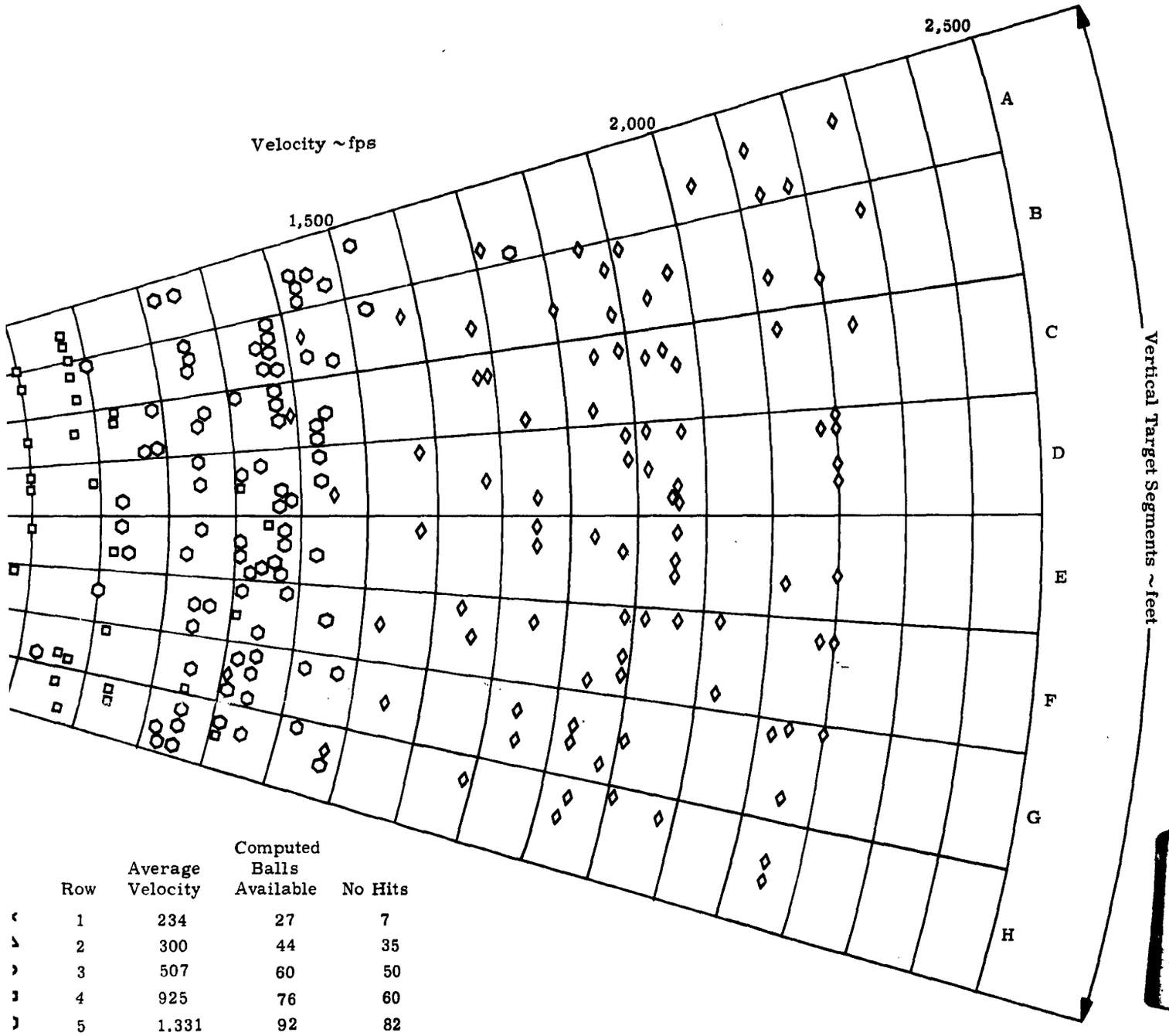


| Row | Average Velocity | Computed Balls Available | No Hits |
|---|---|---|---|
| 1 | 234 | 27 | 7 |
| 2 | 300 | 44 | 35 |
| 3 | 507 | 60 | 50 |
| 4 | 925 | 76 | 60 |
| 5 | 1.331 | 92 | 82 |
| 6 | 1,919 | 108 | 89 |

2

Figure 110. Velocity versus Radial Distribution, Round No. 62

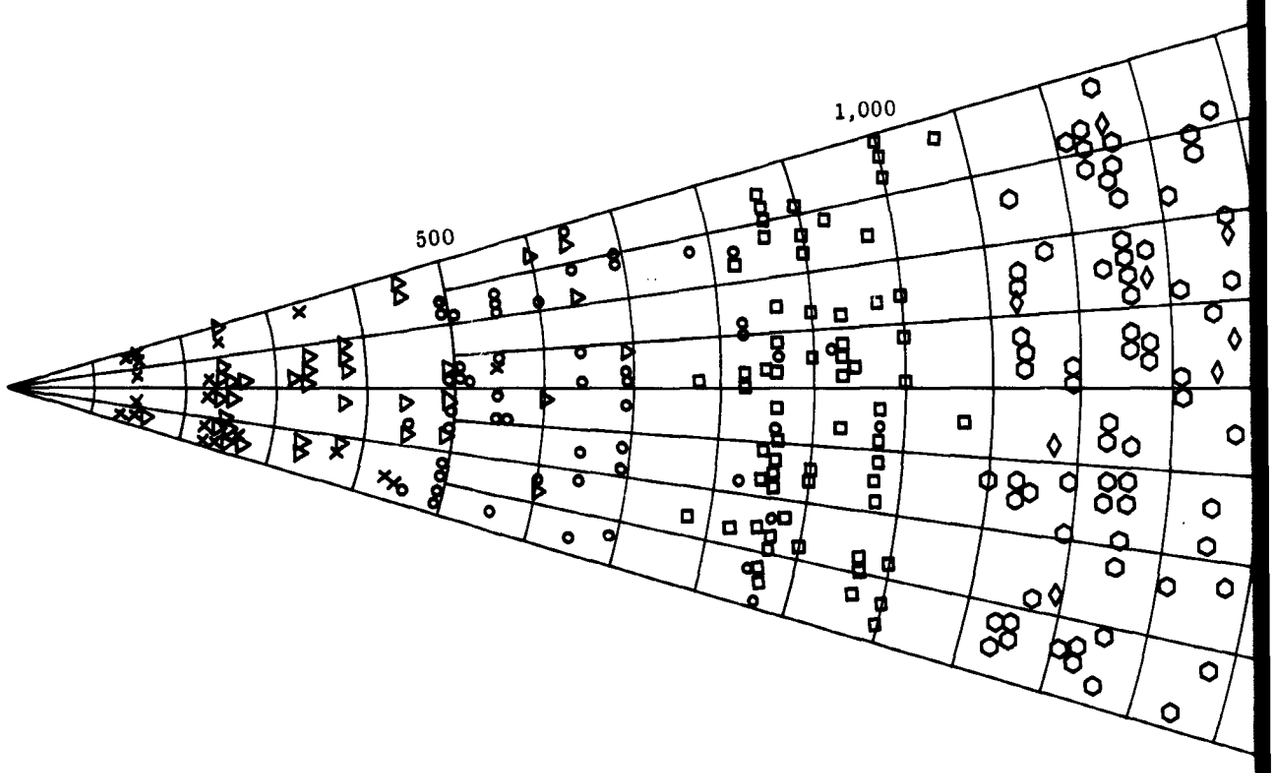


| Row | Average Velocity | Con Balls |
|---|---|---|
| × 1 | 255 | |
| △ 2 | 374 | |
| ○ 3 | 562 | |
| □ 4 | 911 | |
| ⬡ 5 | 1,265 | |
| ◇ 6 | 1,648 | |

Figure 111. Velocity versus Radial Distribution, Round No. 63

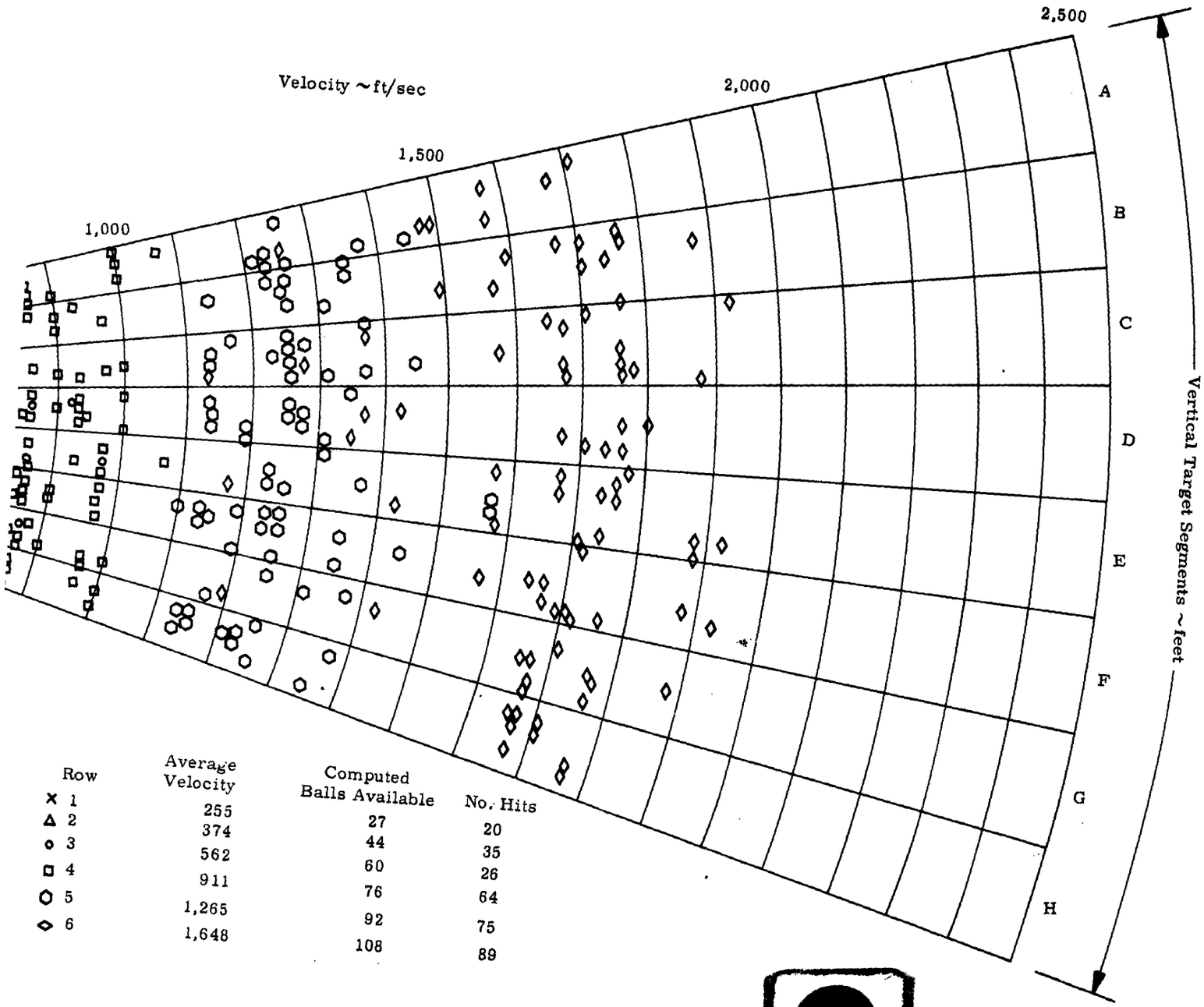


| Row | Average Velocity | Computed Balls Available | No. Hits |
|---|---|---|---|
| × 1 | 255 | 27 | 20 |
| △ 2 | 374 | 44 | 35 |
| ○ 3 | 562 | 60 | 26 |
| □ 4 | 911 | 76 | 64 |
| ⬡ 5 | 1,265 | 92 | 75 |
| ◇ 6 | 1,648 | 108 | 89 |



2

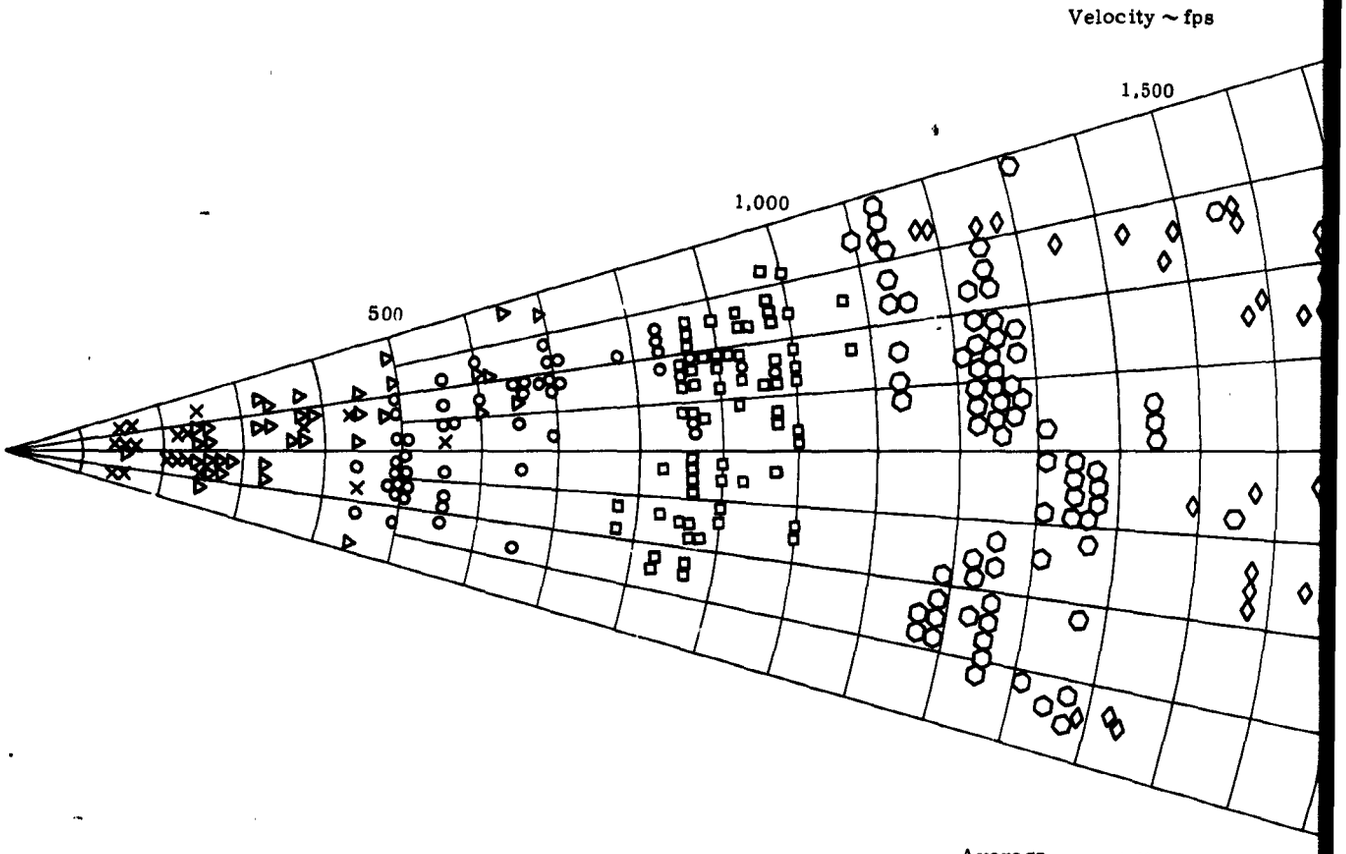


| Row | Average Velocity fps | Balls Available | No. Hits |
|---|---|---|---|
| 1 | 255 | 27 | 20 |
| 2 | 374 | 44 | 35 |
| 3 | 562 | 60 | 26 |
| 4 | 911 | 76 | 64 |
| 5 | 1,265 | 92 | 75 |
| 6 | 1,648 | 108 | 89 |

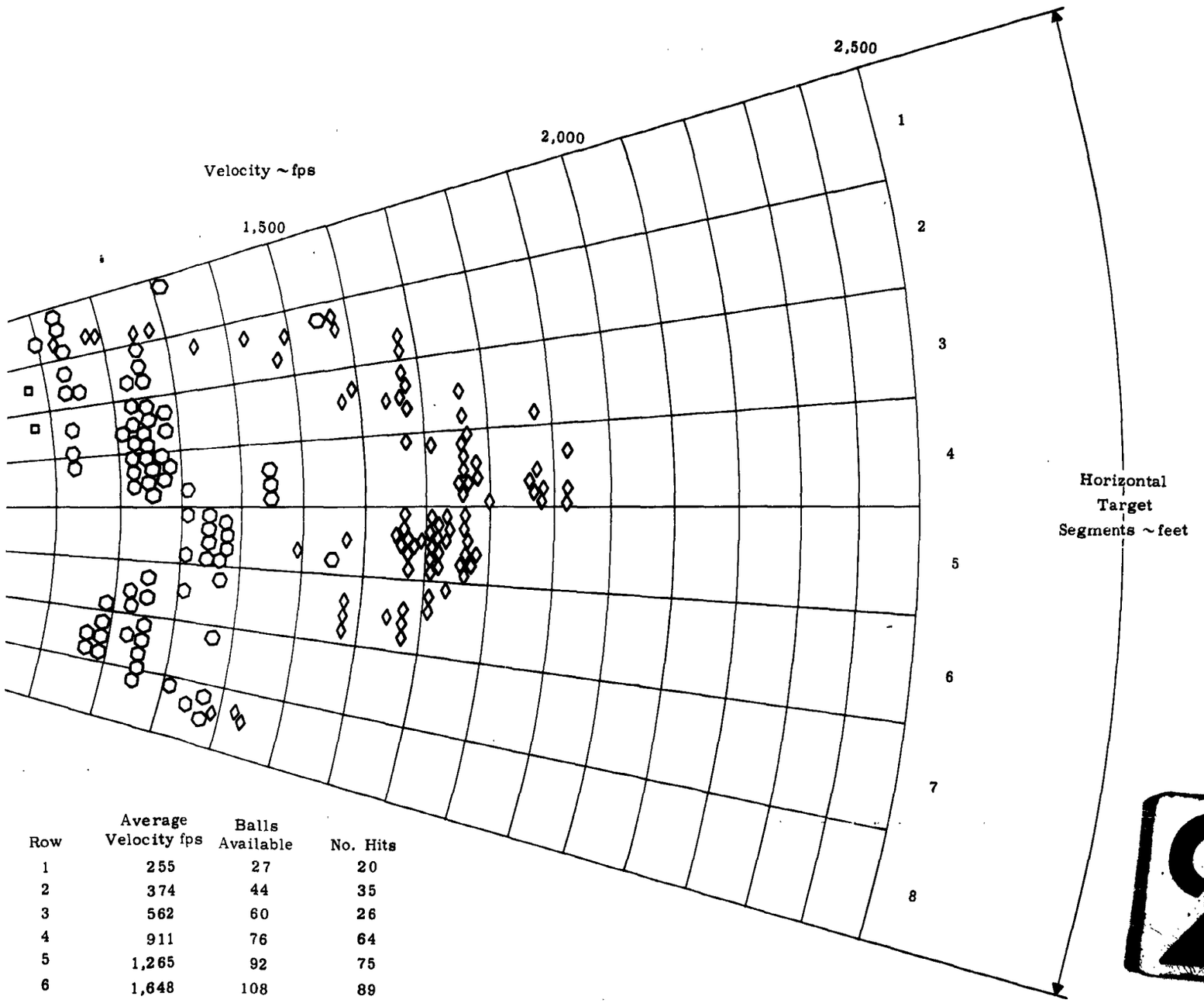


| Row | Average Velocity fps | Balls Available | No. Hits |
|---|---|---|---|
| 1 | 255 | 27 | 20 |
| 2 | 374 | 44 | 35 |
| 3 | 562 | 60 | 26 |
| 4 | 911 | 76 | 64 |
| 5 | 1,265 | 92 | 75 |
| 6 | 1,648 | 108 | 89 |

Figure 112. Velocity versus Radial Distribution, Round No. 63 (Side Cut)

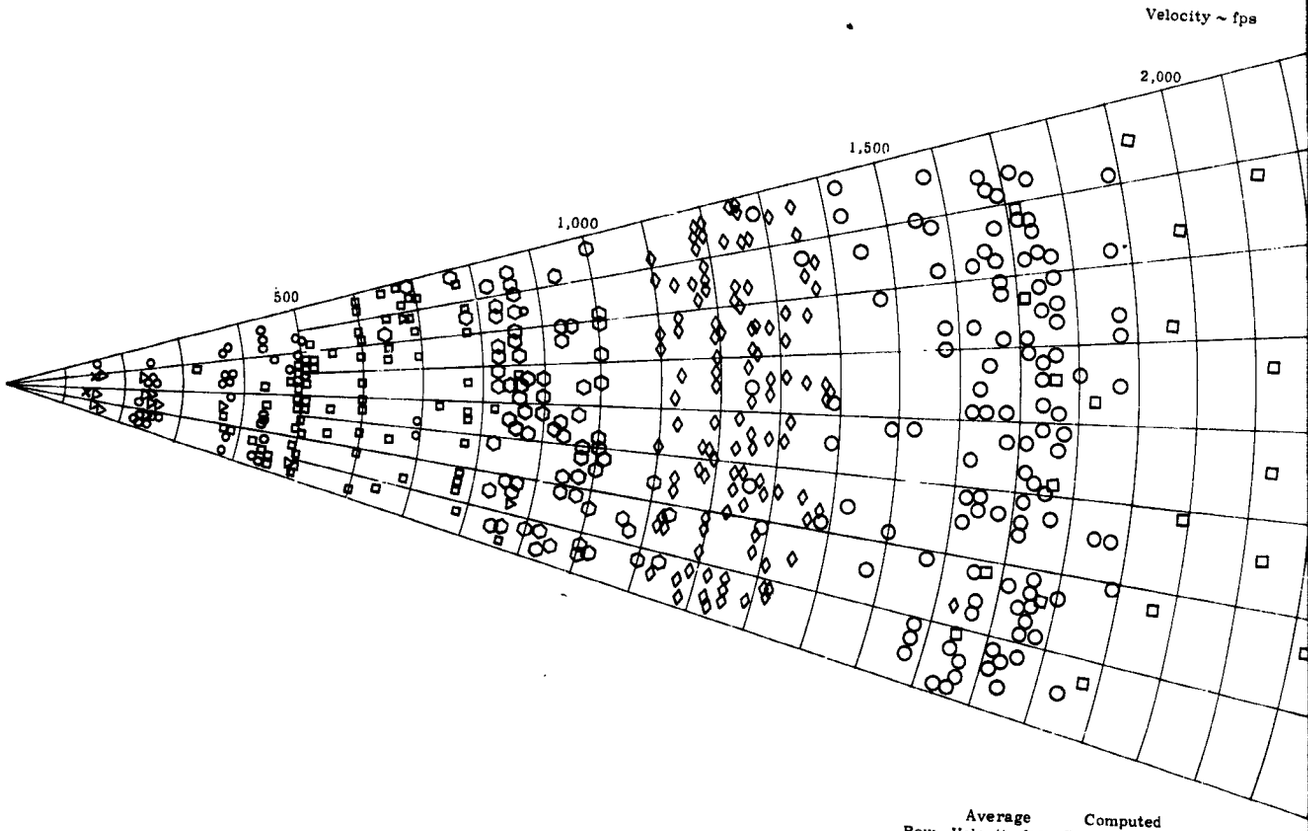


| | Row | Average Velocity fps | Computed Balls Available | No. Hits |
|---|---|---|---|---|
| × | 1 | 150 | 34 | 2 |
| △ | 2 | 324 | 54 | 13 |
| ○ | 3 | 377 | 75 | 39 |
| □ | 4 | 596 | 95 | 74 |
| ⬡ | 5 | 918 | 115 | 74 |
| ◇ | 6 | 1,236 | 135 | 111 |
| ○ | 7 | 1,658 | 155 | 110 |
| □ | 8 | 2,826 | 175 | 145 |

Figure 113. Velocity versus Radial Distribution, Round No. 64

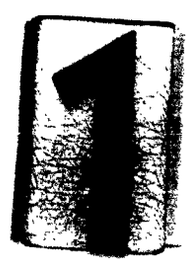

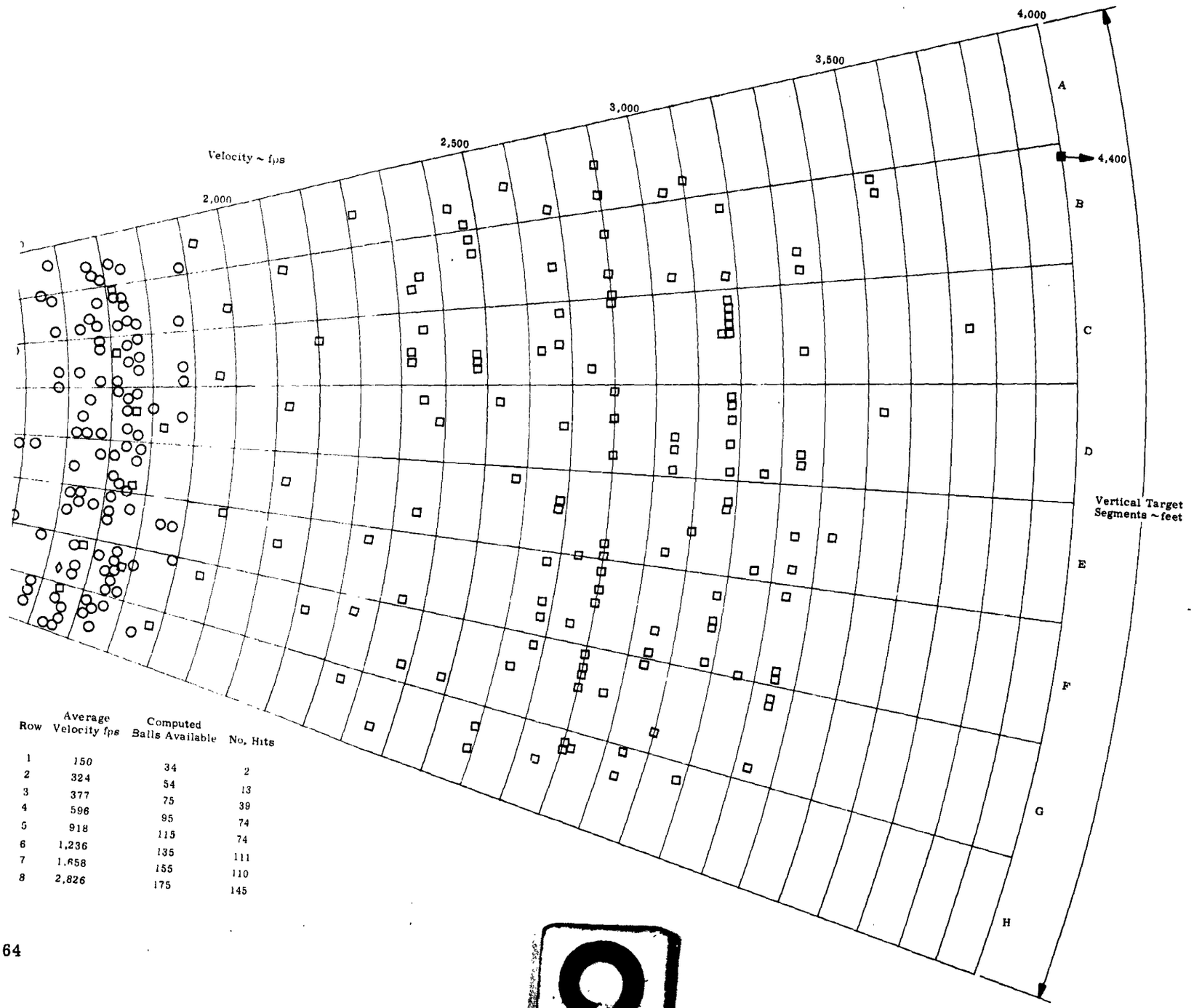


| Row | Average Velocity fps | Computed Balls Available | No. Hits |
|---|---|---|---|
| 1 | 150 | 34 | 2 |
| 2 | 324 | 54 | 13 |
| 3 | 377 | 75 | 39 |
| 4 | 596 | 95 | 74 |
| 5 | 918 | 115 | 74 |
| 6 | 1,236 | 135 | 111 |
| 7 | 1,658 | 155 | 110 |
| 8 | 2,826 | 175 | 145 |



2

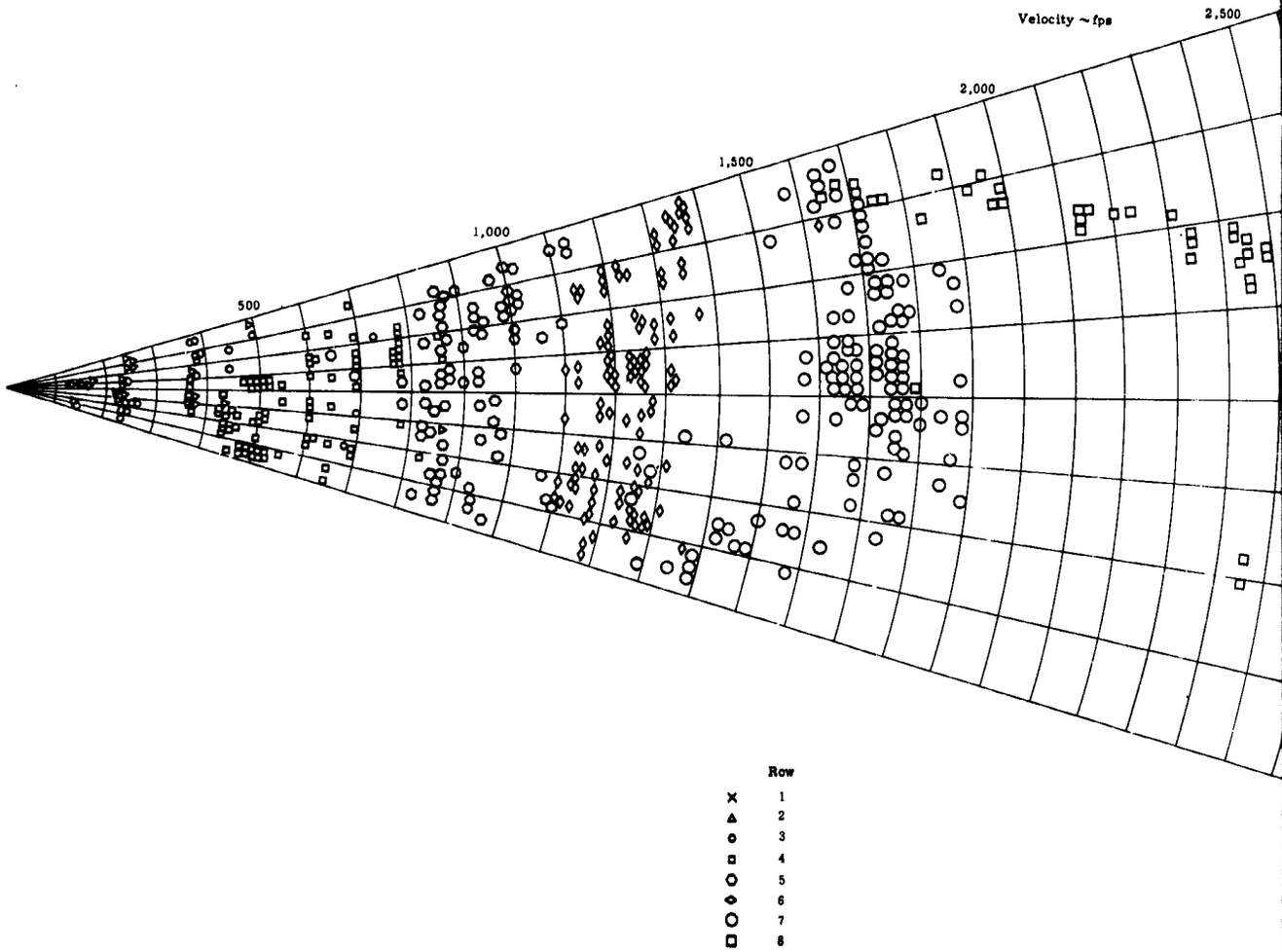


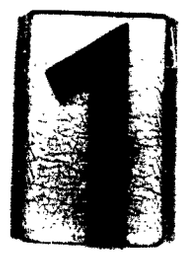

Fi

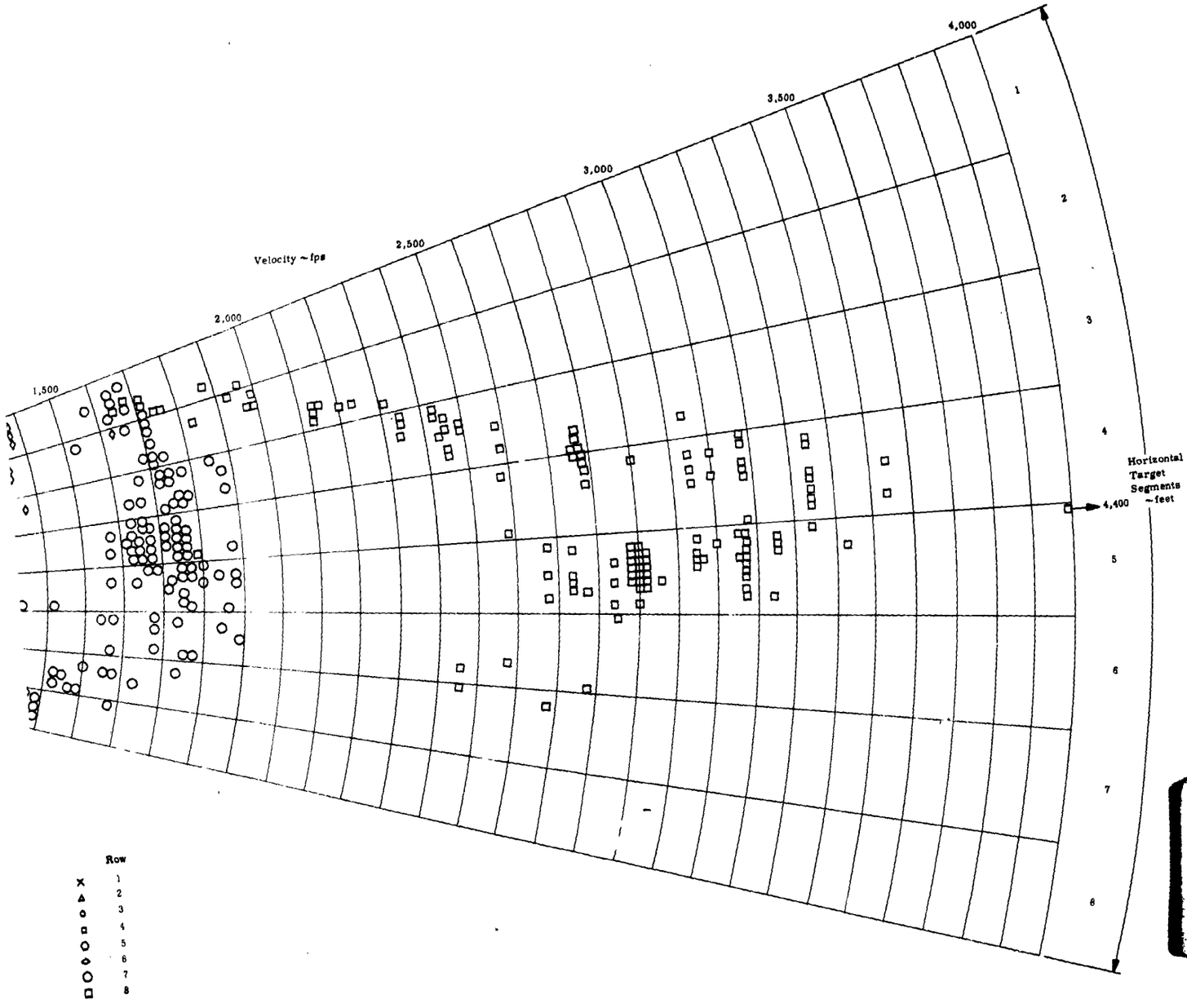


Figure 114. Velocity versus Radial Distribution, Round No. 64 (Side Cut)

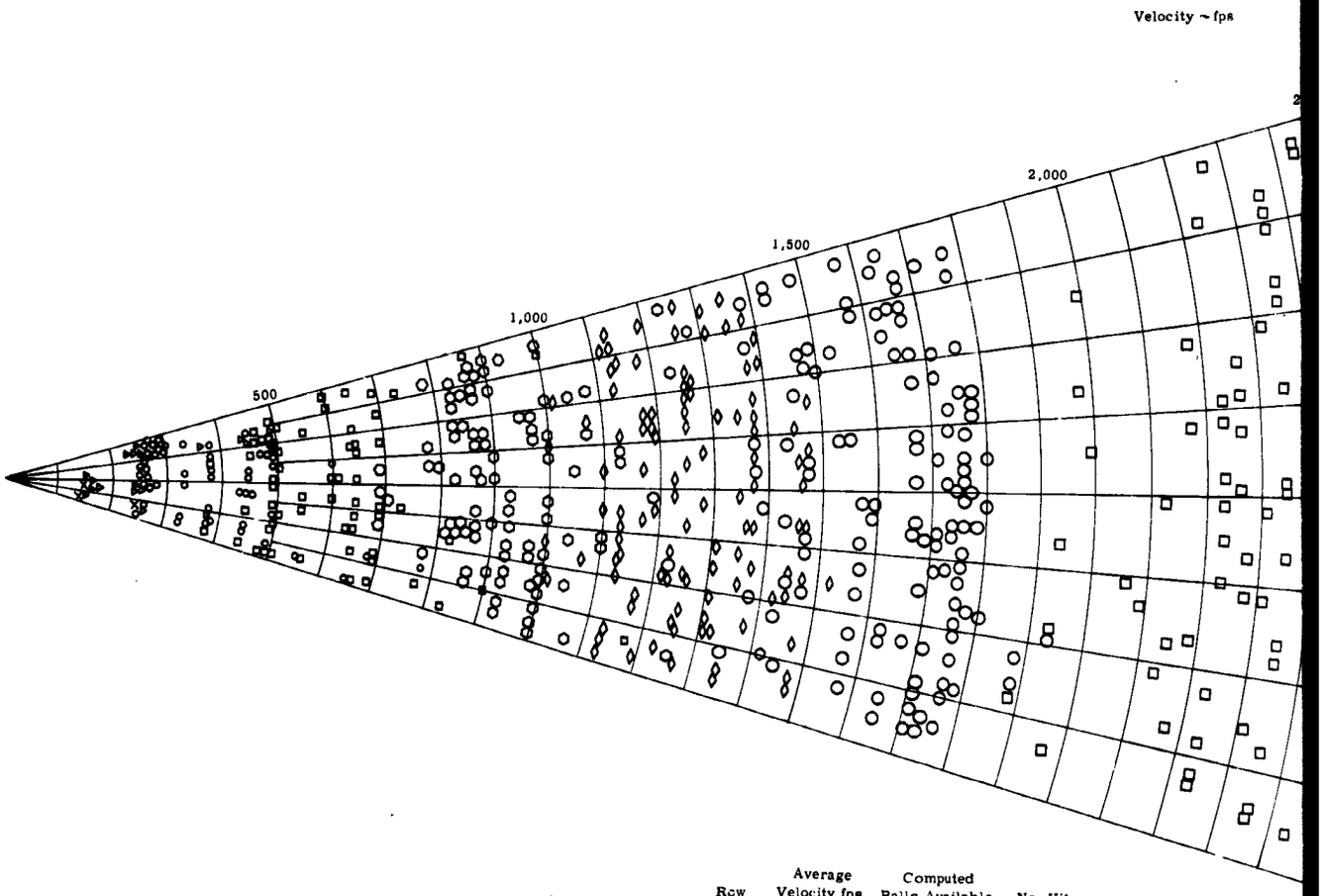


| | Row | Average Velocity fps | Computed Balls Available | No. Hits |
|---|---|---|---|---|
| × | 1 | 258 | 34 | 4 |
| ▲ | 2 | 278 | 54 | 15 |
| o | 3 | 372 | 75 | 47 |
| □ | 4 | 595 | 95 | 62 |
| ○ | 5 | 943 | 115 | 90 |
| ⬭ | 6 | 1,266 | 135 | 106 |
| ○ | 7 | 1,636 | 155 | 120 |
| □ | 8 | 2,768 | 175 | 156 |

Figure 115.

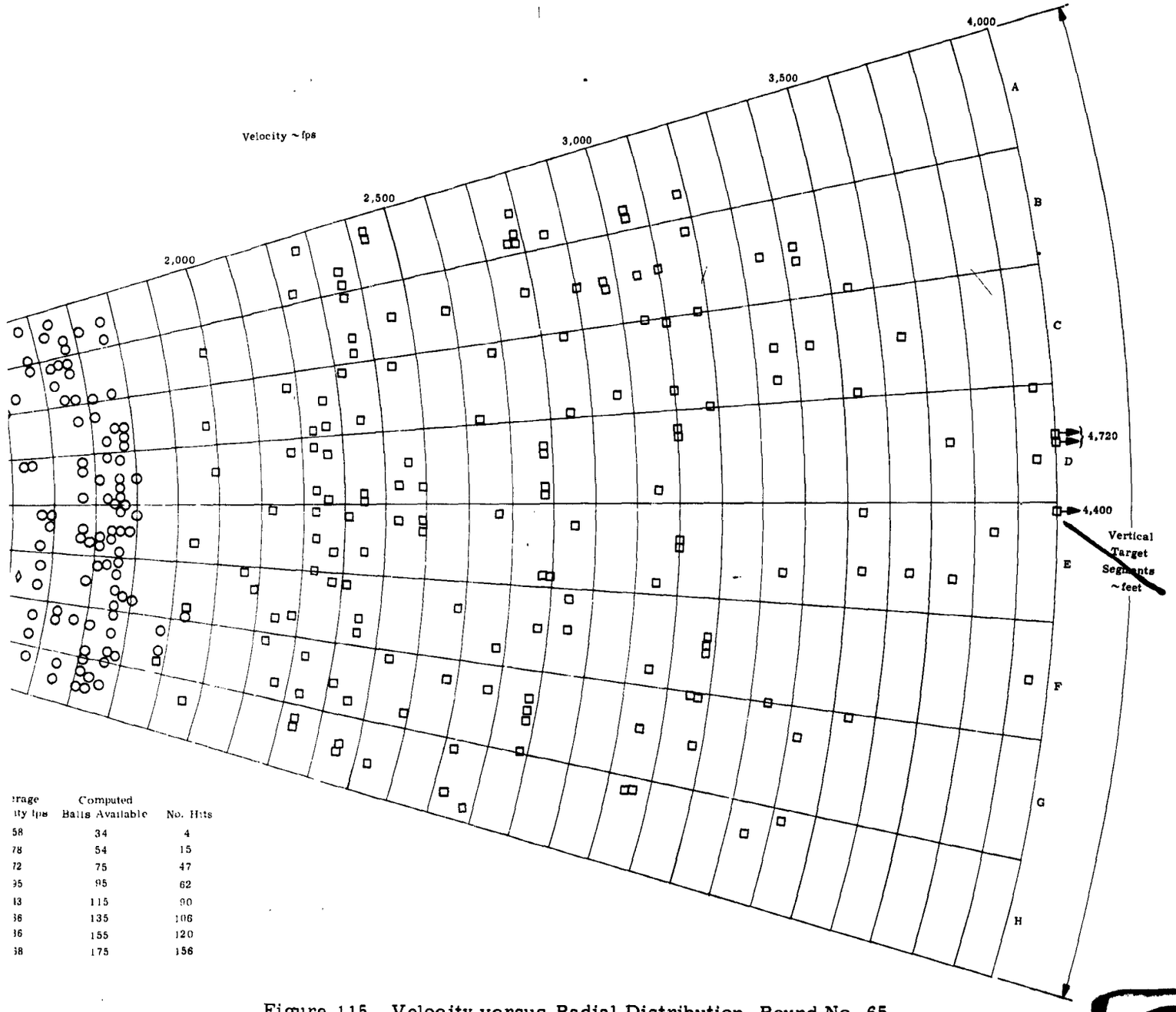


| rage ity fps | Computed Balls Available | No. Hits |
|---|---|---|
| 58 | 34 | 4 |
| 78 | 54 | 15 |
| 72 | 75 | 47 |
| 95 | 95 | 62 |
| 13 | 115 | 90 |
| 36 | 135 | 106 |
| 16 | 155 | 120 |
| 38 | 175 | 156 |

Figure 115. Velocity versus Radial Distribution, Round No. 65

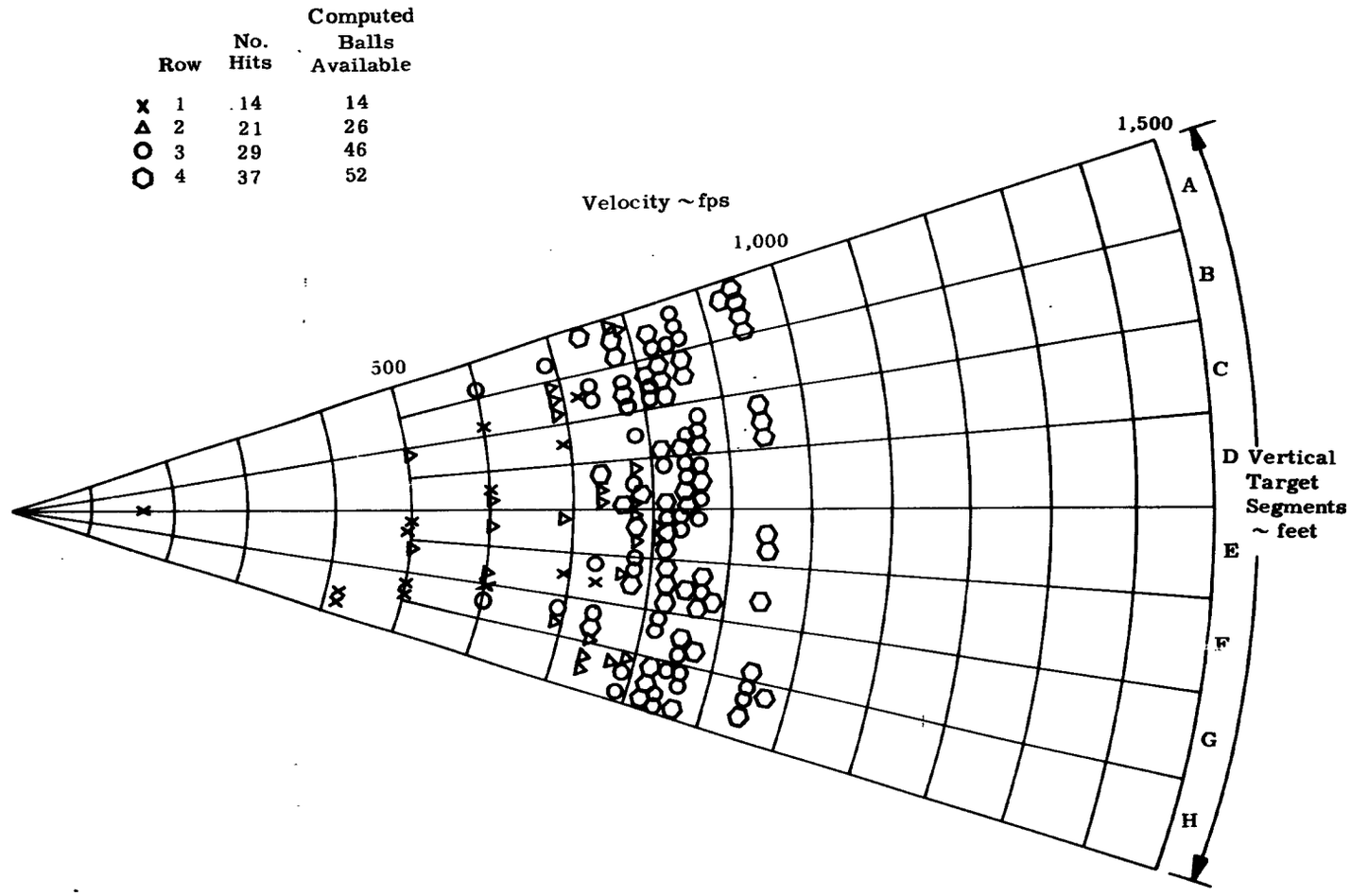


Figure 116. Velocity versus Radial Distribution, Round No. 70

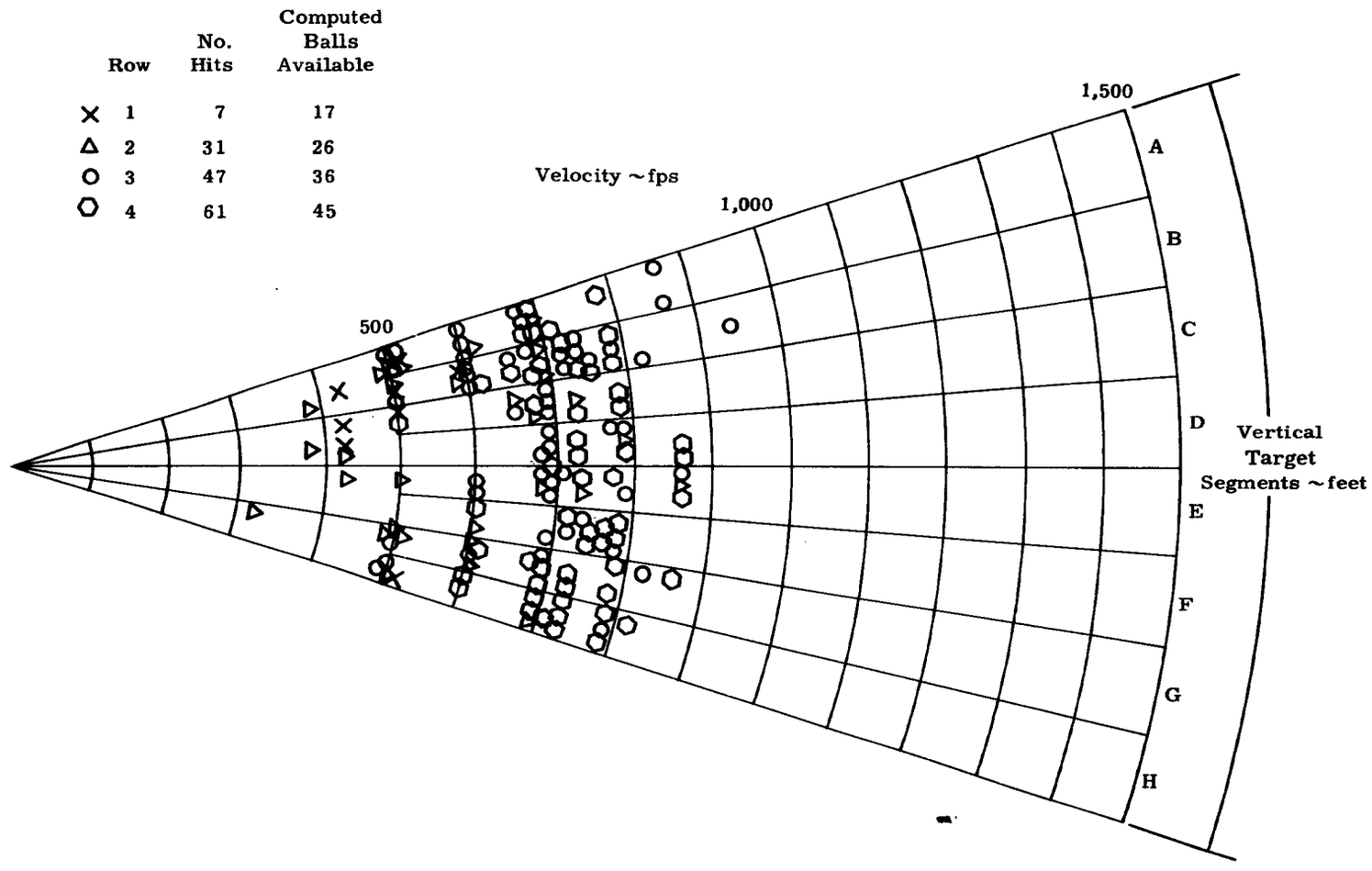


Figure 117. Velocity versus Radial Distribution, Round No. 71





CONFIDENTIAL

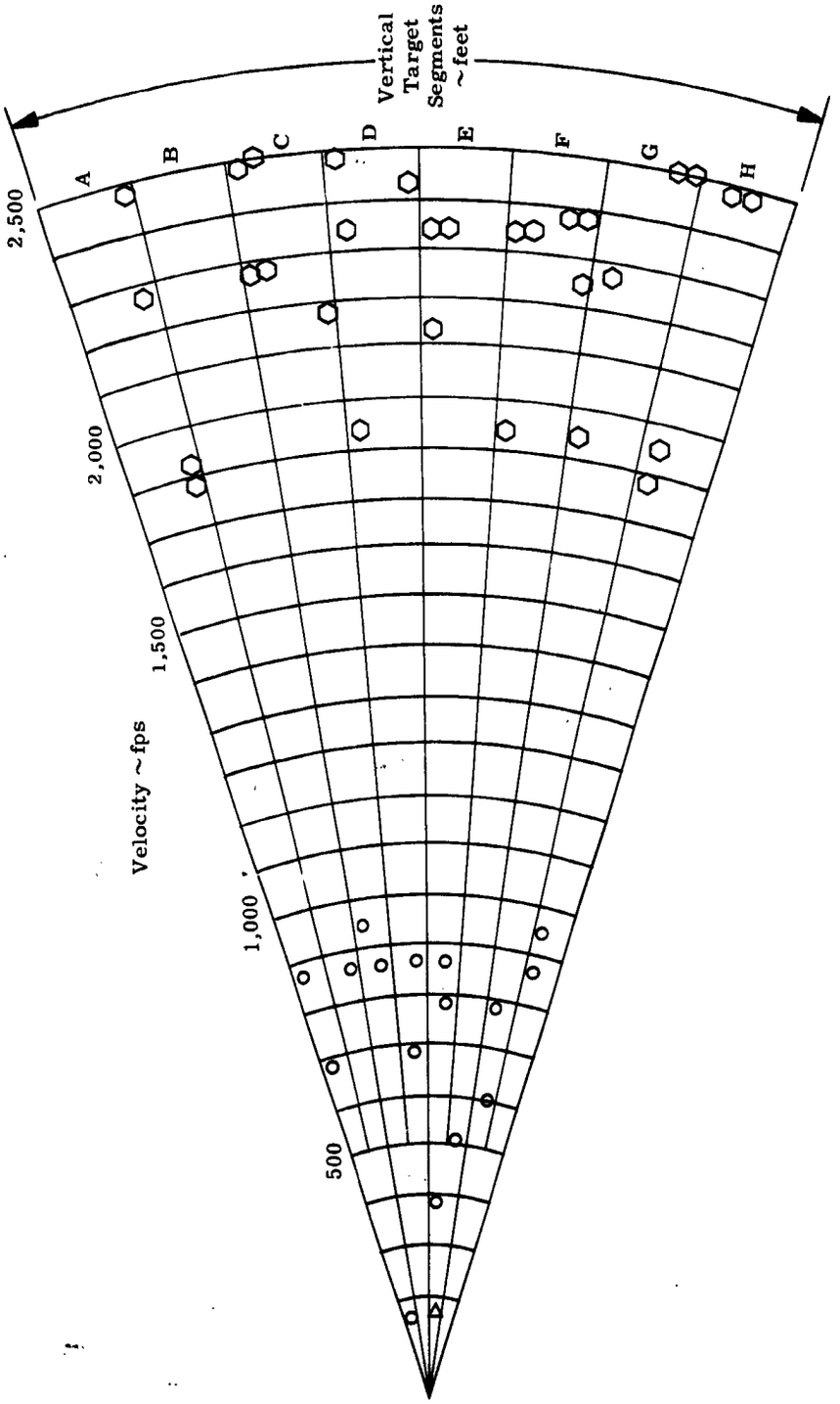


Figure 118. Velocity versus Radial Distribution, Round No. 76

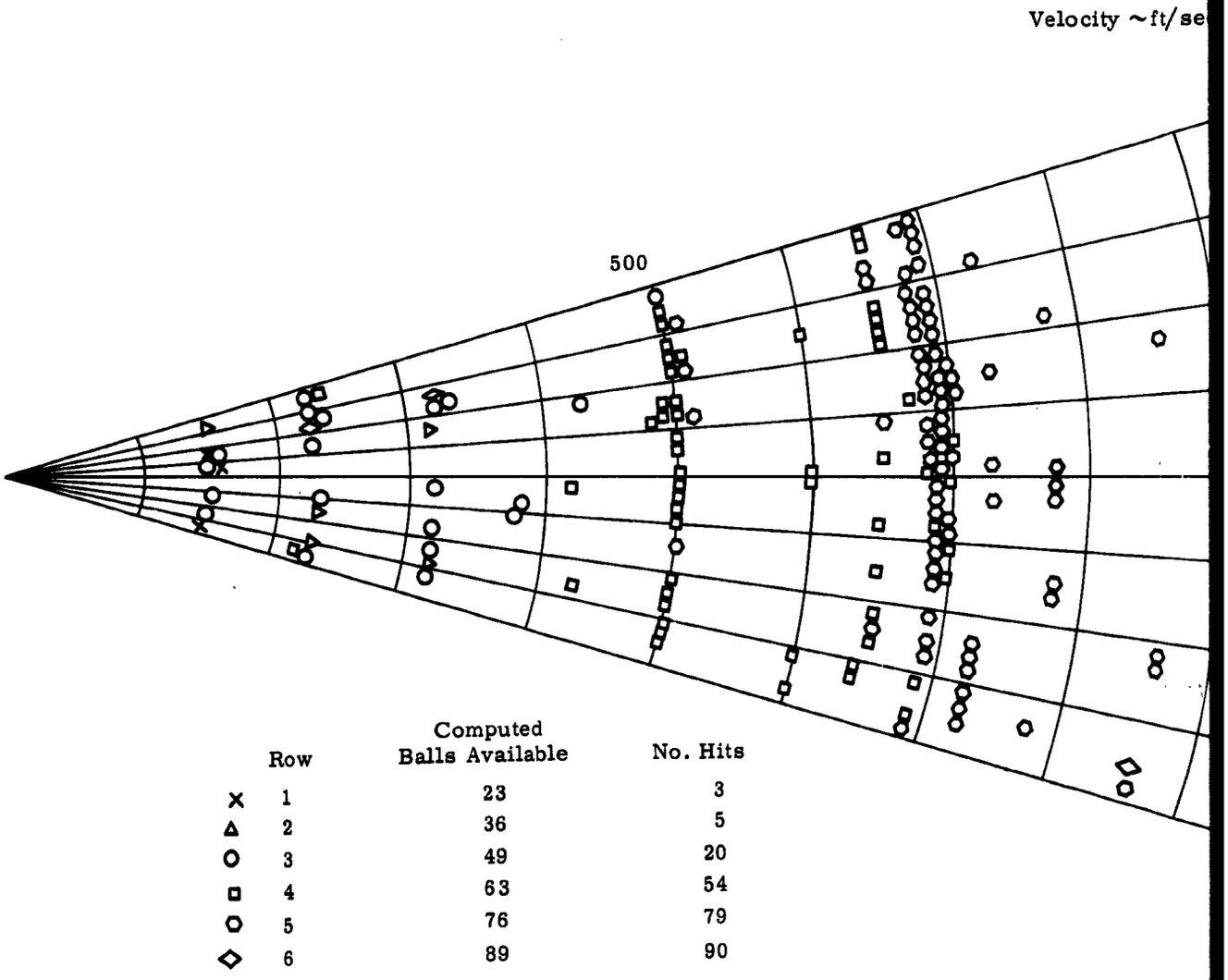


| | Row | Computed Balls Available | No. Hits |
|---|---|---|---|
| × | 1 | 23 | 3 |
| △ | 2 | 36 | 5 |
| ○ | 3 | 49 | 20 |
| □ | 4 | 63 | 54 |
| ⬡ | 5 | 76 | 79 |
| ◇ | 6 | 89 | 90 |

Figure 119. Velocity versus Radial Distribution, Round No. 77

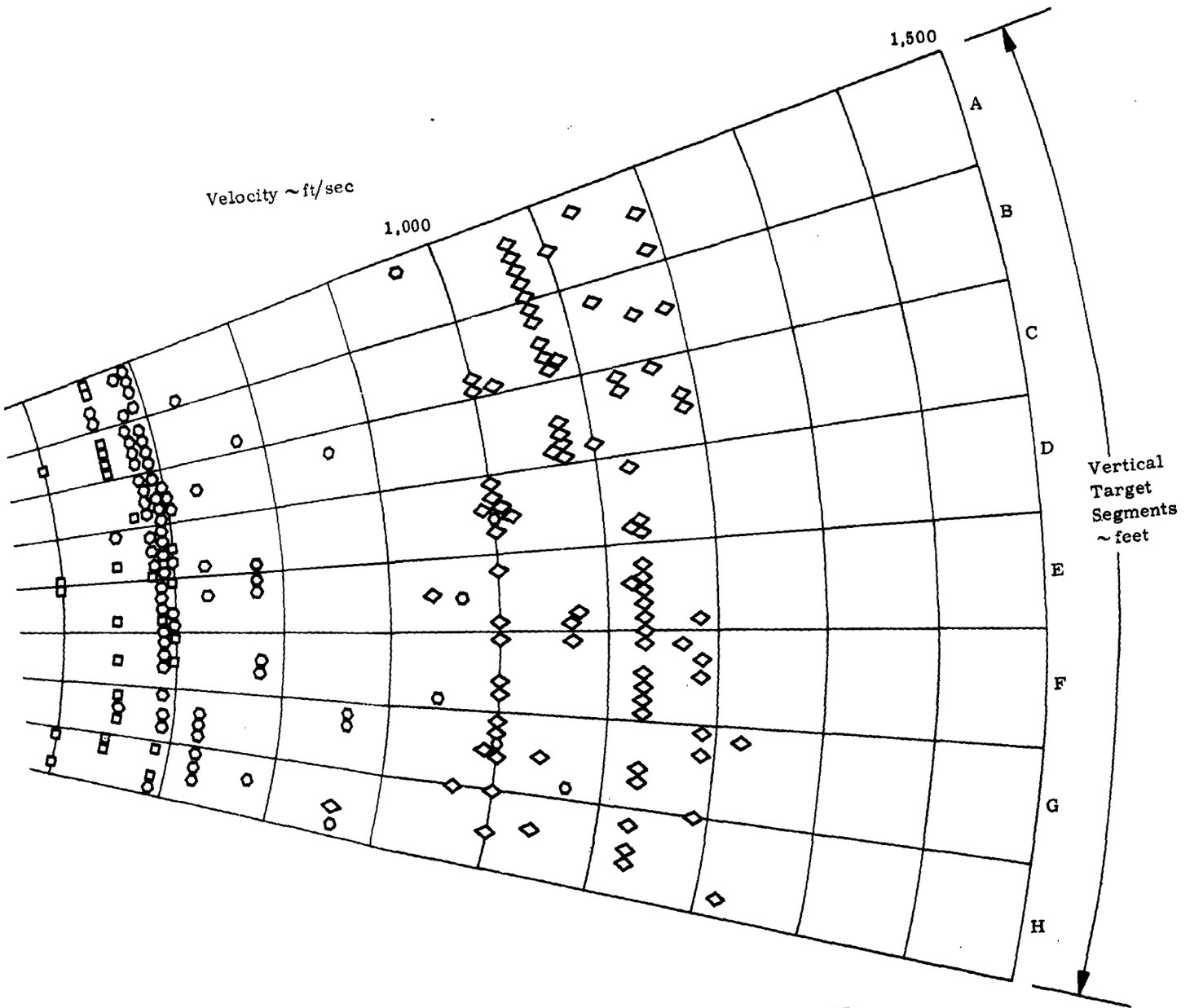
Velocity ~ ft/sec
1,000
1,500
A
B
C
D
E
F
G
H
Vertical
Target
Segments
~ feet

2

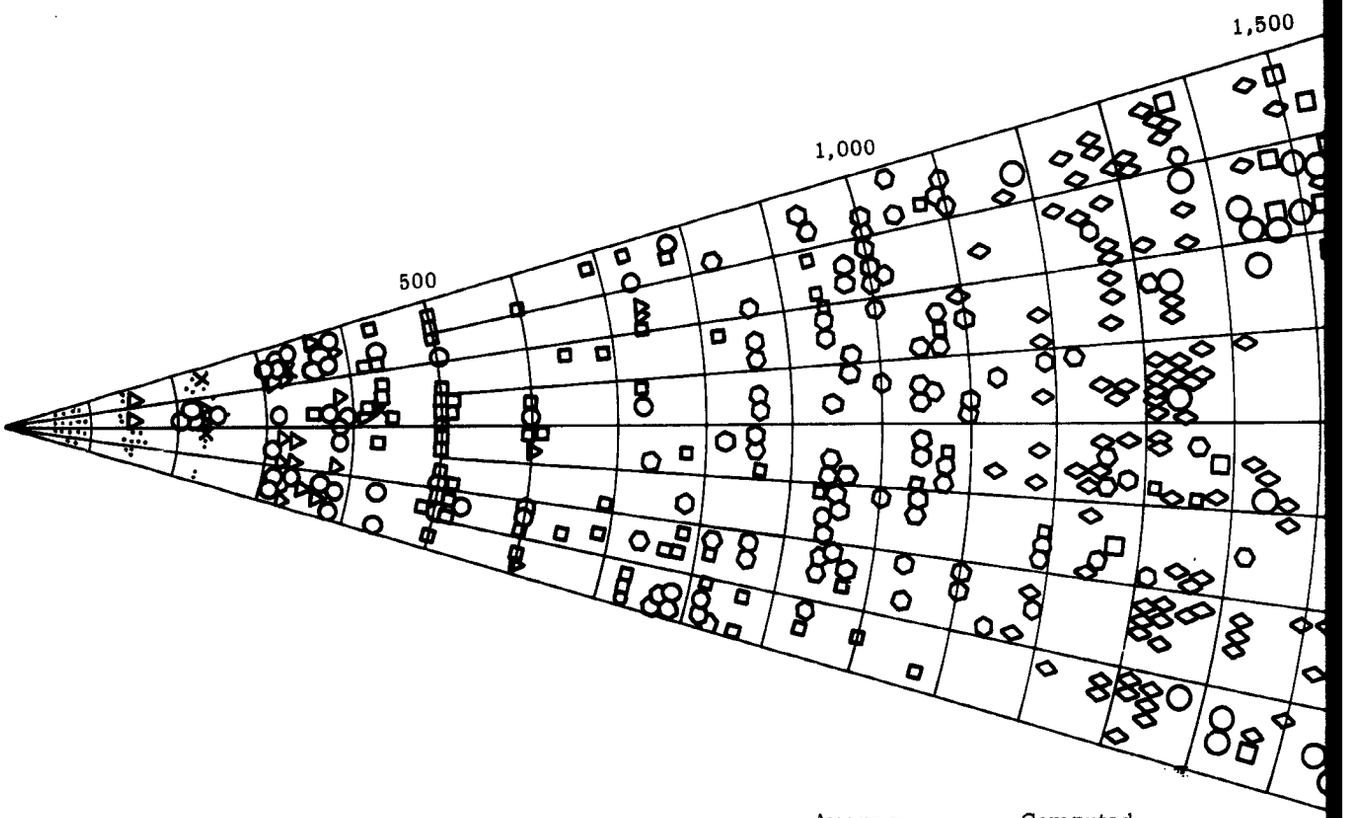


| | Row | Average Velocity | Computed Balls Available | No. Hi |
|---|---|---|---|---|
| × | 1 | 318 | 25 | 5 |
| ▷ | 2 | 380 | 44 | 22 |
| ○ | 3 | 454 | 63 | 40 |
| □ | 4 | 689 | 81 | 69 |
| ⬡ | 5 | 1,018 | 100 | 91 |
| ◇ | 6 | 1,330 | 119 | 100 |
| ○ | 7 | 1,708 | 138 | 134 |
| □ | 8 | 1,937 | 151 | 175 |
| · | Low velocity hits not identifiable | | | 42 |

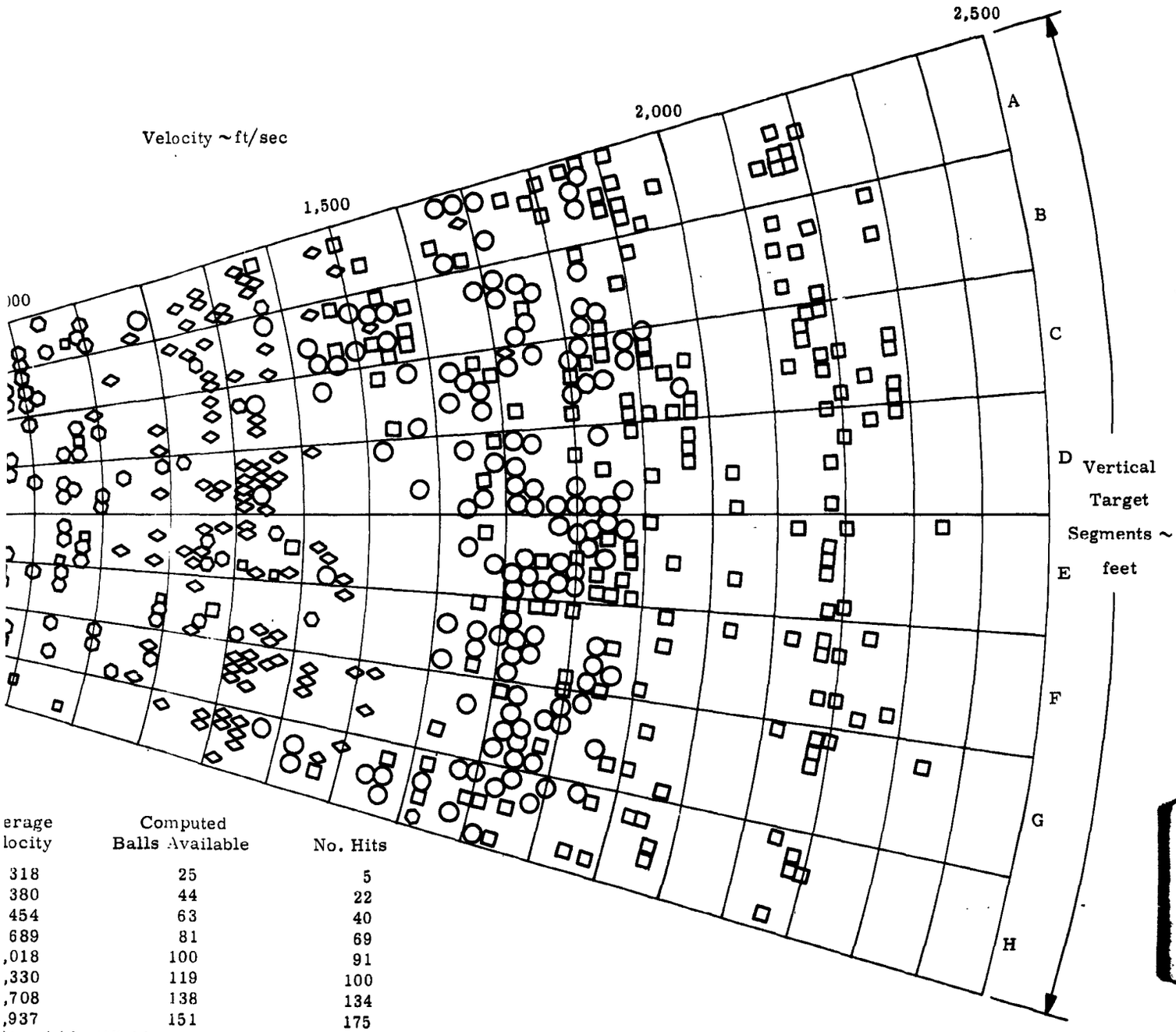


| erage locity | Computed Balls Available | No. Hits |
|---|---|---|
| 318 | 25 | 5 |
| 380 | 44 | 22 |
| 454 | 63 | 40 |
| 689 | 81 | 69 |
| ,018 | 100 | 91 |
| ,330 | 119 | 100 |
| ,708 | 138 | 134 |
| ,937 | 151 | 175 |
| ts not identifiable | | 42 |

Figure 120. Velocity versus Radial Distribution, Round No. 82

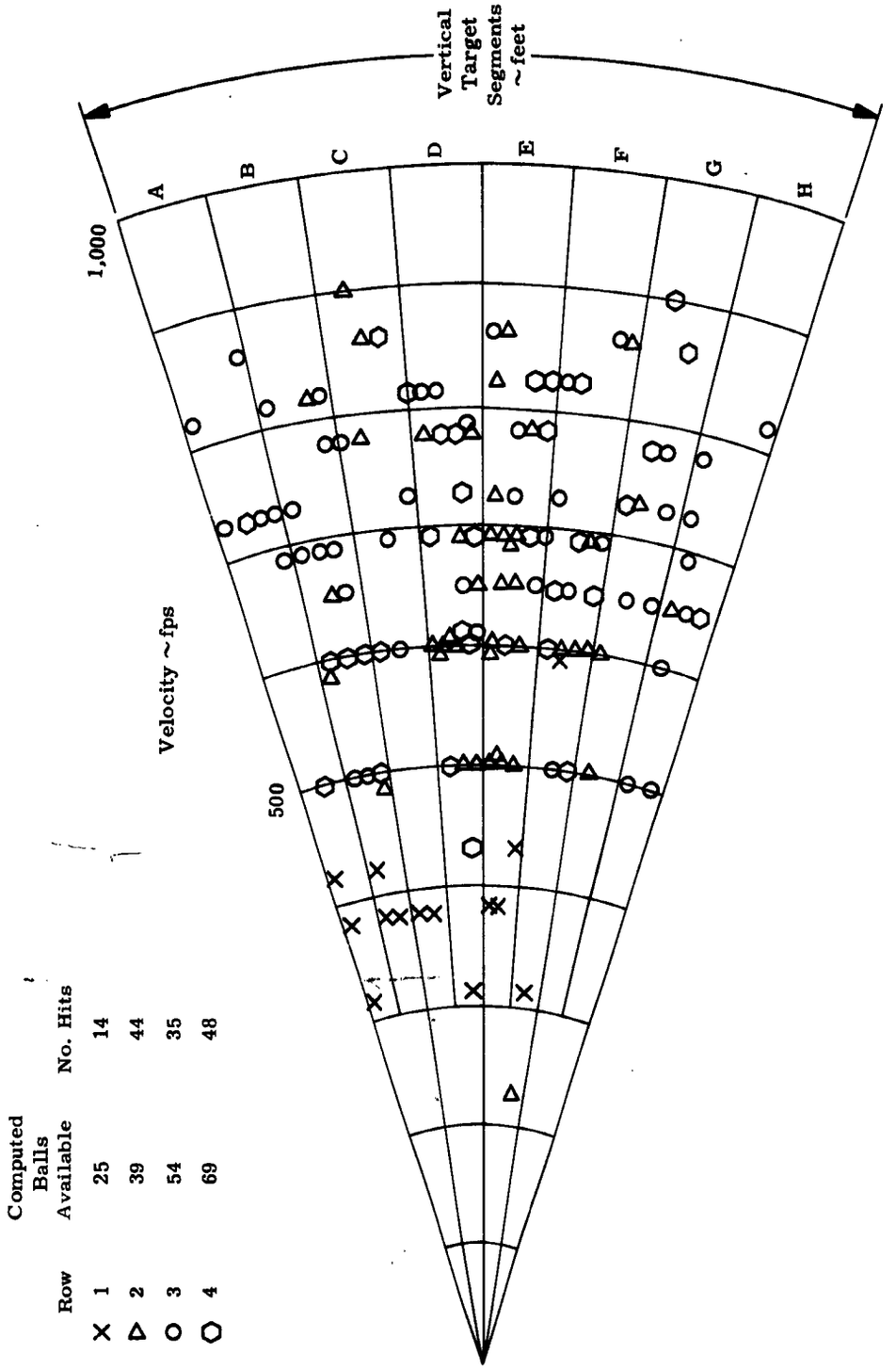


Figure 121. Velocity versus Radial Distribution, Round No. 89

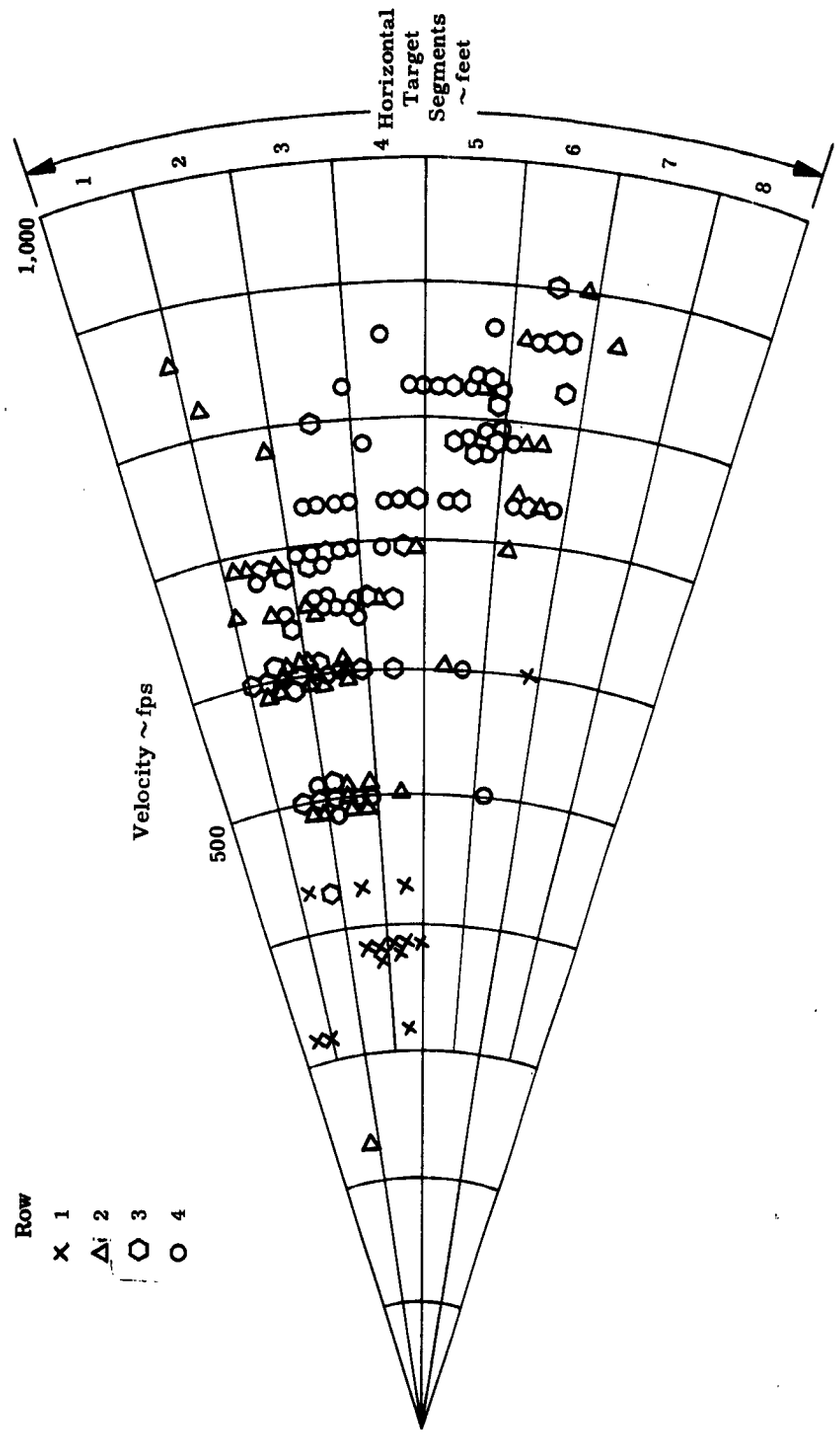


Figure 122. Velocity versus Radial Distribution, Round No. 89 (Side Cut)

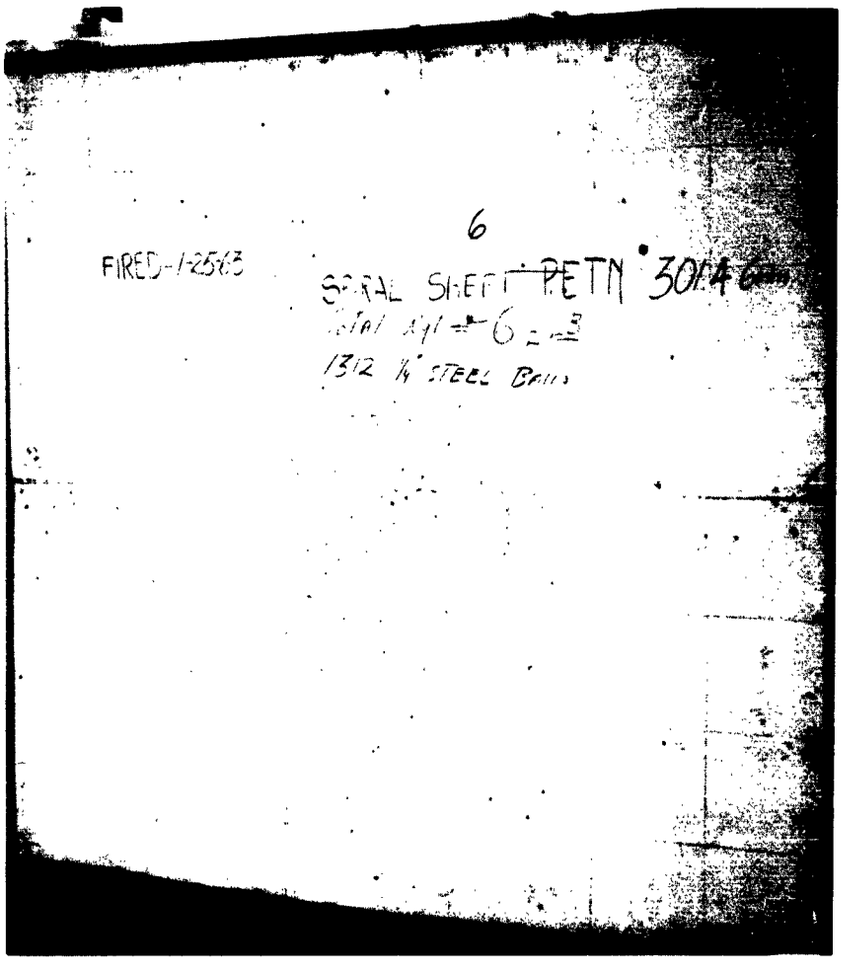


Figure 124. Impact Pattern, Round No. 6

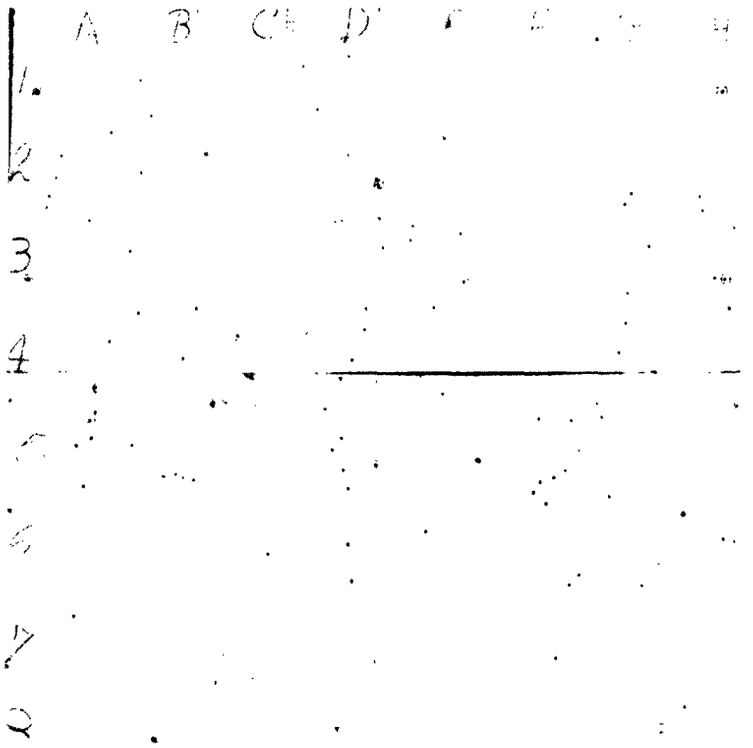

Figure 125. Impact Pattern, Round No. 19

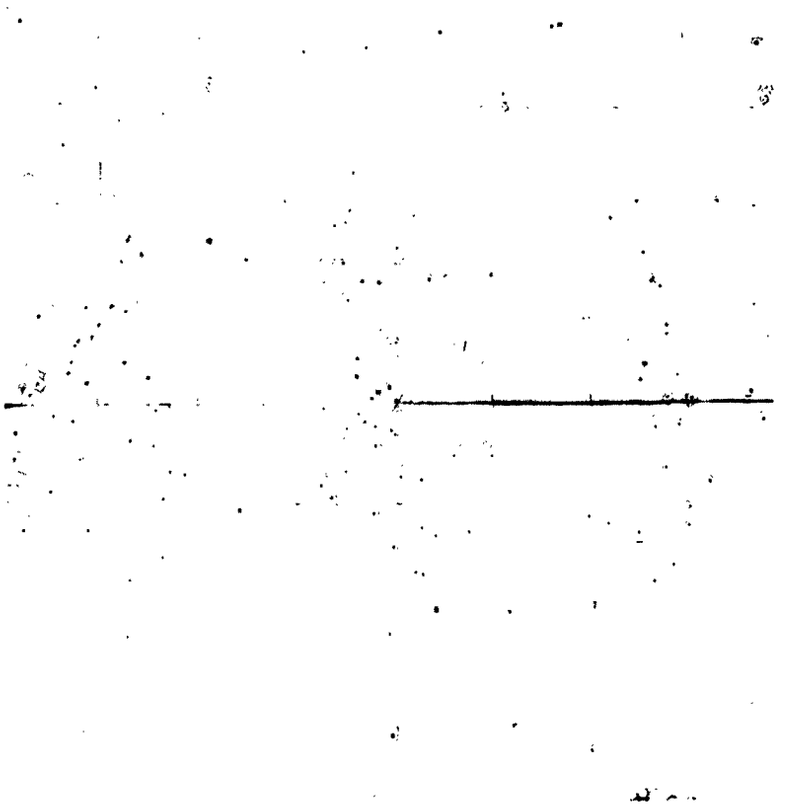

Figure 126. Impact Pattern, Round No. 20

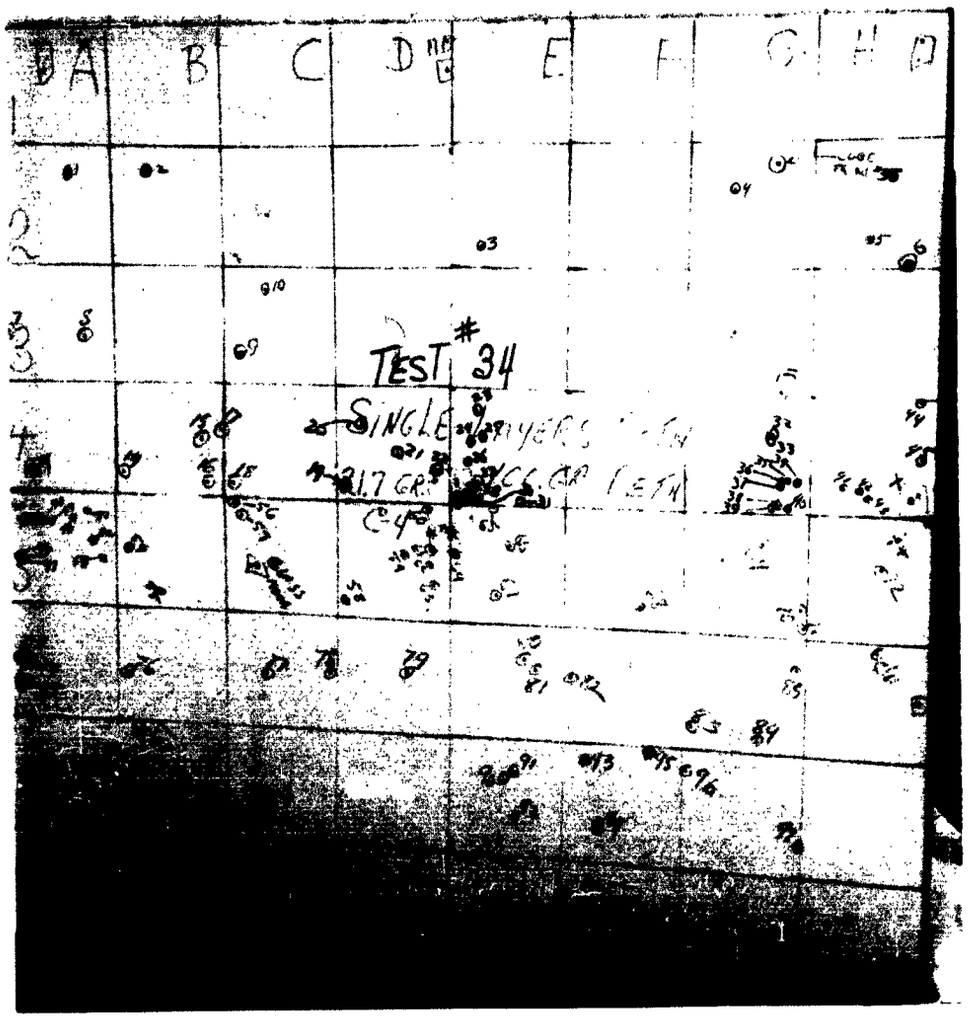


Figure 127. Impact Pattern, Round No. 34

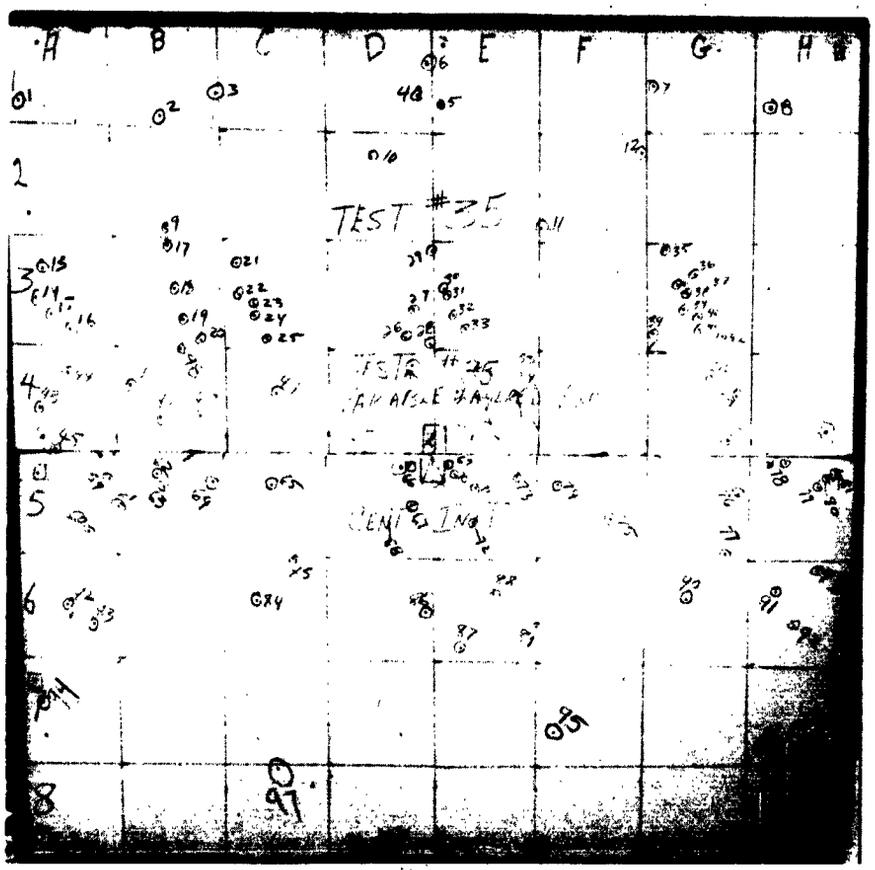


Figure 128. Impact Pattern, Round No. 35

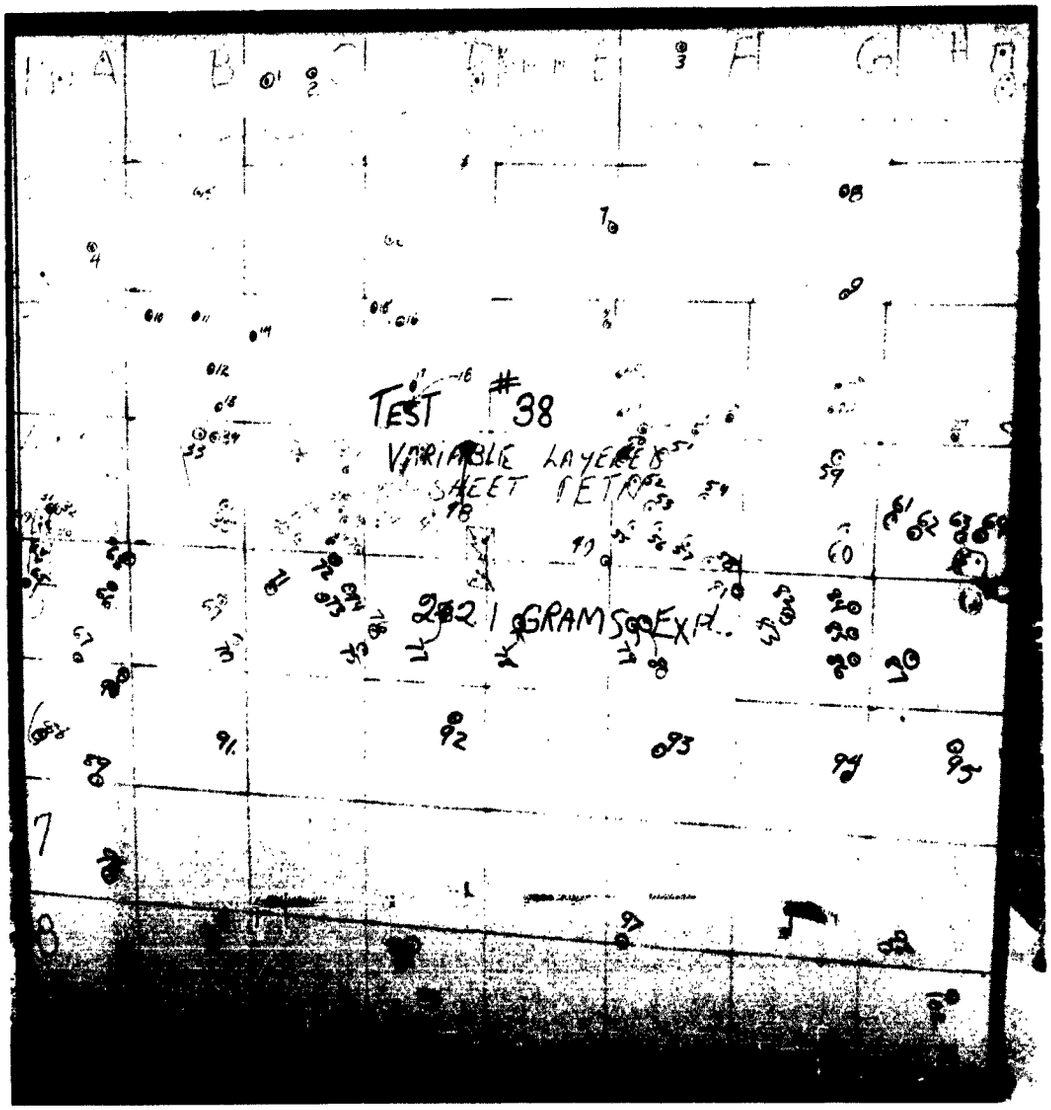


Figure 129. Impact Pattern, Round No. 38


Figure 130. Impact Pattern, Round No. 43

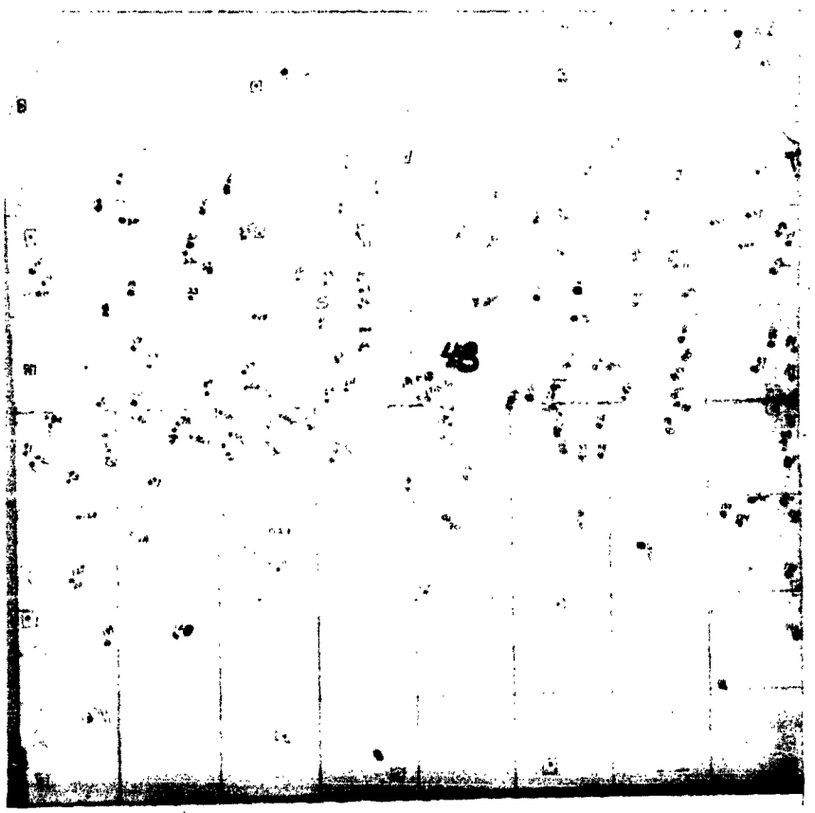


Figure 131. Impact Pattern, Round No. 48

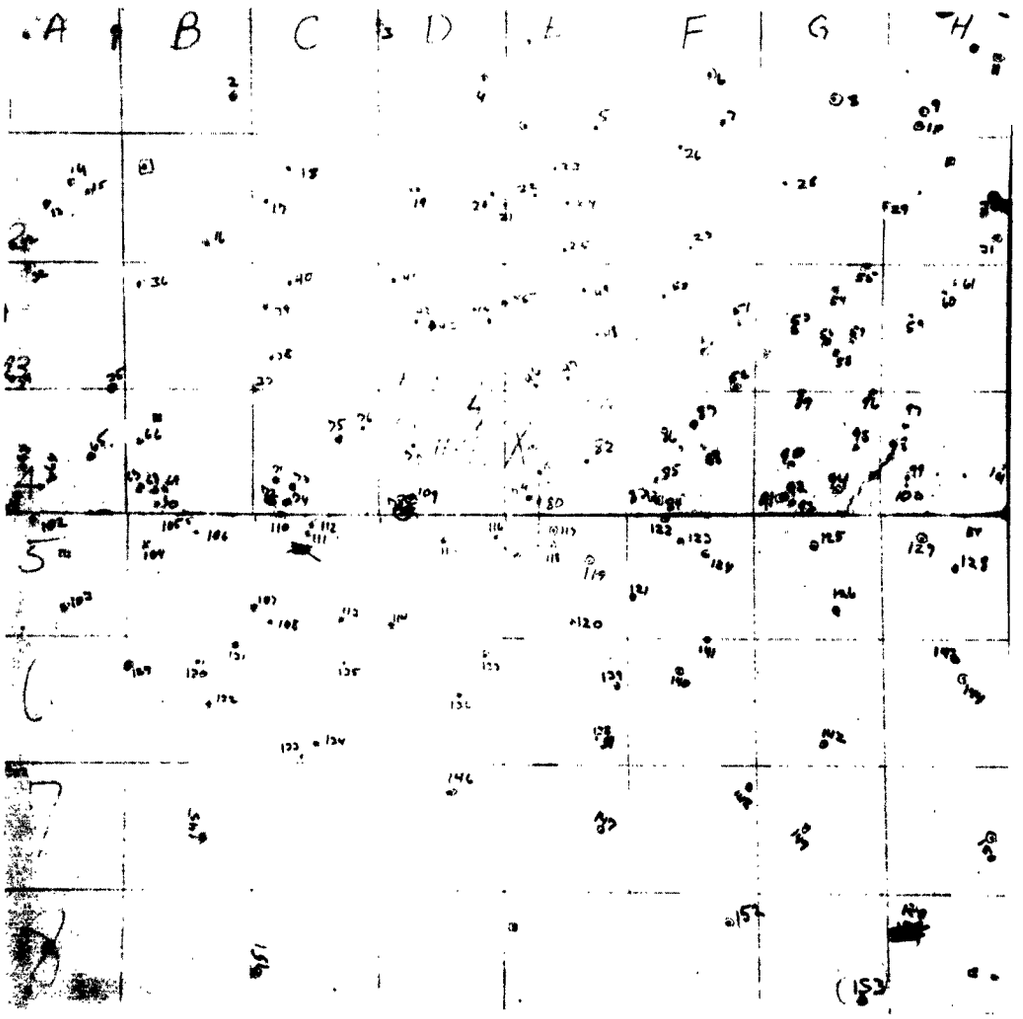


Figure 132. Impact Pattern, Round No. 49X

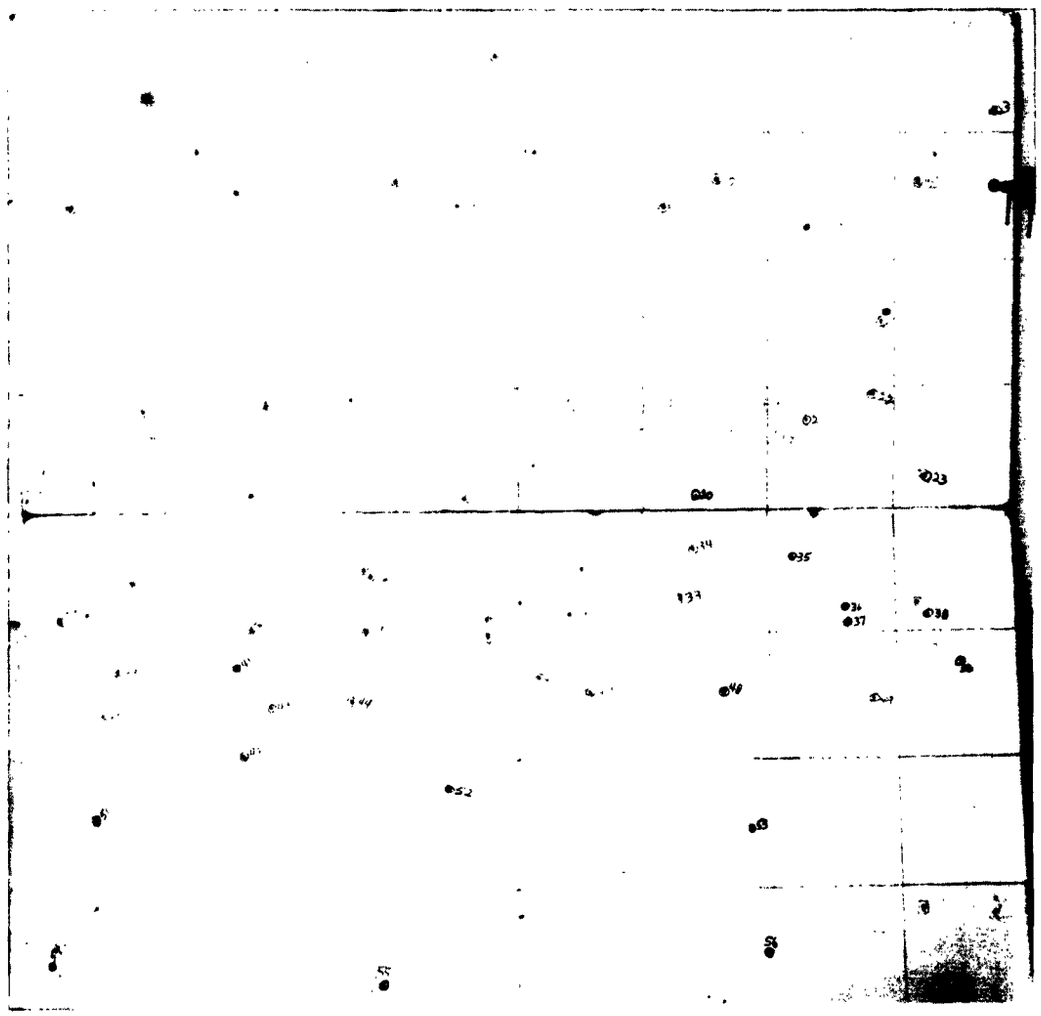

Figure 133. Impact Pattern, Round No. 52X


Figure 134. Impact Pattern, Round No. 53

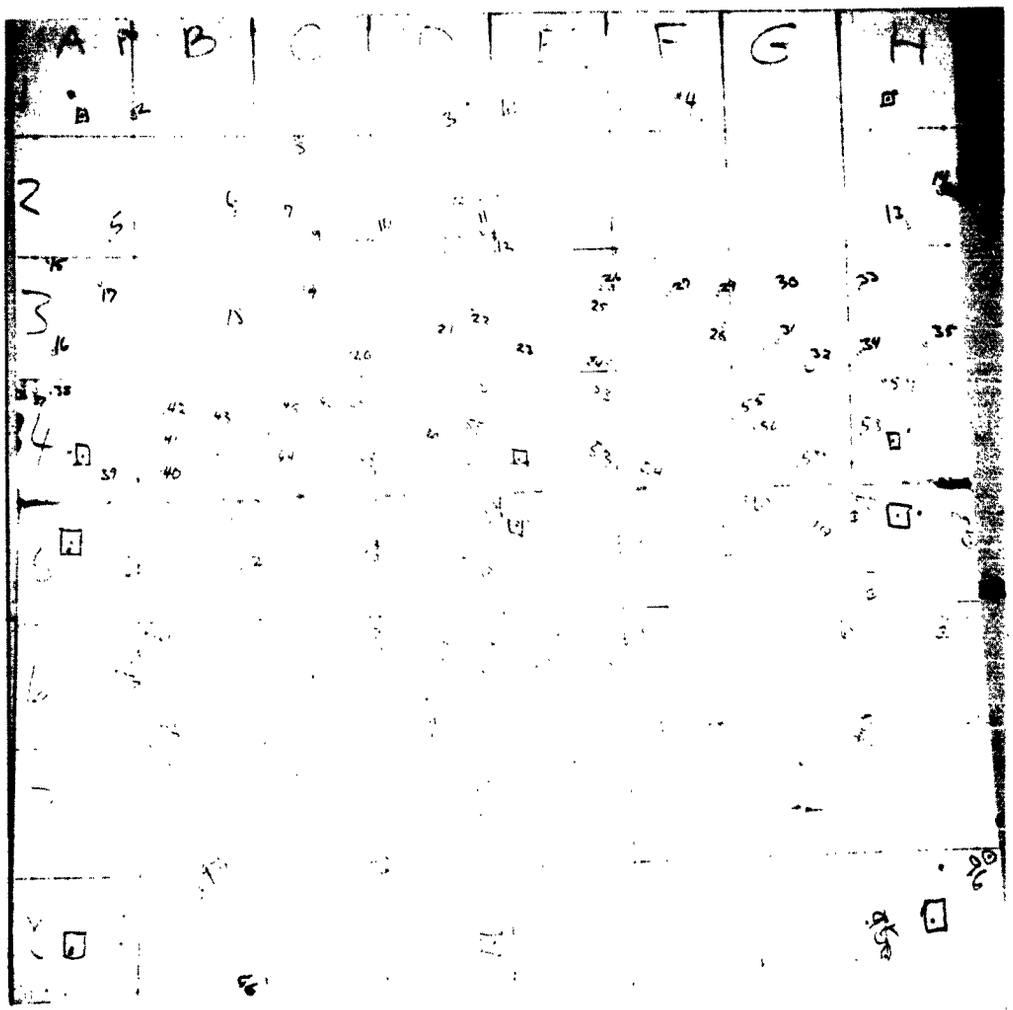


Figure 135. Impact Pattern, Round No. 55

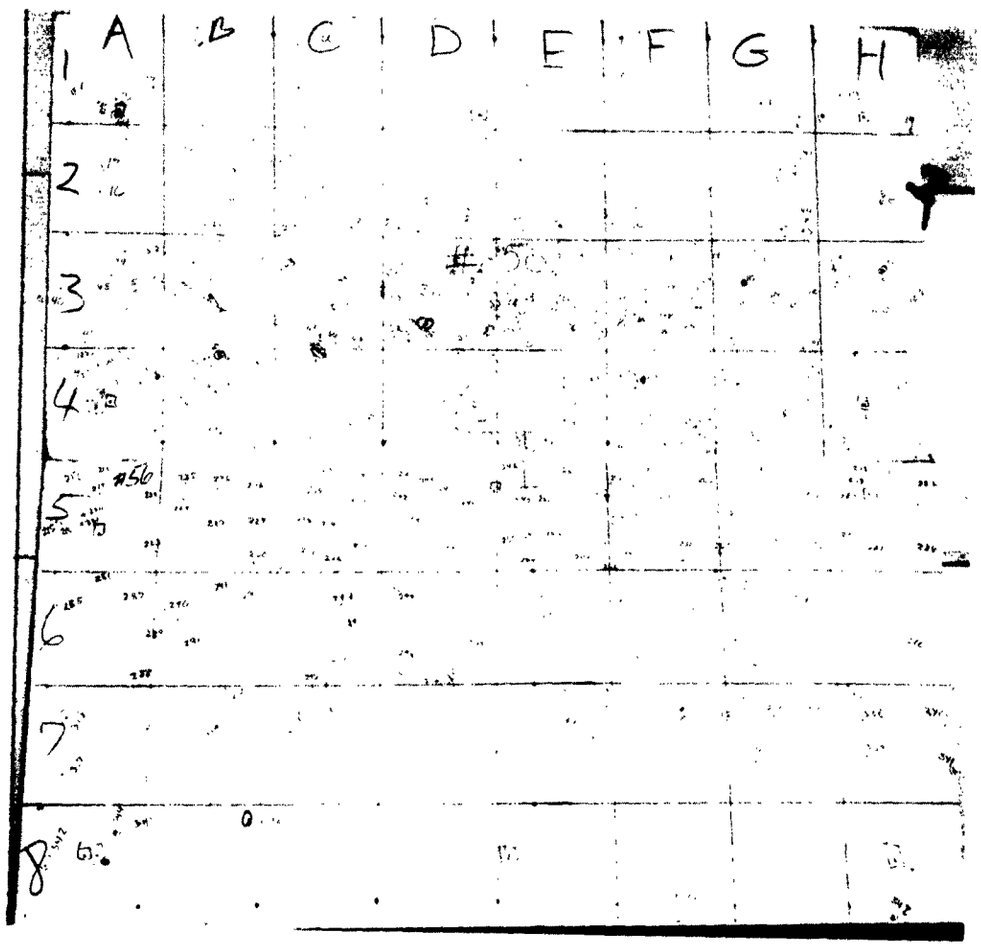


Figure 136. Impact Pattern, Round No. 56

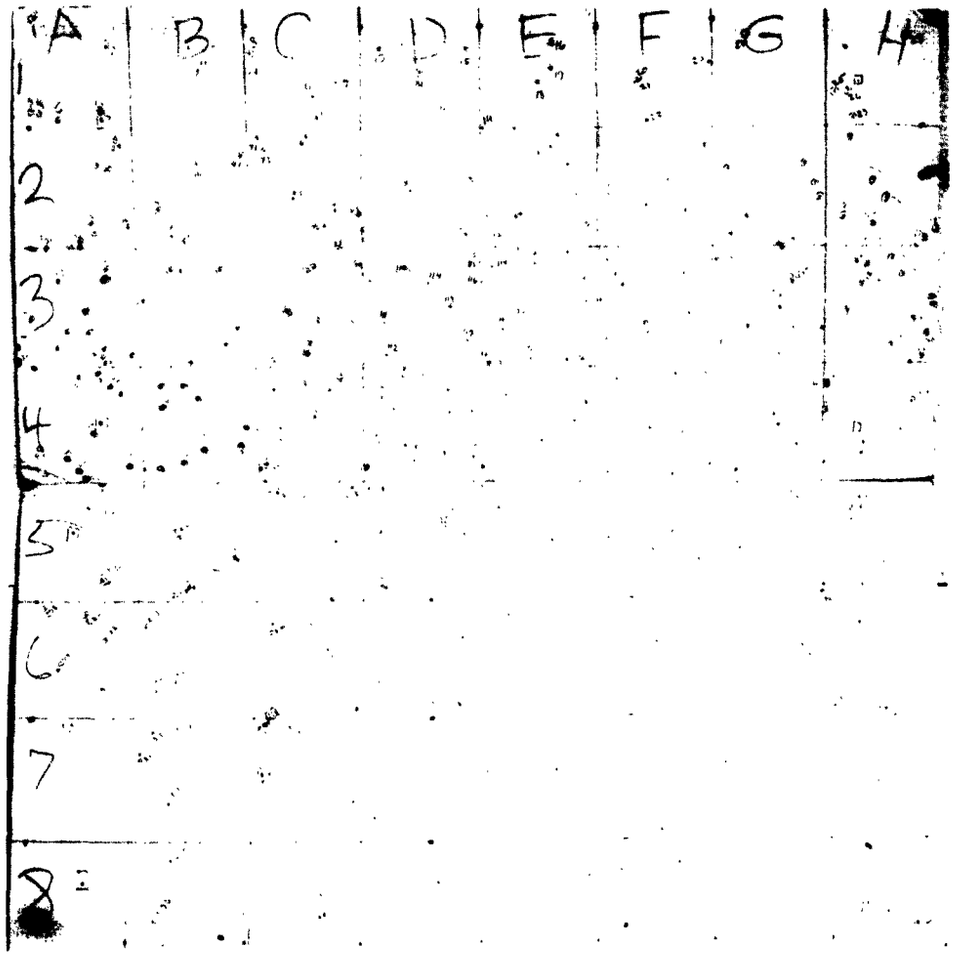


Figure 137. Impact Pattern, Round No. 57

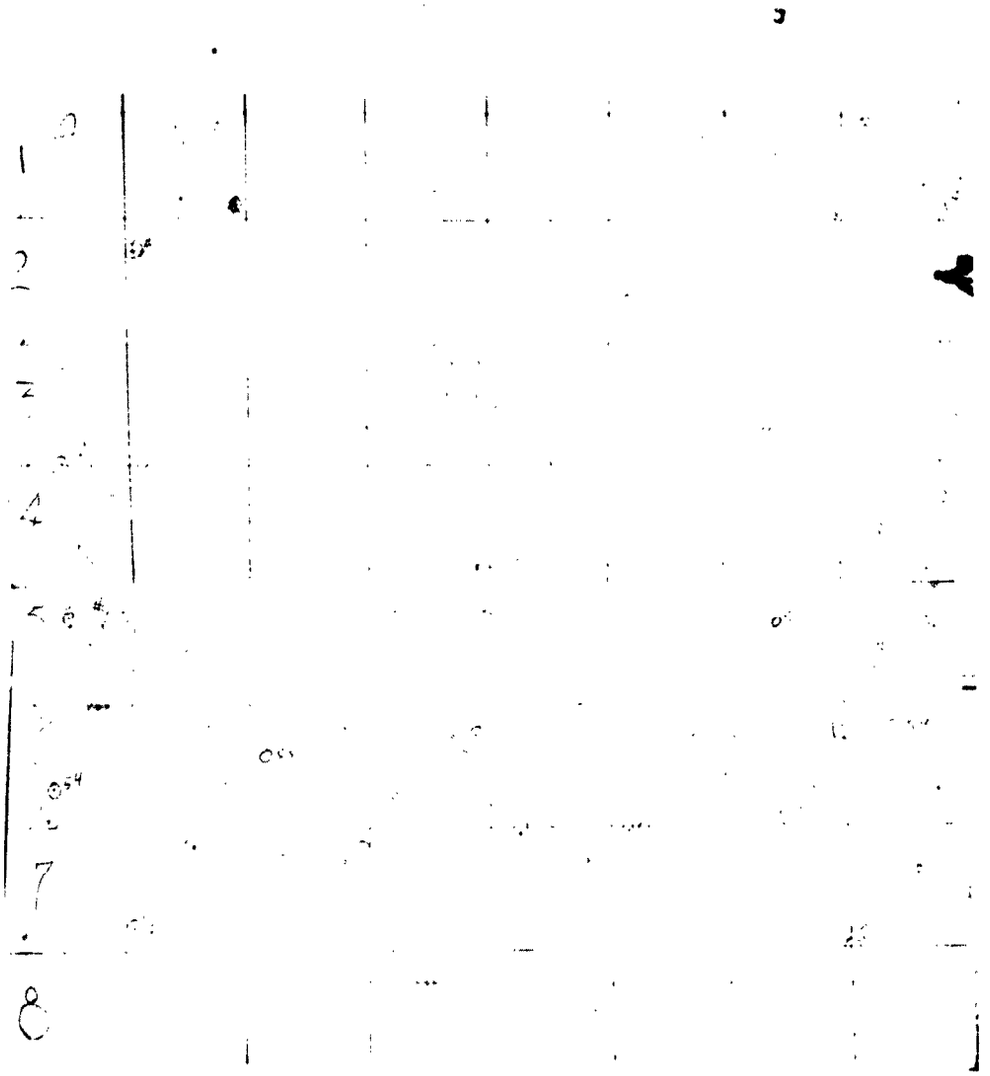

Figure 138. Impact Pattern, Round No. 60

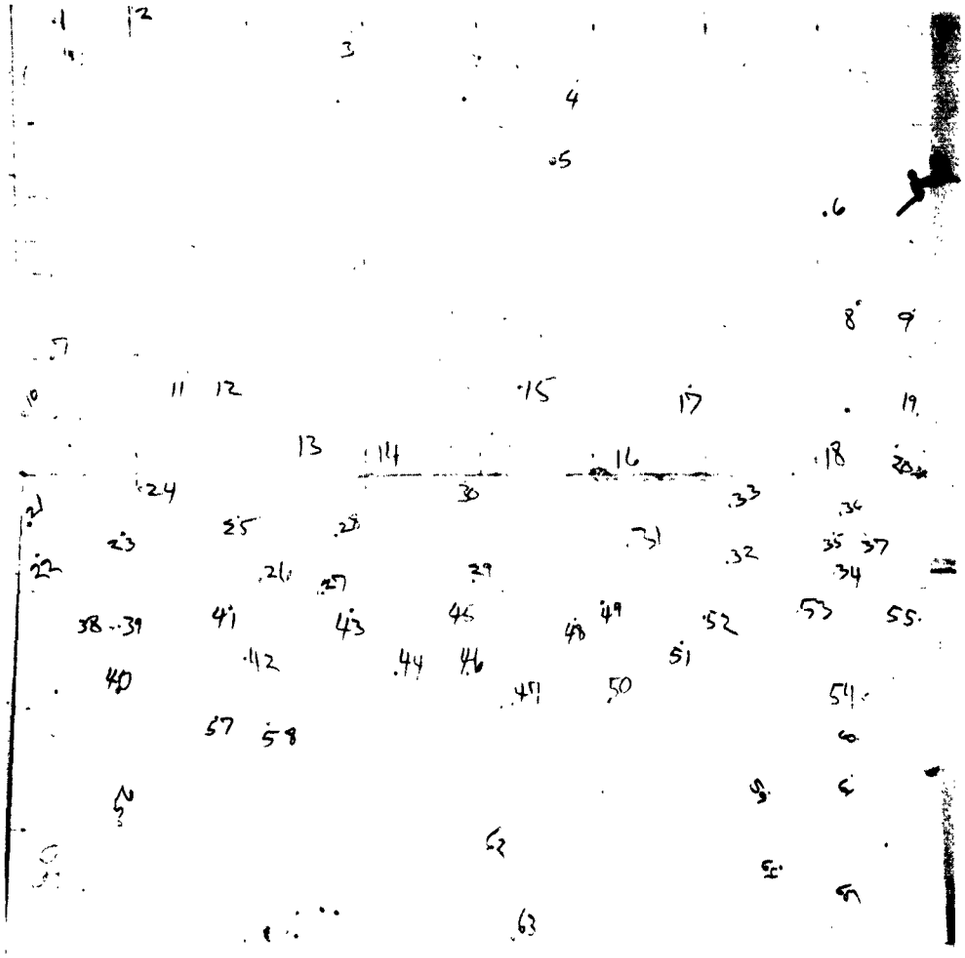

Figure 139. Impact Pattern, Round No. 61

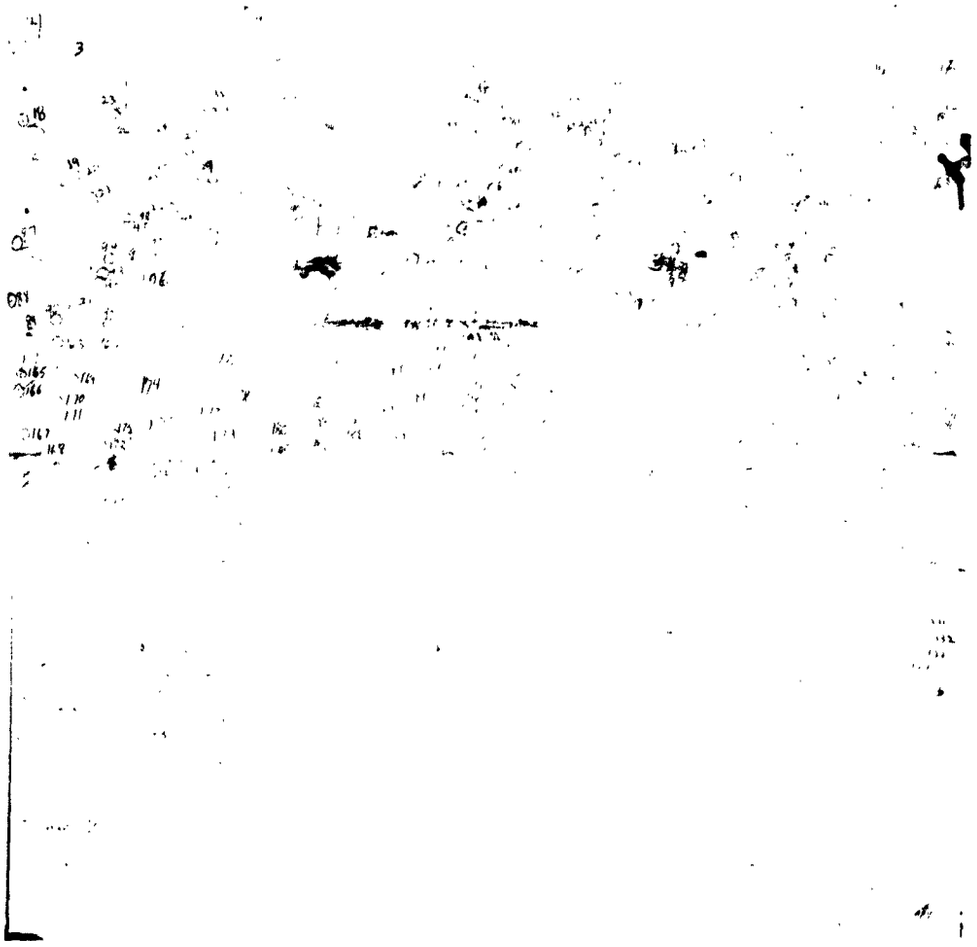

Figure 140. Impact Pattern, Round No. 62


Figure 141. Impact Pattern, Round No. 63

Figure 142. Impact Pattern, Round No. 64

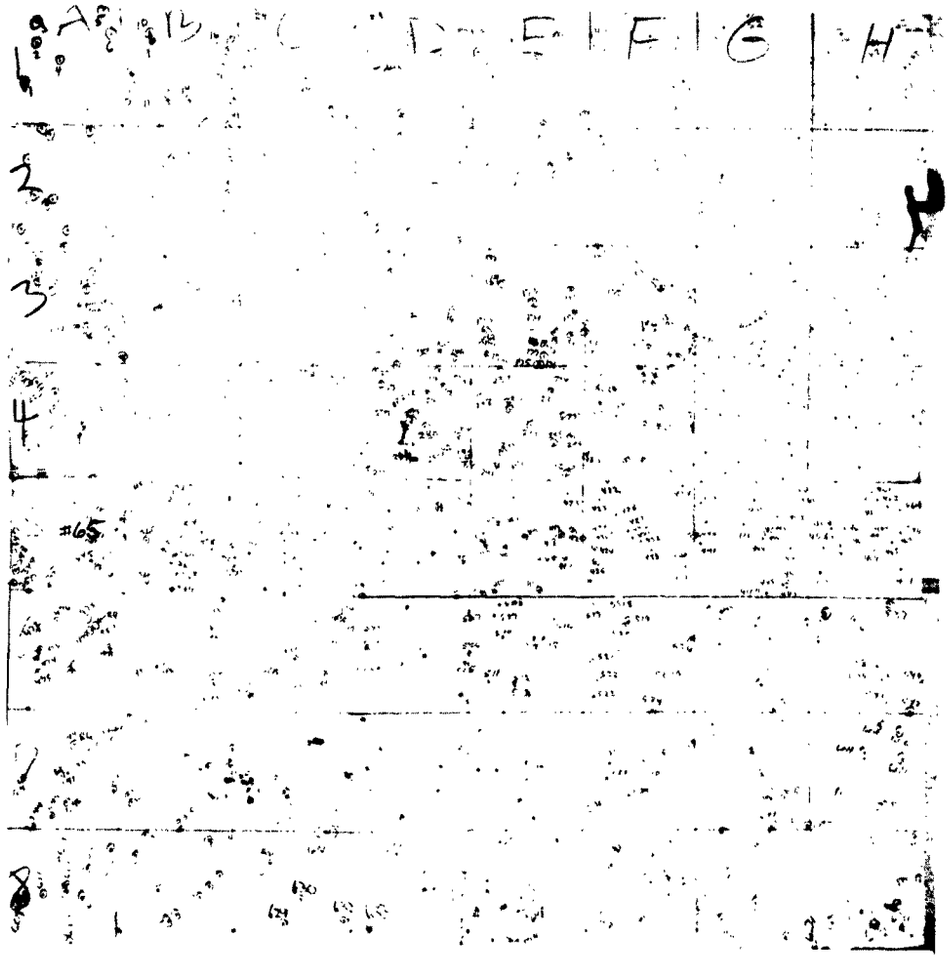

Figure 143. Impact Pattern, Round No. 65

Figure 144. Impact Pattern, Round No. 68

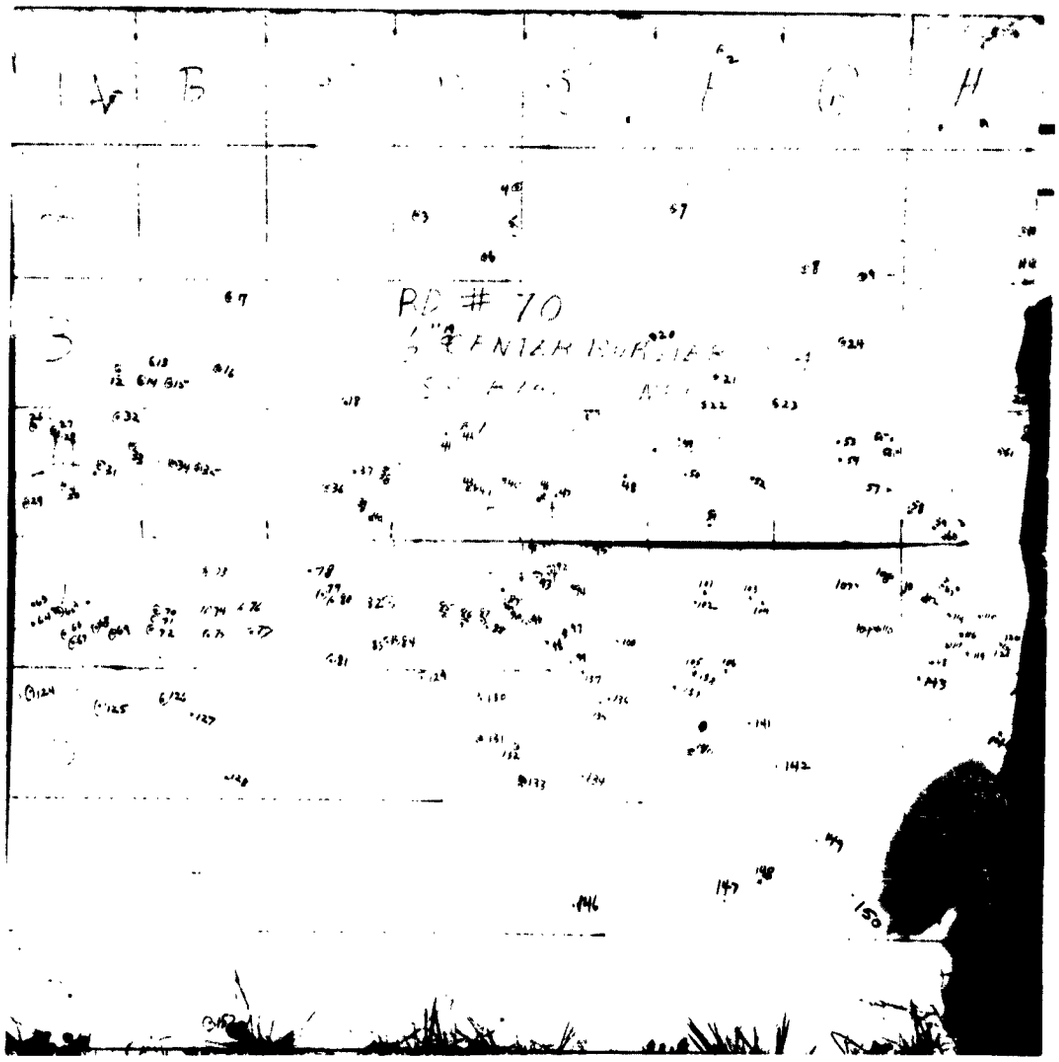


Figure 145. Impact Pattern, Round No. 70

Figure 146. Impact Pattern, Round No. 77


Figure 147. Impact Pattern, Round No. 78

Figure 148. Impact Pattern, Round No. 79

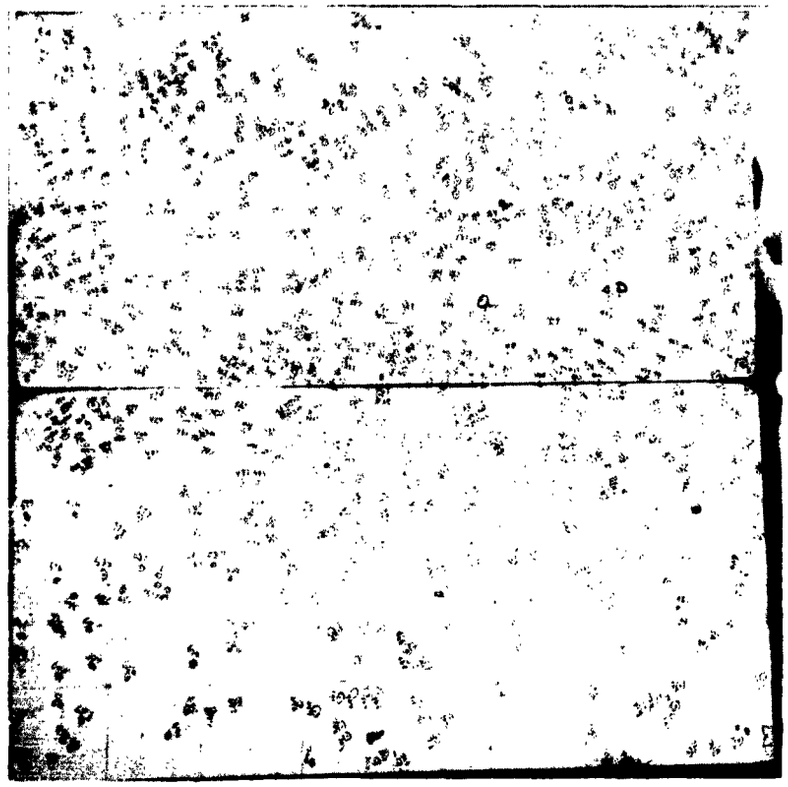

Figure 149. Impact Pattern, Round No. 82

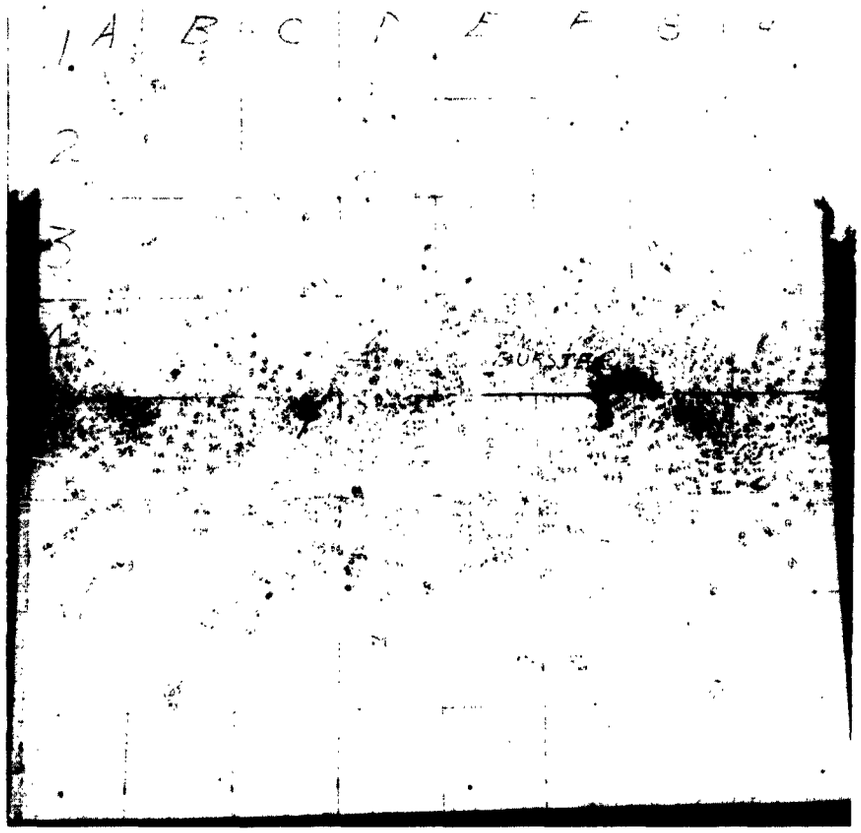

Figure 150. Impact Pattern, Round No. 83

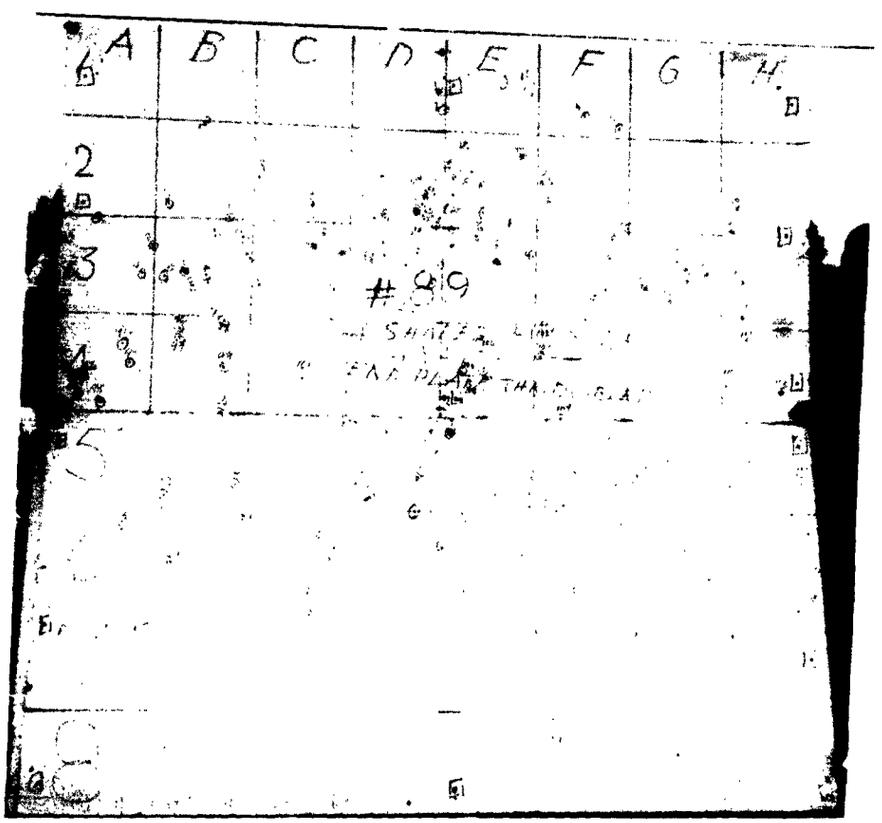


Figure 151. Impact Pattern, Round No. 89

# APPENDIX V

## ALTERNATE CONCEPTS DATA

This appendix summarizes design and test data on alternate concepts investigated during the course of this study.

## TABLE 10

### Basic Design – Data Summary – Speci

| Round No. | Round Description | | | | | | | | | Parameter Varied | Test Objectives | |
|---|---|---|---|---|---|---|---|---|---|---|---|---|
| | Expl Mass (grams) | Frag Mass (grams) | End Plate Mass (grams) | C/M | Type | Cent. Burst Type | Cent. Burst Diam (in.) | Over Dim. Ht (in.) | Over Dim. Diam (in.) | | | |
| 23 | 32.8 | 2636 | 545<br>559 | 0.012 | Fig. 152 | C-4 | 1.19 (max) | 2.5 | 3.5 | Conical center burster | Pattern and velocity gradient from top to bottom of ground | F |
| 24 | 27.4 | 2636 | 607<br>607 | 0.010 | Fig. 152 | C-4 | 1.19 (max) | 2.5 | 3.5 | Same as 23 | Same as 23 | F |
| 44 | 62.2 | 2359 | 297<br>686 | 0.026 | Fig. 153 | C-4 | 1.50 (max) | 2.5 | 2.44 to 3.86 (conical) | Conical center burster Fragments in contact with explosive. Initiation at small end | Same as 23 | F |
| 45 | 61.4 | 2438 | 299<br>685 | 0.027 | Fig. 153 | C-4 | 1.50 (max) | 2.5 | 2.44 to 3.86 (conical) | Same as 44 | Same as 23 | F |
| 46 | 58.0 | 2790 | 612<br>612 | 0.021 | Fig. 152 | C-4 | 1.50 | 2.5 | 3.6 | Same as 44 except air gap between fragments and burster | Same as 23 | F |

## TABLE 10

### Basic Design – Data Summary – Special Concepts

| rst Diam (in.) | Over Dim. Ht (in.) | Over Dim. Diam (in.) | Parameter Varied | Test Objectives | Results: Impact Pattern | Results: Beam Spy Angle | Results: Velocity Gradient | Results: Polar Plot | Conclusions and Comments |
|---|---|---|---|---|---|---|---|---|---|
| .19 max) | 2.5 | 3.5 | Conical center burster | Pattern and velocity gradient from top to bottom of ground | Fig. 159 | 14 Deg | 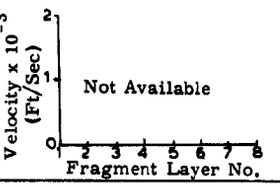  | Not available | Data invalid |
| .19 max) | 2.5 | 3.5 | Same as 23 | Same as 23 | Fig. 160 | 26 Deg | 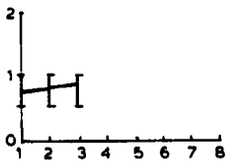  | Not available | Data invalid |
| .50 max) | 2.5 | 2.44 to 3.86 (conical) | Conical center burster Fragments in contact with explosive. Initiation at small end | Same as 23 | Fig. 161 | 20 Deg |   | Fig. 156 | Fragments moved as a group |
| .50 max) | 2.5 | 2.44 to 3.86 (conical) | Same as 44 | Same as 23 | Fig. 162 | 24 Deg | 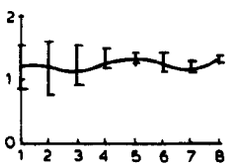  | Fig. 157 | Same as 44 |
| .50 | 2.5 | 3.6 | Same as 44 except air gap between fragments and burster | Same as 23 | Fig. 163 | 28 Deg | 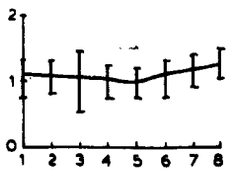  | Fig. 158 | Same as 44 |



TABLE 10 (Cont)

| Round No. | Round Description | | | | | | | | | Parameter Varied | Test Objectives | Im Pa |
|---|---|---|---|---|---|---|---|---|---|---|---|---|
| | Expl Mass (grams) | Frag Mass (grams) | End Plate Mass (grams) | C/M | Type | Cent. Burst Type | Cent. Burst Diam (in.) | Over Dim. Ht (in.) | Over Dim. Diam (in.) | | | |
| 72 | 18.6 | 803 | 6.9 | 0.023 | Fig. 155 | None | None | 7.8 | 2.25 | Explosive end plates as confiner and fragment propellant (Eglin concept) | Reduction of weight and fragment velocity Pattern control | Fi |
| 73 | 18.9 | 801 | 7.3<br>7.0 | 0.024 | Fig. 155 | None | None | 2.8 | 2.5 | Same as 72 | Same as 72 | Fi |
| 74 | 11.5 | 1904 | 394<br>399 | 0.006 | Fig. 154 | Shaped C-4 | 0.625 | 2.88 | 2.77 | Center burster with shaped core; fragments in solid pack | Pattern and velocity from top to bottom of round | Fi |
| 75 | 12.7 | 1897 | 382<br>383 | .007 | Fig. 154 | Shaped C-4 | 0.625 | 2.88 | 2.77 | Same as 74 | Same as 74 | Fi |
| | | | | | | | | | | | | |

TABLE 10 (Cont)

| irst Diam (in.) | Over Dim. Ht (in.) | Over Dim. Diam (in.) | Parameter Varied | Test Objectives | Results: Impact Pattern | Results: Beam Spy Angle | Results: Velocity Gradient | Results: Polar Plot | Conclusions and Comments |
|---|---|---|---|---|---|---|---|---|---|
| None | 7.8 | 2.25 | Explosive end plates as confiner and fragment propellant (Eglin concept) | Reduction of weight and fragment velocity Pattern control | Fig. 164 | Too large | 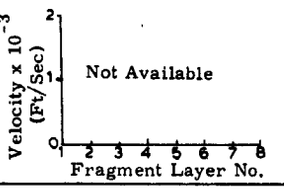  | Not available | Fastax camera data indicate potential for random fragment distribution at low velocities. Maximum velocity for rounds 72 and 73 was 380 fps |
| None | 2.8 | 2.5 | Same as 72 | Same as 72 | Fig. 165 | | 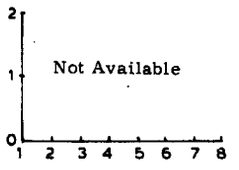  | Not available | Same as 72 |
| 0.625 | 2.88 | 2.77 | Center burster with shaped core; fragments in solid pack | Pattern and velocity from top to bottom of round | Fig. 166 | 12 Deg | 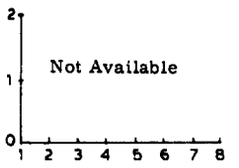  | Not available | Velocities irregular - order to 300 to 400 fps |
| 0.625 | 2.88 | 2.77 | Same as 74 | Same as 74 | Fig. 167 | 12 Deg | 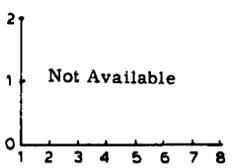  | Not available | Same as 74 |
| | | | | | | | | | |

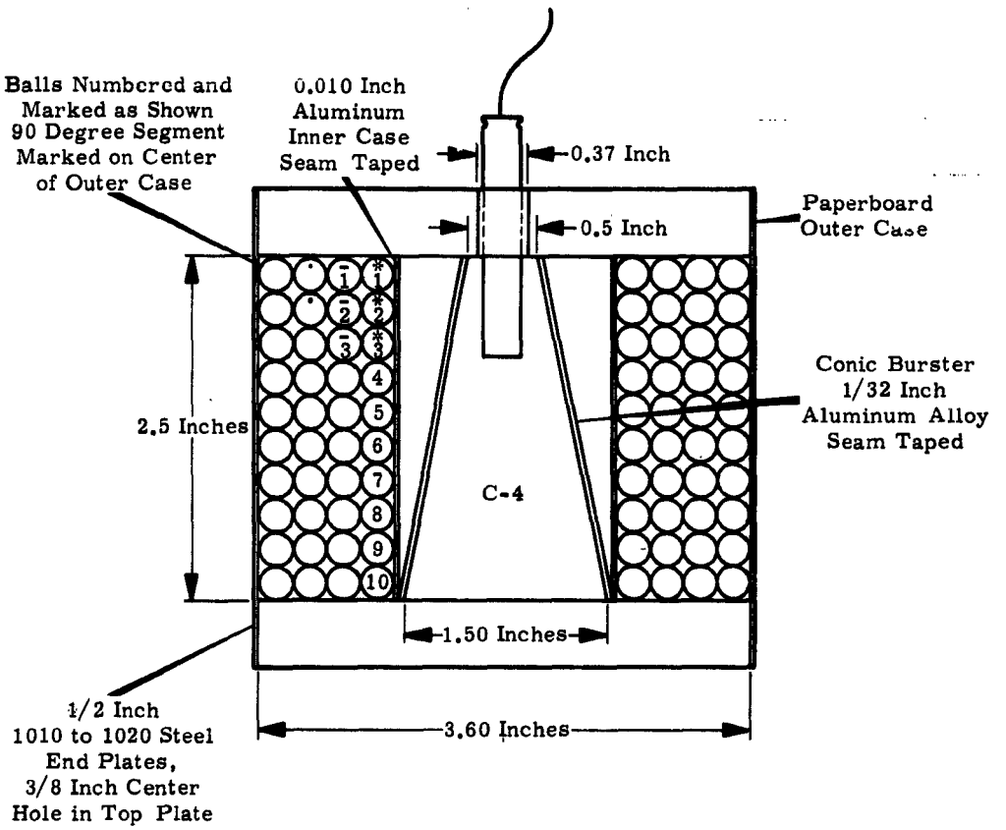


Figure 152. Tapered Burster, Design Concept A

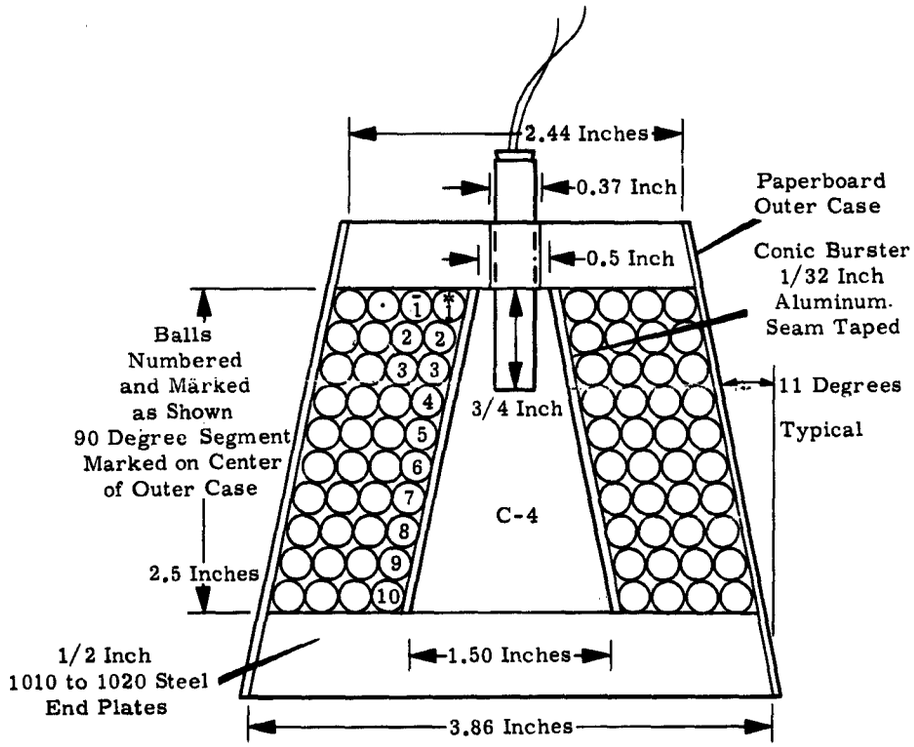


Figure 153. Tapered Burster, Design Concept B

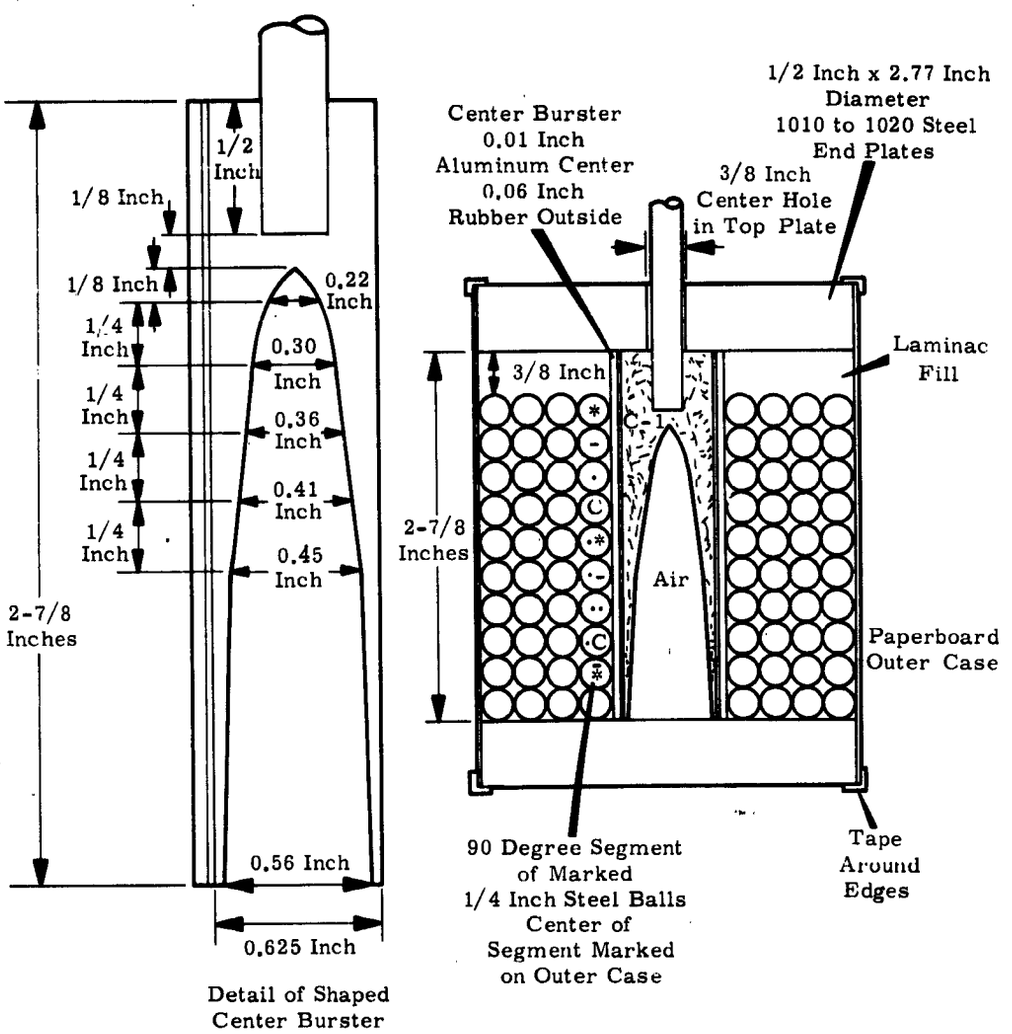


Figure 154. Shaped Burster Design Concept

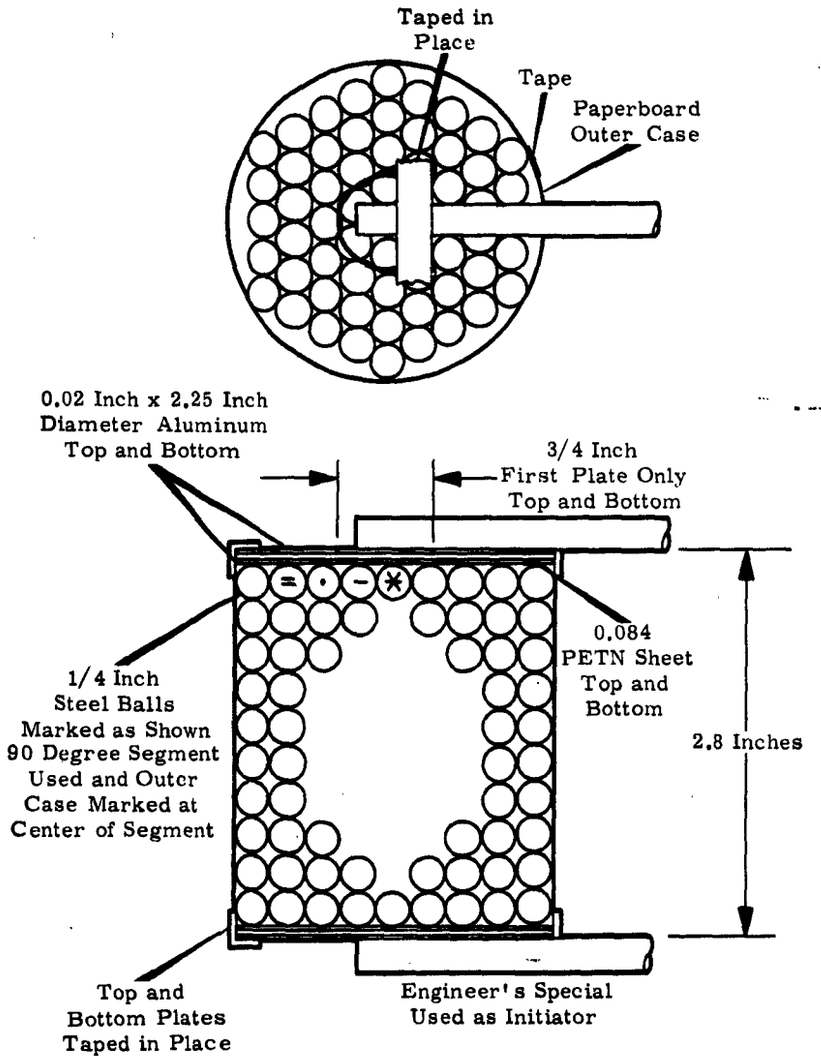


Figure 155. Explosive End Impulse Design Concept

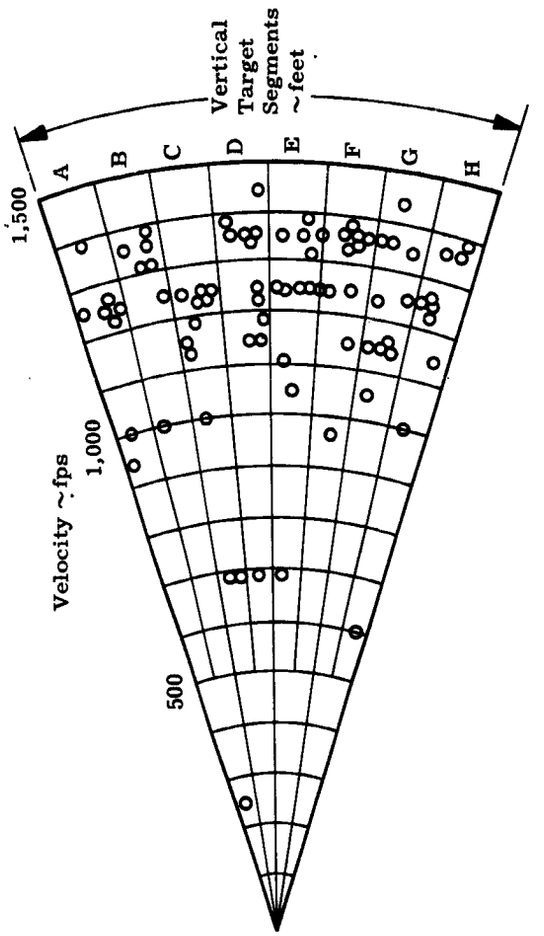


Figure 156. Velocity versus Radial Distribution, Round No. 44

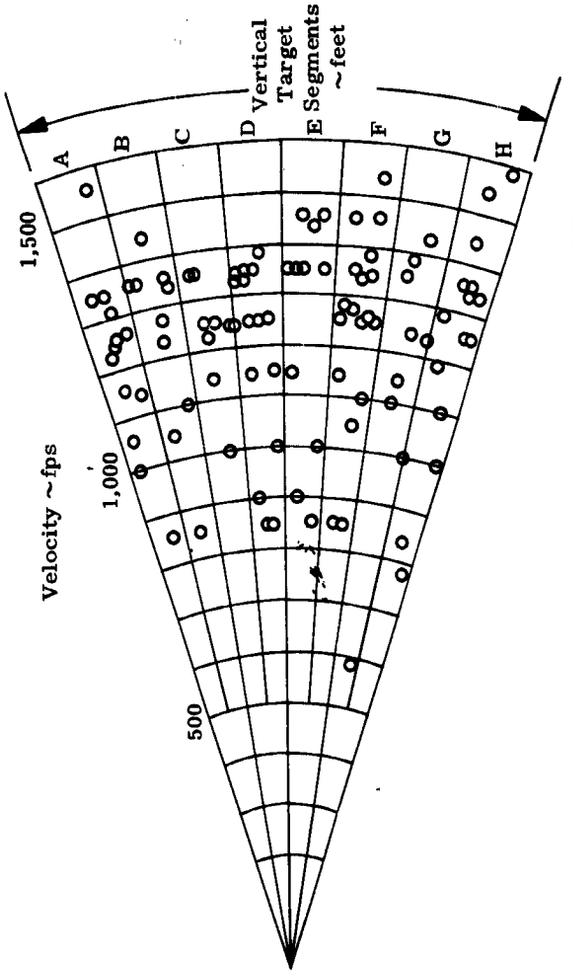


Figure 157. Velocity versus Radial Distribution, Round No. 45

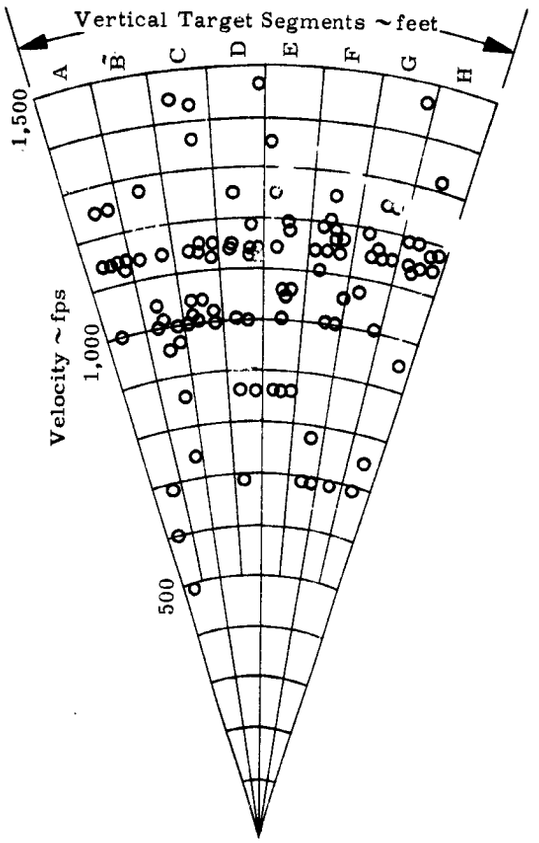


Figure 158. Velocity versus Radial Distribution, Round No. 46

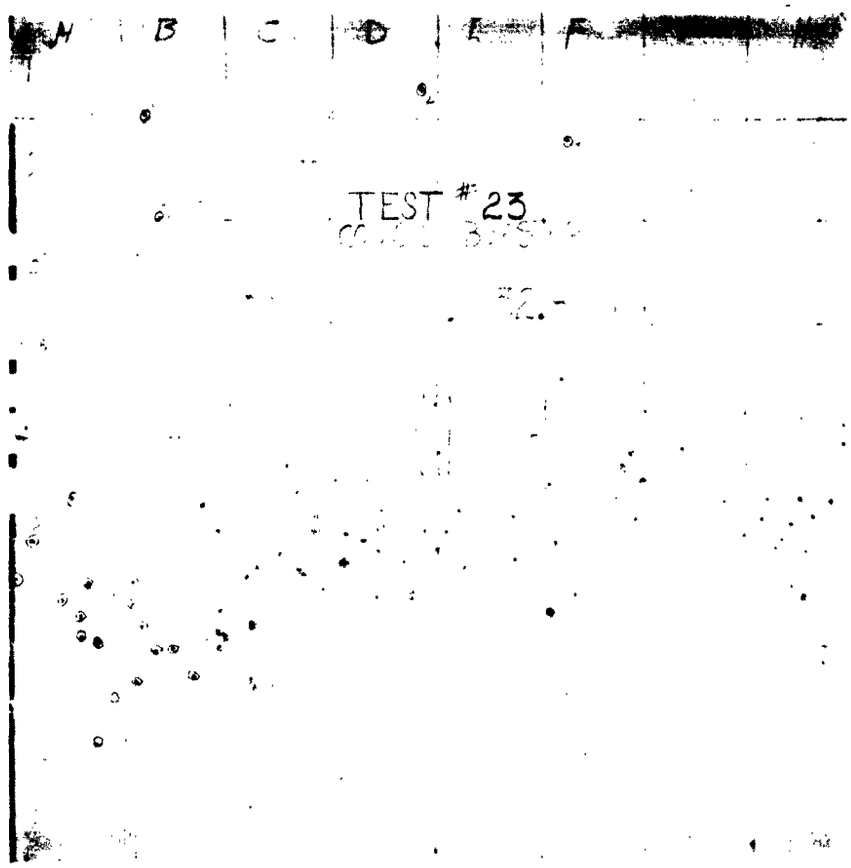


Figure 159. Impact Pattern, Round No. 23

Figure 160. Impact Pattern, Round No. 24

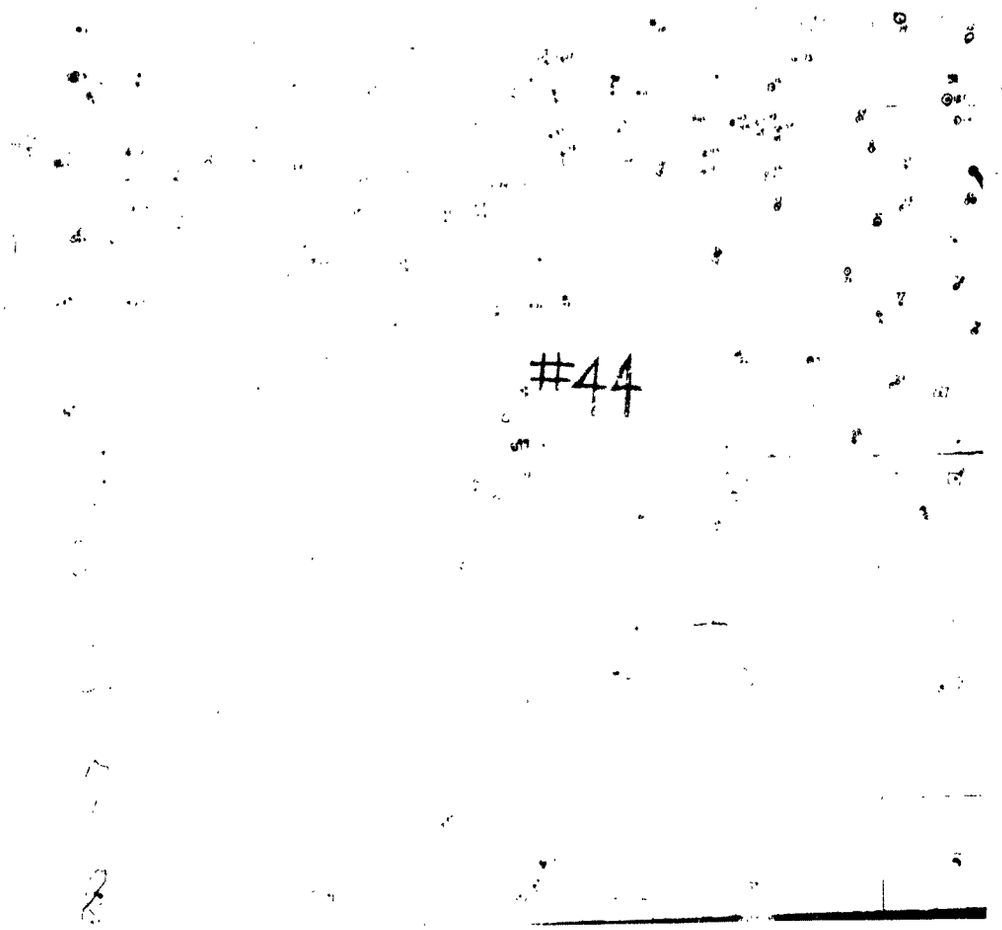


Figure 161. Impact Pattern, Round No. 44

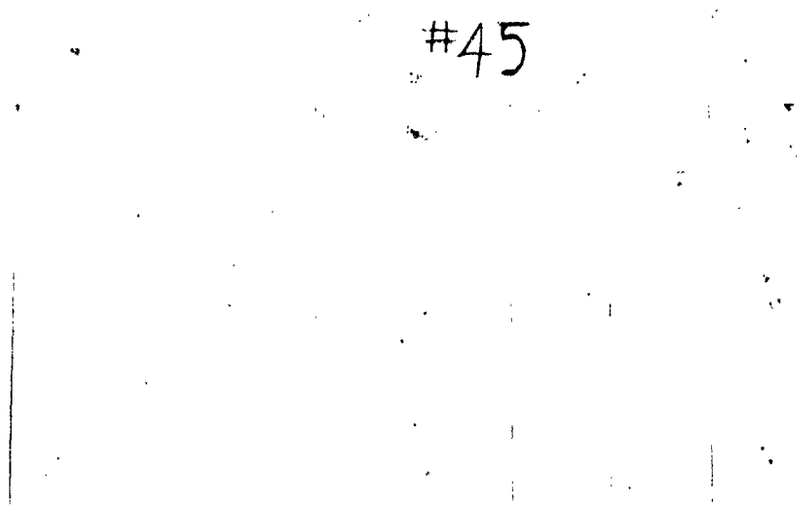


Figure 162. Impact Pattern, Round No. 45

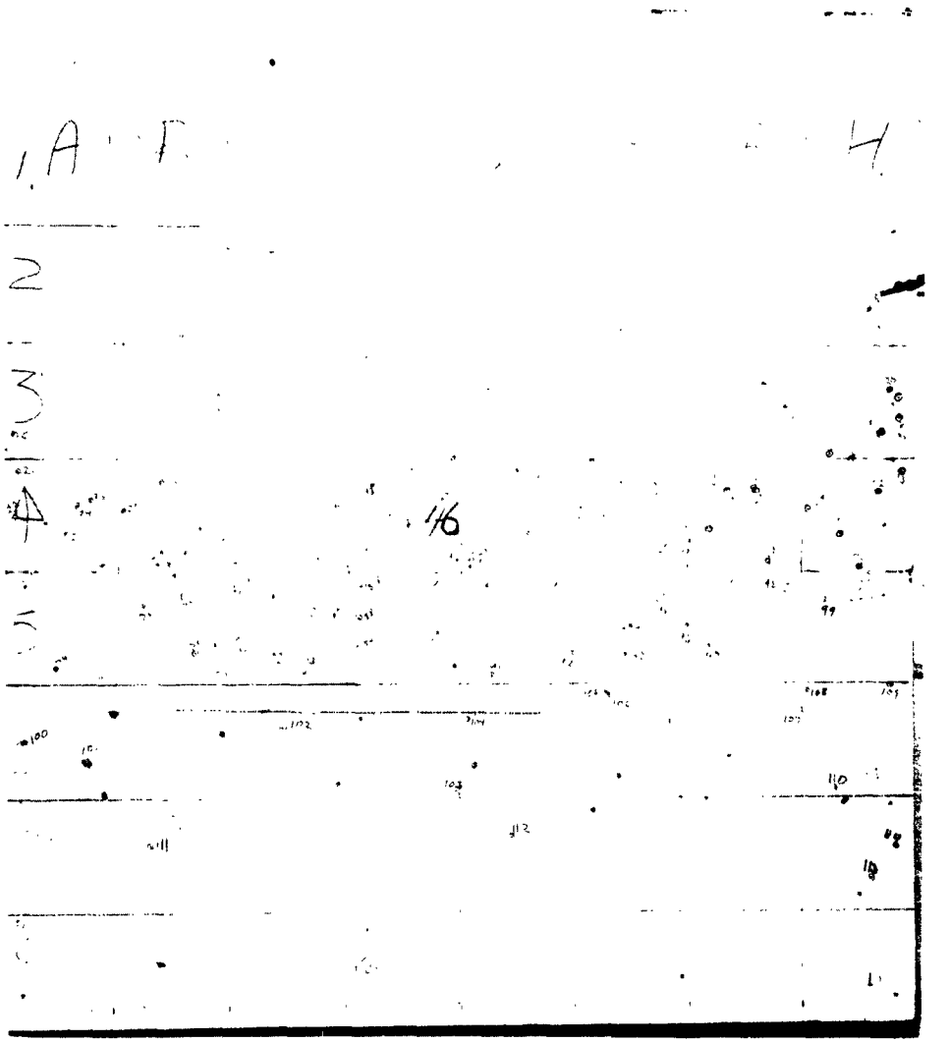

Figure 163. Impact Pattern, Round No. 46

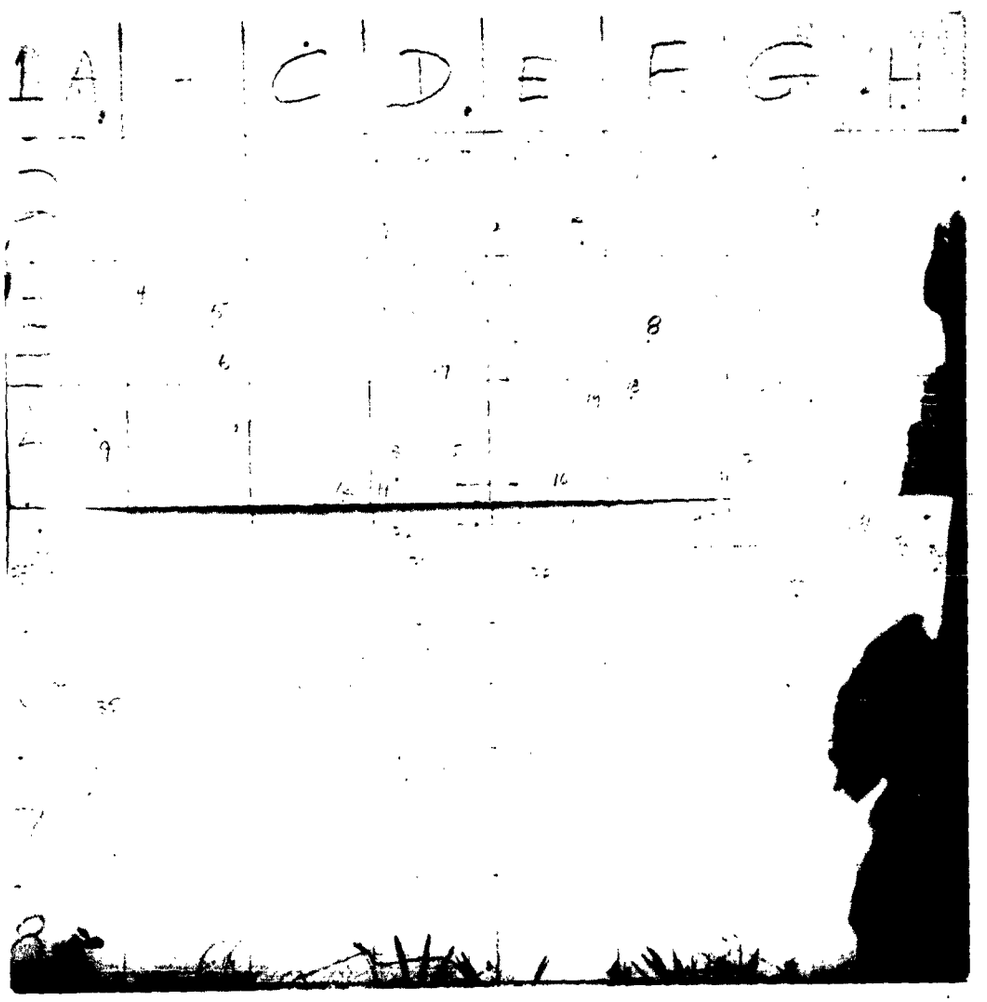


Figure 164. Impact Pattern, Round No. 72

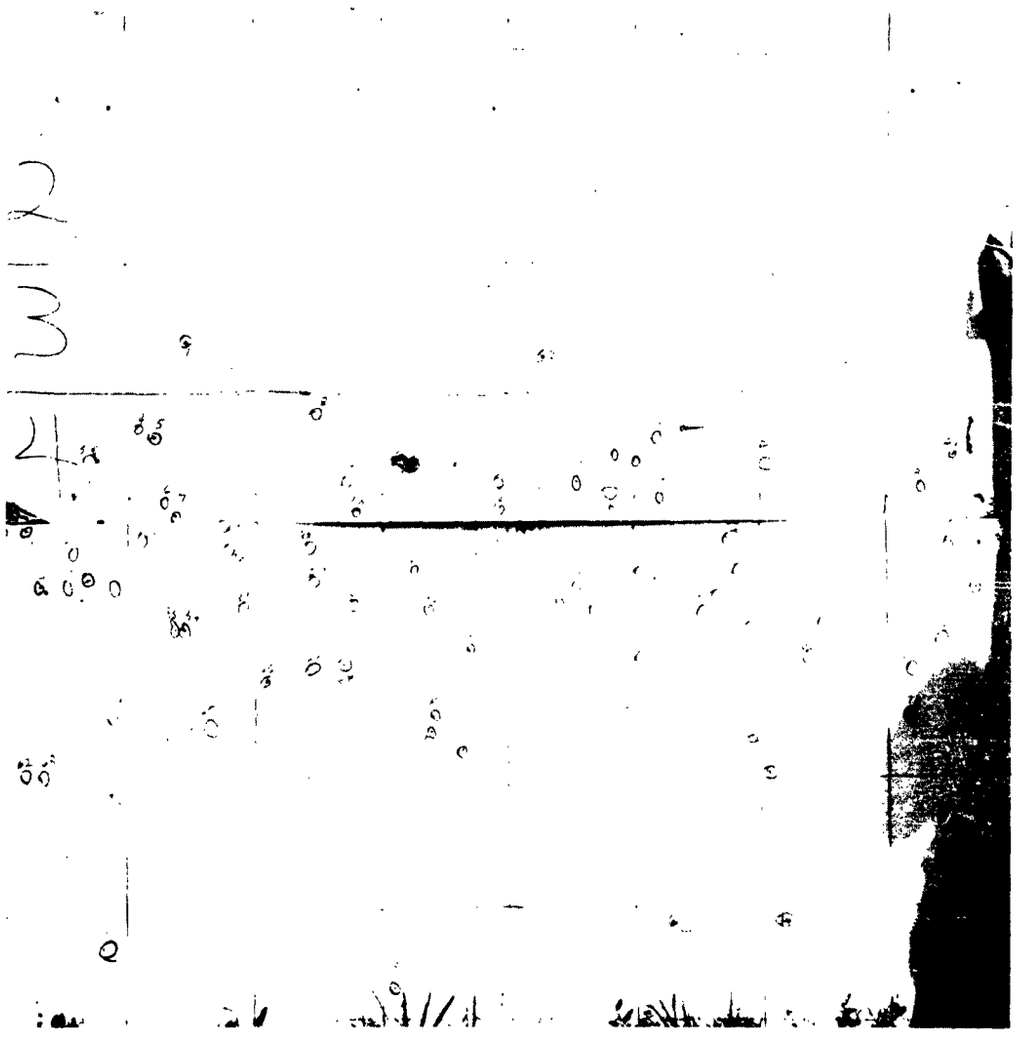

Figure 165. Impact Pattern, Round No. 73


Figure 166. Impact Pattern, Round No. 74

Figure 167. Impact Pattern, Round No. 75